SOLAR RADIATION INDUCED PERTURBATIONS AND CONTROL OF SATELLITE TRAJECTORIES

by

JOZEF CYRILLUS VAN DER HA

M.Sc., TECHNOLOGICAL UNIVERSITY EINDHOVEN, THE NETHERLANDS, 1973

A THESIS SUBMITTED IN PARTIAL FULFILMENT OF

THE REQUIREMENTS FOR THE DEGREE OF

DOCTOR OF PHILOSOPHY

in

THE FACULTY OF GRADUATE STUDIES

(Department of Mechanical Engineering)

We accept this thesis as conforming to the

required standard

THE UNIVERSITY OF BRITISH COLUMBIA

June, 1977

In presenting this thesis in partial fulfilment of the requirements for an advanced degree at the University of British Columbia, I agree that the Library shall make it freely available for reference and study. I further agree that permission for extensive copying of this thesis for scholarly purposes may be granted by the Head of my Department or by his representatives. It is understood that publication, in part or in whole, or the copying of this thesis for financial gain shall not be allowed without my written permission.

JOZEF C. VAN DER HA

Department of Mechanical Engineering

The University of British Columbia,
Vancouver, Canada, V6T 1W5

Date SEPTEMBER 23, 1977

ABSTRACT

The long-term orbital perturbations due to solar radiation forces as well as ways to utilize these effects for corrections in the orbit are investigated. In order to obtain familiarity with relative merits of the formulations and methods relevant to the present objective, the special case of an orbit in the ecliptic plane and a force along the radiation is considered first. The long-term valid analysis is based upon the two-variable expansion method and incorporates the apparent motion of the sun by treating the sun's position as a quasi-orbital element. Analytical representations for orbital elements are derived and the perturbations are conveniently summarized in the form of polar plots showing the long-term evolution of the eccentricity vector. While the eccentricity is periodic with period close to one year, the argument of the perigee contains secular terms. The total energy and thus major axis remain conserved in the long run. However, in the course of one year, the effect of the earth's shadow may lead to small secular changes in the major axis thereby modifying the satellite's period.

Next, the analysis is extended to orbits of an arbitrary inclination with closed-form analytical solutions established in some special cases. An interesting relation between the long-term behavior of the orbital inclination and the in-plane perturbations is discovered. Also, more general satellite configurations are studied: e.g., spacecrafts modelled as a plate in an arbitrary fixed orientation with respect to the earth or solar radiation as well as platforms kept fixed to the inertial space. In all appli-

cations a realistic solar radiation force allowing for diffuse and/or specular reflection as well as for re-emission of absorbed radiation is considered. In a few cases, the analysis is extended to include arbitrarily shaped satellite bodies modelled by a number of surface components of homogeneous material characteristics.

After establishing a comprehensive spectrum of the qualitative and quantitative aspects of solar radiation induced orbital perturbations, the attention is focused on the development of control strategies involving the rotation of solar panels attached to the satellite to manipulate both the direction and magnitude of the resulting force. A few on-off switching strategies are explored and the most effective switching locations for several specific objectives, e.g. maximization of the major axis, are determined. The switching strategies explored here constitute an attractive possibility for orbital corrections. The concept is particularly of interest to modern communications satellite technology since it allows their normal operation to remain unaffected over approximately half the time. Although on-off switching may lead to substantial changes in the major axis, it is not necessarily the best policy when time-varying orientations are also taken into consideration. The optimal control strategy for maximization of the major axis over one revolution is determined by means of the numerical steepest-ascent iteration procedure, and its effectiveness is compared with that of the switching programs. The solution should prove to be of interest in several future missions including the launching of a solar sail from a geocentric orbit into a heliocentric or escape trajectory.

Subsequently, solar radiation effects upon a satellite (usually a solar sail) in a heliocentric orbit are explored. First, the sail is

taken in a fixed but arbitrary orientation to the local frame. Using specific initial conditions, exact solutions in the form of conic sections and three-dimensional logarithmic spirals are established. For an arbitrary initial orbit, long-term approximate representations of the orbital elements are derived. An effective out-of-plane spiral transfer trajectory is obtained by reversing the force component normal to the orbit at specified positions. By choosing the appropriate control angles, any point in space can eventually be reached.

Finally, time-varying optimal control strategies are explored for increasing the total energy (and angular momentum) during one revolution. While analytical approximate results can be established for near-circular orbits, in the general case a numerical steepest-ascent technique is employed. The results are compared with those from the constant sail setting indicating that the latter is a near-optimal strategy for low eccentricity starting orbits.

TABLE OF CONTENTS

Chapter Page

LIST OF TABLES

LIST OF FIGURES

Figure | Page

ACKNOWLEDGEMENT

The author wishes to express his sincere gratitude to Dr. V.J. Modi for his patient guidance and stimulating encouragement throughout the preparation of this thesis.

The investigation reported here was partially supported by the National Research Council of Canada, Grant No. A2181.

LIST OF SYMBOLS

a	semi-major axis
$\hat{a}$	total energy, $-1/a$
$\underline{a}$	vector of orbital elements $(a, \ell, p, q, i, \Omega, \eta)$
$\tilde{\underline{a}}$	vector of orbital elements $\underline{a}$ excluding η
a_r	semi-major axis of reference (24-hour period) orbit, 42,241 km
a_e	semi-major axis of earth's orbit, 1 A.U. = 1.496×10^8 km
$a^j_{nk}, b^j_{nk}, c^j_{nk}, d^j_{nk}$	slowly varying Fourier coefficients, Appendix II
b	constant, $c(1 + d^2)^{1/2}$
c	constant relating ε and δ, $(\delta/\varepsilon)\, a_{00}^{3/2}$
c_1	constant relating ε and δ^2, $(\delta^2/\varepsilon)\, a_{00}^{3/2}$
c_s	constant in spiral trajectory, $-u'(\nu)/u(\nu)$
c_t	constant, Equation (5.9)
c_ε	constant, ε/δ
d	constant, $3\,\varepsilon\, a_{00}^{1/2} / (2\delta)$
e	eccentricity
$\underline{e}$	eccentricity vector, pointing from origin to perigee with length e, Figure 3-1
e_f, e_b	emissivities of front , and back side of surface element
e_p	modified eccentricity, $[e_{00}^2 + 2\varepsilon_s p_{00} R + \varepsilon_s^2 R^2]^{1/2} / (1-\varepsilon_s R)$
$\underline{f}(\underline{a},\nu)$	vector function denoting the right-hand-side of the perturbation equation
$\tilde{\underline{f}}(\underline{a},\nu)$	vector function $\underline{f}$ excluding equation for η
$\underline{g}(\underline{a},\underline{\alpha})$	vector function denoting the right-hand-sides of Equations (4.15)

$\underline{h}$	angular momentum (per unit mass) vector, $\underline{r} \times \underline{v}$
h_1, h_2	components of $\underline{h}$ along x_n and y_n axes, respectively
i	inclination of orbital plane with respect to ecliptic
$\underline{i}$, $\underline{j}$, $\underline{k}$	unit vectors along the x, y, z axes, respectively
$\underline{i}_r$, $\underline{j}_r$, $\underline{k}_r$	(r = 0, 1, 2) unit vectors along the x_r, y_r, z_r axes
$\underline{i}_n$, $\underline{j}_n$, $\underline{k}_n$	unit vectors along the x_n, y_n, z_n axes
j	auxiliary element, $e\cos\omega = p\cos\psi + q\sin\psi$
k	auxiliary element, $e\sin\omega = q\cos\psi - p\sin\psi$
ℓ	semi-latus rectum
$\hat{\ell}$	auxiliary variable, $\ln(\ell)$
ℓ_p	modified semi-latus rectum, $\ell_{00}/(1-\varepsilon_s R)$
m	mass of satellite
n	number of illuminated surface components
$\underline{n}_k^0$	auxiliary vector, $(0, 0, \sin\beta_k)$
$\underline{n}_k^1$	auxiliary vector, $-(\cos\beta_k \cos\hat{\alpha}_k, \cos\beta_k \sin\hat{\alpha}_k, 0)$
$\underline{n}_k^2$	auxiliary vector, $-(\cos\beta_k \sin\hat{\alpha}_k, -\cos\beta_k \cos\hat{\alpha}_k, 0)$
p	auxiliary element, $e\cos\tilde{\omega}$
q	auxiliary element, $e\sin\tilde{\omega}$
$\underline{r}$	radius vector, pointing from origin to satellite, Figure 3-1
s	ratio R_e/ℓ
s_u	sign of $U = (\underline{u}^n \cdot \underline{u}^s)$
$\underline{s}^0$	auxiliary vector, $(0, 0, \sin i_{00} \sin\hat{\eta}_{00})$
$\underline{s}^1$	auxiliary vector, $-(K_{10}, K_{20}, 0)$
$\underline{s}^2$	auxiliary vector, $-(K_{20}, -K_{10}, 0)$

t	time (nondimensional)
u	inverse radius, $1/r$
$\underline{u}_k^n$	$(u_{kx}^n, u_{ky}^n, u_{kz}^n)$, unit vector normal to surface component A_k with components along local coordinate axes
$\underline{u}^s$	(u_x^s, u_y^s, u_z^s), unit vector along direction of radiation with components along local coordinate axes
u_{kx}^n	component of $\underline{u}_k^n$ along local vertical, $-\cos\alpha_k \cos\beta_k$
u_{ky}^n	component of $\underline{u}_k^n$ along local horizontal, $-\sin\alpha_k \cos\beta_k$
u_{kz}^n	component of $\underline{u}_k^n$ normal to orbit, $\sin\beta_k$
u_x^s	component of $\underline{u}^s$ along local vertical, $-\cos^2(i/2)\cos(\nu-\psi-\hat{\eta}) - \sin^2(i/2)\sin(\nu-\psi+\hat{\eta})$
u_y^s	component of $\underline{u}^s$ along local horizontal, $\cos^2(i/2)\sin(\nu-\psi-\hat{\eta}) + \sin^2(i/2)\sin(\nu-\psi+\hat{\eta})$
u_z^s	component of $\underline{u}^s$ normal to orbit, $\sin(i)\sin\hat{\eta}$
$\underline{v}$	velocity vector, $\dot{\underline{r}}$
w	auxiliary element, $1 - (1 - e^2)^{1/2}$
$\underline{w}^r$	rotation vector along instantaneous radius vector, $(rF_z/h)\underline{i}$
x	auxiliary element, $e\sin(\eta-\tilde{\omega}) = p\sin\eta - q\cos\eta$
y	auxiliary element, $e\cos(\eta-\tilde{\omega}) = p\cos\eta + q\sin\eta$
x, y, z	moving frame of reference fixed to osculating plane (geocentric case): x along the radial, y along the circumferential and z along the orbit-normal direction, Figure 3-1
x_1, y_1, z_1	intermediate frame of reference after rotation of surface element by α, Figure 3-2b
x_2, y_2, z_2	reference frame fixed to the plate after Eulerian rotations α and β, Figure 3-2b

x_n, y_n, z_n — reference frame with x_n and y_n axes in the osculating plane (x_n along line of nodes) and z_n normal to orbital plane

A — total effective illuminated surface area of the satellite, cross-sectional area for spherical satellite

$A_0(\bar{\nu})$, $B_0(\bar{\nu})$ — auxiliary functions in expression for M_0, Equation (5.21)

$A_j(\bar{\nu})$, $B_j(\bar{\nu})$ — ($j = 2,3,4,5$) auxiliary functions in second-order results, Equations (5.41)

A_k — k-th surface component (nondimensional)

A_{nk}, B_{nk} — ($n = 1,2,\ldots$; $k = 0,1,2,\ldots$) integrals, defined and evaluated in Appendix I

$\underline{A}^j(\underline{a}_0)$, $\underline{B}^j(\underline{a}_0)$ — vectors of Fourier coefficients in expansion of $\underline{f}(\underline{a}_0,\nu)$

$$\begin{pmatrix} \underline{A}^j(\underline{a}_0) \\ \underline{B}^j(\underline{a}_0) \end{pmatrix} = \int_0^{2\pi} \underline{f}(\underline{a}_0,\tau) \begin{pmatrix} \cos(j\tau) \\ \sin(j\tau) \end{pmatrix} d\tau/\pi$$

B — auxiliary constant, $c_s T/(2S) = \varepsilon_s T/C$

C — constant in spiral trajectory, $u(\nu)\, \ell(\nu)$

$C_0(\bar{\nu})$ — auxiliary function of $\bar{\nu}$, $(A_0^2 + B_0^2)^{1/2}$

$\underline{c}_k^j$ — ($j = 0,1,2$) auxiliary vector, $|U_k| \{\sigma_{1k}\underline{s}^j + [\sigma_{2k} + \rho_k U_k]\, \underline{n}_k^j\}\, A_k$

C_s — abbreviation for $3 \arcsin(s) - s(1 - s^2)^{1/2}$

D_1 — integral constant, $\sin(i_{00})\, (1 - j_{00}^2)^{1/2}$

D_2 — integral constant, $[k_{00} - d\,(1 - e_{00}^2)\, \sin\hat{n}_{00}]\, \sin(i_{00})$

D_3 — integral constant, $[(1 - e_{00}^2)^{1/2} + d\, k_{00} \sin\hat{m}_{00}] \cos(i_{00}) + d\, j_{00} \cos\hat{n}_{00}$

$\underline{D}^j$ — ($j = 0,1,\ldots,4$) auxiliary vector, Equations (3.26)

E — constant, $D_3/[(1 + d^2)\, (1 - D_1^2)]^{1/2}$

$\underline{F} = (F_x, F_y, F_z)$ — solar radiation force (Equation 3.7) with components along local coordinate axes (Equations 3.8)

$\tilde{\underline{F}}(\underline{a},\nu)$	vector function, $\tilde{\underline{f}}$ if ν outside and $\underline{0}$ if ν inside I_s
$F_1(e,\chi)$, $F_2(e,\chi)$	auxiliary functions, Equations (4.3)
$G(\bar{\nu})$	auxiliary function of $\bar{\nu}$, Equation (3.21)
H, H_ℓ	Hamiltonian, Equation (6.4) and (6.19), respectively
$H(e,\chi)$	auxiliary function, Equation (4.8)
I_s	shadow interval, $(\eta+\pi-\beta_1, \eta+\pi+\beta_2)$
I_{nk}	auxiliary integral, Appendix I
I_{on}	interval where force is switched on
I_{off}	interval where force is switched off
K, K_k	component of $\underline{K}$ along orbit-normal and $K(\nu_k)$, respectively
$\underline{K} = (M, L, K)$	unit vector along Z-axis with components along local coordinate axes
$K_1(\bar{\nu})$, $K_2(\bar{\nu})$	auxiliary functions, Equations (3.15)
K_{10}	constant, $\cos^2(i_{00}/2)\cos(\hat{\eta}_{00}+\psi_{00}) + \sin^2(i_{00}/2)\cos(\hat{\eta}_{00}-\psi_{00})$
K_{20}	constant, $\cos^2(i_{00}/2)\sin(\hat{\eta}_{00}+\psi_{00}) - \sin^2(i_{00}/2)\sin(\hat{\eta}_{00}-\psi_{00})$
L	component of $\underline{K}$ along local horizontal
M, M_k	component of $\underline{K}$ along local vertical and $M(\nu_k)$, respectively
P, Q	auxiliary functions, Equations (6.10)
P_ℓ, Q_ℓ	auxiliary functions, Equations (6.22)
R	component of $\underline{R}$ along local vertical
$\underline{R} = (R, S, T)$	functions of rotation angles α and β, and material properties, Equation (5.4), with components along local reference frame
R_e	nondimensional earth's equatorial radius (6378 km), 0.151
S	component of $\underline{R}$ along local horizontal
S_c	solar constant, 1.35 kW/m^2
S'	solar radiation pressure, S_c/(velocity of light), 4.51×10^{-6} N/m^2

T	component of $\underline{R}$ along orbit-normal
T_f, T_b	temperature of front , and back side of surface element
U, U_k	dot-products $(\underline{u}^n \cdot \underline{u}^s)$ and $(\underline{u}_k^n \cdot \underline{u}^s)$, respectively
U_0	constant, $\sin\beta \sin(i_{00}) \sin\hat{n}_{00}$
U_1	constant, $\cos\beta\ [K_{10} \cos\alpha + K_{20} \sin\alpha]$
U_2	constant, $\cos\beta\ [K_{20} \cos\alpha - K_{10} \sin\alpha]$
$\underline{W}$	rotation vector, $\underline{w}^r + \dot{\underline{\nu}}$
X, Y, Z	inertial reference axes, Figures 3-1, 5-1a
$\hat{\alpha}$	modified control angle, $\alpha + \nu$
$\underline{\alpha} = (\alpha, \beta, \gamma)$	Eulerian control angles defining orientation of surface element with respect to orbital plane, Figures 3-2, 5-1b
$\underline{\alpha}^*(\nu)$	optimal control vector
$\underline{\alpha}_0(\nu)$	starting value for control vector
α_1	angle between switching locations, ν_3, ν_4 and sun-earth line
α_k, β_k	Eulerian control angles for surface component A_k
α_p	phase angle in periodic long-term variations of orbital elements, $\arctan\{bx_{00}/[cy_{00} - 3a_{00}^2(1 - e_{00}^2)^{1/2}/2]\}$
α_s	spiral angle, $\arctan(c_s)$
β_1, β_2	shadow angles, Figure 2-1
δ	slow angular rate of motion of the sun with respect to earth, 1/365.2422
δ_1, δ_2	auxiliary angles, Equations (3.27)
δ_3, δ_4	auxiliary angles, Equations (4.6)
$\delta\underline{a}$, $\delta\underline{\alpha}$	variations in $\underline{a}$ and $\underline{\alpha}$, respectively
ε	ratio of solar radiation and gravity forces for geocentric orbits, $2\ S'(A/m)\ a_r^2/\mu = 4.0 \times 10^{-5}\ (A/m)$

ε_s	ratio of solar radiation and gravity forces for heliocentric orbits, $2S'\ (A/m)\ a_e^2/\mu_s = 1.52 \times 10^{-3}\ (A/m)$
η	solar aspect angle measured from inertial X axis
$\hat{\eta}$	modified solar aspect angle measured from line of nodes, $\eta-\Omega$
θ	true anomaly, measured from the instantaneous perigee axis, $\phi - \omega = \nu - \tilde{\omega}$
κ	material parameter, $(e_f T_f^4 - e_b T_b^4)/(e_f T_f^4 + e_b T_b^4)$
λ	constant characterizing the initial conditions, $c(1 - e^2)^{1/2} + 3\, y_{00}\, a_{00}^2/2$
$\underline{\lambda}(\nu)$	vector of adjoint variables
μ	earth's gravitational parameter, $3.986 \times 10^{14}\ m^3/s^2$
μ_s	sun's gravitational parameter, $1.326 \times 10^{20}\ m^3/s^2$
ν	quasi-angle in osculating plane, $\dot{\nu} = \dot{\phi} + \dot{\Omega}\cos(i)$, $\nu(0) = 0$, employed as independent variable
$\bar{\nu}$	slow independent variable, $\varepsilon\nu$
$\tilde{\nu}$	slow independent variable, $\delta\nu$
ν_1, ν_2	points of entry into and exit out of shadow cylinder
ν_f	length of interval before rectification
ν_j	$(j = 1,2,\ldots,6)$ switching points, Figure 4-1
ν_k	$(k = 0,1,2,\ldots)$ abbreviation for $\nu_k = k\pi/(1 + B^2)^{1/2}$
ν_{on}, ν_{off}	on- and off-switching points, respectively
ξ_0, η_0, ζ_0	reference axes, fixed to osculating plane in heliocentric orbits, ξ_0 along the local vertical, η_0 along the local horizontal and ζ_0 along the orbit-normal, Figure 5-1a
ξ_1, η_1, ζ_1	intermediate frame of reference after rotation of solar sail by α, Figure 5-1b
ξ, η, ζ	reference frame fixed to solar sail after rotations by α and β, Figure 5-1b

ρ	material parameter characterizing specular reflectivity of surface component, $\rho_1\rho_2$
ρ_1	portion of incident photons which are reflected
ρ_2	portion of reflected photons which are reflected specularly
ρ_b, ρ_f	specular reflectivity for back and front side of surface element, respectively
ρ_e	ratio R_e/ℓ
ρ_k	specular reflectivity for surface component A_k
σ	material parameter for homogeneous flat plate, $\sigma_1 + \sigma_2 + \rho$, or homogeneous sphere, $(1 - \tau)/2 + 2\sigma_2/3$
σ_1, σ_2	material parameters, $\sigma_1 = (1 - \rho - \tau)/2$ and $\sigma_2 = [\rho_1(1 - \rho_2) + \kappa(1 - \rho_1 - \tau)]/3$
σ_{1k}, σ_{2k}	σ_1 and σ_2 for surface component A_k
τ	material parameter denoting transmissivity of surface element
ϕ	argument of latitude, i.e. position angle of satellite as measured from the line of nodes, $\theta + \omega$, (for ecliptic orbits: $\phi = \nu$), Figure 3-1
χ	angle between projection of sun-earth line and perigee axis (for ecliptic orbits: $\chi = \eta - \omega$), Figure 4-1
ψ	angle characterizing shift of orbital plane, $\nu - \phi$
ω	argument of the perigee with respect to the line of nodes
$\tilde{\omega}$	position of the perigee measured in osculating plane from axis $\nu = 0$ (for ecliptic orbits: $\tilde{\omega} = \omega$), $\omega + \psi$
$\tilde{\omega}_p$	modified position of the perigee, $\arctan [q_{00}/(p_{00} + \varepsilon_s R)]$
$\Delta\underline{a}$	first-order changes in orbital elements after one revolution, $\varepsilon\underline{a}_1(2\pi)$
$\underline{\Lambda}$	vector of influence functions, Equation (4.17)
Φ, Ψ	auxiliary variables, $p \cos\nu + q \sin\nu$ and $p \sin\nu - q \cos\nu$, respectively

Φ_0 , Ψ_0	auxiliary variables, $p_{00} \cos\nu + q_{00} \sin\nu$ and $p_{00} \sin\nu - q_{00} \cos\nu$, respectively
Ω	longitude of ascending node, measured from the autumnal equinox, Figure 3-1

Single subscripts refer to the order of the perturbation terms; 00 indicates initial conditions; dots and primes refer to differentiation with respect to time and ν, respectively. The norm $||\underline{\alpha}(\nu)||$ stands for the integral over $(0,2\pi)$ of the dot-product of $\underline{\alpha}(\nu)$ with itself. It should be mentioned that the branches of the inverse trigonometric functions (e.g. arctan) are not explicitly specified but are readily determined by the initial conditions involved and by continuity.

1. INTRODUCTION

1.1 Preliminary Remarks

Since 1965, when the first Intelsat spacecraft, appropriately named 'Early Bird', provided 240 transatlantic telephone circuits, on-board power requirements for communications satellites have been growing steadily. This in turn has led to the use of larger solar panels, the most widely used source of the photovoltaic power. For example, the experimental Canada/U.S.A. Communications Technology Satellite (CTS), launched on January 17, 1976, is provided with two solar panels 7.32 m × 1.14 m each, generating up to 1.3 kW. The trend suggests future communication systems using more sophisticated satellites with increased capabilities and accommodating a larger number of smaller receiving ground terminals.

It is likely that in the near future, motive power for interplanetary explorations and geocentric transfer missions will be provided by the Solar Electric Propulsion Stage (SEP or SEPS). The electrical power needed for its ion engines is, typically, of the order of 25 kW and, in the present state of the art, will be generated by two, 120 square meter, arrays of solar cells.

Advances in space science and technology are overtaking our wildest imagination. Launching of the space shuttle is about to open up avenues for assembling and servicing of space vehicles in orbit. It is likely to bring into the realm of reality by the turn of the century the concept of Solar Satellite Power Stations (SSPS) equipped with lightweight arrays of solar cells, a few kilometers in area, generating around 5 GW and relaying

this energy by means of microwave transmission to receiving stations on earth.

A promising possibility for large-scale exploration of the planetary system is provided by the concept of solar sailing where the spaceship is propelled by solar radiation forces arising from the impingement of photons upon large sails made of aluminized Mylar or Kapton. A technology assessment of a solar sail mission to Halley's comet in the beginning of the next decade is undertaken by NASA's Jet Propulsion Laboratory. It appears feasible to transfer a scientific package of approximately 850 kg into a trajectory for a rendezvous with the comet using an 850 m × 850 m aluminum-coated 0.1 mil Mylar sail. Figure 1-1 shows the concept of a solar sail.

A characteristic common to all these space programs is the presence of large, lightweight appendages exposed to the solar radiation. Due to the high area/mass ratios involved, substantial perturbative accelerations of the spacecraft may be produced by the solar radiation forces. In fact, this is precisely the intention in the case of a spacecraft equipped with a solar sail. In other situations however, these perturbations may become detrimental to the spacecraft's performance, e.g., a communications satellite may drift away from its preferred location. In any case, a detailed knowledge of the nature of the long-term orbital effects of solar radiation forces would facilitate the process of eliminating undesired influences in certain applications and of enhancing desired capabilities in other situations. With this as a background, the thesis aims at providing better understanding of the long-term orbital implications of the solar radiation forces as well as at assessing the feasibility of utilizing them for effecting prescribed orbital changes.

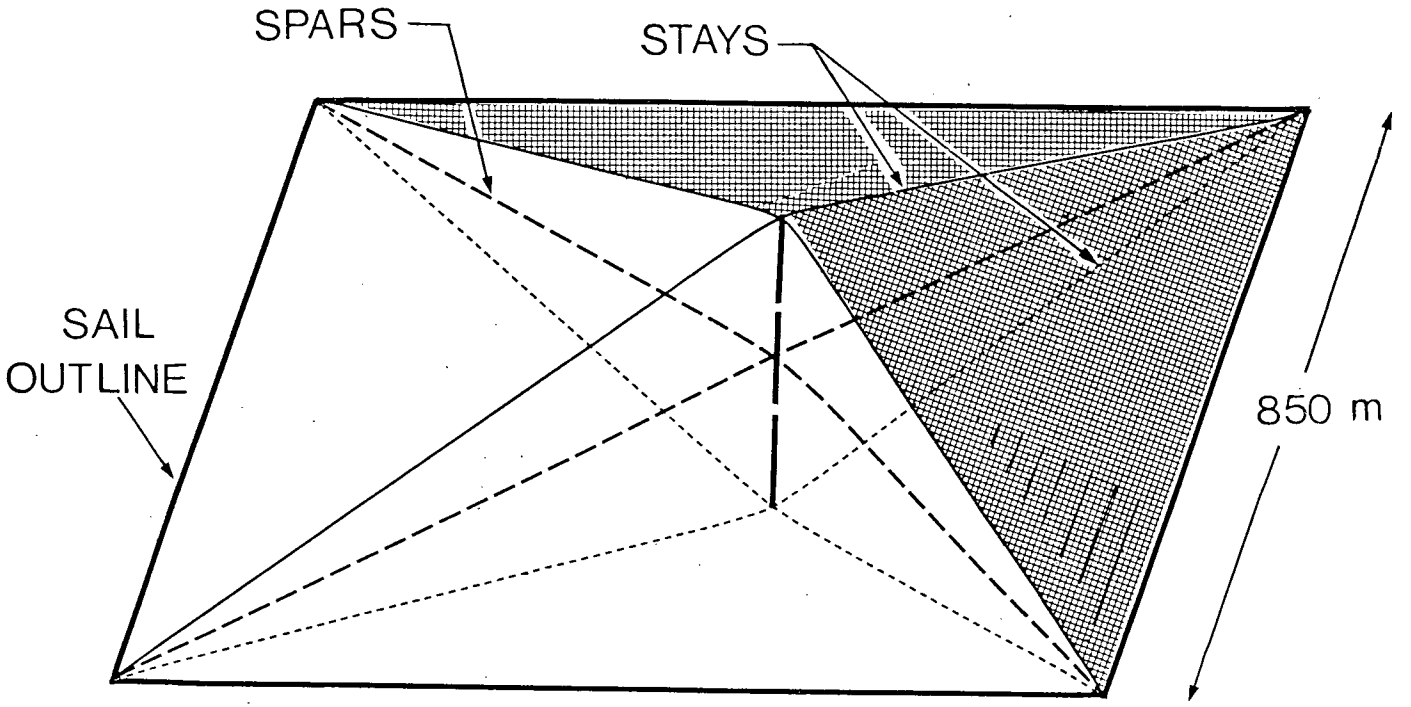

Figure 1-1 A schematic diagram showing the concept of solar sail

1.2 Review of the Literature

1.2.1 Solar radiation induced orbital perturbations

The fact that light carries momentum and exerts pressure when it is incident upon a surface, was known long before the advent of the space age and is inherent in Einstein's famous $E = mc^2$ law. Nevertheless, the first exhibition of solar radiation effects upon an earth's satellite (the Vanguard I, launched on March 17, 1958) caught the observers by surprise: only the classical perturbations due to the higher harmonics of the earth's potential field and luni-solar gravitational influences were taken into consideration. Subsequently, Musen et al.[1] included the solar radiation effect in an attempt to account for the observed discrepancy (of amplitude 2 km and period of 850 days) in its perigee height and found it to be fully responsible. The first theoretical analysis of the effect (Musen[2]), deriving the equations governing the evolution of the orbital elements by means of the vectorial method, appeared soon after. A few of the basic features of the solar radiation pressure effects were discovered, e.g., a significant perturbation in the perigee height and only small short-term periodic variations in the semi-major axis. Furthermore, he established that for certain combinations of altitude and inclination, the solar radiation force interacts with the perturbations due to the earth's oblateness: the most interesting of these so-called 'resonance' cases is the one where the perigee closely follows the motion of the sun producing a long-period, large amplitude variation in the perigee height which could seriously affect the lifetime of the satellite. A study by Parkinson et al.[3] with reference to the lifetime of the Beacon satellite further emphasizes this point.

It was the passive communications balloon-satellite Echo I, launched on August 12, 1960, which provided a dramatic indication as to the possible severity of solar radiation induced orbital change: in about five months the perigee altitude decreased from more than 1500 km to 930 km and subsequently increased again to almost its original value. The property which made Echo I extremely sensitive to solar radiation effects was its high area/mass ratio: the satellite consisted of an aluminum-coated half-mil thick mylar sphere, 30 meter in diameter, weighing some 70 kg. Many papers are devoted to the perturbations of the Echo I [4-8]; the latter two of these provide comprehensive analyses of its orbital behavior. A very readable account on sunlight pressure induced perturbations is given by Shapiro et al.[9], who describe the effect upon orbiting dipoles in the West Ford experiment. Allan[10] extended Musen's results by including the effect of the shadow in the pertubation equations and provided some numerical results. By integration of the classical Lagrange's perturbation equations in terms of the eccentric anomaly, Kozai[11] was probably the first one to establish general analytical results, valid for a short duration. Bryant[12] has indicated how the method of averaging may be employed in deriving the equations underlying the long-term orbital perturbations, but does not provide any results. A very comprehensive account on the effect of solar radiation, including the shadow effect, on the orbital period is given by Wyatt[13], who derives short-term analytical results for several special cases. An admirable attempt to obtain first-order analytical results for the combined effects of solar radiation and the earth's second zonal harmonic was undertaken by Koskela[14], but the validity of the application of the approach beyond the first few revolutions must be questioned. Under certain simplifying

assumptions, Cook et al.[15] have derived an elegant approximate solution to this problem for near-circular, non-resonant orbits in the context of the West Ford experiment. An interesting, subsequent paper by Cook[16] finds a good agreement between this solution and the observed motion of the Echo I and Explorer 9 satellites.

After these pioneering contributions, the attention was directed either to refinements in the basic understanding of solar radiation effects or to applications where the force can be employed in bringing about desired changes. The primary emphasis was focused on the effects of reflected radiation from the earth, e.g. the excellent work of Wyatt[17], which was later extended by Baker[18]. Under no circumstances, however, can this influence rival the dominance of direct solar radiation effects. A very extensive summary of all aspects of solar radiation effects as well as the more traditional sources of orbital perturbations is given by Shapiro[19]. Especially of interest is his exposition on stable near-earth orbits, having the characteristic of constant eccentricity under the combined influences of solar radiation and the second harmonic of the earth's potential field. Another enlightening review of the main solar radiation features, stemming from the Russian literature, is by Polyachova[20]: although the titles of a few figures are interchanged, this paper provides the most detailed information on resonance conditions. Using a formulation in terms of the Hamiltonian expressed in Delaunay variables, Brouwer[21] investigated resonance in the case of polar orbits and finds general agreement with numerical results. Later, Hori[22] extended the analysis to general orbits. It can be concluded that resonance does not occur for orbits with a semi-major axis exceeding three times the earth's radius, except when the

eccentricity is very large. A numerical study of the solar radiation pressure effects on satellites with several different configurations is presented by Lubowe[23]. Levin[24] provides a fresh insight into the nature of the solar radiation effects by analysing the behavior of the radial distance for initially circular orbits. Zee[25,26] has presented an approximate analytical study of the combined influences of gravitational and solar radiation forces for near-circular equatorial orbits. On the other hand, Lidov[27] employs double averaging, both in the motion of the satellite and that of the sun to obtain approximate results valid for extremely long duration. The results obtained by Isayev et al.[28,29] are valid for a short interval only since the position of the sun is kept constant with respect to the earth providing a uniform force field. A high-precision short and long-term numerical integration scheme based on Kozai's equations[11] including the shadow effect was recently presented by Aksnes[30]. Sehnal[31,32] has summarized various aspects of solar radiation influences. A satellite whose orbital behavior attracted almost as much attention as Echo I is Pageos, launched in 1966. Pageos consists of a balloon quite similar in size, structure and mass to Echo I, but its shape approximates a prolate spheroid. Many studies are devoted to explaining the anomalies in its orbital behavior: Sehnal[33], Prior[34], Fea[35], and Gambis[36] analyse the influence of earth-reflected radiation upon this spacecraft. At present, its orbital anomalies are believed to be caused by a unique interplay of attitude and orbital perturbations[37,38]: the orientation of the satellite's spin-axis as well as its spin-rate are changing continually due to solar radiation torques thereby producing a time-dependent orbital perturbation force.

It should be emphasized that almost all studies employ a simplified solar radiation force model taking a constant-magnitude force along the direction of radiation. A more realistic formulation was provided by Georgevic[39] who includes the effects of diffuse reflection and re-emission of absorbed energy. This model proved capable of predicting the actual magnitude of the solar radiation force upon the Mariner 9 Mars orbiter within 0.1 %.

A number of papers are devoted specifically to the effects of the earth's shadow. Escobal[40] presents a detailed analysis of the points of entry and exit of the shadow region. The fraction of the orbit spent in darkness, expressed in true anomaly, is determined by Karymov[41], and by Zhurin[42] in terms of time. An interesting approach for incorporating the shadow effect in the analytical treatment of solar radiation perturbations is proposed by Ferraz-Mello[43], who multiplies the perturbation potential by a shadow function, being unity outside and zero inside the shadow interval. After development of this function in terms of Fourier series, a first-order solution in the form of infinite trigonometric series in the mean anomaly is obtained for the Delaunay variables. Since the computation of the coefficients is extremely laborious, the practicability of the approach must be considered limited. Other shortcomings are pointed out by the author himself in a subsequent paper[44] undertaking a new attack using Von Zeipel's method and a Hamiltonian in extended Delaunay variables. The main outcome of the analysis is the absence of secular perturbations in semi-major axis, eccentricity and inclination. Vilhena de Moraes[45] has found a close correspondence between the outcome of Ferraz-Mello's model applied to the Vanguard II satellite and results by Kozai. Short-term

semi-analytical results were obtained by Lála et al.[46-48], developing their own shadow function but keeping the sun in a fixed position. Meeus[49] studied the observed orbital behavior of a few satellites and found that, in general, the effect of the shadow makes the semi-major axis increase (decrease) when the eccentricity is diminishing (growing).

1.2.2 Orbital control using solar radiation forces

Whereas all of the previous references deal with natural perturbations in the sense that the librational motion of the satellite body is not deliberately manipulated, the following category of papers studies the effects of controlled changes in the orientation of the reflecting surface and thus the resulting solar radiation force. The feasibility of utilizing solar radiation forces for controlled orbital change was assessed quite early in the space age. In 1958, Garwin[50] envisioned an exploration of the solar system by means of large solar sails made of aluminized Mylar. Considering heliocentric solar sail trajectories Tsu[51] derived an approximate solution in the form of a planar logarithmic spiral neglecting the small radial velocity component. London[52] remedied this shortcoming and determined, graphically, the best sail setting and corresponding spiral angle for minimum-time transfer. The spiral solution, naturally, allows only specific initial conditions. Pozzi et al.[53] suggested an iteration scheme to accomodate more general initial conditions. A fairly complete survey of solar sail trajectories and possible missions is given by Kiefer[54]. Modi et al.[55] proposed and on-off strategy with the sail normal to or aligned with the radiation leading to a significant elongation of the orbit as the perigee moves towards and the apogee drifts away from the sun.

Other studies foresaw opportunities for using solar sails in geocentric orbits. Sands[56] proposed to rotate the sail about an axis perpendicular to the orbital plane at half the rate of the satellite's motion around the earth. This strategy enables the satellite to reach an escape trajectory eventually. For an orbit in a plane normal to the ecliptic Fimple[57] determined the control strategy which maximizes the component of the solar radiation force along the instantaneous velocity, thereby continuously increasing the total energy and semi-major axis. Cohen et al.[58] achieved substantial changes in the orbital elements of an orbit in the ecliptic plane by means of an on-off switching strategy: during the on-phase, when the satellite moves away from the sun, the plate is aligned with the radius vector and kept normal to the orbital plane, while during the off-phase the plate is along the radiation. The effects upon a large earth-orbiting mirror in the ecliptic plane reflecting sunlight to the earth were determined by Bosch[59] under certain simplifying assumptions. Ahmad et al.[60] considered this problem as well as that of a perfect absorber facing the sun in a more realistic equatorial orbit and obtained the orbital perturbations using a numerical technique. Furthermore, the forces and torques required to maintain the desired orientations were calculated. Shrivastava et al.[61] determined the panel orientation for obtaining maximum changes in various orbital elements. The feasibility of east-west station-keeping of communications satellites by means of controlled solar radiation forces was demonstrated by Shrivastava et al.[62] and further substantiated by Modi et al.[63].

A different concept for utilizing solar radiation forces in orbital control is presented by Buckingham[64], who studied a balloon with different reflective and absorptive characteristics on either side permitting control

of the force through rotation of the body. The same concept applied to plates is investigated by Black[65].

1.2.3 Small-thrust trajectories

The problem of controlled orbital change by means of solar radiation forces may be studied within the general framework of small-thrust trajectories which normally consider perturbing forces due to micro-thruster units. Although obvious differences exist in the nature of these two sources of orbital change (because of the constraints imposed by the instantaneous position of the sun and thus the direction of the force), a knowledge of the methods and results of the more classical field of small-thrust trajectories would certainly be valuable. The smallness of the thrust is capitalized upon by modelling the problems in terms of perturbation theory using expansions in terms of the ratio of thrust/gravity forces. The problem of either tangential or radial constant small thrust for circular orbits was studied first[66-68]. A comprehensive analysis including intermittent thrust by means of the Krylov-Bogoliubov method has been presented by Lass et al.[69], providing the following results: a constant radial force causes the axis of the orbit to precess, while a tangential thrust changes an initially circular orbit into a spiral. Rider[70] proposed a control strategy for changing the inclination and longitude of nodes of an orbit while Lass et al.[71] study the effects of a thrust normal to the orbital plane. Zee[72,73] refined the analysis for a small tangential thrust and discovered small oscillations in the spiral trajectory. The Russian literature, naturally, abounds with studies related to small-thrust problems as a consequence of the epoch-making work of Krylov, Bogoliubov and Mitropolskii[74] in the field of nonlinear oscil-

lations. Laricheva et al.[75,76] illustrated some of the pitfalls of the method of averaging by a few illustrative examples: for orbits with initial eccentricity smaller or of the same order as the small perturbation parameter, indiscriminate application of averaging may lead to qualitatively incorrect results. Taking a constant tangential acceleration, Okhotsimskii[77] analysed the resulting motion in detail using asymptotic representations near $e = 0$ and $e = 1$, while Cohen[78] has presented an approximate solution accounting for the variation of the mass of the satellite due to the burning of fuel.

The more general problem of a constant small thrust under an arbitrary but fixed angle to the local vertical gained the attention of the investigators next. Johnson et al.[79] derived a solution valid for short duration only. Introducing an independent slow variable in the radial distance and separating the oscillatory and non-oscillatory terms in an ad-hoc manner, Ting et al.[80] offered a prelude to the application of the two-variable expansion procedure to this problem. A later paper by Brofman[81] also treats the case of tangential thrust with variable mass and orbital decay due to drag in a similar manner. Nayfeh[82] found essentially the same results using his more systematic derivative-expansion method. While all these studies consider an initially circular orbit, the problem in its most general form, including a starting orbit of an arbitrary eccentricity, was solved by Shi et al.[83] using the two-variable expansion method. Due to the fact that the ratio of thrust/gravity does not remain small for ascending trajectories, their results do not predict the radial distance correctly near escape. This deficiency is redressed by the same authors[84] through a careful analysis of the rate of change of radial distance in three different regions :

gravity dominant, gravity and thrust of the same order, and thrust dominant. Incorporating the change in the mass of the satellite, Moss[85] studied circumferential thrust by the same (two-variable expansion) method. Flandro[86] obtained approximate long-term solutions for the orbital elements under a low thrust normal to the orbital plane.

For an illustrative description of the two-variable expansion method one is referred to the original presentation by Cole and Kevorkian[87] and the more comprehensive treatment by Kevorkian[88]. Morrison[89] points out the consistency between the results obtained by this method and those derived by the modified method of averaging. A more fundamental treatment of these methods can be found in Perko[90] and Klimas[91]. Kevorkian[92] established the equivalence of the Von Zeipel and the two-variable expansion methods up to first-order in the small parameter. Nayfeh[93] has described the various perturbation methods and their relative advantages in detail.

1.2.4 Optimal trajectories

Finally, a few papers using optimal control theory in determining the best steering and/or thrust program to accomplish a given objective in a prescribed manner should be mentioned. The field of optimal control theory, fostered by the calculus of variations, has become a full-grown science in itself. A theoretical foundation is given by Lee et al.[94] and a practical summary is provided by Bryson et al.[95]. The application of optimal control theory in rocket and satellite trajectories is manifested in numerous papers. A problem which has attracted continuous attention over the last two decades concerns the optimal transfer, i.e. determination of the thrust direction for reaching a prescribed final orbit from a given initial orbit with

minimum fuel consumption. Early contributions dealing with various aspects of this problem are by Lawden[96,97], Faulders[98,99], Melbourne[100,101] and Hinz[102]. Of particular interest is the conclusion by Lawden that the optimal thrust orientation approximately bisects the tangential and circumferential directions. A comprehensive analytical solution for transfer between two close ellipses is presented by Edelbaum[103]. Breakwell et al.[104] studied the problem of reaching a specified energy level with minimum fuel expenditure. An higher-order analytical treatment of the linearized equations for near-circular transfer is presented by McIntyre et al.[105]. A review of the early papers on optimal trajectories is given by Bell[106]. In the Russian literature, the development of the maximum principle by Pontryagin and Boltyanskii[107] has stimulated many researchers in the space sciences. Of particular interest is the work by Lebedev and others[108-110], who consider the minimum-time transfer between coplanar circular orbits by means of a solar sail: a numerical iteration method is employed to solve a system of differential equations with partly initial, partly final boundary conditions. An interesting attempt to find an approximate solution to the problem of transfer between two coplanar orbits in minimum time using the method of averaging is presented by Avramchuk et al.[111]; unfortunately, only the adjoint equations are amenable to closed-form solutions. The book by Grodzovskii et al.[112] provides a somewhat outdated, but exhaustive treatment on various aspects of small-thrust and optimal trajectories. More recently, Brusch[113] has presented a comprehensive treatment of the minimum-fuel transfer from an initial circular to a prescribed coplanar, elliptic orbit. An analytical solution to the optimal (in the sense of least fuel) escape from a circular orbit in terms of a straightforward perturbation solution was

given by Anthony et al.[114]. An essentially similar problem is treated more accurately by Jacobson et al.[115] by means of the two-variable expansion procedure. They discovered small (order ε = thrust/gravity) oscillatory terms in the near-tangential optimal control strategy. These results were substantiated by Reidelhuber et al.[116] using a different formulation. An exhaustive review (up to 1965) of papers using optimal control theory with emphasis on flight mechanics is given by Paiewonsky[117].

Unfortunately, analytical (approximate) solutions to optimal control problems may be derived in very limited situations only. Therefore, many numerical methods have been developed, specifically for this purpose. A very attractive procedure is the steepest-ascent (or gradient) method involving a generalization of a problem in the ordinary calculus, viz. the maximization of a function subject to constraints. An heuristic description of the method is given by Kelley[118], while a general treatment is presented by Bryson et al.[119] and Campbell et al.[120].

1.3 Scope and Objective of the Study

The literature survey indicates that many aspects of solar radiation induced orbital perturbations have been investigated. Resonance conditions leading to large amplitude variations of the orbital elements are well established[2,20,22]. Short-term valid analytical results are available[11,13,14] and approximate representations for the long-term behavior are explored for certain special cases: near-circular[15,24,26,43] or low-inclination orbits[27]. The available solutions are based upon a model where the force is taken along the radiation, which is justified only when the satellite can be modelled as a sphere with homogeneous surface characteristics or as a plate

kept normal to the radiation.

In the present investigation an attempt is made to obtain long-term valid analytical solutions for the orbital elements with no restrictions imposed on the initial orbit and the apparent motion of the sun accounted for. Because of the successful application of the two-variable expansion procedure in small-thrust trajectories[83], it is felt that an approach along these lines should deserve attention in the present situation. In addition to providing valuable information as to the long-term evolution of orbits in general, a comprehensive understanding of the qualitative aspects of solar radiation effects would be a valuable guide in exploring control strategies for desired orbital changes. Furthermore, the analysis is based upon a realistic force model allowing for diffuse and/or specular reflection as well as for re-emission of absorbed radiation. In some cases, the investigation is extended to include arbitrarily shaped satellite structures modelled by a number of flat surface elements of homogeneous material characteristics. Other applications such as space platforms modelled as a flat plate in an arbitrary fixed orientation with respect to the earth as well as those kept fixed to inertial space are also studied.

It should be mentioned that the effects of other perturbation forces are ignored in the present investigation. For an equatorial geosynchronous orbit, the magnitude of the major perturbing forces as compared with the local gravity force are of the following order:

i) solar radiation force : $4\ (A/m)\ 10^{-5}$;

ii) out-of-plane oblateness force: 10^{-4} ;

iii) in-plane oblateness force : 4×10^{-5} ;

iv) lunar attraction force : 1.5×10^{-5} ;

v) solar attraction force : 7×10^{-6} ;

Hence, for satellites with a large A/m ratio (e.g., the SSPS and particularly the solar sail), radiation forces would be the predominant source of perturbations. However, for spacecrafts with a relatively small A/m ratio (e.g., communications satellites) the traditional perturbations, especially those due to the earth's oblateness, need to be incorporated. Except in the resonance cases, the wellknown secular effects caused by the classical perturbations could simply be added to the results obtained for the solar radiation induced orbital changes in the first-order approximation.

Another part of the thesis is concerned with the development of control strategies, involving the rotation of solar panels attached to the main body, thereby producing variations in both the magnitude and direction of the resulting solar radiation force. Considerable attention is given to on-off switching programs, where the plate is aligned with the radiation during the off-phase and normal to the radiation, generating the largest possible force, in the on-phase. The optimal locations for switching are determined for a few specific objectives such as maximum increase in total energy. While on-off switching may lead to substantial changes in the major axis, it is not necessarily the optimal strategy when time-varying orientations are also taken into consideration. Therefore, the determination of the optimal control strategy for maximization of the major axis after one revolution is undertaken and the effectiveness of this control program is compared with that of the switching strategies. This investigation is of relevance for raising a solar sail from a geocentric to a heliocentric or escape trajectory.

Subsequently, the orbital behavior of satellites in an heliocentric orbit is studied in detail. The resulting orbital behavior of a spacecraft in a fixed orientation to the local frame is explored in terms of exact so-

lutions (specific initial conditions) or approximate long-term valid representations (general case). The potential of out-of-plane spiral transfer trajectories is assessed. The results are mainly of interest for interplanetary solar sail missions. While some aspects of interplanetary transfer have been explored[108-110], no studies on optimal escape are reported. Therefore, time-varying optimal control strategies are investigated with the objective to maximize the increase in total energy and angular momentum per revolution. In addition, these results may be used for assessing the relative effectiveness of constant sail settings.

A schematic overview of the plan of study is presented in Figures 1-2 a and b.

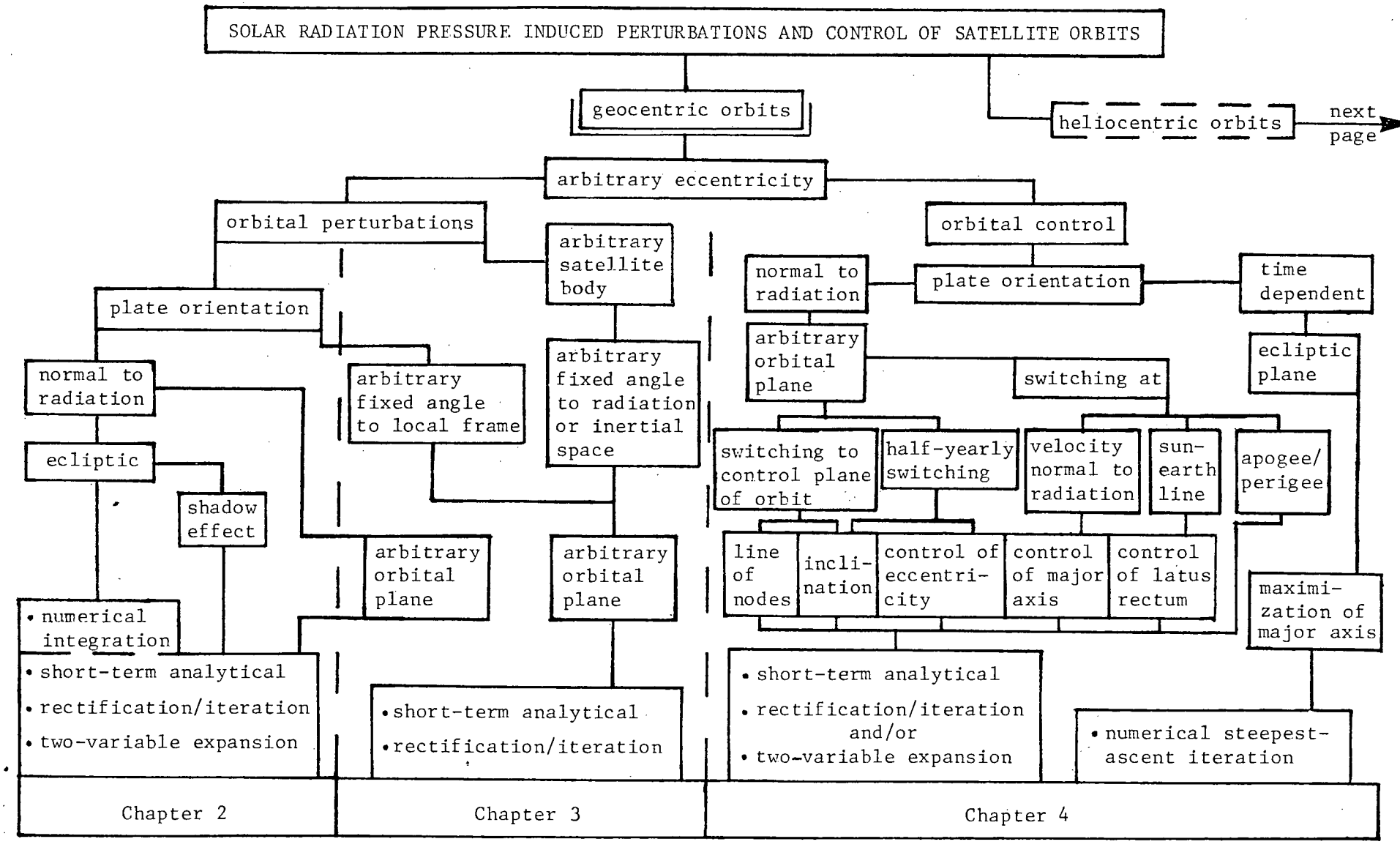

Figure 1-2 Schematic overview of the plan of study: (a) geocentric orbits

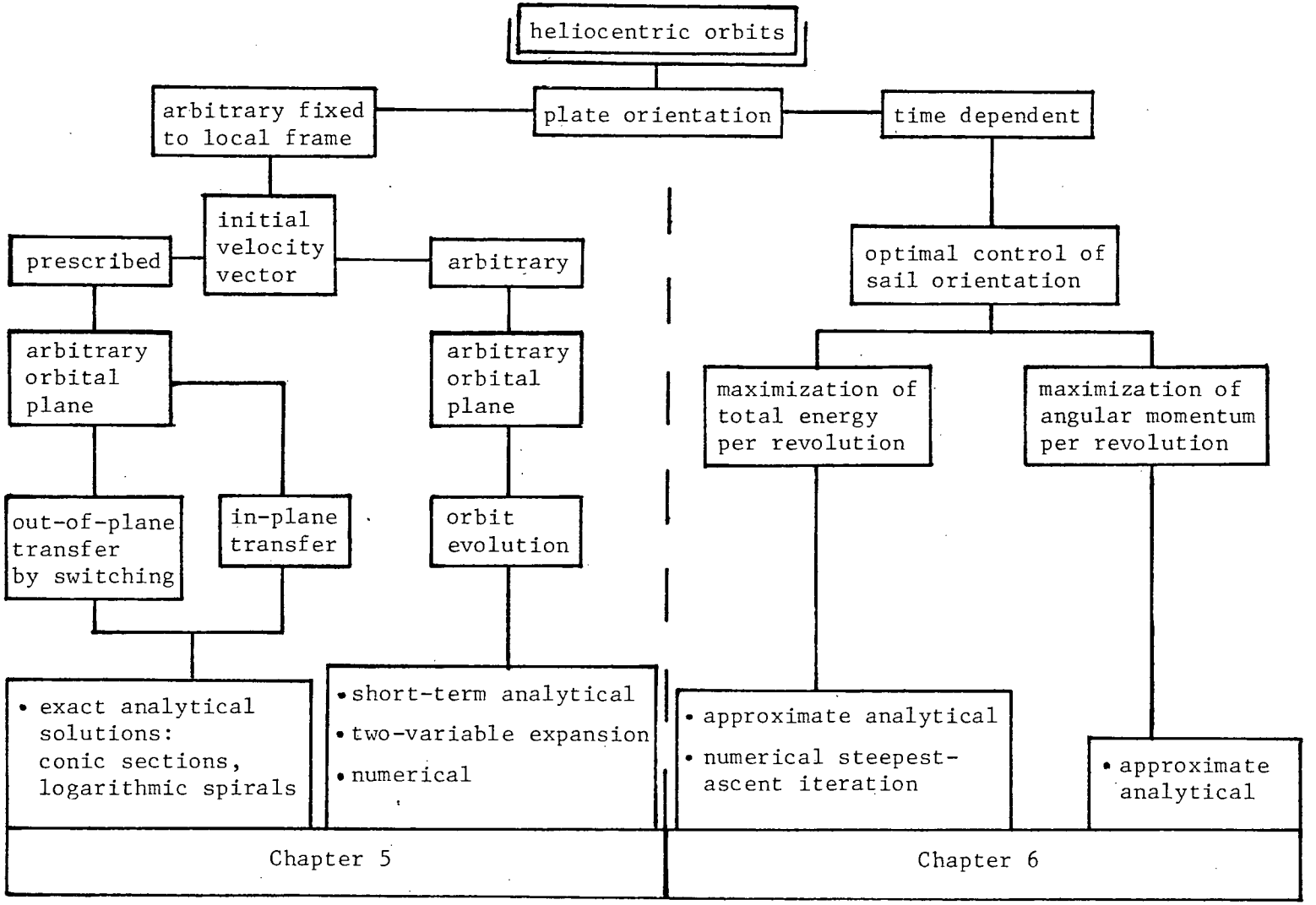

Figure 1-2 Schematic overview of the plan of study: (b) heliocentric orbits

2. SOLAR RADIATION EFFECTS UPON AN ORBIT IN THE ECLIPTIC PLANE

2.1 Preliminary Remarks

In this chapter, the perturbations of a satellite orbit in the ecliptic plane subjected to solar radiation forces are studied. Long-term valid approximate solutions for the orbital elements are derived, by means of the two-variable expansion procedure while accounting for the apparent motion of the sun around the earth. The results are compared with those obtained by repeated rectification of the short-term valid solutions obtained by a straightforward perturbation method and their relative accuracies assessed using a double precision numerical integration routine. In the analysis, the solar radiation force is taken along the direction of the sun-earth line which is considered to be coincident with the sun-satellite line, since for a geocentric orbit the relative distance of a satellite to the earth in comparison with that to the sun can be ignored.

Taking the resulting radiation force along the sun-earth line is justified in the case of a satellite with large solar panels kept normal to the incident radiation for maximum on-board power production, e.g., communications satellites or the proposed SEPS mentioned before. A spherical satellite with homogeneous surface characteristics would also experience a solar radiation force along the sun-earth line.

Two cases of practical importance are studied separately: first, the nondimensional solar radiation force parameter referred to as 'solar parameter' (ε) is taken to be of the same order of magnitude as the 'frequency parameter' (δ) designating relative motion of the sun in the ecliptic plane. This assumption is valid for satellites with a relatively large area/mass ratio, e.g., Echo I (A/m = 10 m^2/kg) or the proposed SSPS[121,122,123]. In the other case, the solar parameter ε is taken to be of the order δ^2 representing a class of satellites with relatively small solar radiation perturbations like the CTS[124].

By expressing the perturbation equations in terms of $p = e \cos \omega$ and $q = e \sin \omega$, the singularity in ω for $e = 0$ is avoided making the analysis uniformly valid for both circular and elliptical osculating orbits. A comprehensive picture of the long-term orbital perturbations is provided by polar plots (p, q-diagrams) for the eccentricity and argument of the perigee. The effect of the earth's shadow is investigated separately. Note that this influence is likely to be strongest for orbits in the ecliptic plane since the satellite is now eclipsed in every revolution. Both short and long-term analytical representations have been established.

The qualitative and quantitative understanding of long-term perturbations of orbits in the ecliptic plane may serve as a guide in predicting the behavior of near-ecliptic, including equatorial, orbits. Furthermore, the analysis yields considerable

insight into the nature and range of validity of the approximate methods, thus providing a basis for establishing a rational approach for the following chapters.

2.2 General Formulation of the Solar Radiation Force

A realistic model for the solar radiation force acting upon a satellite has been provided by Georgevic[39] in his detailed analysis of the radiation force upon the Mariner 9 spacecraft. In case of a satellite in a geocentric orbit up to the geosynchronous altitude, fluctuations in the local value of the solar constant are almost entirely due to the seasonal variations in the solar constant itself, caused by the eccentricity of the earth's orbit. These variations amount to about 3.4% from the mean value and are ignored. The solar radiation force upon an arbitrarily shaped satellite in a geocentric orbit can be represented in the following general form:

$$\underline{F} = 2S' \iint_A | \underline{u}^n \cdot \underline{u}^s | \left\{ \sigma_1 \underline{u}^s + [\sigma_2 + \rho(\underline{u}^n \cdot \underline{u}^s)] \, \underline{u}^n \right\} dA \quad , \qquad .....(2.1)$$

where $\underline{u}^n$ is the unit-normal to the surface element dA and A denotes the total effective surface area of the satellite illuminated by the sun. The absolute sign around $\underline{u}^n \cdot \underline{u}^s$ is necessary to ensure that the force has a non-negative component along the direction of the radiation, $\underline{u}^s$. The material parameters σ_1, σ_2 and ρ may vary over the surface area and are determined by the reflectivity and emissivity of the surface element dA :

$$\rho = \rho_1\rho_2 \; ; \quad \sigma_1 = (1 - \rho - \tau)/2 \; ; \quad \sigma_2 = [\rho_1(1 - \rho_2) + \kappa(1 - \rho_1 - \tau)]/3 \qquad \ldots\ldots (2.2)$$

where ρ_1 denotes the total fraction of the incident photons which are reflected, ρ_2 the portion of these photons which are reflected specularly, and τ the portion of photons transmitted through the surface. The constant κ depends upon the temperatures and emissivities of the front and back sides of the surface element:

$$\kappa = (e_f T_f^4 - e_b T_b^4) / (e_f T_f^4 + e_b T_b^4) \quad .$$

Variations in the material parameters with time due to deterioration of the surface or due to changes in temperature fall outside the scope of the present investigation.

The following table gives an idea of the values of the material constants for a few typical spacecraft components[39] including aluminum-coated mylar solar sails[125]:

Table 2.1 Material Parameters for a Few Typical Spacecraft Components

Components	ρ_1	ρ_2	τ	e_f	e_b	κ	ρ	σ_1	σ_2	σ
Solar panel	0.21	1.00	0	0.81	0.81	0	0.21	0.39	0	0.60
High-gain Antenna	0.30	0.67	0	0.84	0.06	0.87	0.20	0.40	0.23	0.83
Solar Sail	0.88	0.94	0	0.05	0.60	-0.85	0.83	0.09	-0.02	0.90

In most practical cases the total surface area can be divided into components representing different parts of the satellite, each with its own homogeneous material parameters, so that the integral of Equation (2.1) can be written as a summation over the various components. In many applications, most notably solar sail and SSPS, the magnitude of the force upon one component, namely the sail and solar panels, is so predominant over the sum of the forces upon all other components that, effectively, the satellite can be modelled as a plate with homogeneous material characteristics.

2.3 Plate Normal to Radiation

For satellites which can be effectively modelled as a homogeneous plate normal to the incident radiation, the solar radiation force of Equation (2.1) can be simplified as $\underline{F} = 2\sigma\, S'A\, \underline{u}^S$, since $\underline{u}^n$ and $\underline{u}^S$ coincide for that case. It is interesting that the force upon a spherical satellite with homogeneous surface characteristics, takes on the same form with σ equal to $(1 - \tau)/2 + 2[\rho_1(1 - \rho_2) + \kappa(1 - \rho_1 - \tau)]/9$ as obtained by integration over the spherical surface. In this case A represents the cross-sectional area of the sphere.

In an inertial reference frame fixed to the earth, the equations of motion in polar coordinates r and ν become:

$$\ddot{r} - r\dot{\nu}^2 = -\mu/r^2 - 2\sigma\, S'(A/m)\cos[\nu - \eta(\nu)] \;;$$

$$r\ddot{\nu} + 2\dot{r}\dot{\nu} = 2\sigma\, S'(A/m)\sin[\nu - \eta(\nu)] \;. \qquad \text{.....(2.3)}$$

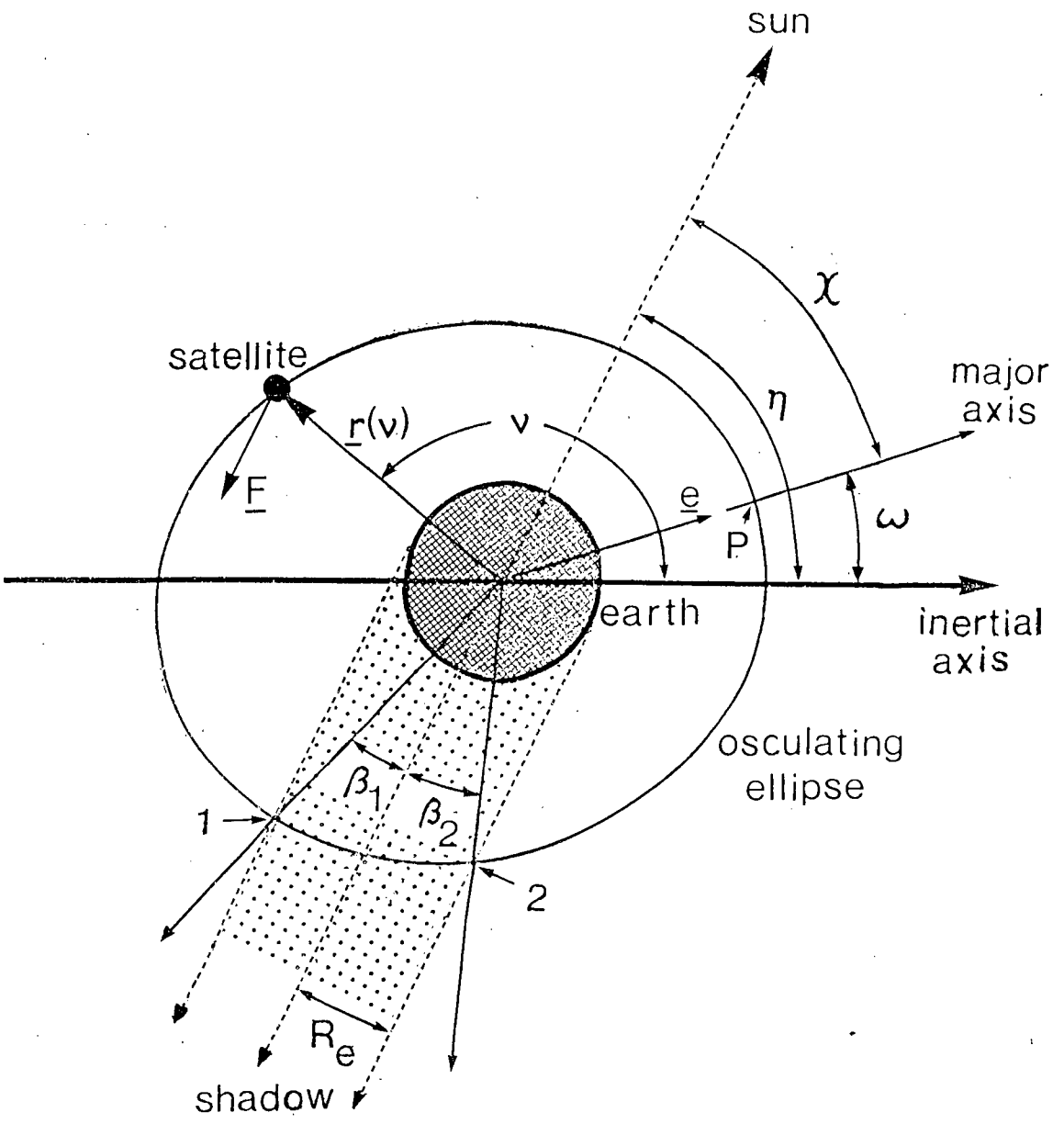

Figure 2-1 Geometry of sun, earth and satellite including shadow region

The solar aspect angle $\eta(\nu)$ denotes the sun's position, Figure 2-1. For the analysis to be valid over a long term, the relative motion of the sun needs to be taken into account: since the sun completes one revolution per year, i.e. $1/\delta = 365.2422$ days, it follows that

$$\eta(\nu) = \delta t(\nu)(\mu/a_r^3)^{1/2} + \eta_{00} \quad . \qquad .....(2.4)$$

It is convenient to nondimensionalize the equations by introducing the reference length and time units $a_r = 42{,}241$ km and $(a_r^3/\mu)^{1/2} = 1/(2\pi)$ day. Forces are nondimensionalized through $a_r^2/(\mu m)$ and become, mathematically, indistinguishable from accelerations. The form of Equations (2.3) is not convenient for finding analytical solutions, therefore, a transformation $u = 1/r$ as in the derivation of the classical Keplerian equations is performed, and the angle ν is taken as independent variable ($\dot{\nu} = h/r^2$) leading to the (nondimensional) equations:

$$u''(\nu) + u(\nu) = 1/\ell(\nu) + \varepsilon \left\{\cos[\nu - \eta(\nu)] - u'(\nu)\sin[\nu - \eta(\nu)]/ u^2(\nu) \right\} / \ell(\nu) \; ;$$

$$\ell'(\nu) = 2\varepsilon \sin[\nu - \eta(\nu)] / u^3(\nu) \; ;$$

$$t'(\nu) = 1/(u^2\ell^{1/2}) \; ; \quad \eta(\nu) = \delta t(\nu) + \eta_{00} \quad . \qquad .....(2.5)$$

The solar parameter ε is defined as

$$\varepsilon = 2S'(A/m)(a_r^2/\mu) = 4.0 \times 10^{-5} (A/m) \quad .$$

It should be noted that the parameter σ is taken equal to unity (i.e., $\rho = 1$, $\tau = 0$) in the present analysis. A different value of σ can readily be accommodated by modifying the parameter ε accordingly.

Since the solar parameter is very small, it may be justified to postulate solutions for the radial distance in the form of conic sections with slowly changing orbital elements, i.e. $u(\nu)$ is written in the form:

$$u(\nu) = [1 + p(\nu)\cos\nu + q(\nu)\sin\nu] / \ell(\nu) \quad , \qquad .....(2.6)$$

where p ($= e\cos\omega$), q ($= e\sin\omega$) and ℓ are slowly varying orbital elements. At any instant $\nu = \nu_1$, the 'ellipse' with elements $p_1 = p(\nu_1)$, q_1 and ℓ_1 is referred to as the osculating ellipse. This orbit may be interpreted as the elliptic trajectory that would be followed by the satellite if the perturbation force were to vanish at $\nu = \nu_1$ instantaneously. This can be seen by taking $\varepsilon = 0$ for $\nu \geq \nu_1$ in Equations (2.5). It can also be understood that both the radius and velocity vectors at any point in the actual (perturbed) trajectory are identical to those of the osculating ellipse corresponding to that point. This is referred to as the condition of osculation

and can be stated mathematically as $u'(\nu) = (-p \sin\nu + q \cos\nu)/\ell$. The second-order equation for $u(\nu)$ can now be replaced by an equivalent system of two first-order equations for $p(\nu)$ and $q(\nu)$. Thus, the complete system of equations to be studied becomes:

$$p'(\nu) = \varepsilon \ell^2 \left\{ -\sin\eta + (p + \cos\nu) \sin(\nu - \eta)/(1 + p\cos\nu + q\sin\nu) \right\} / (1 + p\cos\nu + q\sin\nu)^2 ;$$

$$q'(\nu) = \varepsilon \ell^2 \left\{ \cos\eta + (q + \sin\nu) \sin(\nu - \eta)/(1 + p\cos\nu + q\sin\nu) \right\} / (1 + p\cos\nu + q\sin\nu)^2 ;$$

$$\ell'(\nu) = 2\varepsilon \ell^3 \sin(\nu - \eta)/(1 + p\cos\nu + q\sin\nu)^3 ;$$

$$\eta'(\nu) = \delta \ell^{3/2} / (1 + p\cos\nu + q\sin\nu)^2 . \qquad .....(2.7)$$

It should be noted that the solar aspect angle $\eta(\nu)$ is treated here as a quasi-orbital element. The system of equations (2.7) will be written symbolically as $\underline{a}'(\nu) = \varepsilon \underline{f}(\underline{a},\nu)$ and arbitrary initial conditions $\underline{a}(0) = \underline{a}_{00}$, with the vector $\underline{a}$ containing the pertinent orbital elements. Note that $\underline{f}$ is periodic in the variable ν.

2.3.1 Short-term valid approximations

A short-term valid approximation for the orbital elements can readily be obtained by means of an expansion of the elements in

terms of a simple perturbation series. In case ε is of the same order of magnitude as δ, the expansion may be taken in the form

$$\underline{a}(\nu) = \sum_{j=0}^{N-1} \varepsilon^j \, \underline{a}_j(\nu) + O(\varepsilon^N) \quad . \qquad \ldots\ldots(2.8)$$

On substitution of this series into Equations (2.7), it follows that $\underline{a}_0(\nu) = \underline{a}_{00}$ and integration of the first-order equations leads to

$$\underline{a}_1(\nu) = \int_0^{\nu} \underline{f}\,[\underline{a}_{00}, \tau]\, d\tau \quad ,$$

or explicitly:

$$p_1(\nu) = \ell_{00}^2 \Big\{ \cos \eta_{00} \,[p_{00} B_{31}(\nu) + B_{32}(\nu)/2] - \sin \eta_{00} [A_{20}(\nu) + p_{00}\, A_{31}(\nu) + A_{30}(\nu)/2 + A_{32}(\nu)/2] \Big\} \,,$$

$$q_1(\nu) = \ell_{00}^2 \Big\{ \cos \eta_{00} \,[A_{20}(\nu) + q_{00}\, B_{31}(\nu) + A_{30}(\nu)/2 - A_{32}(\nu)/2] - \sin \eta_{00} \,[q_{00}\, A_{31}(\nu) + B_{32}(\nu)/2] \Big\} \,,$$

$$\ell_1(\nu) = 2\, \ell_{00}^3 \Big\{ B_{31}(\nu) \cos \eta_{00} - A_{31}(\nu) \sin \eta_{00} \Big\} \,,$$

$$\eta_1(\nu) = c(1 - e_{00}^2)^{3/2}\, A_{20}(\nu) \,, \qquad \ldots\ldots(2.9)$$

where the integrals $A_{nk}(\nu)$ and $B_{nk}(\nu)$, which depend on p_{00} and q_{00}, are defined and evaluated in Appendix I. With these and after considerable amount of algebraic manipulation, the orbital elements can be expressed explicitly in terms of initial conditions as follows:

$$a_1(\nu) = -2a_{00}^2 \ell_{00} \left\{ \frac{\cos(\nu - \eta_{00})}{1 + p_{00}\cos\nu + q_{00}\sin\nu)} \right\}\Bigg|_0^\nu ;$$

$$p_1(\nu) = a_{00}^2(1 - e_{00}^2)/2 \left\{ \frac{(1 - e_{00}^2)\sin\nu \sin(\nu - \eta_{00})}{(1 + p_{00}\cos\nu + q_{00}\sin\nu)^2} \right.$$

$$\left. + 3\,\frac{(p_{00}\sin\nu - q_{00}\cos\nu)\sin\eta_{00}}{1 + p_{00}\cos\nu + q_{00}\sin\nu} - 3\,A_{10}(\nu)\sin\eta_{00} \right\}\Bigg|_0^\nu ;$$

$$q_1(\nu) = -a_{00}^2(1 - e_{00}^2)/2 \left\{ \frac{(1 - e_{00}^2)\cos\nu \sin(\nu - \eta_{00})}{(1 + p_{00}\cos\nu + q_{00}\sin\nu)^2} \right.$$

$$\left. + 3\,\frac{(p_{00}\sin\nu - q_{00}\cos\nu)\cos\eta_{00}}{1 + p_{00}\cos\nu + q_{00}\sin\nu} - 3\,A_{10}(\nu)\cos\eta_{00} \right\}\Bigg|_0^\nu ;$$

$$\eta_1(\nu) = c(1 - e_{00}^2)^{1/2} \left\{ A_{10}(\nu) - \frac{(p_{00}\sin\nu - q_{00}\cos\nu)}{1 + p_{00}\cos\nu + q_{oo}\sin\nu} \right\}\Bigg|_0^\nu \quad \ldots(2.10)$$

It is seen that after one orbit ($\nu = 2\pi$), only the terms containing $A_{10}(\nu)$ do not vanish.

While these results provide a reasonable approximation to the orbital elements of the osculating ellipse at any point during the first few revolutions, it is of particular interest to consider the orbital elements at $\nu = 2\pi$. The terms which vanish at $\nu = 2\pi$ can then be identified as short-term periodic contributions and are of secondary importance in the long-term behavior of the orbital elements. Writing $\Delta \underline{a} = \varepsilon \underline{a}_1 (2\pi)$, one obtains by substituting $\nu = 2\pi$ into the integrals of Equations (2.10):

$$\Delta p = -3\pi \varepsilon a_{00}^2 (1 - e_{00}^2)^{1/2} \sin \eta_{00} \quad ;$$

$$\Delta q = 3\pi \varepsilon a_{00}^2 (1 - e_{00}^2)^{1/2} \cos \eta_{00} \quad ;$$

$$\Delta \ell = 6\pi \varepsilon a_{00}^3 (1 - e_{00}^2)^{1/2} [p_{00} \sin \eta_{00} - q_{00} \cos \eta_{00}] \quad ;$$

$$\Delta \eta = 2\pi \delta a_{00}^{3/2} \quad ;$$

$$\Delta t = 3\pi \varepsilon a_{00}^{7/2} \left\{(4 + p_{00}) \cos \eta_{00} + 6 q_{00} \sin \eta_{00}\right\} + O(e_{00}^2) \quad \ldots\ldots (2.11)$$

Here the expression for Δt is obtained by expanding the elements in the integrand $r^2/\ell^{1/2}$ for small e_{00}. The change in semi-major axis can be expressed in terms of the results of Equations (2.11) yielding

$\Delta a = 0$, so that the major axis and hence the total energy return to their original values after one revolution in the first-order theory: the energy added while moving away from the sun is balanced by that removed during the motion towards the sun. In case $e_{00} \neq 0$, the changes in eccentricity and argument of the perigee can also be expressed in terms of Equations (2.11):

$$\Delta e = (p_{00}\Delta_p + q_{00}\Delta q)/e_{00} = -3\pi\varepsilon a_{00}^2(1 - e_{00}^2)^{1/2}\sin(\eta_{00} - \omega_{00});$$

$$\Delta\omega = (p_{00}\Delta q - q_{00}\Delta p)/e_{00}^2 = 3\pi\varepsilon a_{00}^2(1 - e_{00}^2)^{1/2}\cos(\eta_{00} - \omega_{00})/e_{00}. \quad .....(2.12)$$

It is evident that these first-order solutions represent a valid approximation only for a limited duration as the elements tend to move away from their reference values with the passage of time. Eventually, the solution becomes unreliable since it is unable to distinguish long-periodic from truly secular trends. In the following sections, a few approaches for obtaining long-term approximate solutions are studied.

2.3.2 Rectification/iteration procedure

The short-term solutions obtained in the previous subsection can be employed in a scheme to extend the interval of validity of these solutions. Thereto, a certain interval over which the first-order straightforward perturbation solutions provide sufficiently accurate approximations is selected, say $(0, \nu_f)$. For convenience, but not out of necessity, ν_f is usually taken as 2π. At $\nu = \nu_f$, the first-order changes in the elements are added to the initial values, i.e., rectification of the initial conditions:

$$\underline{a}(\nu_f)_{rect.} = \underline{a}_{00} + \varepsilon \underline{a}_1(\nu_f) \quad .$$

Subsequently, the adjusted value $\underline{a}(\nu_f)_{rect.}$ is treated as the initial condition for the next interval, say $(\nu_f, 2\nu_f)$, and again the first-order changes in $\underline{a}(\nu)$ at $\nu = 2\nu_f$ are calculated and the elements are updated. All elements as well as the solar aspect angle are treated in this manner and the procedure can be repeated as often as needed. Eventually, however, neglected second-order influences will affect the desired accuracy adversely.

Mathematically, the procedure is described as follows: the system of differential equations $\underline{a}'(\nu) = \varepsilon \underline{f}(\underline{a},\nu)$ and $\underline{a}(0) = \underline{a}_{00}$ is written in integral form:

$$\underline{a}(\nu) = \underline{a}_{00} + \varepsilon \int_0^{\nu} \underline{f}\,[\underline{a}(\tau),\tau]\, d\tau \quad . \qquad .....(2.13)$$

Application of the first-order straightforward perturbation expansion proposed in Equations (2.9) over the interval $[k\nu_f,(k+1)\nu_f]$, $k = 0,1,2,\cdots$, leads to the result:

$$\underline{a}_1[(k+1)\nu_f] = \int_{k\nu_f}^{(k+1)\nu_f} \underline{f}[\underline{a}(k\nu_f),\tau]\, d\tau \quad . \qquad \ldots\ldots(2.14)$$

Thus, the rectification/iteration procedure can be interpreted as replacing the integral in Equation (2.13) at $\nu = N\nu_f$ by the modified Riemann sum:

$$\underline{a}(N\nu_f) = \underline{a}_{00} + \varepsilon \sum_{k=0}^{N-1} \int_{k\nu_f}^{(k+1)\nu_f} \underline{f}[\underline{a}(k\nu_f),\tau]\, d\tau$$

$$= \underline{a}_{00} + \varepsilon \sum_{j=1}^{N} \underline{a}_1(j\nu_f) \quad . \qquad \ldots\ldots(2.15)$$

Successive calculation of $\underline{a}_1(j\nu_f)$, $j = 1,2,\cdots,N$ by means of Equation (2.14) leads to a piecewise constant approximation for the slowly varying elements. The accuracy of the approximation depends on the choice of the number of intervals N or the length of the interval ν_f. By taking N sufficiently large or ν_f sufficiently small, any desired accuracy can be attained. In fact, in the limit $N \to \infty$ (or $\nu_f \to 0$), the approximation becomes the exact solution. Consequently, accuracies exceeding those obtained by second and higher-order expansions without

rectification can be attained by simply choosing a sufficiently small interval before rectification of the first-order results (Lubowe[126]). Apart from providing physical insight through interpretation of the first-order results, the rectification/iteration procedure is perfectly suited for execution by a digital computer at a considerable saving in cost and effort as compared to a numerical integration of the original system of equations.

2.4 Two-Variable Expansion Procedure

A relatively recent, but extremely popular method for establishing long-term valid asymptotic representations for the solutions of a set of differential equations is the two-variable expansion method[87-93]. It involves the introduction of a so-called slow variable which is to be treated as distinctly independent of the regular independent variable, transforming ordinary into partial differential equations in the two independent variables. The solution of this transformed problem will contain certain indeterminate functions of the slow variable to be ascertained by postulating the mathematical constraint that the problem possesses a consistent asymptotic expansion uniformly valid for times of the order of the reciprocal of the small parameter. Physically, the imposed constraint may be interpreted as the elimination of secular terms.

Formally, the orbital elements (including the solar aspect angle) are expanded in asymptotic series:

$$\underline{a}(\nu) = \sum_{j=0}^{N-1} \varepsilon^j \underline{a}_j(\nu,\bar{\nu}) + O(\varepsilon^N) \quad , \qquad \text{.....(2.16)}$$

with the slow variable $\bar{\nu}$ defined by $\bar{\nu} = \varepsilon\nu$. Substituting these series into the perturbation equations $\underline{a}'(\nu) = \varepsilon \underline{f}(\underline{a},\nu)$ and collecting terms of like order in ε yields $\partial \underline{a}_0 / \partial \nu = 0$ for the zeroth-order elements so that $\underline{a}_0 = \underline{a}_0(\bar{\nu})$ with $\underline{a}_0(0) = \underline{a}_{00}$. The unknown slowly varying functions $\underline{a}_0(\bar{\nu})$ will be determined by requiring that the first-order contributions $\underline{a}_1(\nu,\bar{\nu})$ remain bounded as a function of ν (elimination of secular terms). This condition is equivalent (at least in the problems considered here) to the mathematical constraint mentioned before. The first-order equations are of the following general form:

$$\frac{\partial \underline{a}_1}{\partial \nu} = -\frac{d\underline{a}_0}{d\bar{\nu}} + \underline{f}\,[\underline{a}_0(\bar{\nu}),\nu] \quad , \quad \underline{a}_1(0) = \underline{0} \quad ; \qquad \text{.....(2.17)}$$

with the functions $\underline{f}$ periodic in the variable ν. A convenient way of separating the terms leading to unbounded contributions from those producing bounded results is by expanding the right-hand-side of Equation (2.17) in terms of Fourier series with slowly varying coefficients,

$$\frac{\partial \underline{a}_1}{\partial \nu} = -\frac{d\underline{a}_0}{d\bar{\nu}} + \int_0^{2\pi} \underline{f}\,[\underline{a}_0(\bar{\nu}),\tau]\, d\tau / (2\pi) + \sum_{j=1}^{\infty} \left\{ \underline{A}^j(\underline{a}_0)\cos j\nu \right.$$

$$\left. + \underline{B}^j(\underline{a}_0)\sin j\nu \right\} \quad . \qquad \text{.....(2.18)}$$

It should be realized that the slow variable $\bar{\nu}$ is treated as independent of ν during the integrations (cf. the method of averaging where the slowly changing mean variables are considered constants during integration). The vector functions $\underline{A}^j[\underline{a}_0(\bar{\nu})]$ and $\underline{B}^j[\underline{a}_0(\bar{\nu})]$ can be evaluated explicitly in an obvious and straightforward manner in terms of the Fourier coefficients a^j_{nk}, b^j_{nk}, c^j_{nk} and d^j_{nk}, Appendix II. From Equation (2.18) it is apparent that $\underline{a}_1(\nu,\bar{\nu})$ will be bounded (in fact, periodic) as a function of ν if the following relation for $\underline{a}_0(\bar{\nu})$ is satisfied:

$$\frac{d\underline{a}_0}{d\bar{\nu}} = \int_0^{2\pi} \underline{f}\,[\underline{a}_0(\bar{\nu}),\tau]\, d\tau/(2\pi) \quad , \qquad .....(2.19)$$

meaning that the slow rate of change of $\underline{a}_0(\bar{\nu})$ must equal the averaged (over one revolution) value of the right-hand-side of the perturbation equations. The similarity of the zeroth-order two-variable results, Equation (2.19) with those from first-order averaging is quite apparent: in fact, the equation obtained from first-order averaging is identical to Equation (2.19). It is interesting to compare the zeroth-order terms obtained by the two-variable method with the results from rectification/iteration, written as

$$[\underline{a}_1(2\pi) - \underline{a}_1(0)]\,/\,(2\pi) = \int_0^{2\pi} \underline{f}[\underline{a}_{00},\tau]\, d\tau/(2\pi) \quad . \qquad .....(2.20)$$

Comparing the expressions in Equations (2.19) and (2.20), one can interpret $\underline{a}_0(\bar{\nu})$ in terms of the rectification procedure as portraying a continual rectification (i.e., interval before rectification is infinitesimal) of the first-order results while the periodic dependence of $\underline{f}$ upon ν has been eliminated by averaging. (Note that the left-hand-side of Equations (2.19) and (2.20) may be interpreted as a differential and difference quotient, respectively.) Consequently, the function $\underline{a}_0(\bar{\nu})$ will generally be a better approximation to the exact solution than the results obtained by repeated rectification of the first-order straightforward perturbations when the interval of rectification is $\nu_f = 2\pi$. However, in order to improve upon a certain accuracy, one needs to solve for the higher-order equations in $\underline{a}_1(\nu,\bar{\nu})$ etc., in case of the two-variable expansion procedure, while the accuracy of the rectification/iteration method can be enhanced by simply choosing a smaller interval before rectification of the first-order straightforward perturbation results.

The first-order solutions $\underline{a}_1(\nu,\bar{\nu})$ may be obtained immediately by integration of the remainder of Equation (2.18), yielding:

$$\underline{a}_1(\nu,\bar{\nu}) = \sum_{j=1}^{\infty} (1/j) \left\{ \underline{A}^j(\underline{a}_0)\sin j\nu - \underline{B}^j(\underline{a}_0)\cos j\nu \right\} + \tilde{\underline{a}}_1(\bar{\nu}) \quad , \qquad .....(2.21)$$

where the as yet unknown functions $\tilde{\underline{a}}_1(\bar{\nu})$ must be determined from a constraint (similar as the one upon $\underline{a}_1$) upon the behavior of $\underline{a}_2(\nu,\bar{\nu})$.

The second-order equations can be obtained from $\underline{a}' = \varepsilon \underline{f}(\underline{a},\nu)$ by means of a Taylor expansion of $\underline{f}(\underline{a},\nu)$ around $\underline{a} = \underline{a}_0$, leading to

$$\frac{\partial \underline{a}_2}{\partial \nu} = -\frac{\partial \underline{a}_1}{\partial \nu} + \left[\frac{\partial f_i}{\partial a_j}(\underline{a},\nu)\right]_{\underline{a}=\underline{a}_0} \cdot \underline{a}_1(\nu,\bar{\nu}) \; ; \quad \underline{a}_2(0) = \underline{0} \; . \qquad .....(2.22)$$

Again, a Fourier series expansion of the right-hand-side is used for the separation of the bounded and unbounded contributions and differential equations for $\tilde{\underline{a}}_1(\bar{\nu})$ are obtained when requiring that $\underline{a}_2$ be bounded as a function of ν. This process can be continued for higher orders, if desired, but usually the contributions beyond the first-order can not be expressed in analytical form. Therefore, a sensible policy would consist of attempting to solve for the lower-order two-variable results and, if unsuccessful, or in case a better accuracy is needed, employing the rectification/iteration procedure with a sufficiently small interval ν_f. Note that ν_f must be smaller than 2π if the accuracy of the zeroth-order two-variable terms is to be exceeded.

A fortunate consequence of the similarities of the expressions in Equations (2.19) and (2.20) is that it allows us to write down, automatically, the zeroth-order two-variable equations, once the first-order straightforward solutions at $\nu = 2\pi$ are known (and vice versa).

2.4.1 Long-term valid results, case $\varepsilon = O(\delta)$

In this section the two-variable expansion method will be applied to obtain long-term valid approximations for the orbital elements. First, the case where the solar parameter is of the same order of magnitude as the frequency parameter of the sun in the ecliptic plane is considered.

Applying the resulting expression of Equation (2.19), yields the following zeroth-order equations:

$$\frac{dp_0}{d\bar{\nu}} = \ell_0^2 \left\{ \cos\eta_0 \left[p_0 B_{31}(2\pi) + B_{32}(2\pi)/2 \right] - \sin\eta_0 \left[A_{20}(2\pi) + p_0 A_{31}(2\pi) + A_{30}(2\pi)/2 + A_{32}(2\pi)/2 \right] \right\} / (2\pi) \; ;$$

$$\frac{dq_0}{d\bar{\nu}} = \ell_0^2 \left\{ \cos\eta_0 \left[A_{20}(2\pi) + q_0 B_{31}(2\pi) + A_{30}(2\pi)/2 - A_{32}(2\pi)/2 \right] - \sin\eta_0 \left[q_0 A_{31}(2\pi) + B_{32}(2\pi)/2 \right] \right\} / (2\pi) \; ;$$

$$\frac{d\ell_0}{d\bar{\nu}} = \ell_0^3 \left\{ B_{31}(2\pi)\cos\eta_0 - A_{31}(2\pi)\sin\eta_0 \right\} / \pi$$

$$\frac{d\eta_0}{d\bar{\nu}} = c \, (1 - p_0^2 - q_0^2)^{3/2} \; A_{20}(2\pi)/(2\pi) \; ; \qquad \text{.....(2.23)}$$

with initial conditions $\underline{a}_0(0) = \underline{a}_{00}$. The similarity in the structure of Equations (2.23) and the short-term results of Equations (2.10) with $\nu = 2\pi$ is evident indeed, as explained in the previous subsection. The integrals $A_{nk}(2\pi)$ and $B_{nk}(2\pi)$ now contain the slowly varying zeroth-order elements $p_0(\bar{\nu})$, $q_0(\bar{\nu})$, etc. Upon calculation and substitution of the integrals in Equations (2.23), a coupled nonlinear system of differential equations is obtained:

$$
\begin{aligned}
p_0'(\bar{\nu}) &= -\frac{3}{2} a_{00}^2 (1 - e_0^2)^{1/2} \sin \eta_0 \quad ; \\
q_0'(\bar{\nu}) &= \frac{3}{2} a_{00}^2 (1 - e_0^2)^{1/2} \cos \eta_0 \quad ; \\
\ell_0'(\bar{\nu}) &= 3 a_{00}^3 (1 - e_0^2)^{1/2} [p_0 \sin \eta_0 - q_0 \cos \eta_0] \quad ; \\
\eta_0'(\bar{\nu}) &= c \qquad \qquad \qquad \qquad \qquad \qquad \qquad \qquad \qquad \qquad .....(2.24)
\end{aligned}
$$

where e_0^2 equals $p_0^2 + q_0^2$. It is seen that $\eta_0(\bar{\nu}) = \eta_{00} + c\bar{\nu}$, denoting that the long-term behavior of the solar aspect angle is a linear function of the slow variable $\bar{\nu}$ in the zeroth-order approximation. Also it follows readily from Equations (2.24) that $a_0(\bar{\nu}) = a_{00}$ (write $a_0 = \ell_0/(1 - e_0^2)$), so that the major axis and total energy remain conserved in the long run in this approximation. Another integral can be derived quite readily from the system of Equations (2.24):

$$
c[1 - e_0^2(\bar{\nu})]^{1/2} + 3 a_{00}^2 y_0(\bar{\nu}) / 2 = \lambda = \text{constant.} \qquad .....(2.25)
$$

Introducing auxiliary orbital elements x and y defined by

$$\begin{pmatrix} x \\ y \end{pmatrix} = \begin{pmatrix} \sin\eta & -\cos\eta \\ \cos\eta & \sin\eta \end{pmatrix} \begin{pmatrix} p \\ q \end{pmatrix} = e \begin{pmatrix} \sin(\eta - \omega) \\ \cos(\eta - \omega) \end{pmatrix} , \qquad .....(2.26)$$

so that $x^2 + y^2 = p^2 + q^2 = e^2$, it follows from Equations (2.24) that $x_0(\bar{\nu})$ and $y_0(\bar{\nu})$ satisfy the following set of equations

$$x_0''(\bar{\nu}) + b^2 x_0(\bar{\nu}) = 0 ,$$

$$y_0'(\bar{\nu}) + c\, x_0(\bar{\nu}) = 0 , \qquad .....(2.27)$$

with initial conditions $x_0 = x_{00}$, $x'(0) = c\, y_{00} - 3a_{00}^2(1 - e_{00}^2)^{1/2}/2$ and $y_0(0) = y_{00}$. The constants x_{00} and y_{00} can be expressed in terms of the usual orbital elements according to Equation (2.26). The solutions $x_0(\bar{\nu})$ and $y_0(\bar{\nu})$ can readily be determined from Equations (2.27)

$$x_0(\bar{\nu}) = (b^2 - \lambda^2)^{1/2} \sin(b\bar{\nu} + \alpha_p)/b ,$$

$$y_0(\bar{\nu}) = [c(b^2 - \lambda^2)^{1/2} \cos(b\bar{\nu} + \alpha_p) + 3a_{00}^2\lambda/2]/b^2 , \qquad .....(2.28)$$

The elements $p_0(\bar{\nu})$ and $q_0(\bar{\nu})$ become

$$p_0(\bar{\nu}) = (b^2 - \lambda^2)^{1/2}[\sin(b\bar{\nu} + \alpha_p)\sin\eta_0 + c\cos(b\bar{\nu} + \alpha_p)\cos\eta_0/b\,]/b$$

$$+ 3\lambda a_{00}^2 \cos\eta_0/(2b^2) ,$$

$$q_0(\bar{\nu}) = (b^2 - \lambda^2)^{1/2}[\, c\cos(b\bar{\nu} + \alpha_p)\sin\eta_0/b - \sin(b\bar{\nu} + \alpha_p) *$$

$$*\cos\eta_0]\,/\,b + 3\lambda a_{00}\sin\eta_0/(2b^2) \quad . \qquad .....(2.29)$$

The conventional elements e_0, ℓ_0 and ω_0 can be determined from the results of Equations (2.28) and (2.29)

$$e_0(\bar{\nu}) = \left\{ 1 - [c\lambda - \frac{3}{2} a_{00}^2 (b^2 - \lambda^2)^{1/2}\cos(b\bar{\nu} + \alpha_p)]^2/b^4 \right\}^{1/2} ,$$

$$\ell_0(\bar{\nu}) = a_{00}\,[c\lambda - \frac{3}{2} a_{00}^2 (b^2 - \lambda^2)^{1/2}\cos(b\bar{\nu} + \alpha_p)]^2/b^4 ,$$

$$\omega_0(\bar{\nu}) = \eta_0(\bar{\nu}) - \arcsin\left\{ (b^2 - \lambda^2)^{1/2}\sin(b\bar{\nu} + \alpha_p)/[be_0(\bar{\nu})] \right\} .$$

$$.....(2.30)$$

The result for $\omega_0(\bar{\nu})$ is meaningful only if $e_0(\bar{\nu})$ does not vanish. If e_{00} is small it is recommended to calculate the argument of the perigee from the relation

$$\omega_0(\bar{\nu}) = \arctan\,[q_0(\bar{\nu})\,/\,p_0(\bar{\nu})] \quad .$$

If $\lambda < c$, the argument of the arcsin function can be shown to pass through one and the arcsin function to increase continuously. In case $\lambda > c$, the argument remains less than one and the arcsin function

keeps on oscillating between slowly changing upper and lower bounds. Physically, the two cases correspond to the major axis oscillating around its initial orientation or following the motion of the sun, respectively.

After the determination of the zeroth-order results, the first-order terms can be obtained by explicit calculation of the Fourier coefficients $\underline{A}^j(\underline{a}_0)$ and $\underline{B}^j(\underline{a}_0)$ of Equation (2.21) for the present case. It follows that:

$$p_1(\nu,\bar{\nu}) = \ell_0^2 \cos\eta_0 \sum_{j=1}^{\infty} (1/j) \left\{ [p_0 b_{31}^j + b_{32}^j/2] \sin j\nu + [p_0 d_{31}^j + d_{32}^j/2](1 - \cos j\nu) \right\} - \ell_0^2 \sin\eta_0 \sum_{j=1}^{\infty} (1/j) \left\{ [a_{20}^j + p_0 a_{31}^j + a_{30}^j/2 + a_{32}^j/2] \sin j\nu + [c_{20}^j + p_0 c_{31}^j + c_{30}^j/2 + c_{32}^j/2](1 - \cos j\nu) \right\} + \tilde{p}_1(\bar{\nu}) \quad ;$$

$$q_1(\nu,\bar{\nu}) = \ell_0^2 \cos\eta_0 \sum_{j=1}^{\infty} (1/j) \left\{ [a_{20}^j + q_0 b_{31}^j + a_{30}^j/2 - a_{32}^j/2] \sin j\nu + [c_{20}^j + q_0 d_{31}^j + c_{30}^j/2 - c_{32}^j/2](1 - \cos j\nu) \right\}$$

$$- \ell_0^2 \sin\eta_0 \sum_{j=1}^{\infty} (1/j) \left\{ [q_0 a_{31}^j + b_{32}^j/2] \sin j\nu \right.$$

$$\left. + [q_0 c_{31}^j + d_{32}^j/2](1 - \cos j\nu) \right\} + \tilde{q}_1(\bar{\nu}) \quad ;$$

$$a_1(\nu,\bar{\nu}) = 2a_{00}^3/(1 - e_0^2) \sum_{j=1}^{\infty} (1/j) \left[\cos\eta_0 \left\{ [q_0 a_{20}^j + b_{21}^j] \sin j\nu \right.\right.$$

$$\left. + [q_0 c_{20}^j + d_{21}^j](1 - \cos j\nu) \right\} - \sin\eta_0 \left\{ [p_0 a_{20}^j \right.$$

$$\left.\left. + a_{21}^j] \sin j\nu + [p_0 c_{20}^j + c_{21}^j](1 - \cos j\nu) \right\} \right] + \tilde{a}_1(\bar{\nu}) \quad ;$$

$$\eta_1(\nu,\bar{\nu}) = c(1 - e_0^2)^{3/2} \sum_{j=1}^{\infty} (1/j) \left\{ a_{20}^j \sin j\nu + c_{20}^j(1 - \cos j\nu) \right\}$$

$$+ \tilde{\eta}_1(\bar{\nu}) \quad . \qquad \text{.....(2.31)}$$

The Fourier coefficients a_{nk}^j, b_{nk}^j, etc. are defined and calculated in Appendix II and are functions of p_0, q_0, etc. The unknown 'slow' functions $\tilde{p}_1(\bar{\nu})$, $\tilde{q}_1(\bar{\nu})$, etc. are to be determined from the boundedness

constraint imposed upon the second-order terms and vanish for $\bar{\nu} = 0$. For small e_0, the Fourier coefficients are proportional to $(-e_0)^j$ and converge very rapidly so that usually only the first few terms need to be carried. The periodic terms in Equations (2.31) stay within a band of a width of order ε around the long-term zeroth-order solutions $\underline{a}_0(\bar{\nu})$. The secular contributions of $\tilde{\underline{a}}_1(\bar{\nu})$ in Equations (2.31) are of order ε for ν up to order $1/\varepsilon$, i.e., up to about 800 days for $\varepsilon = 0.0002$.

2.4.2 Long-term valid results, case $\varepsilon = O(\delta^2)$

In the case that the solar parameter ε is of comparable magnitude with δ^2, a similar analysis as in the previous subsection can be followed when the slow variable is taken as $\tilde{\nu} = \delta\nu$ and the elements are expanded in series of powers of δ rather than ε. The zeroth-order results become $p_0 = p_{00}$, $q_0 = q_{00}$, $\ell_0 = \ell_{00}$ and $\eta_0(\tilde{\nu}) = a_{00}^{3/2}\tilde{\nu} + \eta_{00}$, while the first-order results are

$$p_1(\tilde{\nu}) = \frac{3}{2} a_{00}^2 (1 - e_{00}^2)^{1/2} [\cos\eta_0 - \cos\eta_{00}] / c_1 ,$$

$$q_1(\tilde{\nu}) = \frac{3}{2} a_{00}^2 (1 - e_{00}^2)^{1/2} [\sin\eta_0 - \sin\eta_{00}] / c_1 ,$$

$$\ell_1(\tilde{\nu}) = -3 a_{00}^3 (1 - e_{00}^2)^{1/2} [p_{00} (\cos\eta_0 - \cos\eta_{00}) + q_{00}(\sin\eta_0 - \sin\eta_{00})] / c_1 ,$$

$$\eta_1(\tilde{\nu}) = \ell_{00}^{3/2} \sum_{j=1}^{\infty} (1/j) \left\{ a_{20}^j \sin j\nu + c_{20}^j (1 - \cos j\nu) \right\} , \quad .....(2.32)$$

with a_{20}^j and c_{20}^j dependent on p_{00}, q_{00}, etc. In the usual manner, expressions for $e_1(\bar{\nu})$ and $\omega_1(\bar{\nu})$ can be written down, while for small e_{00}, ω becomes indeterminate and the argument of the perigee needs to be found from p_1 and q_1 :

$$\omega_1(\tilde{\nu}) = \arctan \left\{ \frac{q_{00} + \delta q_1(\tilde{\nu}) + O(\delta^2)}{p_{00} + \delta p_1(\tilde{\nu}) + O(\delta^2)} \right\} . \quad .....(2.33)$$

From this relation and Equations (2.32), it follows that for small $\tilde{\nu}$ and $e_{00} = 0$: $\omega_1(\tilde{\nu}) = \eta_{00} + \pi/2$, reaffirming the well-known fact that for an initially circular orbit, the perigee will appear 90° ahead of the sun-earth line.

2.5 Discussion of Results

To assess the validity of the approximate approaches developed in the previous sections, the results are compared with those from a numerical integration of the perturbation equations. The parameters involved were taken corresponding to situations of practical interest: an Echo-type satellite and the SSPS representing the case $\varepsilon = O(\delta)$ and the CTS illustrating the situation $\varepsilon = O(\delta^2)$.

The initial orbital geometry and solar aspect angle were varied systematically.

2.5.1 Case $\varepsilon = O(\delta)$

From the results derived in Section 2.4.1, it is apparent that $e_0(\bar{\nu})$ and $\ell_0(\bar{\nu})$ change periodically with period

$$a_{00}^{3/2} / (b\varepsilon) = 1 / (\delta^2 + 9\varepsilon^2 a_{00} / 4)^{1/2} \text{ days} . \quad .....(2.34)$$

In any case, this period is less than one year and smaller the ε, the closer it approaches one year, which is indeed the period in the case $\varepsilon = O(\delta^2)$ as found in Section 2.4.2. Also, the period increases with decreasing a_{00} (Figure 2-2). For example, taking $a_{00} = 1$ and $\varepsilon = 0.0002$, i.e., $A/m = 10\,m^2/kg$ and $\sigma = 0.5$, which is the case for an SSPS with $\rho = \kappa = \tau = 0$ or a spherical satellite with $\rho = 1$ and $\tau = 0$, the resulting period of the long-term perturbations is approximately 363 days.

The extrema of $e_0(\bar{\nu})$ and $\ell_0(\nu)$ can be determined from Equations (2.30). Limiting λ to the physically meaningful domain $\frac{3}{2} a_{00}^2 \leq \lambda \leq b$, the eccentricity $e_0(\bar{\nu})$ lies between

$$e_{0,max} = [3\lambda a_{00}^2/2 + c(b^2 - \lambda^2)^{1/2}] / b^2 ,$$

at

$$\nu = (2n\pi - \alpha_p) / (b\varepsilon) ,$$

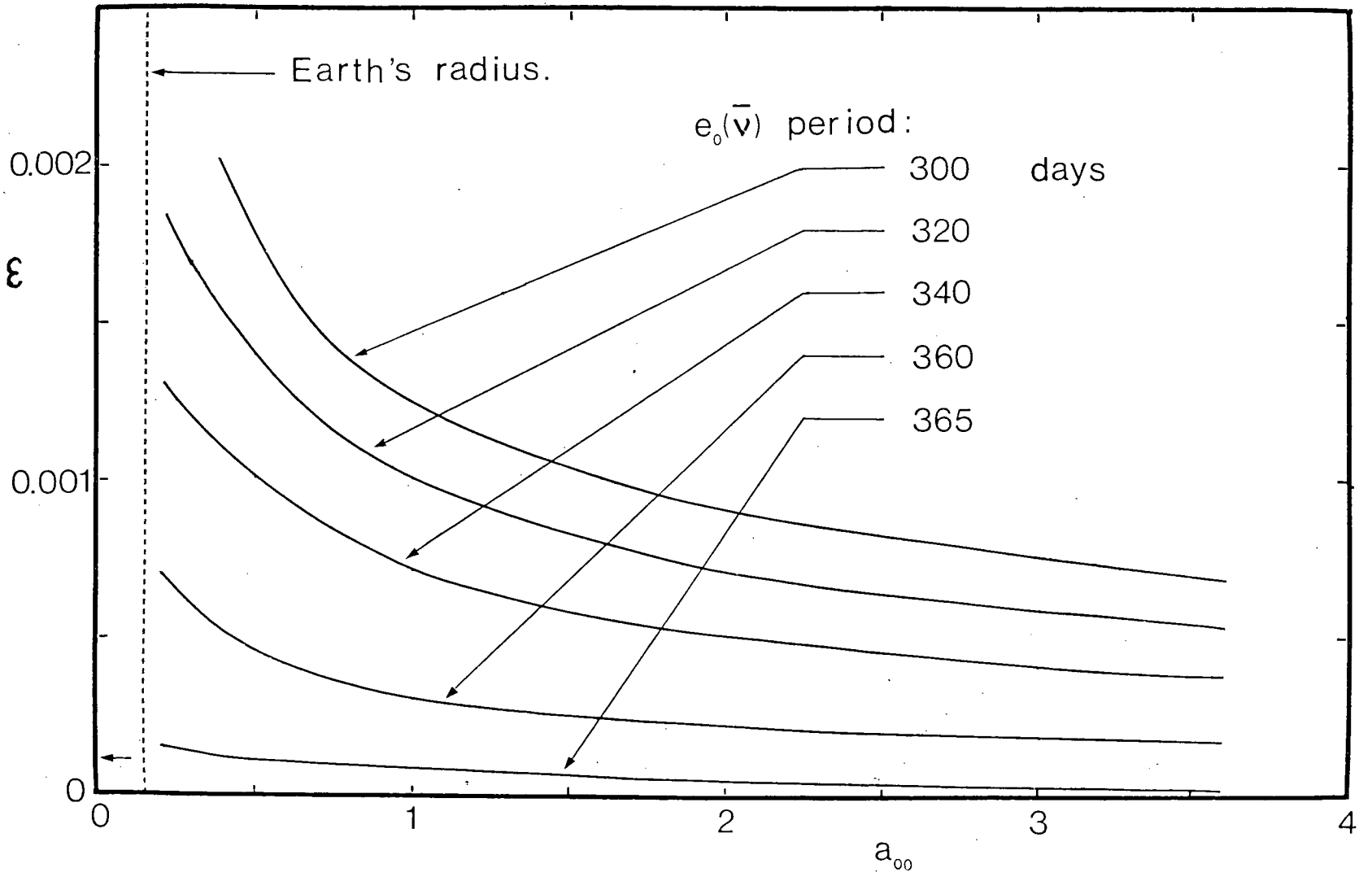

Figure 2-2 Loci in a_{00}, ε plane having same the same period of long-term perturbations

$$e_{0,min} = \left| 3\lambda\, a_{00}^2/2 - c(b^2 - \lambda^2)^{1/2} \right| / b^2 \quad ,$$

at

$$\nu = [(2n+1)\pi - \alpha_p] / (b\varepsilon) \quad , \qquad .....(2.35)$$

with $n = 0,1,2,\cdots$ and $\nu > 0$. It is seen that for $\lambda = b$, the minimum and maximum values are the same. Hence, e_0 and ℓ_0 remain constant: $e_0(\bar{\nu}) = e_{00}$ and $\ell_0(\bar{\nu}) = \ell_{00}$. If $\lambda = c$, the trajectory will become circular at some point as $e_{0,min} = 0$.

Figure 2-3 shows the accuracy of the zeroth-order two-variable solution and the rectification/iteration (with interval $\nu_f = 2\pi$) results in comparison with a double precision Runge-Kutta integration routine. The approximate results proved to be quite effective and their comparison is purposely limited to one case: $e_{00} = 0.5$ and $\eta_{00} = \pi$. The two-variable expansion procedure predicts the eccentricity correctly to three decimal places, while the rectification/iteration method yields results correct to two places. The comparisons were made at $\nu = 2\pi n$, $n = 1,2,\cdots,1200$. It should be noted that the first-order changes in time are incorporated in the rectification/iteration procedure, whereas time is taken proportional to $\bar{\nu}$ in the zeroth-order two-variable expansion results. As can be expected, the value of the initial solar aspect angle has no influence on the resulting behavior of the eccentricity when $e_{00} = 0$, curve (d). The fluctuations in $e_0(\bar{\nu})$ can be as large as 0.2, curves (b) and (d). However, a suitable combination of initial parameters may also result in very small perturbations as indicated by curve (c). In fact, in the

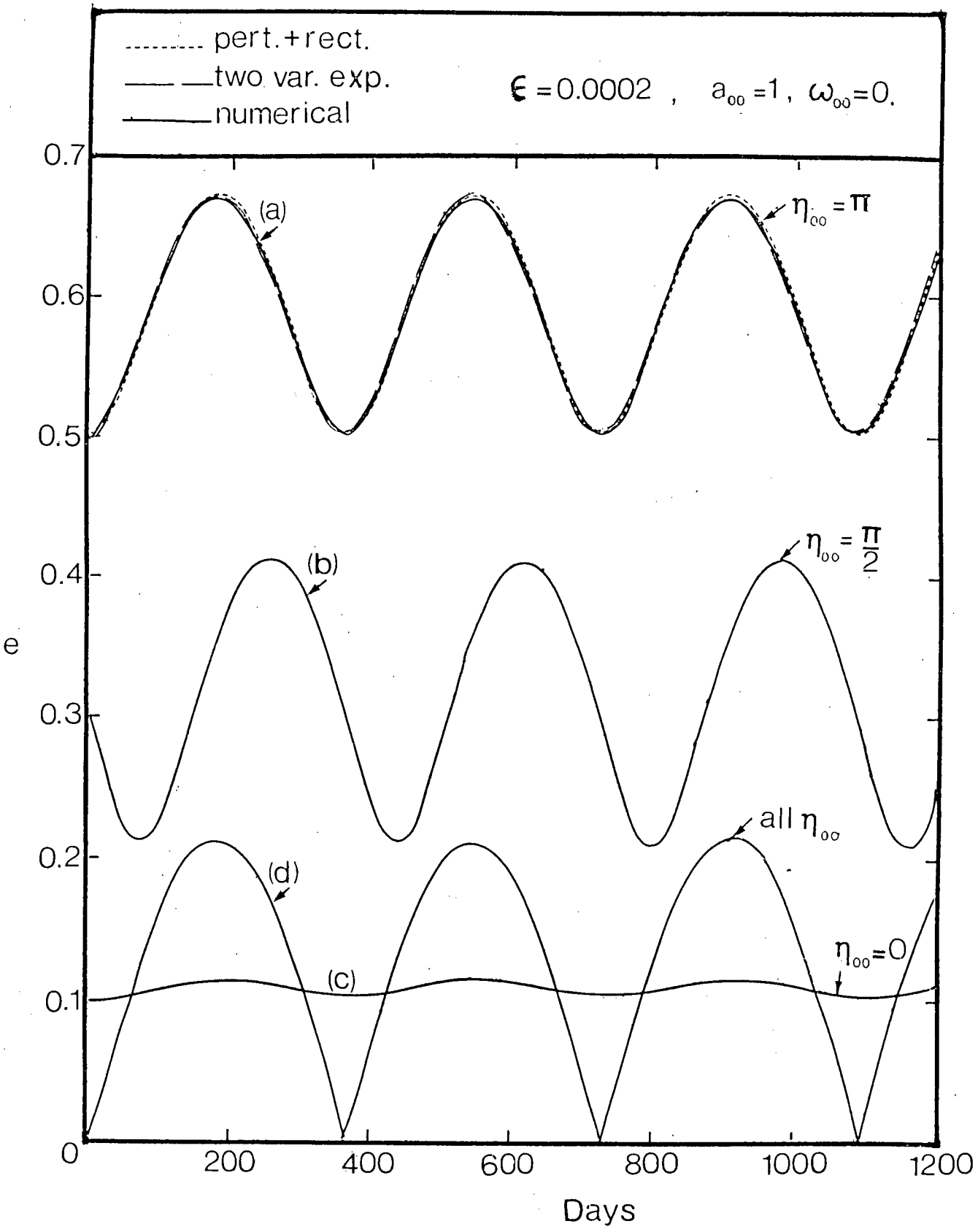

Figure 2-3 Long-term variations in eccentricity as predicted by the three methods

limiting case of $\eta_{00} = 0$ and $e_{00} = 0.109$ the variations in $e_0(\bar{\nu})$ disappeared completely (case $\lambda = b$).

Figure 2-4 shows the predictions of the approximate methods as to the behavior of the semi-latus rectum and argument of the perigee for $\lambda < c$. In case $\lambda > c$, the precession of the major axis is described by a large linear secular variation with a small amplitude periodic motion superimposed on it as shown in Figure 2-5. For $\lambda = c$, the argument of perigee shows periodic discontinuities with a jump through 180°. Note also that in the case $\lambda = b$ (i.e., $e_{00} = 0.109$ and $\eta_{00} = 0$ here), the periodic component disappears completely leaving only the linear variation: the major axis keeps on pointing towards the sun, while the eccentricity remains constant. In the case $\lambda < c$, the axis oscillates between slowly moving upper and lower bounds.

Figure 2-6 shows the very small long-periodic variations in the semi-major axis and the osculating periods for a few values of the initial solar aspect angle obtained from the numerical integration routine. Note that the analytical methods predict that $a(\nu)$ remains constant in the first-order, so that the variations depicted here are second-order effects.

The orbital elements affected most severely by solar radiation forces are eccentricity, semi-latus rectum and argument of the perigee. Since the semi-major axis is not affected in the first-order, the changes in semi-latus rectum can be expressed in terms of those of the osculating eccentricity. Complete visualization of the first-order changes in orbital geometry is thus provided by the two

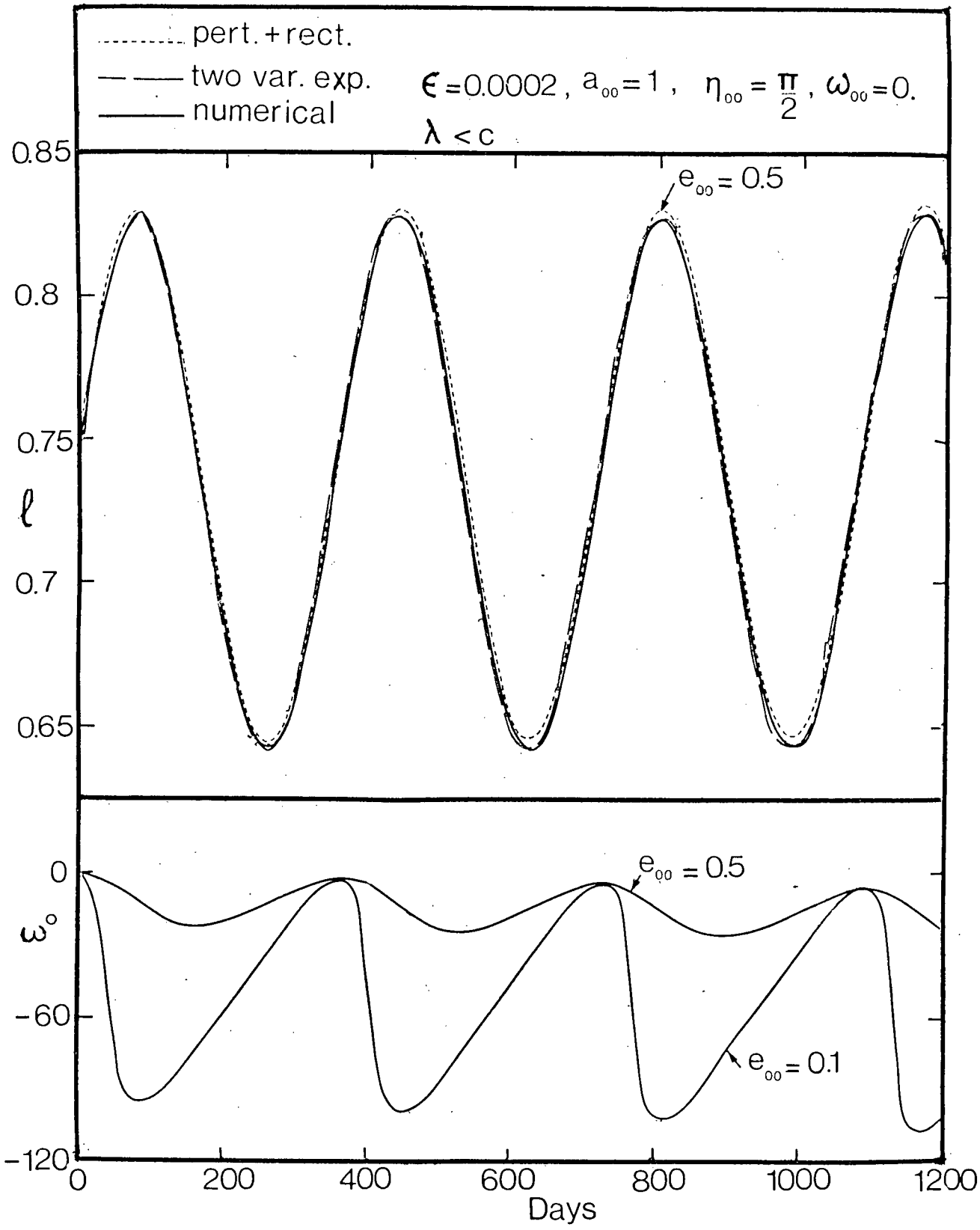

Figure 2-4 Long-term behavior of semi-latus rectum and argument of the perigee

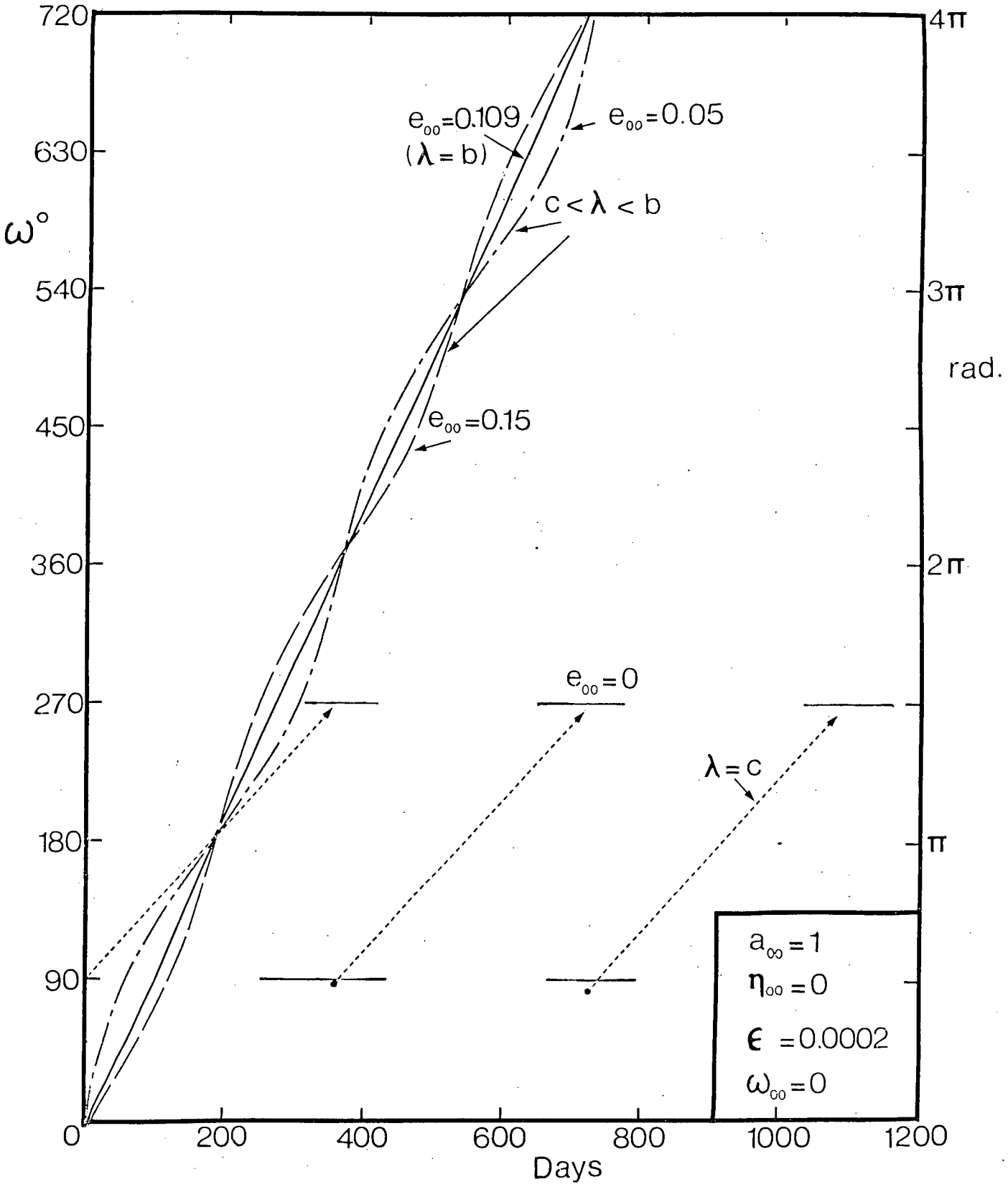

Figure 2-5 Secular variation of the argument of the perigee for $c \leq \lambda \leq b$

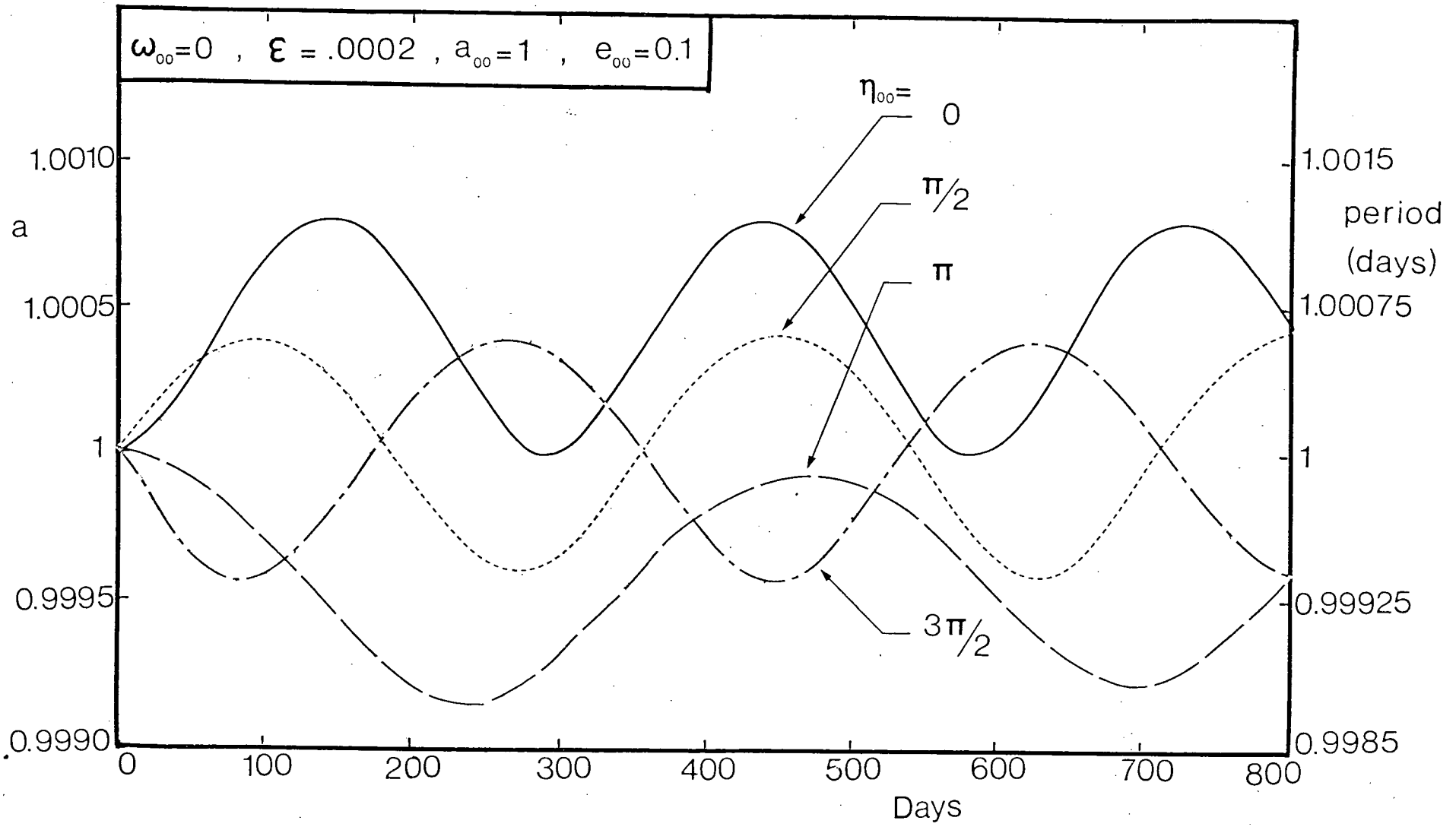

Figure 2-6 Long-term variations in the semi-major axis and orbital period

elements e and ω (or p and q). Complete comprehension of the nature of the orbital perturbations could be obtained from plots showing the long-term behavior of e and ω for various initial conditions and solar aspect angles. One attractive possibility is depicting e and ω as a polar plot in the p,q-plane with e the length and ω the argument of the eccentricity vector $\underline{e}$. It can be observed from Equations (2.24) that the slope of the polar plot as a function of ν is determined from

$$\frac{dq_0}{dp_0}(\nu) = \tan(\delta\, a_{00}^{3/2}\, \nu + \eta_{00} + \pi/2) \quad . \qquad .....(2.36)$$

Considering, for illustration, an orbit with initially $\omega_{00} = 0$ (so that the polar plot starts out from the $q = 0$ axis) it follows that initially the angle at which the tangent to the curve $q_0 = q_0(p_0)$ is inclined to the p axis equals $\eta_{00} + \pi/2$. As ν advances the tangent rotates slowly in an anti-clockwise manner. At $\nu = 2\pi/(c\varepsilon)$, i.e. after slightly less than one year, the tangent returns to its original value indicating that the polar plot describes anti-clockwise loops in the p,q-plane, Figures 2-7a-d. This type of plots allows an easy visualization of the orientation of the major axis as well as the eccentricity of the orbit over a long duration.

The initial configuration is best characterized by the parameter λ as defined by the initial orbital elements and solar aspect angle. It can be shown that $c \geq 3a_{00}^2/2$ provided that

$\varepsilon \leq 2\delta/(3a_{00}^{1/2})$, which covers all practical cases. The physically useful range of λ is limited to $3a_{00}^2/2 \leq \lambda \leq b$. It is informative to study a few special cases:

(a) $\lambda = c$: This case defines the locus of initial conditions for which the ensuing trajectory will have a circular osculating orbit at some time within one year: the corresponding polar plots pass through the origin $p = q = 0$. Figure 2-7a presents a few examples belonging to this class. For any $e_{00} \leq 3ca_{00}^2 / b^2$ (=0.220 in the example), an appropriate value η_{00} can be found so that the resulting curve goes through the origin. It can be seen that the argument of the perigee jumps through 180° at the origin.

(b) $3a_{00}^2/2 < \lambda < c$: Here, the polar plots do not pass through nor encircle the origin and the eccentricity oscillates between the values $e_{0,min}$ and $e_{0,max}$ determined in Equations (2.35). The curves in Figures 2-7b qualitatively indicate the behavior for $e_{00} = 0.5$. While going around in the anti-clockwise manner, a slow precession in the clockwise sense is superimposed on the motion and the result is a trajectory describing loops between the two concentric circles of radii $e_{0,min}$ and $e_{0,max}$. As pointed out before, the period of oscillation in eccentricity is close to but less than one year. Interesting is the behavior of argument of the perigee, ω : after one complete cycle of $e_0(\bar{\nu})$, ω has decreased by $-2\pi(1 - c/b)$, amounting to a precession of -2.14° per year in the example. As the factor $1 - c/b$

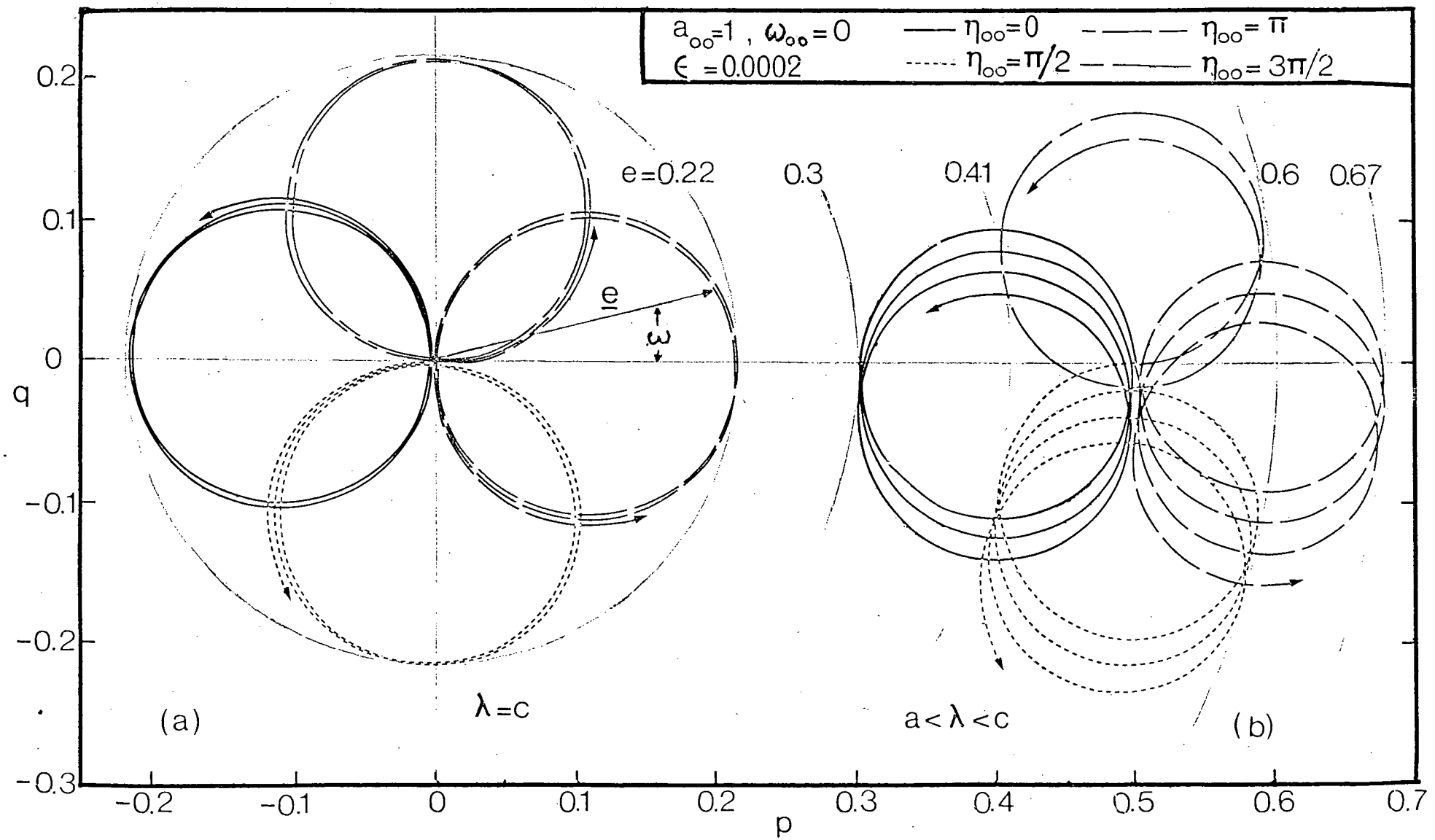

Figure 2-7 Polar plots showing long-term behavior of eccentricity vector $\underline{e}$:
(a) case $\lambda = c$, $e_{00} = 0$; (b) case $3a_{00}^2/2 < \lambda < c$, $e_{00} = 0.5$

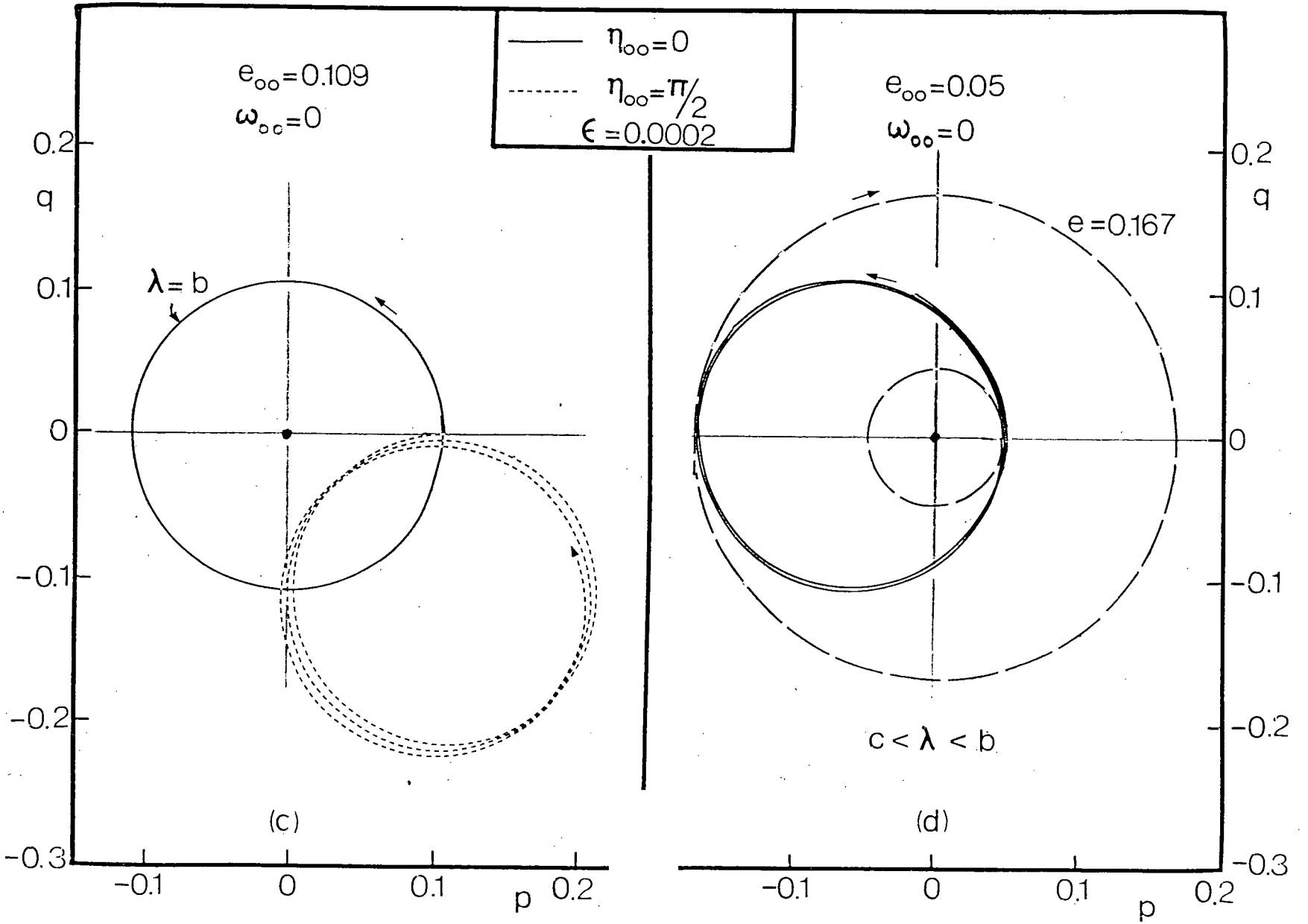

Figure 2-7 Polar plots, showing long-term behavior of eccentricity vector $\underline{e}$:
(c) case $c < \lambda < b$; $e_{00} = 0.109$; (d) case $\lambda = b$; $e_{00} = 0.05$

increases with increasing ε, the precession will be faster for larger ε. Note also that the periodic variations in ω become smaller for increasing e_{00}: physically, the major axis is more 'rigid' for larger e_{00}.

(c) $\lambda = 3a_{00}^2/2$: This case represents the locus of initial conditions which eventually yield a parabolic trajectory ($e = 1$). However, since the semi-major remains constant in the first-order, $e = 1$ would imply that the perigee coincides with the center of attraction. Obviously, the life of the satellite would end long before $e = 1$ is reached. (In fact, for $a_{00} = 1$, $e = 0.84$ will be the maximum physically meaningful eccentricity). The minimum eccentricity to reach an escape trajectory is $e_{0,min} = (c^2 - 9a_{00}^4/4)/b^2$, for $\eta_{00} = \pi$. In the example, $e_{0,min} = 0.976$, hence the locus $\lambda = 3a_{00}^2/2$ is not attainable.

(d) $c < \lambda < b$: For these values of λ the variation of ω is predominantly linear in character, increasing continuously while the curves in the polar plot circle around the origin, Figure 2-7d. From the definition of λ, the criterion for encirclement of the origin ($c < \lambda$) can be expressed in terms of the initial conditions:

$$e_{00} < 3a_{00}^2 c \cos(\eta_{00} - \omega_{00})/[c^2 + 9a_{00}^2 \cos^2(\eta_{00} - \omega_{00})/4] \quad .....(2.37)$$

Note that for $90° \leq \eta_{00} - \omega_{00} \leq 270°$ the loci can not enclose the origin.

(e) $\underline{\lambda = b}$: This interesting case represents only one possible initial configuration, namely, $e_{00} = 3a_{00}^2/(2b)$, i.e. 0.109 in the example, and $\eta_{00} = \omega_{00}$. The resulting eccentricity does not change at all, i.e. $e_0(\bar{\nu}) = e_{00}$ throughout while $\omega_0(\bar{\nu}) = \eta_0(\bar{\nu})$, so that the major axis keeps on pointing towards the sun and the shape of the orbit remains unchanged. The corresponding polar plot consists of a circle of radius $3a_{00}^2/(2b)$ around the origin, Figure 2-7c. The case is interesting since a large region in space can be traversed by a satellite satisfying $\lambda = b$ without altering the shape of the orbit. The annular region is contained by the two concentric circles whose radii are the perigee and apogee heights $a_{00}(1 - e_{00})$ and $a_{00}(1 + e_{00})$, respectively. In the example, the distance between the circles amounts to more than 9,200 km.

The actual orbit based on the result,

$$r_0(\nu,\bar{\nu}) = \ell_0(\bar{\nu}) / [1 + p_0(\bar{\nu})\cos\nu + q_0(\bar{\nu})\sin\nu],$$

is depicted, for a typical case, in Figure 2-8 illustrating the differences in the osculating ellipses at 90 day intervals: the wide band of spatial region reached by the satellite is quite apparent. This is significant in designing a mission aimed at scientific measurements over a vast area in space.

Since the short-term solutions are also known (Section 2.3.1):

$$r(\nu) = r_0(\nu) + \varepsilon r_1(\nu) \quad ,$$

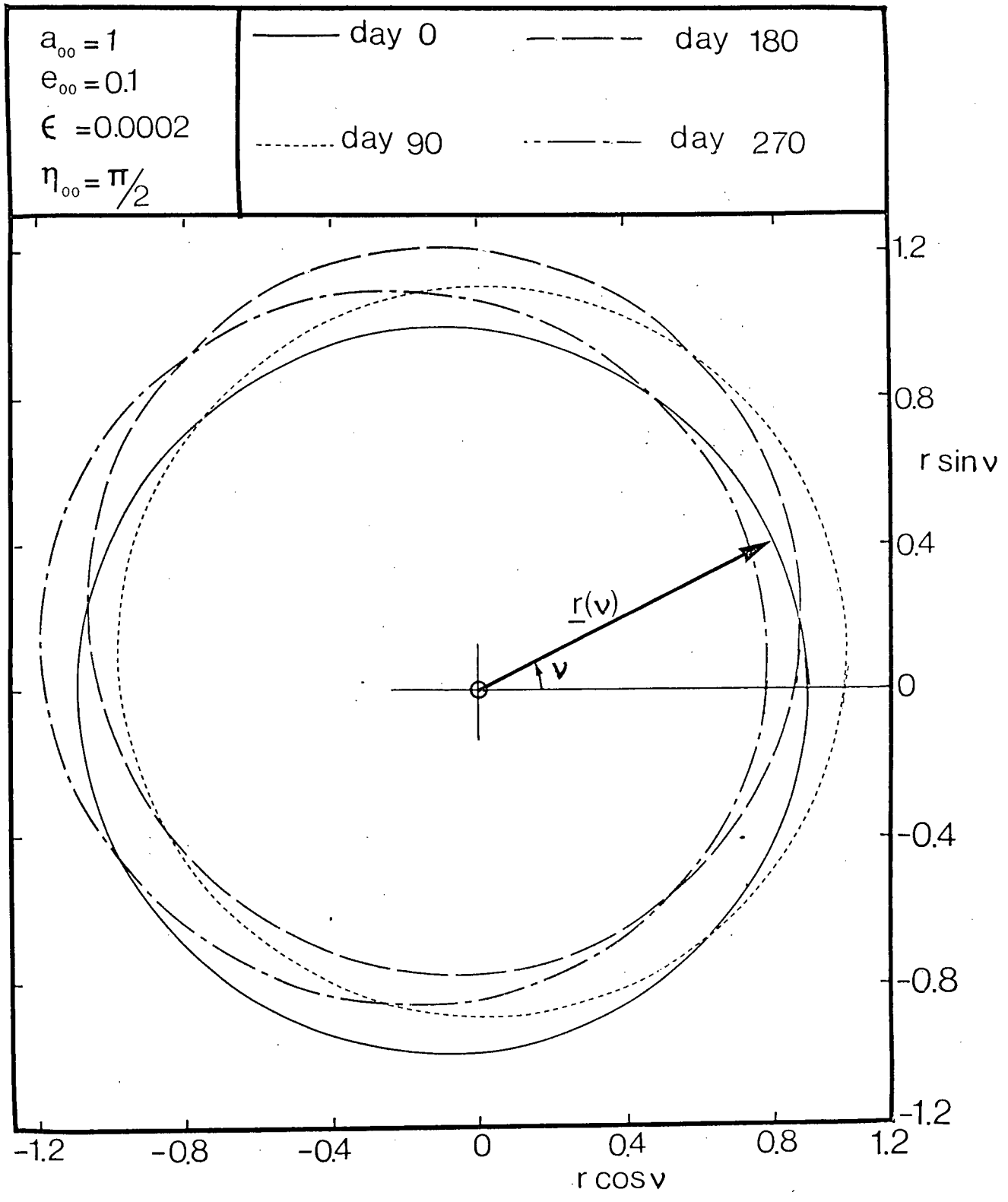

Figure 2-8 Long-term orbital behavior showing traversing of spatial region

with $r_1(\nu)$ readily expressed in terms of ℓ_1, p_1, and q_1 by expansion, it is interesting to show the actual path of the satellite during its first revolution. This has been done in Figure 2-9 for an exaggerated A/m ratio of 1,000 m^2/kg : note that the point of minimum distance to earth occurs about 90° ahead of the sun-earth line.

Finally, loci of λ = constant are plotted in the e_{00}, η_{00} plane (Figure 2-10). They can be used to advantage in assessing the bounds of eccentricity as $e_{0,max}$ and $e_{0,min}$ depend on λ only for given ε and a_{00} (Equations 2.35). Obviously, the lowest and highest values of e_{00} on each curve correspond to the limiting values $e_{0,max}$ and $e_{0,min}$ belonging to that locus. Thus, for any combination of initial eccentricity and solar aspect angle, the corresponding extremes of eccentricity of the ensuing trajectory can be assessed immediately. This should prove useful during the preliminary planning of a mission as it provides a convenient way of determining whether a given satellite will dip into the free molecular environment or not. As can be expected, the point λ = b moves to the right for larger ε with corresponding increase in fluctuations of the eccentricity. The area designated by $\lambda > c$ corresponds with polar plots encircling the origin and the locus λ = c denotes initial conditions with polar plots passing through the origin.

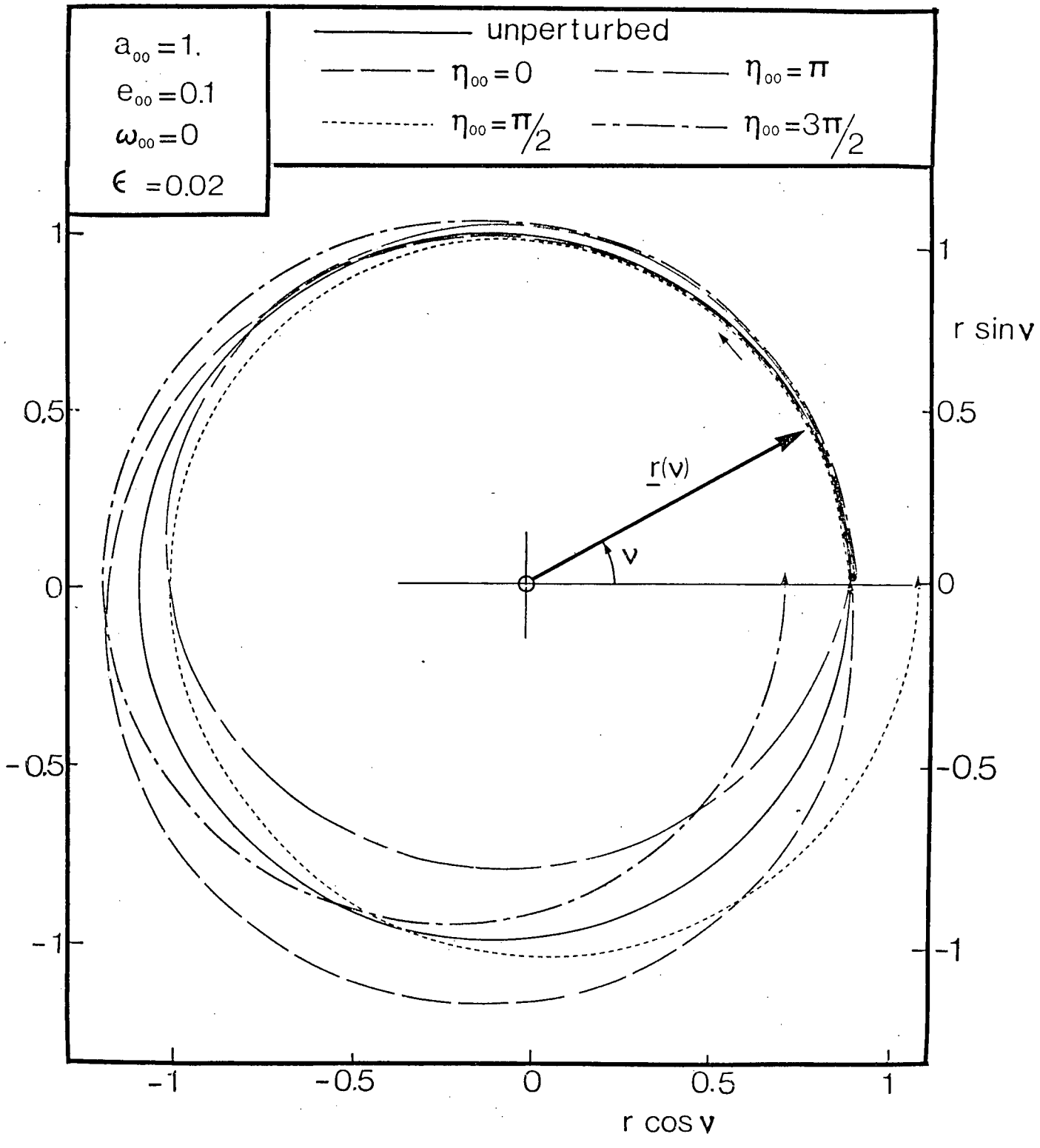

Figure 2-9 Actual path of satellite during first revolution (for exaggerated solar parameter, $\epsilon = 0.02$)

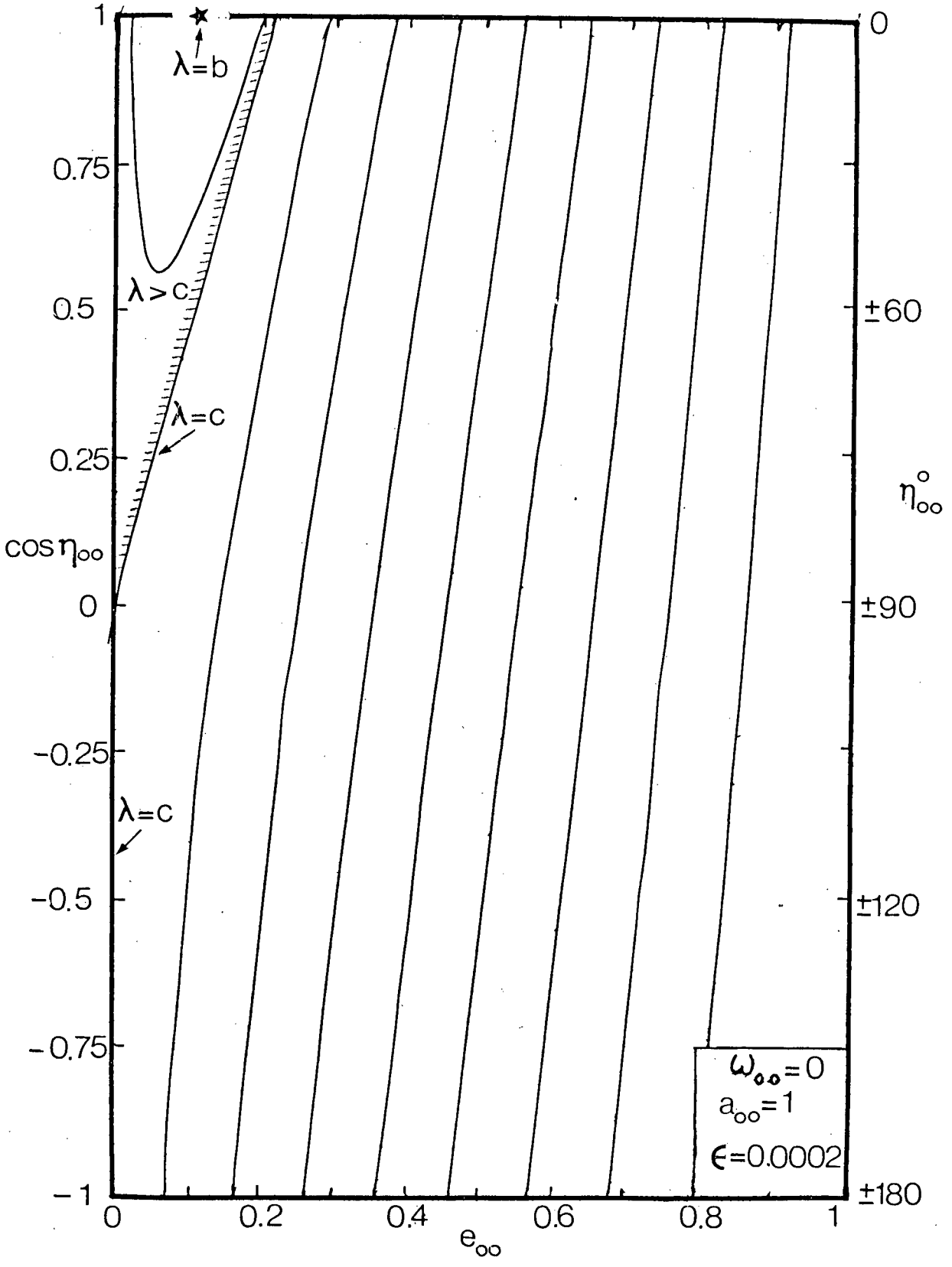

Figure 2-10 Loci of initial conditions, λ = constant, leading to the same extrema of eccentricity

2.5.2 Case $\varepsilon = O(\delta^2)$

It is apparent here that $e_1(\tilde{\nu})$ is periodic with a period of exactly one year and the range of eccentricity is given by

$$e_{1,max} - e_{1,min} = 3\varepsilon \ell_{00}^{1/2} / \delta \quad ,$$

regardless of initial solar aspect angle. For a satellite with the parameters of CTS (i.e. $\varepsilon = 1.4 \times 10^{-6}$, $c_1 = 5.4$) and $a_{00} = 1$, the variation in eccentricity is 1.50×10^{-3}. In terms of perigee distance, this result translates to a maximum fluctuation of some 63 km in six months. In Figure 2-11, the polar plots for $e_{00} = 0$ and 0.1 are shown for a few values of η_{00}. The slope of the polar plots turns out to be exactly the same as in the previous section so that the influence of initial solar aspect angle presented qualitatively in Figures 2-7 remains valid for this case. The periodic variation in ω is over 180° in Figure 2-11a but is reduced to the order 10^{-2} in Figure 2-11b where $e_{00} = 0.1$. A polar plot in the form of a circle around the origin as in the previous section, can also be found here, namely for $e_{00} = 3\delta a_{00}^2/(4c_1^2 + 9a_{00}^4\delta^2)^{1/2}$, i.e. 0.75×10^{-3} in the CTS example, and $\eta_{00} = 0$. In these circumstances, the major axis follows the motion of the sun. Interestingly, the formula for e_{00} found here is identical to the expression of the previous section. If $e_{00} < 6\delta a_{00}^2/(4c_1^2 + 9a_{00}^4\delta^2)^{1/2}$, i.e. 1.50×10^{-3} here, the plots enclose the origin or pass through it provided appropriate values for the

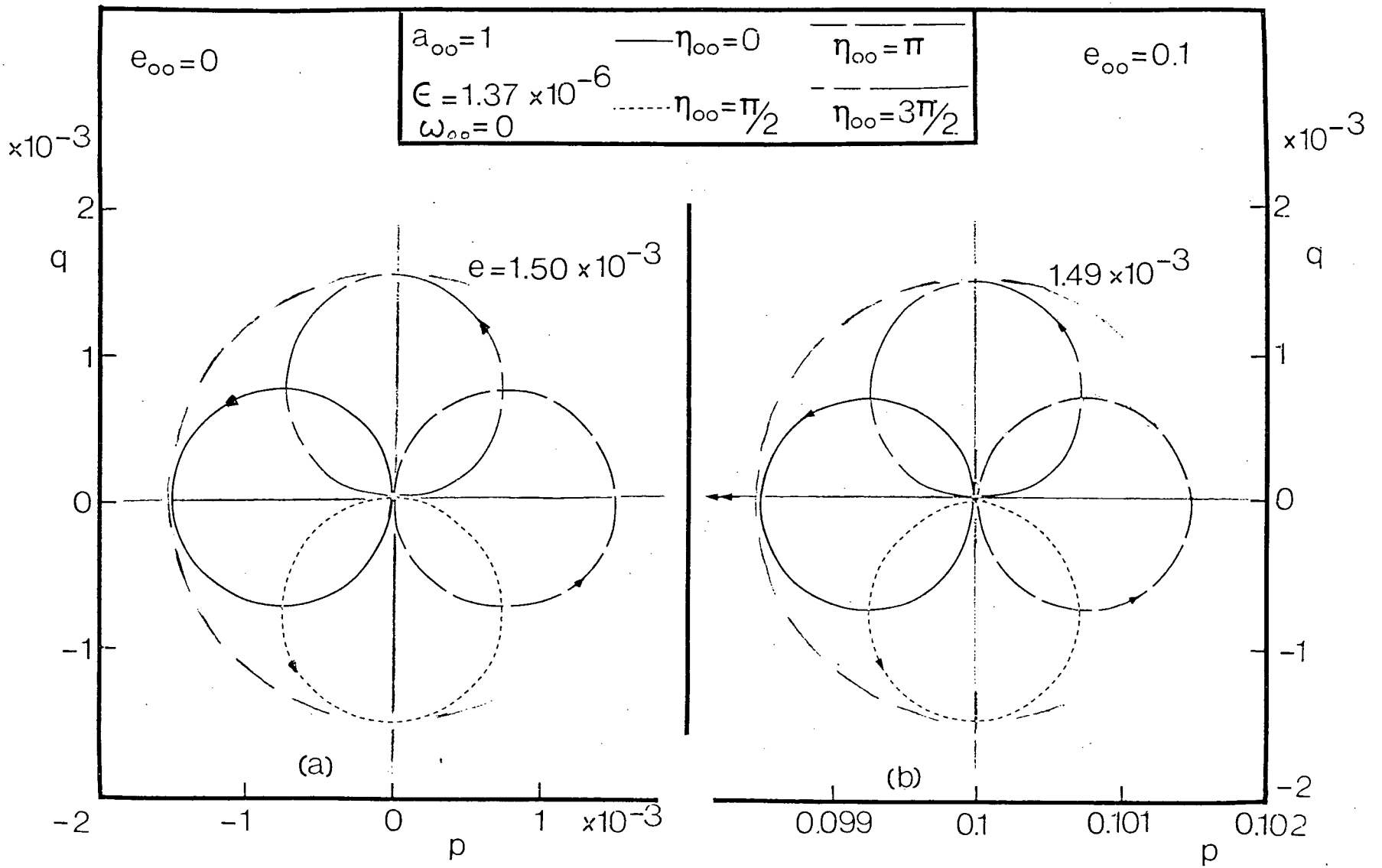

Figure 2-11 Representative polar plots for the Communications Technology Satellite:
(a) $e_{00} = 0$; (b) $e_{00} = 0.1$

solar aspect angle are taken. For e_{00} larger than this value, the orbit will always remain elliptic.

In conclusion, the results here are qualitatively consistent with those of the previous section with two differences: (i) absence of the slow clockwise precession of the polar plot; (ii) amplitude of variation in eccentricity does not depend on initial solar aspect angle.

2.6 Evaluation of the Shadow Effects

The existence of a shadow region, making the solar radiation forces vanish whenever the sun as seen from the satellite is eclipsed by the earth, presents a major obstacle for obtaining realistic long-term solutions for the orbital elements. It is generally assumed that the umbra and penumbra regions may well be replaced by an equivalent simple circular cylinder of radius R_e and axis along the sun-earth line. The space within this cylinder is taken to be completely dark with an abrupt transition to full illumination outside the shadow region. The points of entry and exit of the shadow cylinder satisfy a quartic equation in terms of the cosine of the true anomaly. In general, its solution is too unwieldy for practical use and numerical methods (e.g., successive substitution) is to be preferred. A few special cases exist, however, where the points of entry and exit appear in a more tractable form, e.g. when the

instantaneous orbit is circular or when the orbit lies in the ecliptic plane.

In the present section, the influence of the shadow upon both the short- and long-term results for the orbital elements derived in the previous sections for ecliptic orbits are determined. An interesting approximate relationship linking the small long-term variations in the semi-major axis to the behavior of the auxiliary element $y = e\cos(\eta - \omega)$ is established. While these analytical results match quite well with those found by repeated short-interval rectification and iteration over the first 100 revolutions, relatively large discrepancies arise for longer spans of time. These must be attributed to second-order effects. As to the behavior of the eccentricity, it is found that the no-shadow results are correct to at least two decimals over the first year.

2.6.1 Short-term shadow effects

In case of a prograde* orbit in the ecliptic plane, the points of entry (ν_1) and exit (ν_2) of the shadow cylinder are determined by the equations,

$$r(\nu_1)\sin(\nu_1 - \eta) = R_e \quad , \quad \eta + \pi/2 < \nu_1 < \eta + \pi \quad ,$$

$$r(\nu_2)\sin(\nu_2 - \eta) = -R_e \quad , \quad \eta + \pi < \nu_2 < \eta + 3\pi/2 \quad . \qquad .....(2.38)$$

---

* Prograde means that the motion of the satellite is in the same direction as that of the sun with respect to the earth.

Introduction of the shadow angles β_1 and β_2 (Figure 2-1) through $\beta_1 = \eta + \pi - \nu_1$ and $\beta_2 = \nu_2 - (\eta + \pi)$, and substitution of these angles into Equation (2.38) leads to two quadratic equations from which β_1 and β_2 can be expressed in terms of $\chi = \eta - \omega$ and $s = R_e/\ell$:

$$\beta_{1,2} = \arcsin \left\{ \frac{s(1 \pm es \sin\chi) - es\cos\chi\,(1 - s^2 \pm 2es\sin\chi + e^2s^2)^{1/2}}{1 \pm 2es\sin\chi + e^2 s^2} \right\} \qquad .....(2.39)$$

Note that for a circular orbit, this result simplifies to $\beta_1 = \beta_2 = \arcsin s$ and $\nu_{1,2} = \eta + \pi \mp \arcsin s$.

A first-order approximation for the changes in the orbital elements can be obtained by integration of the perturbation equations as in Section 2.3.1, while excluding the contributions over the shadow interval I_s. Only the resulting change in semi-major axis can be expressed in a tractable form in case of an orbit of arbitrary eccentricity:

$$\Delta a = 2\varepsilon a^2 \ell \left\{ (1 - s^2 + 2es\sin\chi + e^2s^2)^{1/2} - (1 - s^2 - 2es\sin\chi + e^2s^2)^{1/2} + e^2 s \sin 2\chi \right\} / (1 - e^2\cos^2\chi) \quad , \qquad .....(2.40)$$

where the integral over the full cycle $(0,2\pi)$ vanishes. The result indicates that the major axis remains unaffected when the sun lies on the major axis or the orbit is circular. Note that the change in the major axis is maximal for $\chi = \pm \pi/2$, i.e. when the radiation

is normal to the axis. For instance, taking $e = 0.1$, $a = 1$ and $\varepsilon = 0.0002$, it follows that Δa_{max} equals 1.2×10^{-5} amounting to 0.5 km and a change in the period of about 1.5 sec per revolution. In general, the major axis increases (decreases) if the point of entry is farther (closer) to the sun than the point of exit, which is evident from physical considerations. For small eccentricity, the results for the orbital elements p and q can be written explicitly:

$$\Delta p = -\varepsilon a^2 \sin\eta \left\{ 3\pi - C_s - 2es[(1 - s^2)\cos\chi + s^2 \sin\chi/\tan\eta] + O(e^2) \right\} ,$$

$$\Delta q = \varepsilon a^2 \cos\eta \left\{ 3\pi - C_s - 2es[(1 - s^2)\cos\chi - s^2 \sin\chi \tan\eta] + O(e^2) \right\} ,$$

$$\Delta a = 4\varepsilon a^3 es \sin\chi \left\{ 1/(1 - s^2)^{1/2} + e\cos\chi + O(e^2) \right\} , \qquad .....(2.41)$$

where the expansion of Equation (2.40) is also added. Note that the contribution represented by the factor 3π originates from the integration over the full cycle and the abbreviation C_s stands for $3 \arcsin(s) - s(1 - s^2)^{1/2}$. In case $e \neq 0$, the changes in eccentricity and argument of the perigee are obtained quite readily from Equations (2.41):

$$\Delta e = -\varepsilon a^2 \sin\chi \left\{ 3\pi - C_s - 2es\cos\chi + O(e^2) \right\} ,$$

$$e\Delta\omega = \varepsilon a^2 \cos\chi \left\{ 3\pi - C_s - 2es[(1 - s^2)\cos\chi + s^2 \sin\chi \tan\chi] + O(e^2) \right\} . \qquad .....(2.42)$$

It is interesting that for a circular orbit, the shadow effect upon the elements p, q, e and ω can be accounted for by simply multiplying the 'no-shadow' results by a factor $1 - C_s/(3\pi)$. For a geosynchronous orbit, this factor is approximately 0.97 so that the shadow effect reduces the 'no-shadow' perturbations in e and ω by about three percent.

2.6.2 Long-term shadow effects

The long-term implications of the shadow effects upon the orbital elements will be assessed both analytically (for near-circular orbits) and semi-analytically by numerical rectification and iteration of the short-term results. The interval before rectification is, usually, taken as $\pi/2$ and, for assessing the accuracy of the results, a few runs with an interval of $\pi/3$ are performed. Since the short-term (i.e., within one revolution) perturbations in the semi-major axis could be larger than the net long-term changes, care must be taken for proper separation of the latter effects from the former ones. The elements at $\nu_k = 2\pi k$, $k = 1,2,3,\cdots$ are taken as representative for the long-term trend. The upcoming points of entry and exit of the shadow region are reassessed after each interval by substituting the most recent orbital elements into Equations (2.39). It is estimated that a rectification interval of $\pi/2$ predicts the semi-major axis accurately to four decimal places and the elements e and ω to at least two decimals uniformly over a 400 day time-span. These accuracies were established by means of a comparison with results obtained by rectification after $\pi/3$ radians.

For near-circular orbits, it is possible to describe the long-term evolution of the orbital elements analytically by means of the two-variable expansion procedure. Provided the initial position of the sun is close to the perigee axis, the eccentricity will not become much greater than its initial value e_{00} and a general upper limit for $e_0(\bar{\nu})$ may be taken $e_{00} + 3c_\varepsilon a_{00}^{1/2}/(1 + 9a_{00}c_\varepsilon^2/4)$ regardless of η_{00}. These results have been established in the previous sections disregarding the shadow effects. Presuming that this influence does not affect the order of magnitude of the perturbations in eccentricity, the aforementioned value may be used for assessing whether the eccentricity will remain sufficiently small throughout or not. (This is mainly determined by e_{00} and the parameter $c_\varepsilon = \varepsilon/\delta$).

As in Section 2.4, the orbital elements (including η) are expanded in asymptotic series in ν and $\bar{\nu}$. While the zeroth-order results readily lead to $\underline{a}_0 = \underline{a}_0(\bar{\nu})$, the first-order equations can be written symbolically as

$$\frac{\partial \tilde{\underline{a}}_1}{\partial \nu} = -\frac{d\tilde{\underline{a}}_0}{d\bar{\nu}} + \tilde{\underline{F}}\,(\underline{a}_0, \nu) \quad ,$$

$$\frac{\partial \eta_1}{\partial \nu} = -\frac{d\eta_0}{d\bar{\nu}} + a_0^{3/2}/[c_\varepsilon(1 + p_0 \cos\nu + q_0 \sin\nu)^2] \quad , \quad .....(2.43)$$

where $\tilde{\underline{F}}$ equals $\tilde{\underline{f}}$ except in the interval $I_s(\bar{\nu})$ where $\tilde{\underline{F}}$ vanishes. In the present order of approximation, the shadow interval lies between

$$\nu_1(\underline{a}_0) = \pi + \eta_0 - \beta_1(\underline{a}_0) ,$$

and

$$\nu_2(\underline{a}_0) = \pi + \eta_0 + \beta_2(a_0) .$$

The slowly varying shadow angles $\beta_1(\underline{a}_0)$ and $\beta_2(\underline{a}_0)$ are identical in structure as in Equation (2.39) except for the fact that e, s and χ are now all dependent upon $\bar{\nu}$. The vector-function $\underline{\tilde{F}}(\underline{a}_0,\nu)$, though discontinuous, is 2π-periodic in the fast variable ν and can, in principle at least, be expanded in Fourier series with coefficients depending on the slow variable $\bar{\nu}$. In practice, however, these series converge much slower than those for the corresponding continuous vector-function $\underline{f}(\underline{a}_0,\nu)$ discussed in Section 2.4. Nevertheless, representative trends are illustrated by the zeroth-order solutions. The requirement that first-order terms $\underline{a}_1$ remain bounded in the variable ν, leads to the following constraints (Equations 2.43),

$$\underline{\tilde{a}}_0'(\bar{\nu}) = \int_{2\pi-I_s} \underline{\tilde{F}}\,[\underline{a}_0(\bar{\nu}),\, \tau]\, d\tau / (2\pi) \quad , \qquad .....(2.44)$$

$$\eta_0'(\bar{\nu}) = a_0^{3/2}\,(\bar{\nu}) \,/\, c_\varepsilon \quad .$$

Performing the integrations, a set of coupled differential equations in terms of a_0, p_0 and q_0 is obtained. This system can readily be reduced to the following set of equations in a_0, $x_0 = e_0 \sin\chi_0$ and $y_0 = e_0 \cos\chi_0$:

$$a_0'(\bar{\nu}) = 2R_e a_0^2 x_0/\pi \, [a_0 + y_0(a_0^2 - R_e^2)^{1/2}]/(a_0^2 - R_e^2)^{1/2} + O(e_0^3) \quad ,$$

$$x'_0(\bar{\nu}) = y_0 a_0^{3/2} / c_\varepsilon - 3a_0^2 \, [\pi - \arcsin(R_e/a_0)]/(2\pi)$$

$$-R_e(a_0^2 - R_e^2)^{1/2}/(2\pi) + R_e(a_0^2 - R_e^2)y_0/(\pi a_0) + O(e_0^2) \quad ,$$

$$y_0'(\bar{\nu}) = - x_0 a_0^{3/2} / c_\varepsilon + R_e^3 x_0 /(\pi a_0) + O(e_0^2) \quad , \qquad .....(2.45)$$

for uniformly small eccentricity. As mentioned before, the maximum eccentricity will be of the order c_ε for a near-circular initial orbit. For consistency, terms of the order $c_\varepsilon e_0$ and c_ε^2 must be treated as e_0^2. The following expression for $a_0(\bar{\nu})$ is obtained from Equations (2.45) when terms of the orders e_0^3, $(R_e/a_{00})^4$ and higher are ignored:

$$a_0(\bar{\nu}) = a_{00} - R_e c_\varepsilon \, a_{00}^{1/2} \, (2 + R_e^2/a_{00}^2)[y_0(\bar{\nu}) - y_{00}]/\pi \quad . .....(2.46)$$

Utilizing this result, the equations for x_0 and y_0 can be written as

$$c_\varepsilon y_0''(\bar{\nu}) + a_{00}^3 y_0(\bar{\nu})/c_\varepsilon = 3a_{00}^{7/2} / 2 - R_e a_{00}^{5/2} \, [1 + y_0(\bar{\nu})]/\pi \quad ,$$

$$x_0(\bar{\nu}) = - y_0'(\bar{\nu}) / c \quad , \qquad .....(2.47)$$

where terms of order e_0^2 and $(R_e/a_{00})^3$ have been neglected. These

equations are solved readily ,

$$y_0(\bar{\nu}) = c_\varepsilon\, a_{00}^{1/2}\,[3/2 - R_e/(\pi a_{00})][1 - \cos(\Omega_1\bar{\nu})] + y_{00}\cos[\Omega_1\bar{\nu}) - x_{00}\sin(\Omega_1\bar{\nu}) \quad ,$$

$$x_0(\bar{\nu}) = \left\{ y_{00} - c_\varepsilon\, a_{00}^{1/2}\,[3/2 - R_e/(\pi a_{00})] \right\} \sin(\Omega_1\bar{\nu}) + x_{00}\cos(\Omega_1\bar{\nu}) \quad , \qquad .....(2.48)$$

showing that y_0 and x_0 are periodic with a slightly modified frequency as compared to the no-shadow case. The parameter Ω_1 stands for:

$$\Omega_1 = a_{00}^{3/2}\,[1 + R_e\, c_\varepsilon/(\pi a_{00}^{1/2})]^{1/2} / c_\varepsilon \quad . \qquad .....(2.49)$$

It has been checked that the solutions of Equations (2.46) and (2.48) after substitution of $R_e = 0$ are identical to the expansions for small e_0 of the long-term no-shadow solutions of Section 2.4.1.

2.6.3 Discussion of results

The validity of the approximate long-term analytical solution has been assessed by comparing the results with those from repeated

rectification and iteration of the first-order short-term solutions. Figure 2-12 shows the comparison for a satellite with $\varepsilon = 0.0002$ in a geosynchronous orbit with initial eccentricity of 0.1 and solar aspect angle $\eta_{00} = \pi/2$ over a 400 day time-span. The solid line represents the most accurate result obtained by rectification after not more than $\pi/3$ radians where all orbital elements, the solar aspect angle as well as the next point of entry of the shadow region are reassessed. By taking larger intervals before rectification, the maximum discrepancy in semi-major axis compared to the solid line is found to be 2×10^{-4} for an interval of π and 5×10^{-5} for an interval of $\pi/2$ (not shown) over a 400 day period. Also shown in Figure 2-12a is the result obtained by rectification after a full revolution (2π). The difference between this and the aforementioned approximations is quite notable and must be attributed to the fact that second-order contributions are not picked up in this case. The importance of higher-order terms may be evaluated by considering the no-shadow situation, where in the first-order theory, the semi-major axis returns to its original value after one complete cycle. Precise numerical integration, however, reveals variations in the semi-major axis up to an amplitude of almost 10^{-3} in the long run due to higher order influences (Figure 2-6). When the effect of the shadow is incorporated in the analysis, the first-order changes in semi-major axis are caused by a difference in the distance of the points of entry and exit with respect to the sun. The change in semi-major

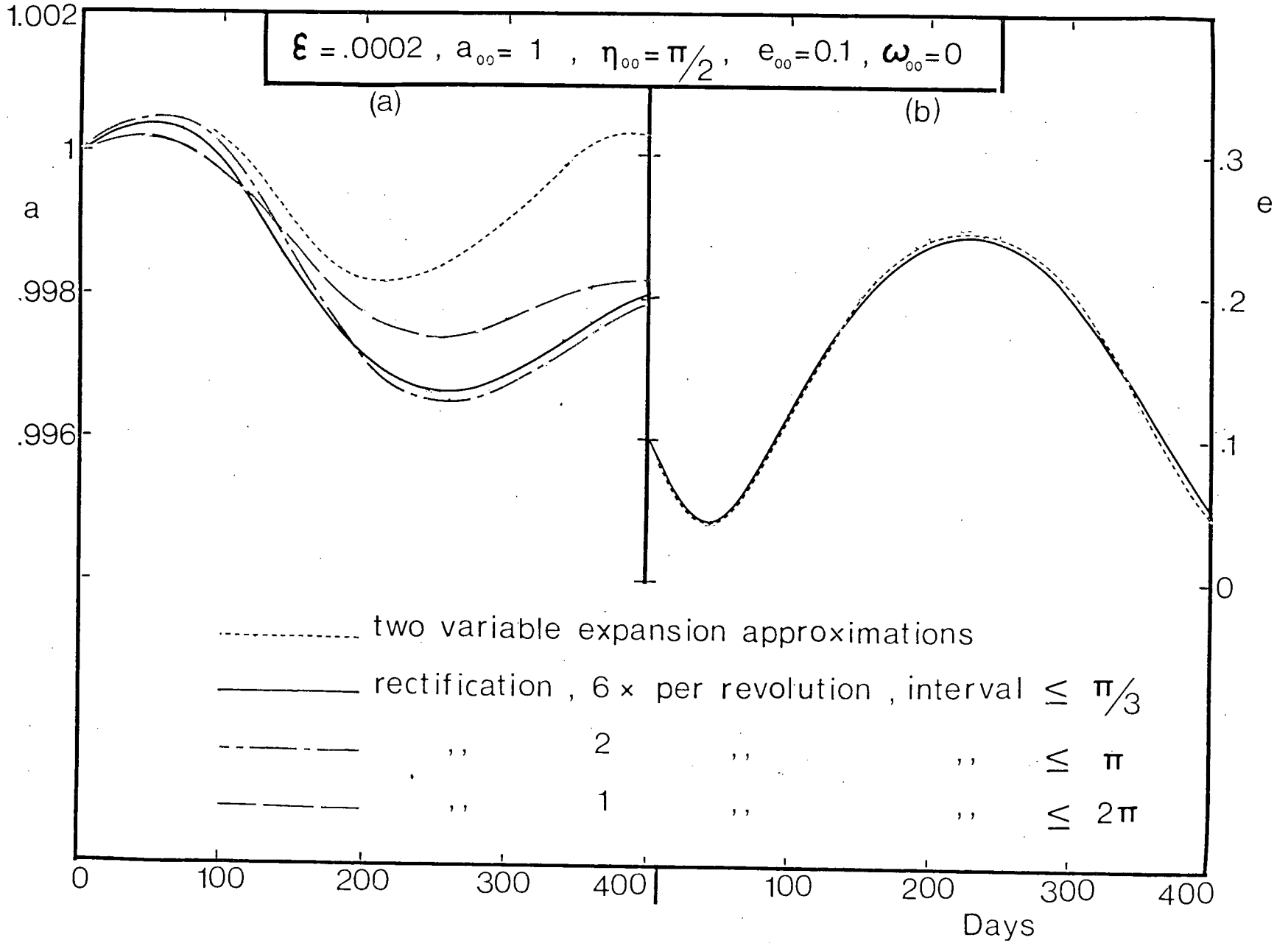

Figure 2-12 Comparison of the analytical long-term approximate solutions for the shadow effects upon: (a) semi-major axis; (b) eccentricity

axis over one revolution amounts to approximately $4 \varepsilon e R_e a^2 \sin\chi$ (Equations 2.41). Since R_e and e are small and e as well as $\sin\chi$ are often oscillatory in the long run, it is not surprising that the total of the higher-order effects (enhanced by the addition of 'interrupted' periodic terms) can build up to and even exceed the magnitude of the first-order shadow effect.

The dotted curve in Figure 2-12a represents the long-term approximate analytical solution $a_0(\bar{\nu})$ of Equation (2.46). Since only the first-order shadow effect is incorporated in this solution, it is evident that it is closer to the 2π-rectification approximation than to the actual solution. Nevertheless, the analytical solution provides a reasonable prediction for the behavior of the semi-major axis over the first half year.

The main objective in determining the perturbations of the semi-major axis is to evaluate changes in the orbital period which is of interest for assessing the drift in the overhead position of the satellite. A change in the semi-major axis of 0.002 (after about 200 days) translates to a change in the orbital period of more than four minutes and a drift in overhead position of 120 km per revolution at geo-synchronous altitude. Figure 2-12b shows the comparison for the eccentricity in the same circumstances. In contrast to the behavior of the semi-major axis, the eccentricity exhibits fairly large perturbations in the first-order 'no-shadow theory' so that in comparison the shadow affects the resulting perturbations only in a minor way (due to the factor $1 - C_s/(3\pi)$ in the short-term Equations 2.41). Comparing the results

with those obtained by neglecting the shadow effect, it is found that, in the case of eccentricity, the influence of the shadow does not show up in the first two decimal places over a 400 day time-span. Nevertheless, its effect is more dominant than that of the higher-order terms in eccentricity which are not felt up to three decimal places over 1200 days.

When studying the observed perigee distances and orbital periods of the Echo I, Pageos and 1963-30D satellites, Meeus[49] conjectured the following rule: "The orbital period (and thus also the semi-major axis) diminishes when the orbit becomes more eccentric and increases when the eccentricity is decreasing." The results depicted in Figure 2-12 seem to obey this rule quite well. However, from Equations (2.46) a slightly modified rule can be formulated: "the changes in the major axis due to the shadow effect are proportional to the behavior of the slowly varying function $-e\cos(\eta - \omega)$." In the case where the major axis follows the sun's motion, which happens if e_{00} is sufficiently small and the initial solar aspect angle is close to the perigee axis, $\eta - \omega$ will be nearly constant and the two rules are consistent.

2.7 Concluding Remarks

The important conclusions of the present chapter may be summarized as follows:

(i) Considering a satellite in the ecliptic plane and taking the solar radiation force along the direction of radiation, both short and long-term valid approximations for the orbital elements are derived using a straightforward and a two-variable perturbation method, respectively.

(ii) The two-variable expansion procedure is found convenient for deriving closed-form analytical results for the long-term orbital perturbations. The accuracy of the zeroth-order solutions compares favorably with those obtained by repeated rectification of the short-term solutions. Numerical results successfully assess their relative accuracies.

(iii) The results show that the variations in eccentricity and semi-latus rectum are periodic, while the argument of the perigee may show a secular trend in certain cases. The semi-major axis remains constant in the first-order.

(iv) Polar plots provide an attractive and concise visualization of the long-term orbital perturbations. Loci of initial conditions resulting in specified extremes of eccentricity should prove useful in preliminary mission studies.

(v) The effect of the shadow both in the short-term and the long-term context has been assessed. It induces small first-order changes in the semi-major axis, while affecting

the already large variations in eccentricity only in a minor way.

(vi) An analytical approximation for the long-term behavior of the major axis is derived for near-circular orbits using the two-variable expansion procedure. Unfortunately, its accuracy degenerates after about half a year due to the build-up of second-order effects.

(vii) A simple rule linking the long-term perturbations in the semi-major axis to a function depending on eccentricity, solar aspect angle and argument of the perigee is established, which may be useful for estimating changes in the orbital period. This rule appears to be consistent with the observed satellite motion.

3. SOLAR RADIATION INDUCED PERTURBATIONS OF AN ARBITRARY GEOCENTRIC ORBIT

The analysis of the previous chapter is now extended to satellites in an arbitrary orbital plane. Another generalization concerns the direction of the solar radiation force: whereas, up to now, this force was taken along the direction of the radiation, in later sections of this chapter, more general configurations are studied, e.g. spacecrafts modelled as a plate in an arbitrary, fixed orientation with respect to the local reference frame. Also the orbital behavior of a satellite in an arbitrary fixed orientation to the radiation or inertial space is explored. The latter situations are of considerable practical interest since they serve as accurate models for satellites with solar arrays (e.g., CTS and SSPS) and instrumentation for deep-space studies (e.g., orbiting telescope). Finally, the analysis is extended to an arbitrarily shaped satellite which may require a number of flat plates for accurate modelling.

3.1 Derivation of the Perturbation Equations

A researcher in orbital mechanics finds himself surrounded by a multitude of procedures for analyzing perturbations of trajectories. Most of these methods originate with the great mathematicians of the last two centuries like Lagrange, Delaunay, Gauss and Hansen in their

analyses of planetary motion. The 'space age' has produced many new and revised techniques for dealing with situations not previously encountered, e.g. air drag. The choice of a particular formulation depends upon the specific nature and objective of the work, the perturbation forces involved and the availability of a digital computer as well as personal preferences. In the present case, a formulation is desired which is suitable for solar radiation forces, remains valid for all eccentricities and inclinations, is conducive to geometrical interpretation and, moreover, is capable of producing closed-form long-term solutions or short-term results fit for rectification and iteration. Probably the most popular approach is the one based on Lagrange's planetary equations using an anomaly, referred to the osculating ellipse, as independent variable. These equations contain singularities for $e = 0$ and $i = 0$, which can be removed by suitable transformations. Unfortunately, the equations rarely yield closed-form solutions for an orbit of arbitrary eccentricity due to the intricate coupling of the motion of the orbital plane (described by i and Ω) and the in-plane perturbations (ℓ, e, ω).

In his search for an effective algorithm for computing (manually!) planetary ephemerides, Hansen in the previous century employed a frame of 'ideal' coordinate axes fixed to the instantaneous orbital plane[127]. The in-plane equations of perturbed motion in this frame take on a form, identical to the equations for planar perturbations alone, thereby effecting an uncoupling of the motion

in the osculating plane from the out-of-plane orbital changes. This approach retains some of the desirable features, like easy geometric visualization, inherent in the osculating elements. Furthermore, a uniquely qualified candidate to serve as independent variable emerges in a natural manner.

In order to convey a physical appreciation for the qualitative effects of the components of the solar radiation force, a simple direct derivation of the perturbation equations based on Newton's second law is presented. These equations can also be obtained from Lagrange's planetary equations by introduction of new variables and algebraic manipulations.

The motion of a satellite in the inertial X,Y,Z frame, Figure 3-1, under the influence of gravitational attraction of the primary (having radially symmetric mass distribution) and an arbitrary perturbation force $\underline{F}$ can be described by Newton's second law (in nondimensional form):

$$\ddot{\underline{r}} + \underline{r} / r^3 = \underline{F} \quad , \qquad \text{.....(3.1)}$$

where the radius vector $\underline{r}(t)$ denotes the position of the satellite measured from the origin at the center of the primary. It is well-known that in absence of perturbation forces, i.e. when $\underline{F} = \underline{0}$, the resulting motion of the satellite $\underline{r}(t)$ describes a conic section in a fixed plane formed by the initial position $\underline{r}(0)$ and velocity

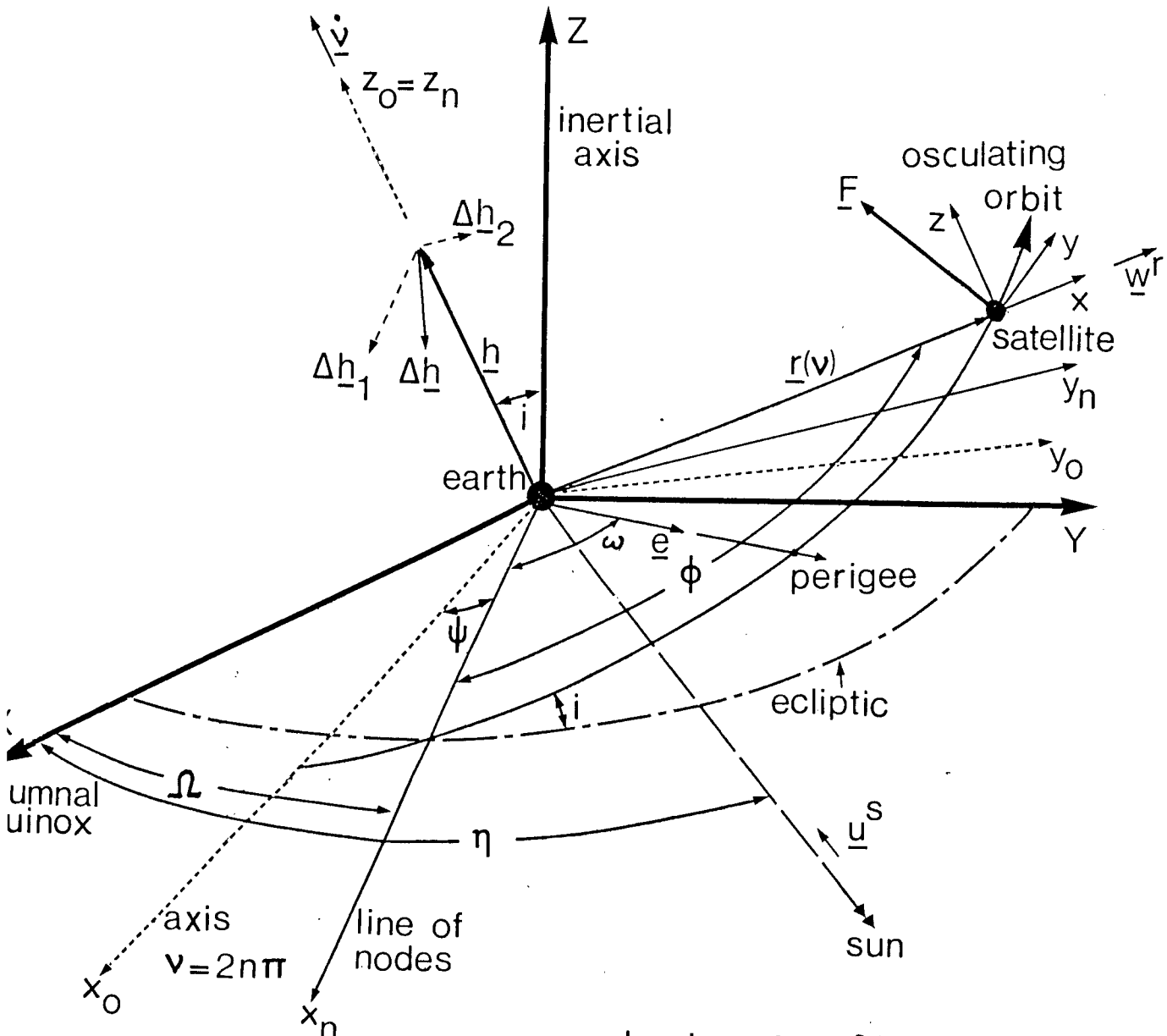

Figure 3-1 General three-dimensional configuration of the earth, satellite and the sun

vector $\dot{\underline{r}}(0)$. The five elements a, e, ω, Ω and i are constants determined by the initial conditions, and the true anomaly θ is implicitly related to time through Kepler's equation. To study effects of the perturbation force $\underline{F}$, a moving local frame of reference x,y,z is introduced, Figure 3-1. At each instant, the x axis points along the radial direction, the y axis lies in the orbital plane such that the velocity vector has a positive component along this axis, and the z axis is normal to the osculating plane. The force $\underline{F}$ is expanded in components (F_x, F_y, F_z) along the local reference frame. The influence of F_x and F_y is limited to an in-plane rate of change in velocity and leaves the orientation of the orbital plane unaffected, while F_z causes an out-of-plane rotation of the velocity vector without affecting its magnitude. The component F_z generates a torque $\underline{r} \times F_z\underline{k} = -rF_z\underline{j}$ along the negative y axis causing the vector $\underline{h}$ to rotate in the y,z plane with instantaneous angular rate $\underline{w}^r = (rF_z/h)\underline{i}$ along the x axis. Thus, the effect of F_z is interpreted as imparting a rotation $\underline{w}^r$ of the orbital plane about the instantaneous radial direction (gyroscopic effect).

The motion of the local x,y,z frame in the inertial X,Y,Z frame is completely described by the sum, $\underline{W}$, of the angular rates $\underline{w}^r$ and $\dot{\underline{\nu}}$, where $\dot{\underline{\nu}}$ points along the instantaneous z axis and represents the rotation of the radius vector in the osculating plane. It must be emphasized that the angle ν is measured from a fixed axis in the instantaneous orbital plane indicated by x_0, Figure 3-1. The angular

momentum vector $\underline{h}$, defined by $\underline{r} \times \underline{v}$, is equal to $\underline{r} \times (\underline{W} \times \underline{r}) = r^2 \dot{\nu} \underline{k}$, which is, interestingly, of the same form as that for the planar perturbations.

The motion of the x,y,z frame can also be described in terms of the Eulerian angles Ω, i and ϕ. The precession $\dot{\underline{\Omega}}$ is taken along the inertial Z-axis, the nutation $(\underline{i})^{\cdot}$ along the line of nodes, i.e. the intersection of the osculating and the X,Y planes, and the spin $\dot{\phi}$ along the z axis. A comparison of the components of the angular velocities along the x,y,z axes leads to:

$$W_x = rF_z/h = (i)^{\cdot} \cos\phi + \dot{\Omega} \sin i \cos\phi \quad ;$$

$$W_y = 0 \quad = (i)^{\cdot} \sin\phi - \dot{\Omega} \sin i \cos\phi \quad ;$$

$$W_z = \dot{\nu} = h/r^2 = \dot{\phi} + \dot{\Omega} \cos i \quad . \qquad \ldots\ldots(3.2)$$

The first two equations yield the standard Lagrange's perturbation equations for the orientation of the orbital plane:

$$(i)^{\cdot} = r F_z \cos\phi / h \quad ;$$

$$\dot{\Omega} = r F_z \sin\phi / (h \sin i) \quad . \qquad \ldots\ldots(3.3)$$

Taking into account the motion of the x,y,z frame, described by the rotation vector $\underline{W}$, with respect to inertial space, the components of Newton's law along the local x,y, and z axes become:

$$\ddot{r} - r\dot{\nu}^2 + 1/r^2 = F_x \quad ;$$

$$r\ddot{\nu} + 2\dot{r}\dot{\nu} = F_y \quad ;$$

$$r\dot{\nu} W_x = F_z \quad . \qquad \text{.....(3.4)}$$

Note that the first two equations do not contain the out-of-plane component of the perturbation force F_z. It is natural to employ the quasi-angle ν as independent variable since $\dot{\nu} = h/r^2$ is free of any out-of-plane elements. Using the transformation $u = 1/r$ as in the previous chapter and rewriting the out-of-plane Equations (3.3) in terms of the angle ν leads to the following complete system of equations:

$$u''(\nu) + u(\nu) = 1/\ell - (F_x + F_y\, u'/u)/(u^2\ell) \quad ;$$

$$\ell'(\nu) = 2\,F_y / u^3 \quad ;$$

$$i'(\nu) = F_z \cos(\nu - \psi) / (\ell u^3) \quad ;$$

$$\Omega'(\nu) = F_z \sin(\nu - \psi) / (\ell u^3 \sin i) \quad ;$$

$$\psi'(\nu) = \Omega' \cos i \quad ;$$

$$t'(\nu) = 1 / (u^2 \ell^{1/2}) \quad , \qquad \text{.....(3.5)}$$

where $\psi \equiv \nu - \phi$. It may be noted that the role of angular momentum is taken over by the semi-latus rectum $\ell = h^2$. The elements ℓ, i and Ω

correspond to Lagrange's osculating elements and can be interpreted as such. As in the planar case, u is written as $(1 + p\cos\nu + q\sin\nu)/\ell$ where p, q and ℓ are slowly varying osculating elements. The dependence of ℓ upon ν is given in the second relation of Equations (3.5) while the condition of osculation, i.e., $u'(\nu) = (-p\sin\nu + q\cos\nu)/\ell$, leads to a set of first-order equations for $p(\nu)$ and $q(\nu)$ replacing the equation for u'' in Equations (3.5),

$$p'(\nu) = \left\{(F_x - F_y u'/u)\sin\nu + 2F_y\cos\nu\right\}/u^2 \quad ,$$

$$q'(\nu) = \left\{-(F_x - F_y\, u'/u)\cos\nu + 2F_y\sin\nu\right\}/u^2 \quad , \quad .....(3.6)$$

with u and u' to be expressed in terms of p, q, ℓ and ν. The usual form $u = (1 + e\cos\theta)/\ell$, where θ is the true anomaly, is retained since $\theta = \phi - \omega = \nu - \tilde{\omega}$ with $\tilde{\omega}$ denoting $\omega + \psi$. It can now be seen that $p = e\cos\tilde{\omega}$ and $q = e\sin\tilde{\omega}$. (Note that for an ecliptic orbit ($i = 0$), there is no distinction between ω and $\tilde{\omega}$ nor between ϕ and ν.) Consequently, the familiar orbital elements e and ω can be derived readily from the formulation above: $e = (p^2 + q^2)^{1/2}$ and $\omega = \arctan(q/p) - \psi$. The auxiliary orbital elements p and q can be interpreted geometrically as the projections of the eccentricity vector $\underline{e}$ (pointing towards the instantaneous perigee position) upon the x_0 and y_0 coordinate axes, Figure 3-1.

3.2 Determination of the Solar Radiation Force

The perturbation force $\underline{F}$ with its components F_x, F_y and F_z along the local frame of reference is evaluated next for a fairly general satellite configuration consisting of n components. Each of these has its own material properties σ_{1k}, σ_{2k}, ρ_k, k=1,2,...,n defined in Equations (2.2), its orientation designated by the normal $\underline{u}_k^n$ and an effective flat surface area A_k. A curved surface component may be replaced by an equivalent flat area with material characteristics determined by integration. The total (nondimensional) solar radiation force acting upon the satellite becomes (Equation 2.1):

$$\underline{F} = \varepsilon \sum_{k=1}^{n} |\underline{u}_k^n \cdot \underline{u}^s| \left\{ \sigma_{1k} \underline{u}^s + [\sigma_{2k} + \rho_k (\underline{u}_k^n \cdot \underline{u}^s)] \underline{u}_k^n \right\} A_k \quad . \qquad .....(3.7)$$

Two Eulerian rotations α_k and β_k are sufficient to describe an arbitrary spatial orientation of the surface element A_k with respect to the osculating plane, Figure 3-2b. The normal $\underline{u}_k^n$ points along the negative x axis when $\alpha_k = \beta_k = 0$. The rotation α_k about the z axis takes A_k to the required line of intersection with the orbital plane and, subsequently, β_k along the y_1 axis adjusts the surface element A_k to the desired inclination with the orbital plane so that $\underline{u}_k^n$ points along the x_2 axis. The components of the vectors $\underline{u}_k^n$ in the x,y,z frame are written symbolically as $\underline{u}_k^n = u_{kx}^n \underline{i} + u_{ky}^n \underline{j} + u_{kz}^n \underline{k}$. Also the direction of the radiation $\underline{u}^s$ is expanded along the local coordinate frame:

$$\underline{u}^s = u_x^s(\nu)\, \underline{i} + u_y^s(\nu)\, \underline{j} + u_z^s(\nu)\, \underline{k} .$$

The components of the solar radiation force can now be written as

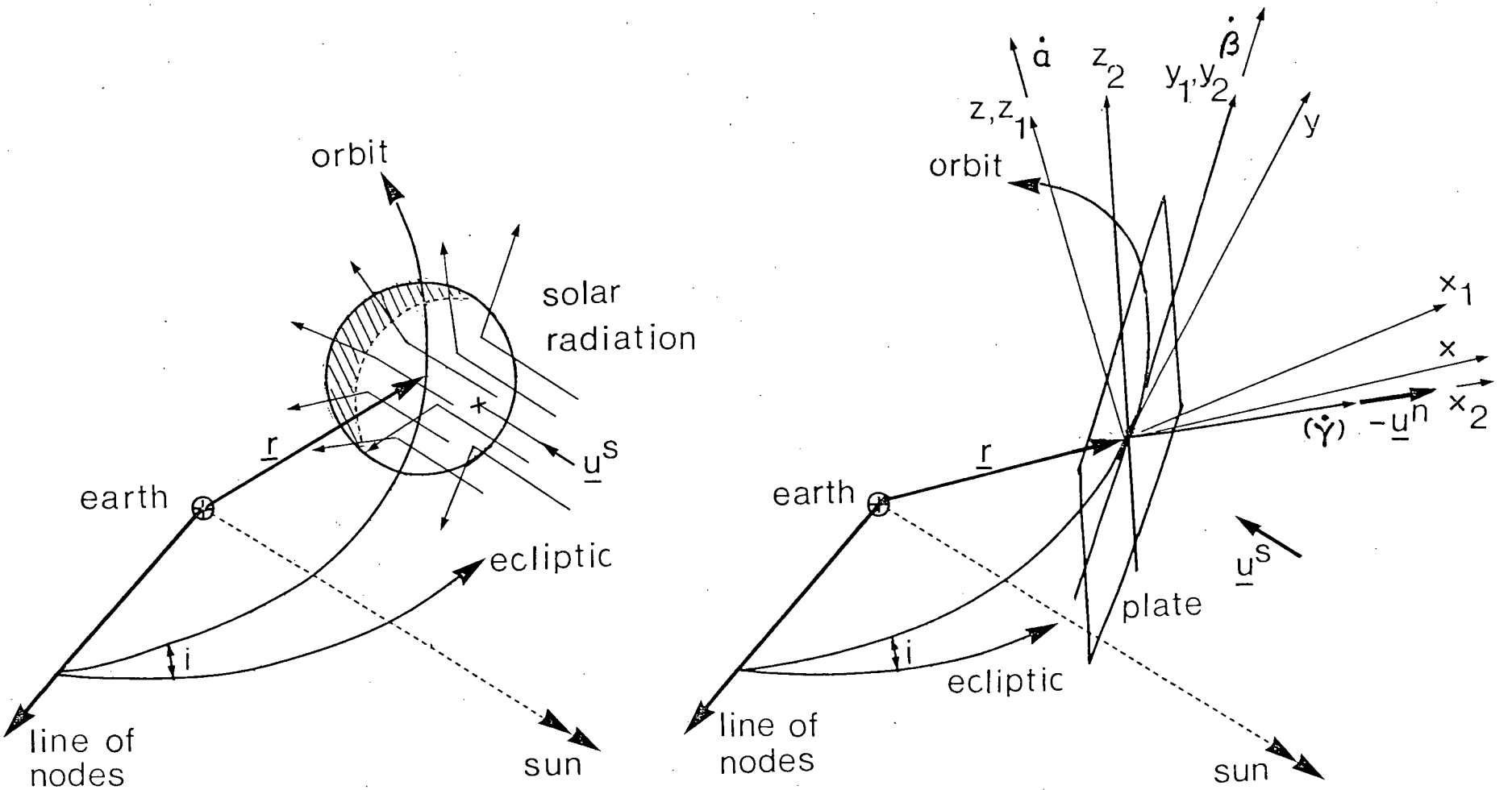

Figure 3-2 Idealized satellite configurations:

(a) sphere
(b) flat plate or surface component in arbitrary orientation to orbital plane

$$F_x = \varepsilon \sum_{k=1}^{n} |U_k| \left\{ \sigma_{1k}\, u_x^s + [\sigma_{2k} + \rho_k U_k]\, u_{kx}^n \right\} A_k \quad ,$$

$$F_y = \varepsilon \sum_{k=1}^{n} |U_k| \left\{ \sigma_{1k}\, u_y^s + [\sigma_{2k} + \rho_k U_k]\, u_{ky}^n \right\} A_k \quad ,$$

$$F_z = \varepsilon \sum_{k=1}^{n} |U_k| \left\{ \sigma_{1k}\, u_z^s + [\sigma_{2k} + \rho_k U_k]\, u_{kz}^n \right\} A_k \quad , \qquad .....(3.8)$$

where A_k has been nondimensionalized by A, the sum of all surface elements illuminated by the sun, and U_k denotes the dot-product $(\underline{u}_k^n \cdot \underline{u}^s)$. It should be noted that, in general, $\underline{u}_k^n$ are functions of ν since the satellite may experience librational motion in the local reference frame.

3.3 Plate Normal to Radiation

In many present and proposed applications, large solar panels are employed for power production either for on-board requirements (e.g. SEPS) or for external needs (e.g. SSPS). The efficiency in terms of power production per unit area of solar cells will be largest if the panels are kept normal to the radiation. This orientation is achieved when $\underline{u}^n = \underline{u}^s$ or in terms of the Eulerian control angles α and β :

$$\alpha(\nu) = -\nu + \psi + \arctan\,[\cos i \tan \hat{\eta}] \quad ,$$

$$\beta = \arcsin\,[\sin i \sin \hat{\eta}] \quad , \qquad .....(3.9)$$

where the modified solar aspect angle $\hat{\eta}$ stands for $\eta - \Omega$. The resulting radiation force becomes $\underline{F} = \varepsilon \underline{u}^S$ for this case (taking $\sigma = 1$). As mentioned before, this model can also serve for calculating perturbations of a spherical satellite with homogeneous surface properties, Figure 3-2a. Since the perturbation equations are written in terms of the independent variable ν, the explicit dependence of the components of $\underline{F}$ and thus $\underline{u}^S$ upon ν is needed:

$$u_x^S(\nu) = -[\cos^2(i/2)\cos(\nu - \psi - \hat{\eta}) + \sin^2(i/2)\cos(\nu - \psi + \hat{\eta})] \quad ;$$

$$u_y^S(\nu) = \cos^2(i/2)\sin(\nu - \psi - \hat{\eta}) + \sin^2(i/2)\sin(\nu - \psi - \hat{\eta}) \quad ;$$

$$u_z^S = \sin i \sin \hat{\eta} \quad . \qquad .....(3.10)$$

The complete set of equations, including the motion of the sun (represented by the angular rate δ) can be found from the preliminaries in Section 3.1:

$$\ell'(\nu) = 2\varepsilon r^3 u_y^S \quad ;$$

$$p'(\nu) = \varepsilon r^2 \{u_x^S \sin\nu + u_y^S [\cos\nu + (p + \cos\nu)\, r/\ell]\} \quad ;$$

$$q'(\nu) = \varepsilon r^2 \{-u_x^s \cos\nu + u_y^s [\sin\nu + (q + \sin\nu)\, r/\ell]\} \;;$$

$$i'(\nu) = \varepsilon r^3 u_z^s \cos(\nu - \psi)/\ell \;;$$

$$\Omega'(\nu) = \varepsilon r^3 u_z^s \sin(\nu - \psi)/(\ell \sin i) \;;$$

$$\psi'(\nu) = \Omega'(\nu) \cos i \;;$$

$$\eta'(\nu) = \delta r^2 / \ell^{1/2} \;. \qquad \text{.....(3.11)}$$

Here the radius r stands for $r(\nu) = \ell/(1 + p\cos\nu + q\sin\nu)$. It must be emphasized that the singularities in the equations for Ω and ψ for $i = 0$ cancel out since u_z^s also contains a term $\sin i$. In this chapter ε will be taken of the same order of magnitude as δ and the system of Equations (3.11) will be referred to as $\underline{a}'(\nu) = \varepsilon \underline{f}(\underline{a},\nu)$.

3.3.1 Short-term analysis

As in Section 2.3.1 for the ecliptic case, initially valid approximations can be obtained by expanding the elements in simple perturbation series, Equation (2.8). After substitution of these series into the system of Equations (3.11) it follows that $\underline{a}_0(\nu) = \underline{a}_{00}$ and the following first-order results are found upon integration:

$$\ell_1(\nu) = 2\ell_{00}^3 \{K_{10}B_{31}(\nu) - K_{20}A_{31}(\nu)\} \quad ;$$

$$p_1(\nu) = \ell_{00}^2\{K_{10}[p_{00}B_{31}(\nu) + B_{32}(\nu)/2] - K_{20}[A_{20}(\nu)$$

$$+ p_{00}A_{31}(\nu) + A_{30}(\nu)/2 + A_{32}(\nu)/2]\} \quad ;$$

$$q_1(\nu) = \ell_{00}^2\{K_{10}[A_{20}(\nu) + q_{00}B_{31}(\nu) + A_{30}(\nu)/2 - A_{32}(\nu)/2]$$

$$- K_{20}[q_{00}A_{31}(\nu) + B_{32}(\nu)/2]\} \quad ;$$

$$i_1(\nu) = \ell_{00}^2 \sin i_{00} \sin \hat{\eta}_{00} [A_{31}(\nu)\cos \psi_{00} + B_{31}(\nu)\sin \psi_{00}] \quad ;$$

$$\Omega_1(\nu) = \ell_{00}^2 \sin \hat{\eta}_{00}[B_{31}(\nu)\cos \psi_{00} - A_{31}(\nu)\sin \psi_{00}] \quad ;$$

$$\psi_1(\nu) = \Omega_1(\nu) \cos i_{00} \quad ;$$

$$\eta_1(\nu) = \ell_{00}^{3/2} A_{20}(\nu) / c_\varepsilon \quad . \qquad .....(3.12)$$

Here the auxiliary constants K_{10} and K_{20} depend upon $\hat{\eta}_{00}$, i_{00}, ψ_{00} and the integrals $A_{nk}(\nu)$ and $B_{nk}(\nu)$ contain p_{00} and q_{00}. The similarity between the results for p_1, q_1, ℓ_1, and η_1 found here and the corresponding results of the previous chapter (Equations 2.9) is evident, hence the explicit results of Equations (2.10) for the in-plane

perturbations remain valid here provided $\cos \eta_{00}$ and $\sin \eta_{00}$ are replaced by K_{10} and K_{20}, respectively. Of special importance are the results for $\nu = 2\pi$ where the short-period terms vanish; they may serve as a basis for obtaining long-term valid solutions. As in the planar case, it follows that $\Delta a = 0$, so that the major axis remains constant in the long run. Similarly, the remaining independent elements can be written as:

$$\Delta e = -3\pi\varepsilon\, a_{00}^2 (1 - e_{00}^2)^{1/2} (p_{00}K_{20} - q_{00}K_{10}) / e_{00} \quad ;$$

$$\Delta \omega = 3\pi\varepsilon\, a_{00}^2 (1 - e_{00}^2)^{1/2} (p_{00}K_{10} + q_{00}K_{20}) / e_{00}^2 - \cos i_{00}\ \Delta\Omega \ ;$$

$$\Delta i = -3\pi\varepsilon\, e_{00} a_{00}^2 \sin \hat{\eta}_{00} \cos \omega_{00} / (1 - e_{00}^2)^{1/2} \quad ;$$

$$\Delta\Omega = -3\pi\varepsilon\, e_{00} a_{00}^2 \sin \hat{\eta}_{00} \sin \omega_{00} / (1 - e_{00}^2)^{1/2} \quad ;$$

$$\Delta t = 3\pi\varepsilon\, a_{00}^{7/2} \left\{(4 + p_{00})K_{10} + 6q_{00}K_{20}\right\} + O(e_{00}^2) \quad . \qquad .....(3.13)$$

It may be noted that the result for Δt can be used for calculating the change in overhead position of a communications satellite after one revolution: e.g., for CTS ($\varepsilon = 1.37 \times 10^{-6}$) it follows that the satellite may drift as much as 330 meters per day. Note also that the possible existence of a shadow region is overlooked here. For a geosynchronous equatorial orbit, there is no eclipse by the earth during about 9 months of the year. Only when the sun is near one of

the equinox positions will there be a shadow interval with duration varying from a maximum of 70 minutes when the sun is on the equinox axis to zero about 22 days before and after that epoch. It should be emphasized that the effect of the earth's shadow upon an equatorial satellite is, quantitatively, less pronounced than that for a space probe in the ecliptic plane analyzed in the previous chapter. Points of entry into and exit from the shadow region as well as their long-term effects upon the orbital elements can best be studied numerically for this arbitrary case.

3.3.2 Long-term approximations

As in the previous chapter, Section 2.3.2, long-term results can be derived from the short-term analysis by repeated rectification and iteration of the initial conditions. This approach has indeed been followed in the present case and the results will be discussed in the next section. Here, analytical closed-form approximate solutions are explored by means of the two-variable expansion method. Following the procedure outlined in Section 2.4.1, the equations for the zeroth-order approximations become:

$$\ell_0'(\bar{\nu}) = \ell_0^3 \left\{ K_1 B_{31}(2\pi) - K_2 A_{31}(2\pi) \right\} / \pi \quad ;$$

$$p_0'(\bar{\nu}) = \ell_0^2 \left\{ K_1 [p_0 B_{31}(2\pi) + B_{32}(2\pi)/2] - K_2 [A_{20}(2\pi) + p_0 A_{31}(2\pi) + A_{30}(2\pi)/2 + A_{32}(2\pi)/2] \right\} / (2\pi) \quad ;$$

$$q_0'(\bar{\nu}) = \ell_0^2 \left\{ K_1[A_{20}(2\pi) + q_0 B_{31}(2\pi) + A_{30}(2\pi)/2 - A_{32}(2\pi)/2] \right.$$

$$\left. - K_2[q_0 A_{31}(2\pi) + B_{32}(2\pi)/2] \right\} / (2\pi) \quad ;$$

$$i_0'(\bar{\nu}) = \ell_0^2 \sin i_0 \sin \hat{\eta}_0 [A_{31}(2\pi) \cos \psi_0 + B_{31}(2\pi) \sin \psi_0]/(2\pi) \quad ;$$

$$\Omega_0'(\bar{\nu}) = \ell_0^2 \sin \hat{\eta}_0 [B_{31}(2\pi) \cos \psi_0 - A_{31}(2\pi) \sin \psi_0] / (2\pi) \quad ;$$

$$\psi_0'(\bar{\nu}) = \Omega_0'(\bar{\nu}) \cos i_0 \quad ;$$

$$\eta_0'(\bar{\nu}) = \ell_0^{3/2} A_{20}(2\pi) / (2\pi c_\varepsilon) \quad . \qquad \text{.....(3.14)}$$

Here the integrals $A_{nk}(2\pi)$ and $B_{nk}(2\pi)$ depend upon $p_0(\bar{\nu})$ and $q_0(\bar{\nu})$ and are evaluated in Appendix I. The slowly varying functions $K_1(\bar{\nu})$ and $K_2(\bar{\nu})$ stand for

$$K_1(\bar{\nu}) = \cos^2(i_0/2)\cos(\hat{\eta}_0 + \psi_0) + \sin^2(i_0/2)\cos(\hat{\eta}_0 - \psi_0) \quad ,$$

$$K_2(\bar{\nu}) = \cos^2(i_0/2)\sin(\hat{\eta}_0 + \psi_0) - \sin^2(i_0/2)\sin(\hat{\eta}_0 - \psi_0) \quad \text{.....(3.15)}$$

The first integral of the system of Equations (3.14) can readily be found as

$$a_0(\bar{\nu}) = \ell_0(\bar{\nu}) / [1 - p_0^2(\bar{\nu}) - q_0^2(\bar{\nu})] = a_{00} \quad . \qquad .....(3.16)$$

Thus, the major axis and total energy of the satellite are conserved in the long run and the motion of the sun does not alter the conclusion reached from the short-term analysis.

On substituting the explicit results for the integrals $A_{nk}(2\pi)$ and $B_{nk}(2\pi)$, evaluated in Appendix I, into Equations (3.14) and performing some algebraic manipulations, the system can be written in a fairly compact form as:

$$\begin{aligned}
(\ell_0^{1/2})' &= 3a_{00}^{5/2} / 2 \, [j_0 \cos i_0 \sin \hat{\eta}_0 - k_0 \cos \hat{\eta}_0] \quad ; \\
j_0' &= -(3/2) a_{00}^{3/2} \ell_0^{1/2} \cos i_0 \sin \hat{\eta}_0 + k_0 \cos i_0 \Omega_0' \quad ; \\
k_0' &= (3/2) \, a_{00}^{3/2} \ell_0^{1/2} \cos \hat{\eta}_0 - j_0 \cos i_0 \, \Omega_0' \quad ; \\
i_0' &= -(3/2) \, a_{00}^{5/2} j_0 \sin i_0 \sin \hat{\eta}_0 / \ell_0^{1/2} \quad ; \\
\Omega_0' &= -(3/2) \, a_{00}^{5/2} k_0 \sin \hat{\eta}_0 / \ell_0^{1/2} \quad ; \\
\hat{\eta}_0' &= c - \Omega_0' \quad . \qquad .....(3.17)
\end{aligned}$$

Here, the auxiliary elements $\hat{\eta} = \eta - \Omega$, $j = e \cos \omega$ and $k = e \sin \omega$ have been introduced for convenience. Note that $j = p \cos \psi + q \sin \psi$ and

$k = q \cos\psi - p \sin\psi$. The simplicity of the equation for $\eta_0(\bar{\nu})$ is a direct consequence of the fact that $a_0(\bar{\nu}) = a_{00}$ so that the orbital period remains constant in the long run. Integration yields $\eta_0(\bar{\nu}) = \eta_{00} + c\bar{\nu}$ indicating that (in this order of approximation) the motion of the sun is proportional to $\bar{\nu}$, relegating the non-uniformity of the sun's motion (with respect to ν) to higher-orders. Apart from $a_0(\bar{\nu}) = a_{00}$, at least three additional integrals can be constructed, namely

$$(1 - j_0^2)^{1/2} \sin i_0 = D_1 \quad ,$$

$$[k_0 - d(1 - e_0^2)^{1/2} \sin \hat{\eta}_0] \sin i_0 = D_2 \quad ,$$

$$[(1 - e_0^2)^{1/2} + d\, k_0 \sin \hat{\eta}_0] \cos i_0 + d\, j_0 \cos \hat{\eta}_0 = D_3 \quad , \qquad .....(3.18)$$

where d stands for $3\varepsilon a_{00}^{1/2} / (2\delta)$. For the orbit to remain closed, i.e., $e_0(\bar{\nu}) < 1$, the constant d must be less than unity or in terms of ε : $\varepsilon < 0.0018$ (for $a_{00} = 1$), which is true for virtually all practical cases. It is interesting that by the first and second relations of Equations (3.18), the orientation of the orbital plane, described by elements $i_0(\bar{\nu})$ and $\Omega_0(\bar{\nu})$, can be expressed in terms of the in-plane perturbations represented by $j_0(\bar{\nu})$ and $k_0(\bar{\nu})$. Note also that the first relation in Equations (3.18) yields the obvious result that an orbit initially lying in the ecliptic plane, i.e. $i_{00} = 0$, will remain in that plane, $i_0(\bar{\nu}) = 0$. The constants D_i, $i = 1,2,3$ are determined from the

initial conditions. Due to the fact that the last relation of Equations (3.18) admits, in principle, that k_0 be eliminated in favor of j_0, only one remaining equation of the system (Equations 3.17) need to be integrated for obtaining a complete analytical long-term representation for the orbital elements. For the general case, an uncoupled and tractable equation has not been found. Fortunately, special situations for which closed-form solutions can be derived more readily exist. In case the sun's position initially lies on the line of nodes and either the initial orbit is circular or has the perigee lying on the line of nodes, it follows that $\hat{\eta}_{00} = 0$ or π and $k_{00} = 0$, implying that the constant D_2 vanishes. In that case $\hat{\eta}_0'(\bar{\nu})$ is readily integrable, yielding the result:

$$\Omega_0(\bar{\nu}) = \eta_0(\bar{\nu}) - \arctan\left[\tan(b\bar{\nu}) / (1 + d^2)^{1/2}\right] . \qquad .....(3.19)$$

Employing the integrals of Equations (3.18), the remaining elements can now be derived:

$$j_0(\bar{\nu}) = (1 - D_1^2)^{1/2} G(\bar{\nu}) / [1 + d^2 \cos^2(b\bar{\nu})]^{1/2} \quad ;$$

$$k_0(\bar{\nu}) = d \sin(b\bar{\nu}) \left\{1 - (1 - D_1^2) G^2(\bar{\nu}) / [1 + d^2 \cos^2(b\bar{\nu})]\right\}^{1/2} / (1 + d^2)^{1/2}$$

$$e_0(\bar{\nu}) = \left\{ d^2 \sin^2(b\bar{\nu}) + (1 - D_1^2) G^2(\bar{\nu}) \right\}^{1/2} / (1 + d^2)^{1/2} \quad ;$$

$$\omega_0(\bar{\nu}) = \arcsin \left\{ \frac{d \sin(b\bar{\nu}) [1 + d^2 \cos^2(b\bar{\nu}) - (1 - D_1^2) G^2(\bar{\nu})]^{1/2}}{[1 + d^2 \cos^2(b\bar{\nu})]^{1/2} [d^2 \sin^2(b\bar{\nu}) + (1 - D_1^2) G^2(\bar{\nu})]^{1/2}} \right\} ;$$

$$i_0(\bar{\nu}) = \arcsin \left\{ D_1[1 + d^2\cos^2(b\bar{\nu})]^{1/2}/[1 + d^2\cos^2(b\bar{\nu}) - (1 - D_1^2)\, G^2(\bar{\nu})]^{1/2} \right\} , \qquad .....(3.20)$$

with appropriate branches of the arcsin functions determined from initial conditions and by continuity. The auxiliary function $G(\bar{\nu})$ stands for

$$G(\bar{\nu}) = d\,E\cos(b\bar{\nu}) - \text{sign}(\cos i_{00})\,(1 - E^2)^{1/2} . \qquad .....(3.21)$$

It is noteworthy that all of the functions $\hat{\eta}_0$, k_0, j_0, e_0, ω_0 and i_0 are periodic with a period of $1/(1 + d^2)^{1/2}$ year, so that the elements return to their original values just before the sun has made a full revolution. These results are consistent with those obtained for the ecliptic orbit in the previous chapter. Note also that Ω_0, ψ_0, $\tilde{\omega}_0$, p_0 and q_0 contain terms of two different but close periods, namely one year and $1/(1 + d^2)^{1/2}$ year, resulting in a slow secular trend in the long run.

The higher-order terms can readily be determined by formal integration, yielding similar (when $\cos \eta_0$, $\sin \eta_0$ are replaced by $K_1(\bar{\nu})$ and $K_2(\bar{\nu})$, respectively) expressions as in Equations (2.31) for the in-plane orbital elements ℓ_1, a_1, p_1 and q_1, while the out-of-plane results are given by

$$i_1(\nu,\bar{\nu}) = \ell_0^2 \sin i_0 \sin \hat{\eta}_0 \left\{ [a_{31}^j \cos \psi_0 + b_{31}^j \sin \psi_0] \sin j\nu \right.$$

$$+ [c_{31}^j \cos\psi_0 + d_{31}^j \sin\psi_0](1 - \cos j\nu) \Big\} + \tilde{i}_1(\bar{\nu}) \quad ,$$

$$\Omega_1(\nu,\bar{\nu}) = \ell_0^2 \sin\hat{n}_0 \Big\{[b_{31}^j \cos\psi_0 - a_{31}^j \sin\psi_0] \sin j\nu + [d_{31}^j \cos\psi_0$$

$$- c_{31}^j \sin\psi_0](1 - \cos j\nu) \Big\} + \tilde{\Omega}_1(\bar{\nu}) \quad , \qquad .....(3.22)$$

with the slow functions $\tilde{i}_1$ and $\tilde{\Omega}_1$ determined from the boundedness constraint upon the second-order terms (Appendix III). However, the complexity of the equations involved precludes any possibility of extracting, analytically, information on the long-range trends of these terms.

3.3.3 Discussion of results

Since an analytical long-term solution has been found only for the case of $D_2 = 0$, the rectification/iteration procedure needs to be employed for cases where the initial conditions are different. As an example, a satellite in a geosynchronous equatorial orbit with $\epsilon = 0.0002$ is considered. A rectification interval $\nu_f = 2\pi$ is chosen yielding sufficiently accurate results over a 1200 day span of time.

As the major axis remains constant in the long run, the in-plane perturbations are fully described by the eccentricity vector $\underline{e}$ or its Cartesian components p and q. Concise representation of the in-plane changes can be provided by polar plots for $\underline{e}$ in the x_0,y_0 plane. From the zeroth-order long-term results, the slope of the polar plot at any instant is given by (Equations 3.14),

$$\frac{dq_0}{dp_0} = \frac{q_0'(\bar{\nu})}{p_0'(\bar{\nu})} = -\frac{K_1(\bar{\nu})}{K_2(\bar{\nu})} \quad \text{.....(3.23)}$$

For an equatorial orbit, $\cos^2(i_0/2)$ is about 25 times $\sin^2(i_0/2)$ so that the polar plots should be similar in shape to those obtained for ecliptic orbits in the previous chapter, Figure 2-7 a-d. Figures 3-3 a,b show the resulting polar plots for initially circular as well as highly eccentric orbits ($e_{00} = 0.5$). The eccentricity is periodic with a period of about 363 days, and the orientation of the major axis depends critically upon the initial eccentricity: for e_{00} sufficiently large, the orbit remains elliptic with its axis exhibiting periodic oscillations (amplitude of about 12° for $e_{00} = 0.5$) as well as a slow clockwise rotation (about 2° per year, Figure 3-3b). For an initially circular orbit, Figure 3-3a, the behavior of $\tilde{\omega}$ is completely different, showing an increase of 180° over one year followed by an instantaneous jump of 180° when the eccentricity passes through the origin again. Also the slow clockwise rotation is apparent. The small differences in the in-plane perturbations for an arbitrary as compared to an ecliptic orbit are due to the fact that the magnitude of the in-plane component of the solar radiation force varies slightly with the position of the sun in the former case. The behavior of an initially circular near-ecliptic orbit may be visualized as follows: the solar radiation force changes the circular orbit into an ellipse with increasing eccentricity and perigee at 90° ahead of the projection of the sun-earth line. Subsequently, the major axis tries to maintain the 90° lead over the moving sun, but as the eccentricity increases the orientation of the major axis becomes more rigid and the sun overtakes the perigee after about half a year.

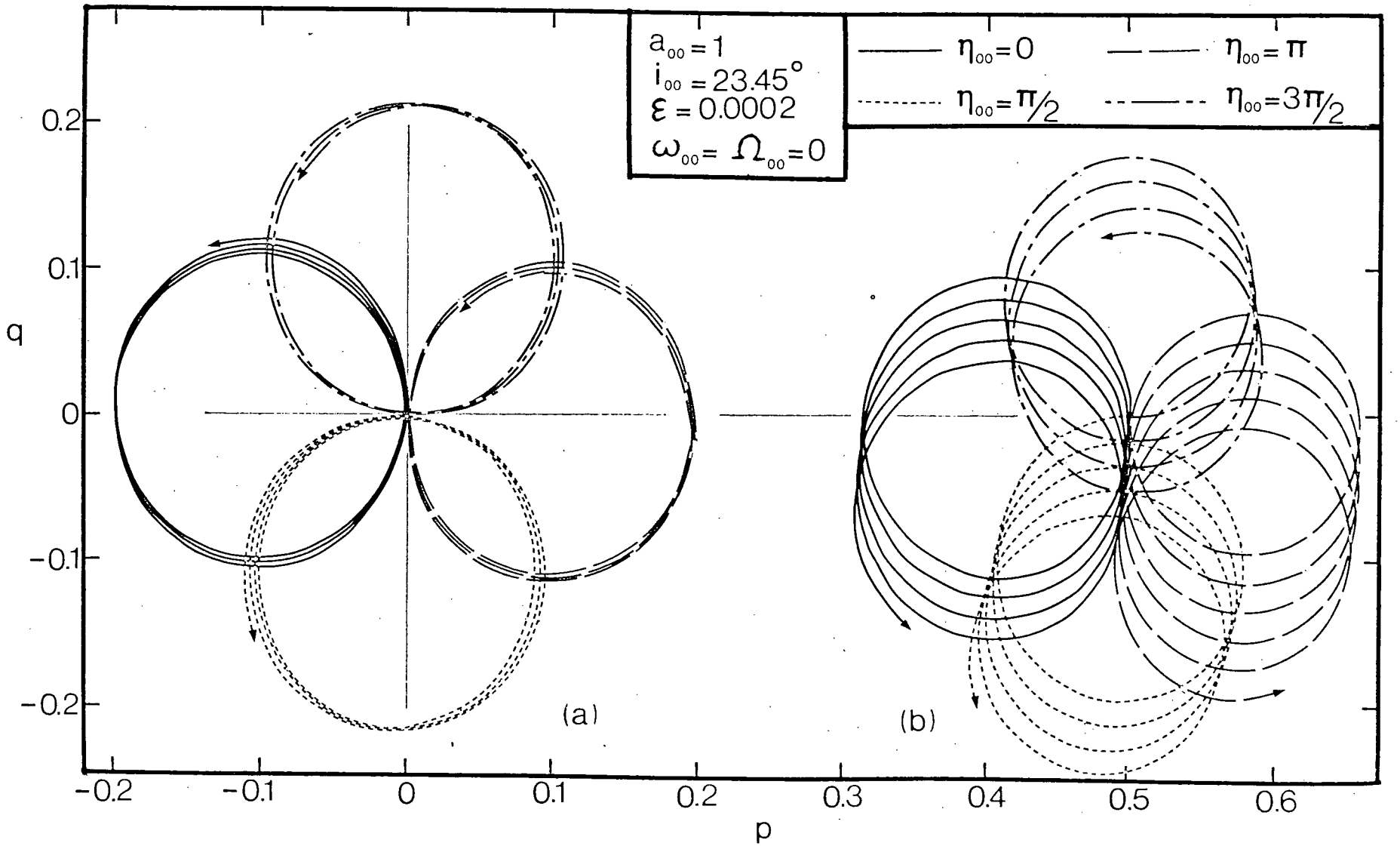

Figure 3-3 Polar plots, illustrating long-term behavior of the eccentricity vector $\underline{e}$:
(a) $e_{00} = 0$; (b) $e_{00} = 0.5$

At this point, the eccentricity has reached its maximum value and will start to decline while the sun moves ahead of the perigee position. After almost a year the perigee is about 90° behind the sun and, while the eccentricity vanishes again, makes a jump of 180°. The original situation is now re-established and the cycle repeats itself.

According to the results of the two-variable expansion procedure, Equations (3.20), the auxiliary elements $j_0(\bar{\nu})$ and $k_0(\bar{\nu})$ are periodic with a period of $1/(1 + d^2)^{1/2}$ year, i.e. about 363 days in the present example. Their behavior can be visualized through polar plots as in Figures 3-3 without the slow clockwise rotation. Since the j,k axes are obtained from the p,q axes by rotation through the angle ψ, the slow clockwise trends in the polar plots of Figures 3-3 can be interpreted as the negative secular growth of the angle ψ.

In Figure 3-4, the behavior of the longitude of the ascending node Ω is depicted for an equatorial orbit and a few values of the initial solar aspect angle η_{00}. Of particular interest is the insensitivity of its behavior to different values of the initial eccentricity in the range 0 - 0.5. Results of the two-variable expansion procedure indicate quite close correspondence with those obtained by rectification/iteration. As seen in Equation (3.19), the long-term behavior of the longitude of nodes is independent of initial eccentricity. The qualitative behavior of $\Omega_0(\nu)$ may be visualized by considering $\Omega_0'(\bar{\nu})$, Equations (3.17): the rate of change of $\Omega_0(\bar{\nu})$ is proportional to $-k_0 \sin\hat{\eta}_0$, which remains negative in case $\eta_{00} = 0$ or π due to the nature of the polar plot for j_0,k_0. By following the behavior of k_0 in conjunction with that of $\hat{\eta}_0$, it becomes evident that the total regression of Ω_0 after one revolution should be essentially independent

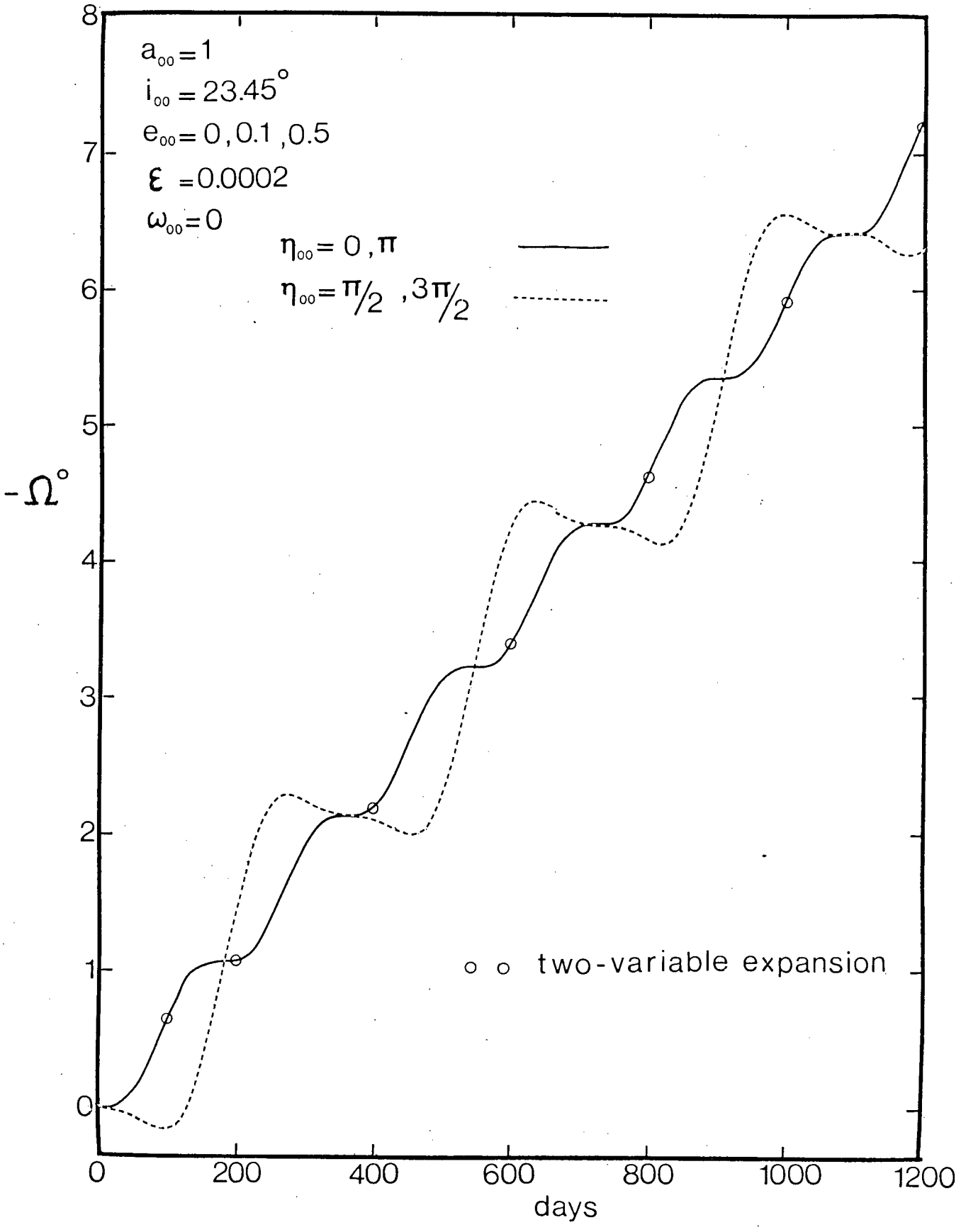

Figure 3-4 Typical long-term behavior of the longitude of nodes as affected by the initial solar aspect angle

of the initial eccentricity and solar aspect angle.

Figure 3-5 shows the long-term behavior of the inclination of the orbital plane for a few values of the solar aspect angle. The results of the two-variable expansion method match quite well with those obtained by rectification and iteration. The fact that the period of oscillation for $\eta_{00} = \pi/2$ and $3\pi/2$ is half that for $\eta_{00} = 0$ and π can be understood from the first relation in Equations (3.18) in conjunction with the in-plane perturbations of j_0. The polar plots indicate that the behavior of j_0^2 is the same for $\eta_{00} = 0$ and π : amplitude $(e_{0,max})^2$ and period 363 days. On the other hand, when $\eta_{00} = \pi/2$ and $3\pi/2$, j_0^2 oscillates with period of 181.5 days and an amplitude of $(e_{0,max}/2)^2$. This explains the occurence of two different frequencies as well as the dependence of the amplitude of variation of i_0 on the initial solar aspect angle. The behavior of the inclination for an initially eccentric orbit, $e_{00} = 0.1$, is both quantitatively and qualitatively different from an initially circular orbit, Figure 3-6. The relatively large differences in amplitude depending on the solar aspect angle can be understood by visualizing the behavior of j_0^2 in the corresponding polar plots. Figure 3-7 shows the variation of the inclination for a very eccentric orbit, $e_{00} = 0.5$. The differences in amplitudes for various values of η_{00} are much smaller than those in Figures 3-5 and 3-6, although the magnitudes themselves are much larger (note the differences in scale). Finally, it may be mentioned that only when $i_{00} = 0$ or π the inclination remains constant throughout in the long run.

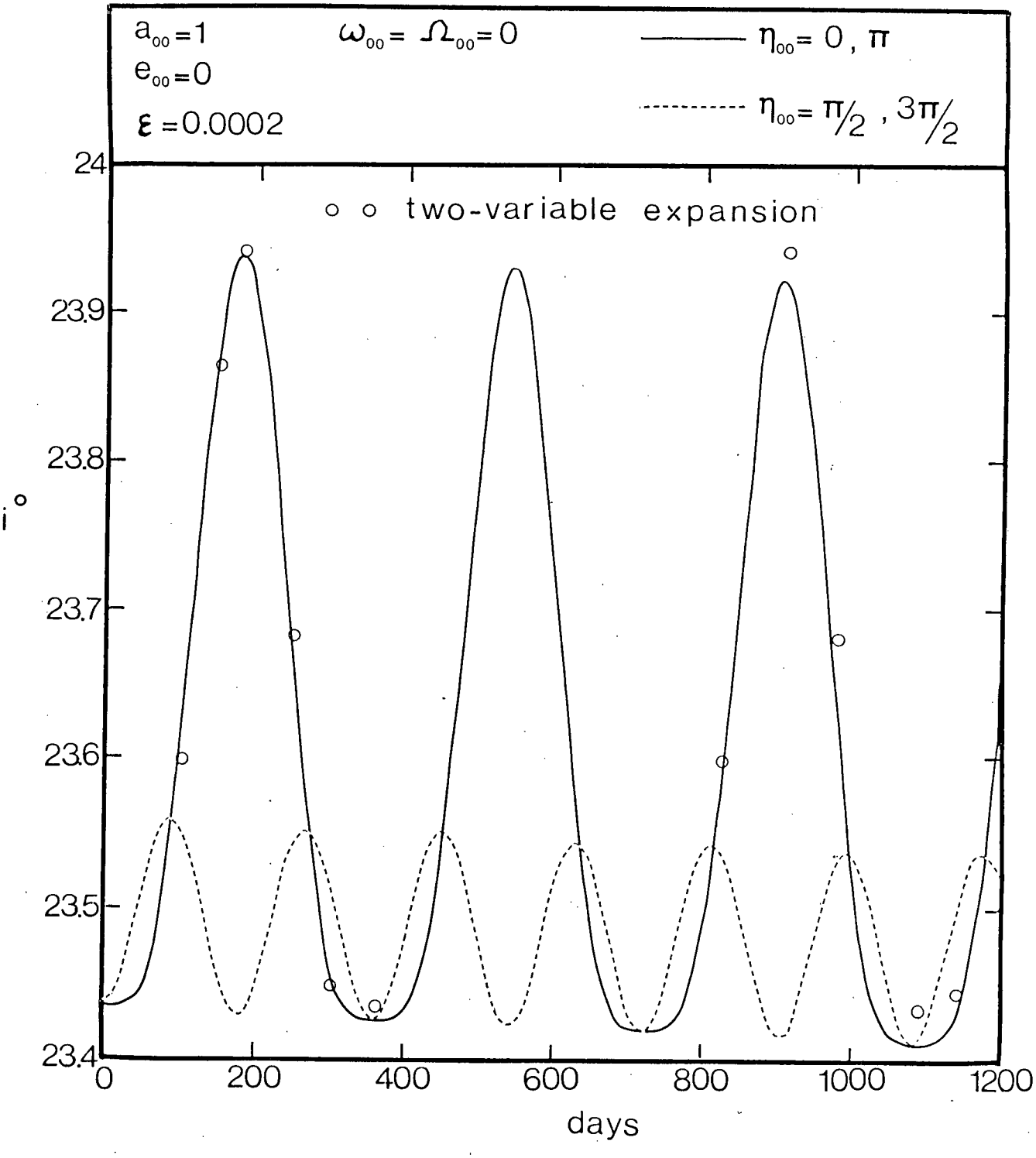

Figure 3-5 Long-term behavior of the inclination for initially circular equatorial orbit

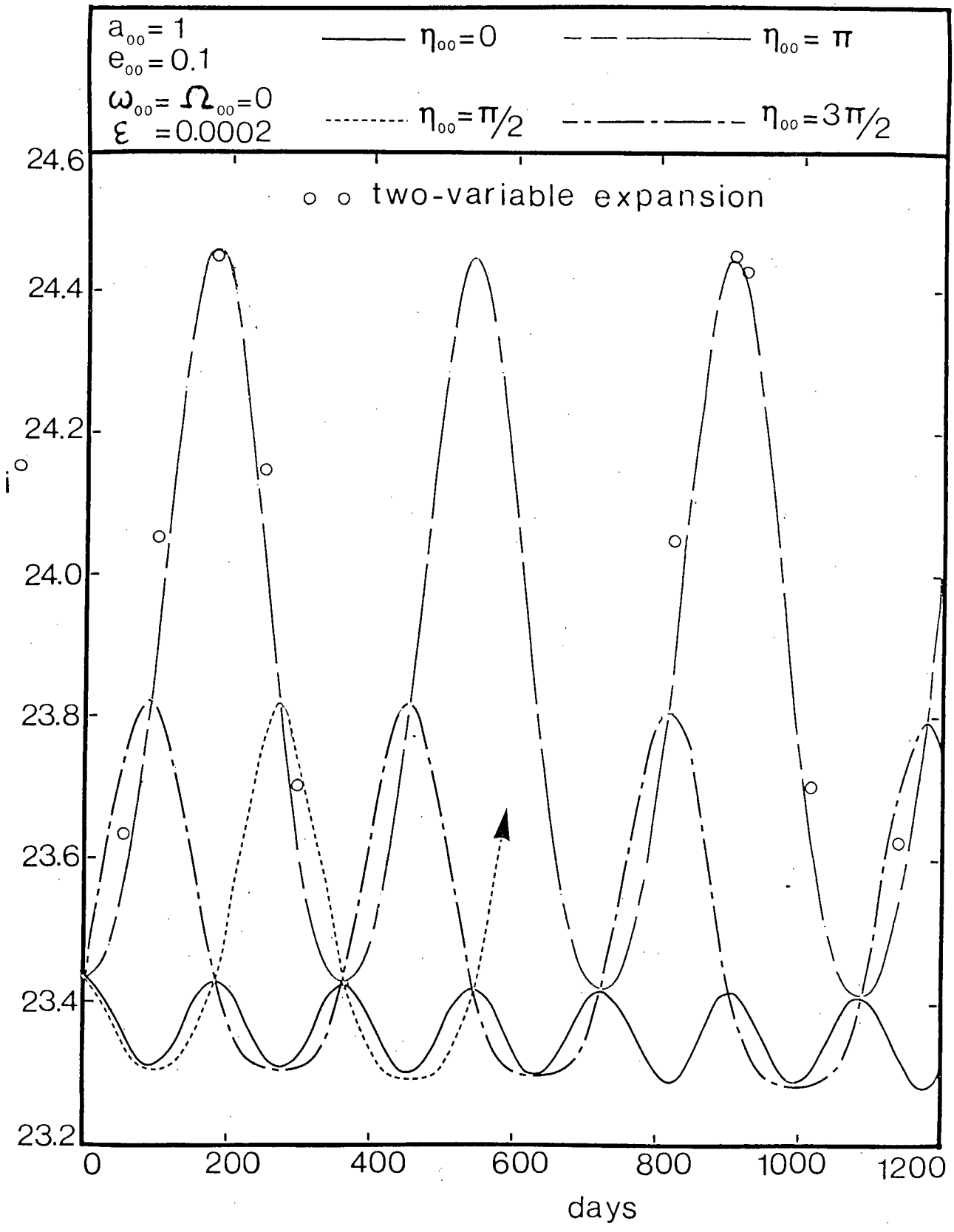

Figure 3-6 Variations in orbital inclination for initially equatorial orbit of eccentricity 0.1

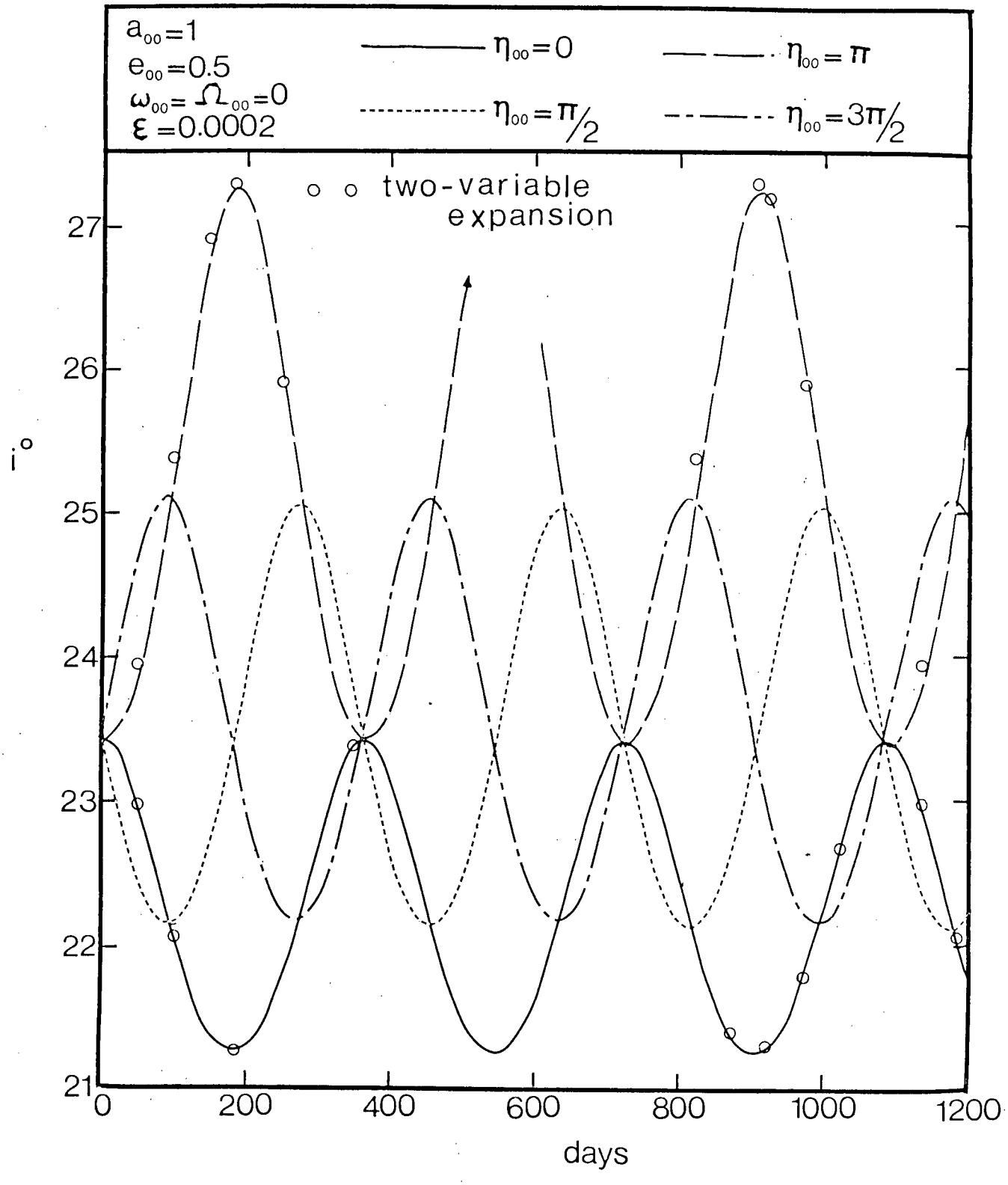

Figure 3-7 Behavior of orbital inclination for initially equatorial orbit of eccentricity 0.5

3.4 Satellite in Arbitrary Fixed Orientation to Radiation

The case considered here constitutes a generalization of the analysis of the previous sections in the sense that now the plate is kept at a fixed but arbitrary angle to the incident radiation. It serves as a fairly accurate model for communications and other satellites having one or two-axis attitude control. The CTS satellite with solar arrays which can be rotated about an axis normal to the orbital plane for maximization of the amount of solar energy intercepted is an obvious example. Furthermore, the analysis is relevant to the solar radiation induced orbital perturbations of a satellite with a fixed orientation in the inertial space, e.g. a platform for deep-space studies. It is noteworthy that the analysis can be extended quite readily to an arbitrarily shaped satellite modelled by n flat surfaces A_k each with its own characteristic material parameters represented by σ_{1k}, σ_{2k} and ρ_k. The orientation of the surface A_k with respect to the instantaneous orbital plane is determined by the two Eulerian rotations, α_k and β_k. A fixed orientation of the satellite with respect to inertial space or the radiation (in a short-term sense) is maintained if $\alpha_k = -\nu + \hat{\alpha}_k$, $k = 1,2,\ldots n$, with arbitrary fixed angles $\hat{\alpha}_k$ and β_k. For instance, the surface element A_k is normal to the radiation if $\hat{\alpha}_k = \psi + \arctan[\cos(i)\tan\hat{\eta}]$ and $\beta_k = \arcsin[\sin(i)\sin\hat{\eta}]$, which corresponds to the control law of Equations (3.9). Replacing the elements i, ψ and $\hat{\eta}$ by their respective initial (or mean) values i_{00}, ψ_{00} and $\hat{\eta}_{00}$, writing

$$\underline{u}^s = \underline{s}^0 + \underline{s}^1 \cos\nu + \underline{s}^2 \sin\nu \quad \text{and} \quad \underline{u}_k^n = \underline{n}_k^0 + \underline{n}_k^1 \cos\nu + \underline{n}_k^2 \sin\nu ,$$

the force expression of Equations (3.8) can be rewritten in the following compact form:

$$\underline{F} = \varepsilon \sum_{k=1}^{n} \{\underline{C}_k^0 + \underline{C}_k^1 \cos\nu + \underline{C}_k^2 \sin\nu\} ,$$

where $\underline{C}_k^j = |U_k| \{\sigma_{1k} \underline{s}^j + [\sigma_{2k} + \rho_k U_k] \underline{n}_k^j\} A_k, \quad j = 0,1,2;$

$$U_k = \cos\beta_k [K_{10} \cos\hat{\alpha}_k + K_{20} \sin\hat{\alpha}_k] + \sin\beta_k \sin(i_{00}) \sin\hat{n}_{00} . \quad .....(3.24)$$

It may be noted that $U_k = (\underline{u}_k^n \cdot \underline{u}^s)$ is constant in the short-term analysis since the satellite as well as the sun maintain a fixed orientation in space. In practise, one needs to update the solar aspect angle $\hat{n}_{00}$ and the control angle $\hat{\alpha}_k$ to account for the slow motion of the sun. Naturally, also the orbital elements change continually and need rectification after a certain time.

Employing the usual perturbation Equations (3.5) and (3.6), integration over a short-term interval (ν_{00},ν) yields the following first-order changes in the orbital elements:

$$\ell_1(\nu) = 2\varepsilon \ell_{00}^3 \sum_{k=1}^{n} \{C_{ky}^1 A_{31} + C_{ky}^2 B_{31}\} ;$$

$$a_1(\nu) = 2\varepsilon a_{00}^2 \ell_{00} \sum_{k=1}^{n} \{C_{kx}^1 [B_{11} - B_{21} - q_{00} A_{20}] + C_{ky}^1 A_{11} + C_{ky}^2 B_{11} - C_{kx}^2 [A_{11} - A_{21} - p_{00} A_{20}]\} ;$$

$$p_1(\nu) = \varepsilon \ell_{00}^2 \sum_{k=1}^{n} \{C_{kx}^1 B_{22} + C_{ky}^1 [A_{20} + A_{22} + A_{30} + A_{32} + 2p_{00} A_{31}] + C_{kx}^2 (A_{20} - A_{22}) + C_{ky}^2 [B_{32} + B_{22} + 2p_{00} B_{31}]\}/2 ;$$

$$q_1(\nu) = \varepsilon \ell_{00}^2 \sum_{k=1}^{n} \{ - C_{kx}^2 B_{22} + C_{ky}^2[A_{20} - A_{22} + A_{30} - A_{32} + 2q_{00} B_{31}]$$

$$- C_{kx}^1(A_{20} + A_{22}) + C_{ky}^1[B_{32} + B_{22} + 2q_{00} A_{31}]\}/2 ;$$

$$i_1(\nu) = \varepsilon \ell_{00}^2[A_{31} \cos\psi_{00} + B_{31} \sin\psi_{00}] \sum_{k=1}^{n} C_{kz}^0 ;$$

$$\Omega_1(\nu) = \varepsilon \ell_{00}^2[B_{31} \cos\psi_{00} - A_{31} \sin\psi_{00}] \sum_{k=1}^{n} C_{kz}^0/\sin(i_{00}) ;$$

$$\psi_1(\nu) = \cos(i_{00})\, \Omega_1 ; \quad \eta_1(\nu) = \ell_{00}^{3/2} A_{20}/c . \qquad .....(3.25)$$

Here, the abbreviations A_{nk} and B_{nk} stand for $A_{nk}(\nu) - A_{nk}(\nu_{00})$ and $B_{nk}(\nu) - B_{nk}(\nu_{00})$, respectively, and depend upon the elements p_{00} and q_{00} (Appendix I). It may be noted that for $i_{00} = 0$, Ω and ψ lose their meaning and the angles ν, $\tilde{\omega}$, measured from a fixed axis in the orbital plane, coincide with ϕ and ω, respectively.

After one revolution, the reduced expressions of the integrals for $\nu = 2\pi$ may be substituted. The result for $a_1(2\pi)$ vanishes after one revolution so that, also in the present situation, first-order secular changes in the major axis are absent. By rectification of the orbital elements, as well as the force expression of Equations (3.24) at $\nu = 2\pi$ and iteration of the results of Equations (3.25), a good approximation for the long-term perturbations may be obtained. This process has been executed for a variety of plate orientations, reflectivities, and initial conditions leading to the following general conclusions. In case $\beta = 0$, i.e. when the plate is kept normal to the orbital plane, the long-term changes in eccentricity, position of the perigee and inclination are periodic with period of about one year

regardless of the (specular) reflectivity ρ. In the examples cosidered, the fluctuations in inclination range from zero when $\rho = 1$ (resulting in a force in the orbital plane) to about 0.5° when $\rho = 0$. Typical long-term in-plane perturbations for a few values of reflectivity are presented in Figure 3-8b. Here the plate is in an equatorial orbit and $\hat{\alpha} = \psi +$ arctan[cos(i) tan$\hat{\eta}$] , aligning the plate-normal with the projection of the radiation in the orbital plane.

When the second rotation $\beta \neq 0$ is imposed, and part of the radiation is absorbed, the qualitative nature of the in-plane perturbations changes drastically as shown in Figure 3-8a. Note that the polar plots show severe secular perturbations in the in-plane elements e and $\tilde{\omega}$.

The orbital inclination may also exhibit long-term secular changes up to about 0.7° per year in the examples considered. The variations in the longitude of nodes are of a long-term secular nature with a rate of regression between 0 and -0.5 degrees per year in the case of $\beta = 0$. The smaller the reflectivity the higher this rate. When the plate is not normal to the orbital plane ($\beta \neq 0$) , higher rates of precession have been observed, e.g. -2.4° per year for $\hat{\alpha} = \hat{\eta}$, $\beta = 23°$ and $\rho = 1$.

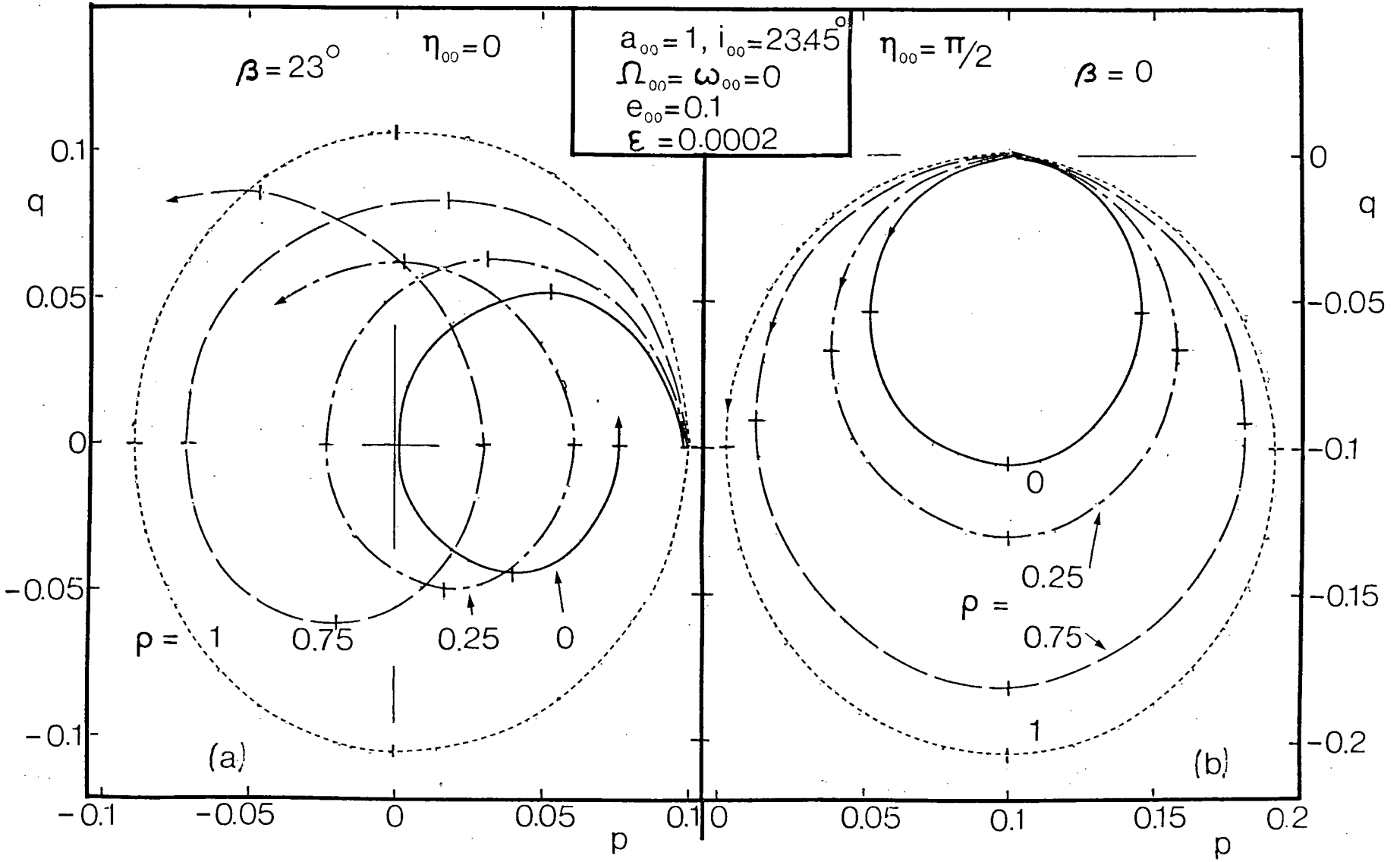

Figure 3-8 Typical polar plots for plate maintaining fixed orientation to radiation, $\hat{\alpha} = \psi + \arctan\{\cos(i) \tan \hat{\eta}\}$ and: (a) $\beta = 23°$; (b) $\beta = 0$

3.5 Plate in Arbitrary Fixed Orientation to Local Frame

In this section a satellite modelled as a flat plate, with arbitrary but homogeneous material characteristics, kept in a general fixed orientation with respect to the local coordinate frame is studied. The analysis is relevant to orbiting platforms or mirrors in a fixed orientation with respect to the earth. In particular, large space structures aligned with the local vertical due to gravity-gradient torques represent an obvious example. The major distinction between the present situation and those encountered previously, is the fact that now both sides of the plate will be exposed to the solar radiation, each during about half a revolution. The change-over occurs when the plate is aligned with the sun-earth line. This raises an interesting question as to the orbital perturbations for a plate with different material properties on the front and back sides.

The orientation of the plate is, as usual, described by the two Eulerian rotations α and β, which are arbitrary constants now. In a short-term analysis, the orbital elements are considered constant (i.e. equal to their initial or mean values) during integration of the perturbation equations and in the evaluation of the force expression. Writing $\underline{u}^s(\nu) = \underline{s}^0 + \underline{s}^1 \cos\nu + \underline{s}^2 \sin\nu$ and $U(\nu) = (\underline{u}^n \cdot \underline{u}^s) = U_0 + U_1\cos\nu + U_2\sin\nu$, the force can be expressed in the form:

$$\underline{F} = \varepsilon\, s_u \{\underline{D}^0 + \underline{D}^1\cos\nu + \underline{D}^2\sin\nu + \underline{D}^3\cos(2\nu) + \underline{D}^4\sin(2\nu)\} ,$$

with: $$\underline{D}^0 = \sigma_1[U_0\,\underline{s}^0 + (U_1\,\underline{s}^1 + U_2\,\underline{s}^2)/2] + [\sigma_2\,U_0 + \rho U_0^2 + \rho(U_1^2 + U_2^2)/2]\,\underline{u}^n ;$$

$$\underline{D}^1 = \sigma_1(U_0\,\underline{s}^1 + U_1\,\underline{s}^0) + (\sigma_2\,U_1 + 2\rho U_0\,U_1)\,\underline{u}^n ;$$

$$\underline{D}^2 = \sigma_1 (U_0 \underline{s}^2 + U_2 \underline{s}^0) + (\sigma_2 U_2 + 2\rho U_0 U_2) \underline{u}^n ;$$

$$\underline{D}^3 = \sigma_1 (U_1 \underline{s}^1 - U_2 \underline{s}^2)/2 + \rho(U_1^2 - U_2^2)/2 \underline{u}^n ;$$

$$\underline{D}^4 = \sigma_1 (U_1 \underline{s}^2 + U_2 \underline{s}^1)/2 + \rho U_1 U_2 \underline{u}^n . \qquad .....(3.26)$$

It may be noted that the vector $\underline{u}^n$ is fixed in the local x,y,z frame and is determined by the angles α and β in such a manner that it points towards the earth for $\alpha = \beta = 0$. When the plate has different material properties on either side, care must be taken to identify the side facing the sun initially and make necessary adjustments after about half a revolution when the other side becomes illuminated. The side facing the earth for $\alpha = \beta = 0$ will be designated as the back side of the plate and its material properties will carry the subscript b. Similarly, the front side will be recognized by the subscript f. Consequently, the value of s_u equals 1 if the front side is illuminated and -1 for the back. The switch-over points ν_1, ν_2 are determinated by $U(\nu) = 0$ and can be written in the following form:

$$\nu_1 = \pi/2 - \alpha + \hat{\eta} + \psi + 2\pi(k-1) + \delta_1 ,$$

$$\nu_2 = 3\pi/2 - \alpha + \hat{\eta} + \psi + 2\pi(k-1) - \delta_2 , \qquad .....(3.27)$$

where the index k designates the appropriate revolution. The angles δ_1 and δ_2 vanish in the case $i = 0$ and for arbitrary inclination ($< \pi/2$) can be found from the following iteration scheme: $\delta_1^{(0)} = \delta_2^{(0)} = 0$ and

$$\delta_1^{(n)} = \arcsin \{\tan(i/2)[2 \tan\beta \sin\hat{\eta} - \tan(i/2) \sin(\delta_1^{(n-1)} + 2\hat{\eta})]\} ,$$

$$\delta_2^{(n)} = \arcsin \{\tan(i/2)[2 \tan\beta \sin\hat{\eta} - \tan(i/2) \sin(\delta_2^{(n-1)} - 2\hat{\eta})]\} , \qquad .....(3.28)$$

$n = 1,2,3,\ldots$. This procedure converges very rapidly for small inclination

since the angles δ_1 and δ_2 are small in that case. Retrograde orbits may be accommodated by reversing the sun's motion.

The short-term perturbations in the orbital elements can be obtained analytically by integration of the perturbation equations over the interval (ν_{00}, ν). Provided the interval does not contain any switch-over points, the integration yields:

$$\ell_1(\nu) = 2s_u \ell_{00}^3 \{D_y^0 A_{30} + D_y^1 A_{31} + D_y^2 B_{31} + D_y^3 A_{32} + D_y^4 B_{32}\} ;$$

$$\begin{aligned} a_1(\nu) = s_u a_{00}^2 \ell_{00} \{ & p_{00} [D_x^2 A_{20} + D_x^4 A_{21} + (2 D_x^0 - D_x^3) B_{21} - D_x^2 A_{22} \\ & + D_x^1 B_{22} - D_x^4 A_{23} + D_x^3 B_{23}] - q_{00} [D_x^1 A_{20} + (2 D_x^0 + D_x^3 A_{21} \\ & + D_x^4 B_{21} + D_x^1 A_{22} + D_x^2 B_{22} + D_x^3 A_{23} + D_x^4 B_{23}] \\ & + 2 [D_y^0 A_{10} + D_y^1 A_{11} + D_y^2 B_{11} + D_y^3 A_{12} + D_y^4 B_{12}]\} ; \end{aligned}$$

$$\begin{aligned} p_1(\nu) = s_u \ell_{00}^2 \{ & (D_x^2 + D_y^1) A_{20} + (D_x^4 + 2 D_y^0 + D_y^3) A_{21} + (2 D_x^0 - D_x^3 \\ & + D_y^4) B_{21} + (D_y^1 - D_x^2) A_{22} + (D_x^1 + D_y^2) B_{22} + (D_y^3 - D_x^4) A_{23} \\ & + (D_x^3 + D_y^4) B_{23} + (D_y^1 + 2p_{00} D_y^0) A_{30} + (2p_{00} D_y^1 + 2 D_y^0 + D_y^3) * \\ & * A_{31} + (2p_{00} D_y^2 + D_y^4) B_{31} + (2p_{00} D_y^3 + D_y^1) A_{32} + (2p_{00} D_y^4 + \\ & + D_y^2) B_{32} + D_y^3 A_{33} + D_y^4 B_{33} \}/2 ; \end{aligned}$$

$$q_1(\nu) = s_u \ell_{00}^2 \{ (D_y^2 - D_x^1) A_{20} + (D_y^4 - 2 D_x^0 - D_x^3) A_{21} + (2 D_y^0 - D_y^3 - D_x^4) *$$

$$* B_{21} - (D_y^2 + D_x^1) A_{22} + (D_y^1 - D_x^2) B_{22} - (D_y^4 + D_x^3) A_{23}$$

$$+ (D_y^3 - D_x^4) B_{23} + (D_y^2 + 2q_{00} D_y^0) A_{30} + (D_y^4 + 2q_{00} D_y^1) A_{31}$$

$$+ (2q_{00} D_y^2 + 2 D_y^0 - D_y^3) B_{31} + (2q_{00} D_y^3 - D_y^2) A_{32}$$

$$+ (2p_{00} D_y^4 + D_y^1) B_{32} - D_y^4 A_{33} + D_y^3 B_{33} \}/2 ;$$

$$i_1(\nu) = s_u \ell_{00}^2 \{ \cos \psi_{00} [D_z^1 A_{30} + (2 D_z^0 + D_z^3) A_{31} + D_z^4 B_{31} + D_z^1 A_{32}$$

$$+ D_z^2 B_{32} + D_z^3 A_{33} + D_z^4 B_{33}]$$

$$+ \sin \psi_{00} [D_z^2 A_{30} + D_z^4 A_{31} + (2 D_z^0 - D_z^3) B_{31} - D_z^2 A_{32}$$

$$+ D_z^1 B_{32} - D_z^4 A_{33} + D_z^3 B_{33}] \}/2 ;$$

$$\Omega_1(\nu) = s_u \ell_{00}^2 \{ \cos \psi_{00} [D_z^2 A_{30} + D_z^4 A_{31} + (2 D_z^0 - D_z^3) B_{31} - D_z^2 A_{32}$$

$$+ D_z^1 B_{32} - D_z^4 A_{33} + D_z^3 B_{33}] \}/2 ;$$

$$- \sin \psi_{00} [D_z^1 A_{30} + (2 D_z^0 + D_z^3) A_{31} + D_z^4 B_{31} + D_z^1 A_{32}$$

$$+ D_z^2 B_{32} + D_z^3 A_{33} + D_z^4 B_{33}] \}/[2 \sin(i_{00})] ;$$

.....(3.29)

and $\psi_1(\nu) = \Omega_1(\nu) \cos(i_{00})$; $\eta_1(\nu) = \ell_{00}^{3/2} A_{20}(\nu)/c_\varepsilon$. The abbreviations A_{nk} and B_{nk} stand for $A_{nk}(\nu) - A_{nk}(\nu_{00})$ and $B_{nk}(\nu) - B_{nk}(\nu_{00})$, respectively, and are functions of the initial or rectified elements p_{00}, q_{00} (Appendix I). The coefficients $\underline{D}^j$, $j = 0,1,\ldots,4$ were given in Equations

(3.26) and s_u is either +1 or -1 over the interval (ν_{00}, ν).

The more interesting long-term perturbations are obtained by repeated rectification of the initial conditions, i.e. iteration of the short-term results of Equations (3.29). The switch-over points ν_1 and ν_2 of Equations (3.27) are the appropriate locations for rectification since s_u needs to be updated at those points in any case. This rectification/iteration procedure was carried out numerically for a few examples representing satellites modelled as a plate in a geosynchronous equatorial orbit. The plate surface was taken as perfectly specular reflective either on both sides $(\rho_b = \rho_f = 1)$ or on one side with the other side perfectly absorptive $(\rho_b$ or $\rho_f = 0)$. A few representative results are shown in Figure 3-9.

Under the influence of the gravity-gradient torque, a plate in a near-circular orbit will tend to be oriented along the local vertical which is the stable equilibrium position. When the plate has different reflecting properties on either side, a gradual increase or decrease in major axis is obtained. For instance, if the plate is kept normal to the orbital plane $(\beta = 0)$ it is obvious that more energy is transferred during the phase when the sunlight strikes the reflecting rather than the absorbing side, since the magnitude of the force is larger and its direction (in an averaged sense) is closer to the instantaneous velocity vector in the former case. This differential in energy transfer results in a continuously growing major axis when the reflecting side is illuminated with the satellite moving away from the sun (curve 1) and a decreasing major axis when the absorbing side is facing the sun during that phase (not shown). The polar plot belonging to case 1, Figure 3-9b, is qualitatively similar to the ones for the case when the plate is kept normal to the radiation (Figure 3-3) except that the

area enclosed by the eccentricity vector after one year is much smaller here. If both sides of the plate have the same reflectivity, the long-term changes in major axis will be relatively small (curves 2 and 4). Also when the plate is kept along the local horizontal (e.g., a reflecting mirror in orbit), the semi-major axis remains virtually constant regardless of the reflectivities on both sides, since the net effect over one half revolution tends to vanish. Curve 3 is a representative example for this case. Note that the polar plot is quite different from the others. Curve 5 illustrates the behavior of a plate along the local vertical with its normal inclined by 30° to the orbital plane and different reflecting properties on either side. It should be noted that the polar plot for this case shows a long-term secular trend. In general, one should expect a closed polar plot only in case $\rho_b = \rho_f$ or when $\beta = 0$ (regardless of the values for ρ_b and ρ_f).

As to the perturbations of the orbital plane, it is found that no changes in its orientation take place when $\rho_b = \rho_f = 1$ and $\beta = 0$, since the force has no component normal to the orbital plane. Otherwise, widely varying perturbations in i and Ω occur with the inclination staying within 1.2 degree of the equatorial plane. On the other hand, perturbations in the longitude of nodes may be oscillatory (within 1.5 degrees) or secular (less than 2 degrees per year) in the long run for the examples considered.

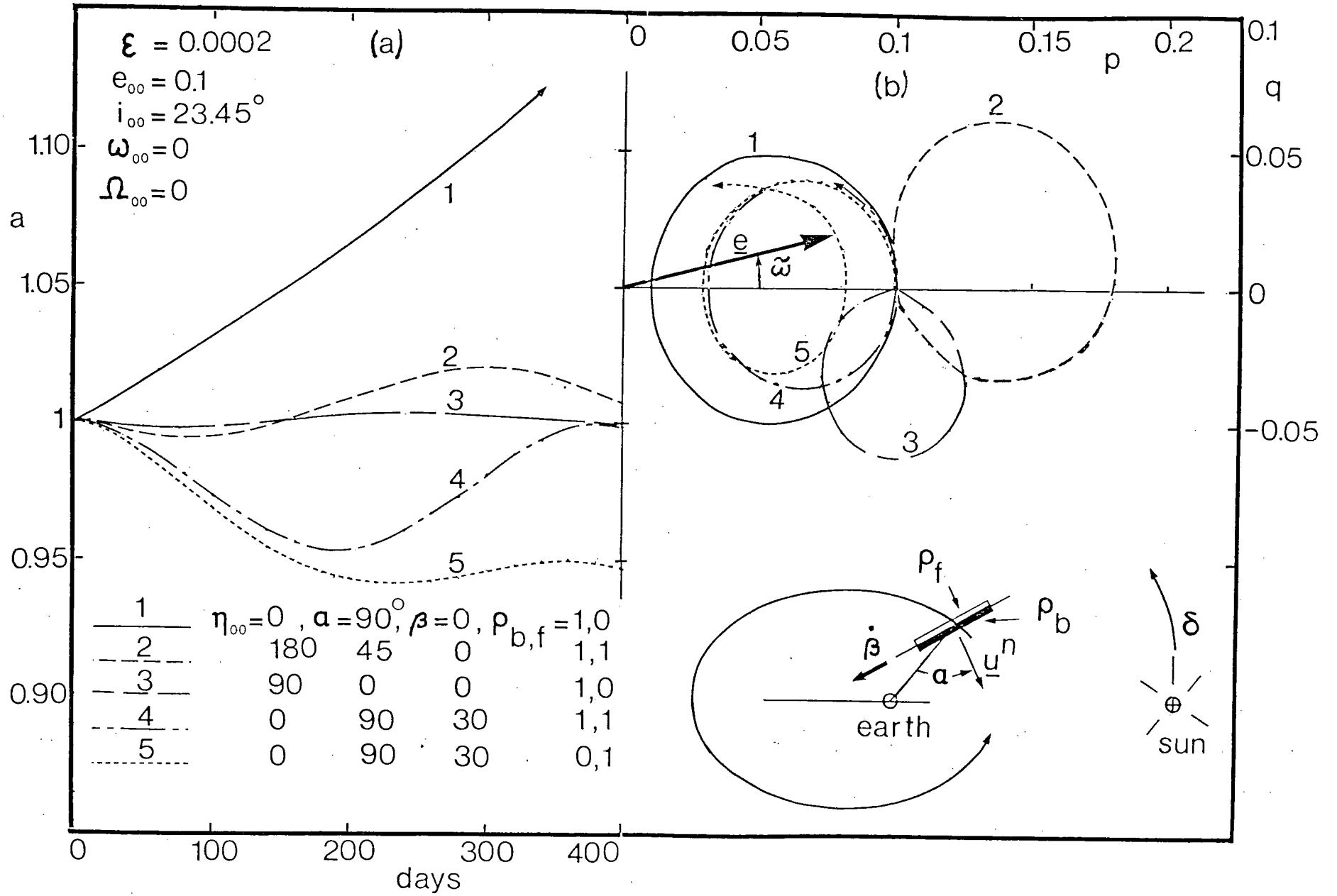

Figure 3-9 Long-term in-plane perturbations for plate fixed to local frame:
(a) semi-major axis; (b) polar plot for eccentricity vector $\underline{e}$

3.6 Concluding Remarks

The important aspects of the investigation and resulting conclusions may be summarized as follows:

(i) A formulation in which the out-of-plane perturbations are uncoupled from the in-plane variations, while retaining a geometric interpretation in terms of osculating elements, is found attractive for studying the influence of the solar radiation force upon the orbital geometry.

(ii) For a plate normal to the radiation, short- and long-term analytical solutions have been formulated using a straightforward and a two-variable expansion perturbation methods. The in-plane changes are illustrated by means of polar plots. The long-term behavior of the orbital inclination can be interpreted in terms of the in-plane perturbations.

(iii) A short-term analytical solution is presented for the case where a satellite is kept in a fixed arbitrary orientation with respect to the radiation or inertial space. The long-term perturbations in eccentricity and argument of the perigee may be of a secular nature when part of the radiation is absorbed.

(iv) Solutions for a satellite modelled as a plate in a fixed orientation with respect to the local reference frame are obtained. Relatively large perturbations in the semi-major axis are observed when the reflecting properties on the two sides are not the same.

4. GEOCENTRIC ORBITAL CONTROL USING SOLAR RADIATION FORCES

4.1 Preliminary Remarks

In many situations, the perturbing effects of the solar radiation force as assessed in the previous two chapters are detrimental in nature, e.g. a communications satellite drifts away from its desired overhead position. On the other hand, these forces have a potential for effecting desired changes in satellite orbits as demonstrated most dramatically by the concept of a solar sail. The transfer of the sail from a low or intermediate orbit around the earth into a heliocentric orbit forms an important and time-consuming phase of the mission. Therefore, strategies for raising the orbit of a spacecraft by means of solar radiation would represent an important aspect of this maneuver. In particular, the chapter studies optimal sail settings for maximum increase in major axis over one revolution. However, the analysis has a wider range of applicability since it also provides ways for orbital correction of a satellite with controllable solar arrays. The proper orientation of these panels can be maintained by means of small solar-electric servomotors. While an interesting procedure for increasing the total energy (plate with different reflectivities on either side) was considered in Section 3.5, a more effective on-off switching strategy is studied here. During the off-phase when the satellite moves towards the sun, the plates are aligned with the radiation, while in the on-phase (when moving away from the sun) the arrays are kept normal to the radiation for generating the maximum force. The most effective switching points for correction of the orbital elements are assessed and their res-

ponses evaluated.

Another interesting application for which the analysis presented here would be relevant consists of a mylar-coated plastic sphere with a pumping device which inflates and deflates the balloon at prescribed instants. This concept has the advantage that it does not require the continuous orientation control of a solar sail.

For convenience the switchings are assumed to take place instantaneously since the time needed for completion of the operation would usually represent a negligible fraction of the orbital period. For a particular strategy, the first-order changes in the orbital elements after one revolution are evaluated by integration of the perturbation Equations (3.11) over the appropriate on-interval $I_{on} = (\nu_{on}, \nu_{off})$, while keeping the orbital elements on the right-hand-side constant.

4.2 Switching at Perigee and Apogee

An obvious switching strategy would be to switch off at apogee and on again at the subsequent perigee, Figure 4-1. Upon integration over the interval $I_{on} = (\tilde{\omega}_{00}, \tilde{\omega}_{00} + \pi)$, the following explicit results are found, using the integrals of Appendix I:

$$\Delta\ell = 3\pi\,\varepsilon\, a^3(1 - e^2)^{1/2}\,[pK_{20} - qK_{10}]/e + 4\varepsilon\, a^3(1 - e^2)\,[pK_{10} + qK_{20}]/e\ ;$$

$$\Delta a = 4\varepsilon\, a^3(pK_{10} + qK_{20})/e\ ;$$

$$\Delta e = 3\pi\,\varepsilon\, a^2(1 - e^2)^{1/2}\,[pK_{10} + qK_{20}]/(2e) + 2\varepsilon\, a^2[pK_{20} - qK_{10}\ ;$$

$$\Delta\Omega = \varepsilon\, a^2\, \sin\hat{n}[2\cos\omega - (3\pi/2)\sin\omega/(1 - e^2)^{1/2}];$$

$$\Delta i = -\varepsilon\, a^2 \sin(i)\, \sin\hat{n}[2\sin\omega + (3\pi/2)\cos\omega/(1 - e^2)^{1/2}]\,. \qquad .....(4.1)$$

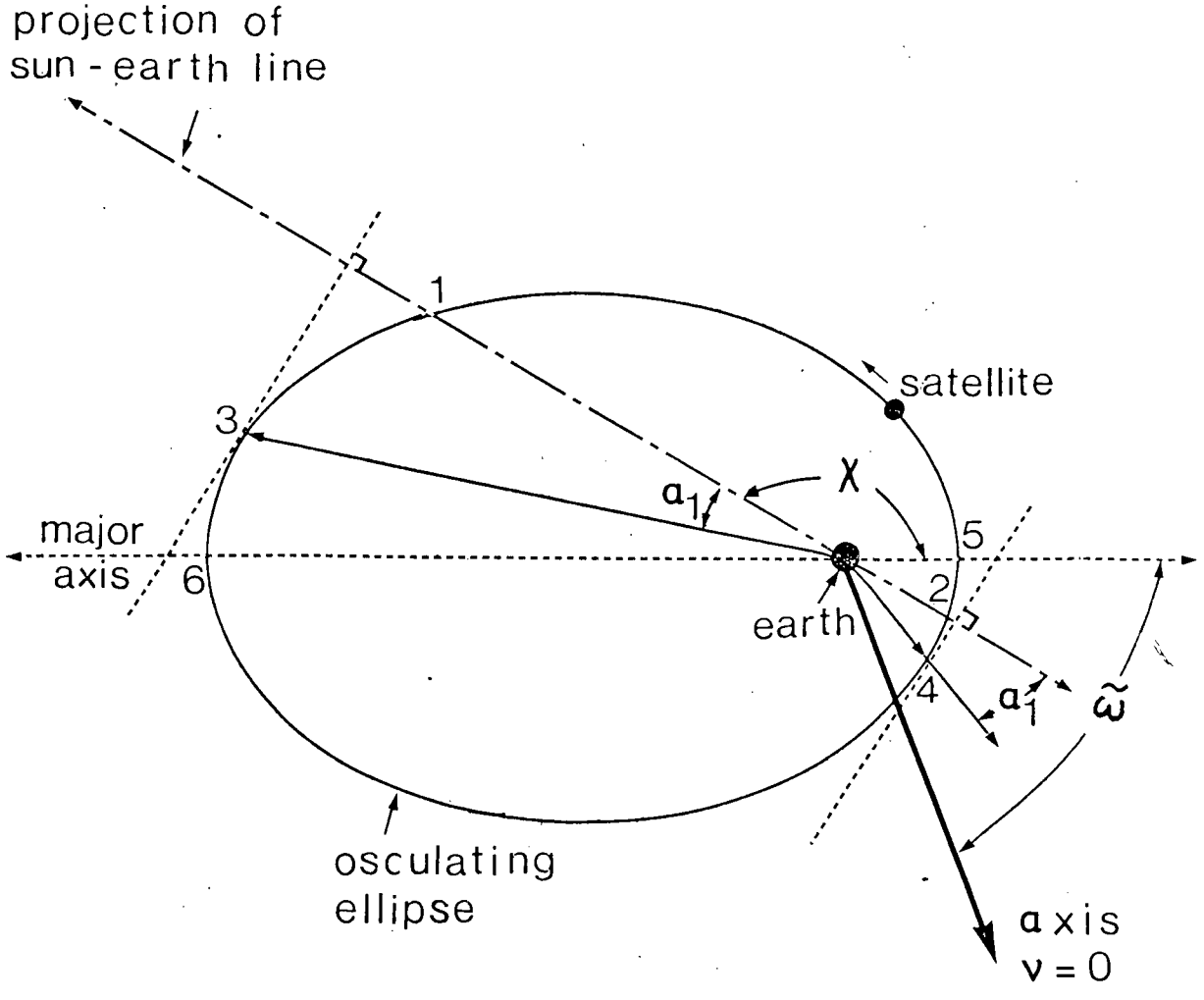

Figure 4-1 Configuration of switching points for controlled orbital change

Here, it is assumed that e does not vanish. It must be mentioned that the subscripts 00 are omitted in the present chapter for brevity. It is interesting that the change in eccentricity is exactly half of the amount obtained when the force acts continuously, Equations (3.13). For near-ecliptic orbits, the expressions $pK_{10} + qK_{20}$ and $pK_{20} - qK_{10}$ may be replaced by $\cos\chi$ and $\sin\chi$ respectively, where χ is the angle between the projection of the sun-earth line and the major axis, Figure 4-1. It is seen that if $0 < \chi < \pi$ the satellite moves against the direction of radiation and looses energy, while if $\pi < \chi < 2\pi$ the major axis increases.

Obviously, the expressions of Equations (4.1) are only valid for one revolution. Long-term results are derived by rectification and iteration of the short-term orbital changes. Figure 4-2 shows the resulting long-term response for the particular case of an orbit in the ecliptic plane. There is a wide range of variation in the behavior of the semi-latus rectum depending on the initial solar aspect angle. In the case that the major axis follows the motion of the sun, a favorable situation is maintained leading to a continuous increase in ℓ: (curve 1). However, in most cases, especially for larger e_{00}, the axis rotation fails to keep up with the sun (Chapter II), so that in the long run no systematic build-up in the latus rectum or the major axis occurs as shown by the other curves. The long-term variations in eccentricity are found to be of approximately half the amplitude as compared to the case of a continuously acting force.

4.3 Systematic Increase in Angular Momentum

Since the nature of the response in the previous on-off switching strategy seems to be strongly dependent upon the initial conditions, a more

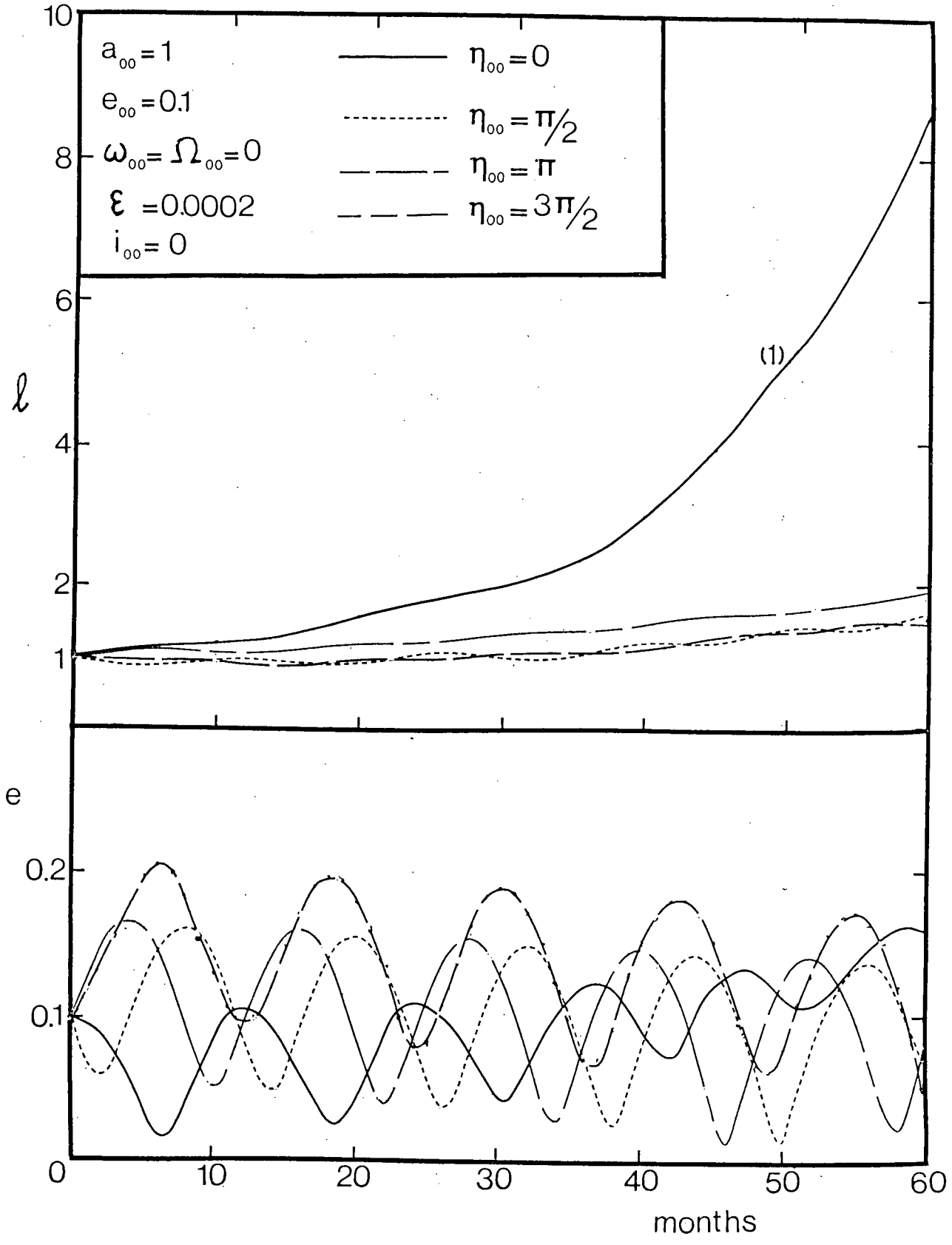

Figure 4-2 Results of perigee-apogee switching strategy

systematic approach is needed to generate a certain prescribed trend. In this section, a switching control strategy with the objective to change the orbital size by increasing the semi-latus rectum as much as possible is explored.

The most effective switching instants are the points where $\ell'(\nu)$ vanishes: ν_1 and ν_2, Figure 4-1. The on-phase (ν_1, ν_2) coincides with $\ell'(\nu) > 0$ and the off-phase $(\nu_2, \nu_1 + 2\pi)$ with $\ell'(\nu) < 0$. The points ν_1 and ν_2 satisfy the equation $u_y^s = 0$ and represent, geometrically, the points of intersection of the orbit with the projection of the sun-earth line into the orbital plane: $\nu_1 = \psi + \arctan[\cos(i) \tan\hat{\eta}]$ and $\nu_2 = \nu_1 + \pi$. During the on-phase the force has a positive component along the circumferential direction and produces a torque $\underline{r} \times \underline{F}$ adding to the magnitude of the angular momentum vector $\underline{h}$ and the semi-latus rectum $\ell = h^2$.

While the orbital changes can be determined readily by means of a digital computer, analytical results are established for an orbit in the ecliptic plane where $I_{on} = (\eta, \eta + \pi)$:

$$\Delta\ell = 2\varepsilon a^2\ell[3 - (1 - e^2)/(1 - e^2\cos^2\chi) + 3e F_1(e,\chi) \sin\chi] ;$$

$$\Delta a = 4\varepsilon a^2\ell/(1 - e^2\cos^2\chi) ;$$

$$\Delta p = -3\varepsilon a\ell F_2(e,\chi) \sin\eta ; \qquad \Delta q = 3\varepsilon a\ell F_2(e,\chi) \cos\eta ;$$

$$\Delta e = -3\varepsilon a\ell F_2(e,\chi) \sin\chi ; \qquad \Delta\omega = 3\varepsilon a\ell F_2(e,\chi) \cos\chi . \quad .....(4.2)$$

The functions $F_1(e,\chi)$ and $F_2(e,\chi)$ are defined by

$$F_1(e,\chi) = \{\pi/2 + \arctan[e \sin\chi/(1 - e^2)^{1/2}]\}/(1 - e^2)^{1/2} ;$$

$$F_2(e,\chi) = e \sin\chi/(1 - e^2 \cos^2\chi) + F_1(e,\chi) \; . \qquad .....(4.3)$$

The most favorable position of the sun for the increase $\Delta\ell$ occurs when the sun-earth line is normal to the major axis. While the expressions in Equations (4.2) designate the changes in the orbital elements after one revolution, the long-term behavior is determined by repeated rectification and iteration of these results. Figure 4-3 shows the long-term implications of this switching strategy: taking a satellite with the parameter $\varepsilon = 0.0002$, i.e. $A/m = 5\ m^2/kg$, the semi-latus rectum increases ten-fold in less than five years when starting out from geosynchronous altitude. The response is almost insensitive to changes in initial eccentricity and solar aspect angle.

4.4 Systematic Increase in Total Energy

While the strategy proposed in the previous section is the most effective on-off switching control for increasing the angular momentum, this policy is (in the case of a non-circular orbit) not the most favorable one for increasing the total energy of the satellite.

The on-off switching points ν_3 and ν_4 representing the zeros of $a'(\nu) = 0$ correspond to the instants at which the in-plane component of the solar radiation force is normal to the instantaneous velocity vector, i.e. the tangent to the osculating ellipse:

$$a'(\nu) = 2a^2 (\underline{F} \cdot \dot{\underline{r}})/\dot{\nu} =$$

$$= 2\varepsilon\, a r^2 \{u_x^s (p \sin\nu - q \cos\nu) + u_y^s (1 + p \cos\nu + q \sin\nu)\}/(1-e^2). \qquad .....(4.4)$$

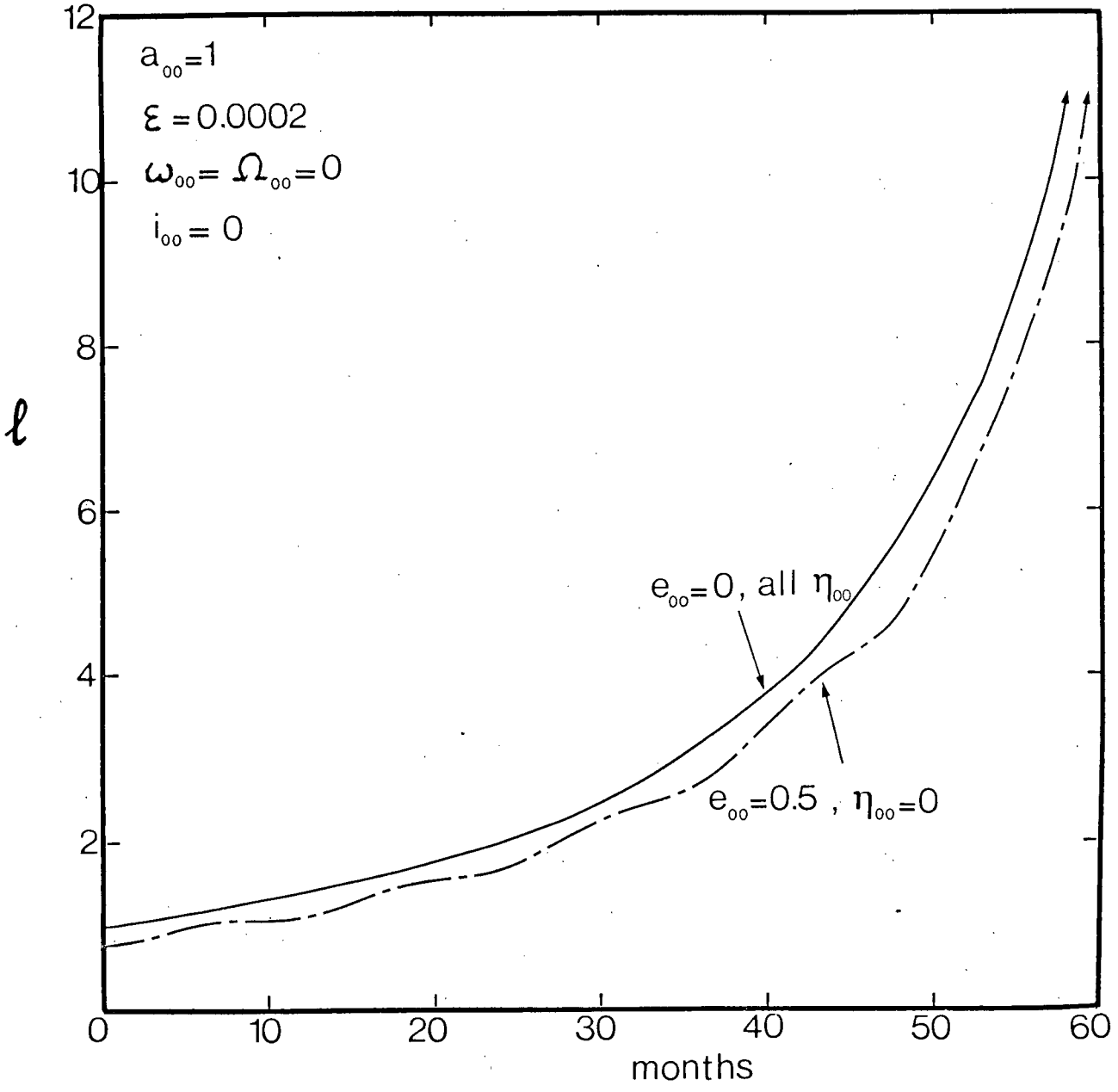

Figure 4-3 Behavior of semi-latus rectum in (ν_1, ν_2) switching program

Locations of the switching points ν_3 and ν_4 are indicated in Figure 4-1 and can be expressed in the following form (for inclination less than 90°),

$$\nu_3 = \hat{\eta} + \psi + \delta_3 + 2\pi(k-1) , \quad \nu_4 = \pi + \hat{\eta} + \psi - \delta_4 + 2\pi(k-1), \quad ..(4.5)$$

where k denotes the appropriate revolution and δ_3 and δ_4 are to be determined by iteration: $\delta_3^{(0)} = \delta_4^{(0)} = \alpha_1 = \arcsin[e \sin(\hat{\eta} - \omega)]$ and

$$\delta_3^{(n)} = \arcsin\{e \sin(\hat{\eta} - \omega) + \tan(i^2/2)[\sin(\delta_3^{(n-1)} + 2\hat{\eta}) + e \sin(\hat{\eta} + \omega)]\},$$

$$\delta_4^{(n)} = \arcsin\{e \sin(\hat{\eta} - \omega) + \tan(i^2/2)[\sin(\delta_4^{(n-1)} - 2\hat{\eta}) + e \sin(\hat{\eta} + \omega)]\}, \quad (4.6)$$

for n = 1,2,3,.... This process converges very rapidly (only four iterations are needed for accuracy to four significant decimal places) for an equatorial orbit.

While the resulting orbital changes for this switching strategy are determined numerically in the case of an arbitrary orbit, analytical expressions can be obtained for an orbit in the ecliptic plane. In that case, $\hat{\eta} - \omega$ equals $\chi = \eta - \tilde{\omega}$ and represents the angle between the sun-earth line and the major axis, Figure 4-1. Writing $\alpha_1 = \arcsin(e \sin\chi)$, it follows that $\nu_3 = \eta + \alpha_1$ and $\nu_4 = \eta + \pi - \alpha_1$. The on-phase (ν_3,ν_4) is less than π radians if χ lies in $(0,\pi)$ and more than π if χ is in $(\pi,2\pi)$. If $e = 0$, it follows that $\alpha_1 = 0$ and the present control strategy, obviously, coincides with the one of the previous section. The response of the orbital elements is obtained by substitution of the limits of integration ν_3 and ν_4 into the integrated results of Equations (3.11). After considerable algebraic simplification, the changes in the elements can be written as,

$$\Delta a = 4\varepsilon a^3(1 - e^2 \sin^2\chi)^{1/2} ,$$

$$\Delta \ell = 3\pi \varepsilon a^3 e \sin\chi (1 - e^2)^{1/2}$$

$$+ 4\varepsilon a^2 \ell(1 + e^2 \sin^2\chi)/(1 - e^2 \sin^2\chi)^{1/2} ,$$

$$\Delta p = -\varepsilon a^2 G(e,\chi)\sin\eta - \varepsilon a^2 e^2 q \sin(2\chi)/(1 - e^2 \sin^2\chi)^{1/2} ,$$

$$\Delta q = \varepsilon a^2 H(e,\chi)\cos\eta + \varepsilon a^2 e^2 p \sin(2\chi)/(1 - e^2 \sin^2\chi)^{1/2} ,$$

$$\Delta e = -\varepsilon a^2 H(e,\chi)\sin\chi ,$$

$$\Delta \omega = \varepsilon a^2 H(e,\chi)\cos\chi/e + \varepsilon a^2 e^2 \sin(2\chi)/(1 - e^2 \sin^2\chi)^{1/2} , \quad .....(4.7)$$

with the auxiliary function $H(e,\chi)$ defined by

$$H(e,\chi) = 3\pi(1 - e^2)^{1/2}/2 + 4 e(1 - e^2)\sin\chi/(1 - e^2 \sin^2\chi)^{1/2}. \quad .....(4.8)$$

It can be shown that Δa is larger while $\Delta \ell$ is smaller than the corresponding expressions of the previous section when $e > 0$ and that the results coincide for $e = 0$. Furthermore, the two switching policies are identical when $\chi = 0$ or π for any eccentricity.

While the long-term implications of the present switching strategy can be assessed by repeated rectification and iteration of the results of Equations (4.7), an additional insight into the long-term orbital behavior can be obtained by means of the two-variable expansion procedure. The system of equations considered here has a (partly) discontinuous right-hand-side and is written symbolically as

$$\tilde{\underline{a}}'(\nu) = \begin{cases} \varepsilon\, \tilde{\underline{f}}(\underline{a},\nu) & , \ \nu \text{ in } I_{on} \ , \\ \underline{0} & , \ \nu \text{ in } I_{off} \ , \end{cases}$$

$$\eta'(\nu) = \delta\, r^2/\ell^{1/2}, \qquad \text{.....(4.9)}$$

where the vector $\tilde{\underline{\alpha}}$ stands for the set of usual orbital elements, excluding the solar aspect angle η. As usual, the zeroth-order two-variable expansion results yield $\underline{a}_0 = \underline{a}_0(\bar{\nu})$ with $\underline{a}_0(0) = \underline{a}_{00}$. The first-order equations are found to be of the form:

$$\frac{\partial \tilde{\underline{\alpha}}_1}{\partial \nu} = \begin{cases} -\tilde{\underline{a}}_0'(\bar{\nu}) + \tilde{\underline{f}}[\underline{a}_0(\bar{\nu}),\, \nu] & , \ \nu \text{ in } I_{on}(\bar{\nu}) \ , \\ -\tilde{\underline{a}}_0'(\bar{\nu}) & , \ \nu \text{ in } I_{off}(\bar{\nu}) \ , \end{cases}$$

$$\frac{\partial \eta_1}{\partial \nu} = -\eta_0'(\bar{\nu}) + \ell_0^{3/2}/[c_\varepsilon(1 + p_0 \cos\nu + q_0 \sin\nu)^2] \ , \qquad \text{.....(4.10)}$$

where it should be emphasized that the limits of the intervals I_{on} and I_{off} are functions of the slow variable $\bar{\nu}$. In order to eliminate secular contributions to the first-order terms $\underline{a}_1(\nu,\bar{\nu})$, average values of the right-hand-sides are required to vanish, yielding

$$\frac{\partial \tilde{\underline{a}}_0}{\partial \bar{\nu}} = \int_{I_{on}(\bar{\nu})} \tilde{\underline{f}}[\underline{a}_0(\bar{\nu}),\, \tau]\, d\tau/(2\pi) \ ;$$

$$\frac{\partial \eta_0}{\partial \bar{\nu}} = a_0^{3/2}(\bar{\nu})/c_\varepsilon \ . \qquad \text{.....(4.11)}$$

The first-order equations for $\underline{a}_1$ may be determined by a Fourier expansion of the discontinuous, yet periodic, function on the right-hand-side of

Equations (4.10), although convergence of the series is expected to be slow.

This scheme leads to the following set of equations in a_0, $x_0 = e_0 \sin(\eta_0 - \tilde{\omega}_0)$ and $y_0 = e_0 \cos(\eta_0 - \tilde{\omega}_0)$:

$$a_0'(\bar{\nu}) = 2a_0^3(1 - x_0^2)^{1/2}/\pi \ ;$$

$$x_0'(\bar{\nu}) = y_0\, a_0^{3/2}/c_\varepsilon - x_0\, a_0^2[1 + (1 - x_0^2 - y_0^2)/(1 - x_0^2)^{1/2}]/\pi \ ;$$

$$y_0'(\bar{\nu}) = -x_0\, a_0^{3/2}/c_\varepsilon + y_0\, a_0^2\, x_0^2/[\pi(1 - x_0^2)^{1/2}] \ . \qquad .....(4.12)$$

The system of Equations (4.12) was integrated numerically using a double-precision Runge Kutta routine with error control. The solution was found to be in good agreement with the one from the rectification and iteration method: over approximately four years, the results are consistent up to the first decimal place, Figure 4-4. Eventually, however, they diverge. Also shown is the response to the switching in case of a lower orbit, $a_{00} = 0.34$, i.e. about 8000 km above the earth. As the gravity force is more dominant here, the advance to higher orbits is much slower. Nevertheless, geosynchronous altitude can be reached within five years. This would be of interest for future space stations like the SSPS, which are to be constructed in a low-altitude orbit: employing the present switching strategy, these structures could propel themselves to a geosynchronous location.

An analytical estimate (i.e. upper bound) for $a_0(\bar{\nu})$ is readily obtained from Equations (4.12),

$$a_0(\bar{\nu}) \leq a_{00}/(1 - 4\,\bar{\nu}\, a_{00}^2/\pi)^{1/2} \ . \qquad .....(4.13)$$

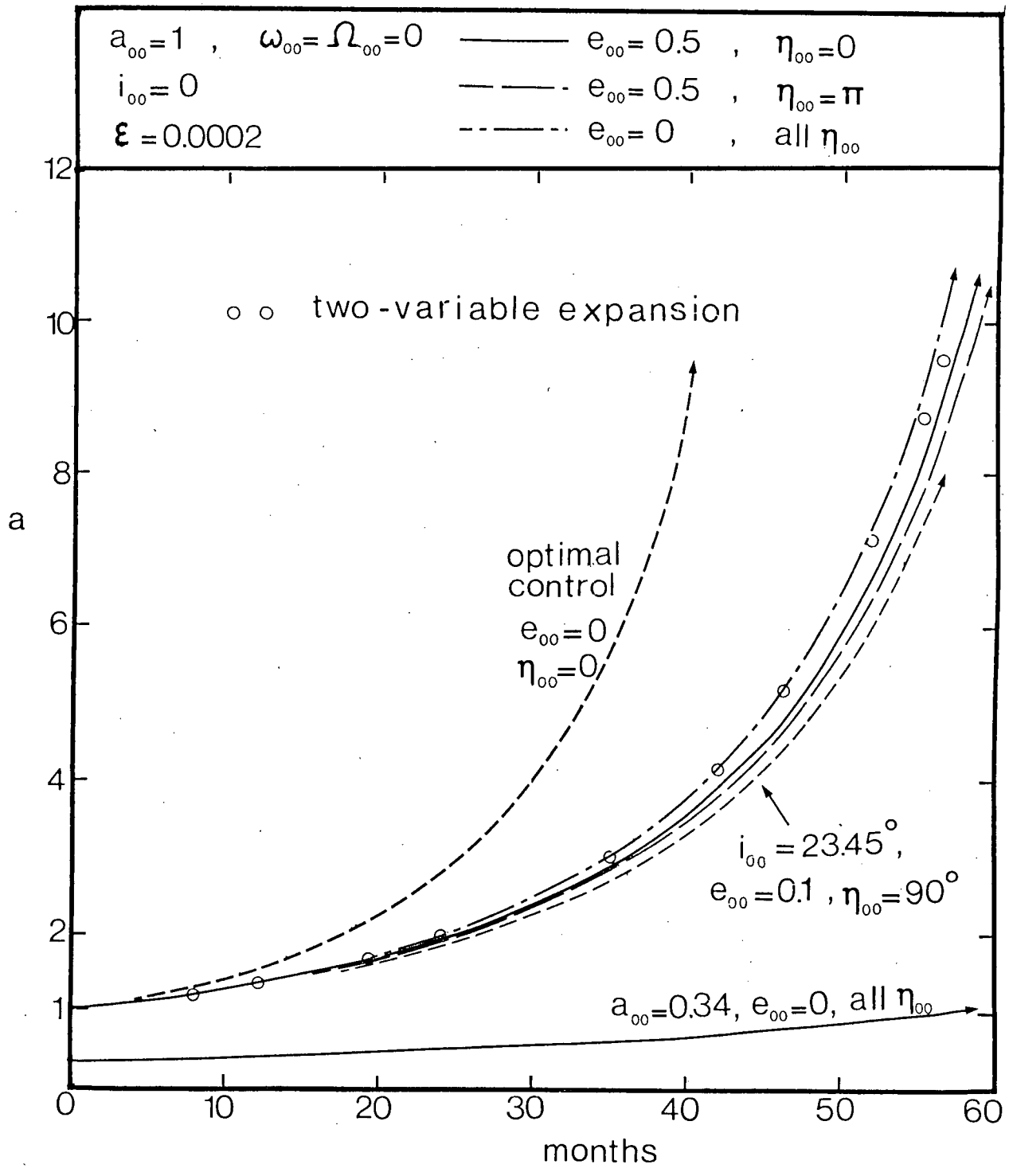

Figure 4-4 Controlled variation of the semi-major axis for (ν_3, ν_4) switching program and optimal control strategy

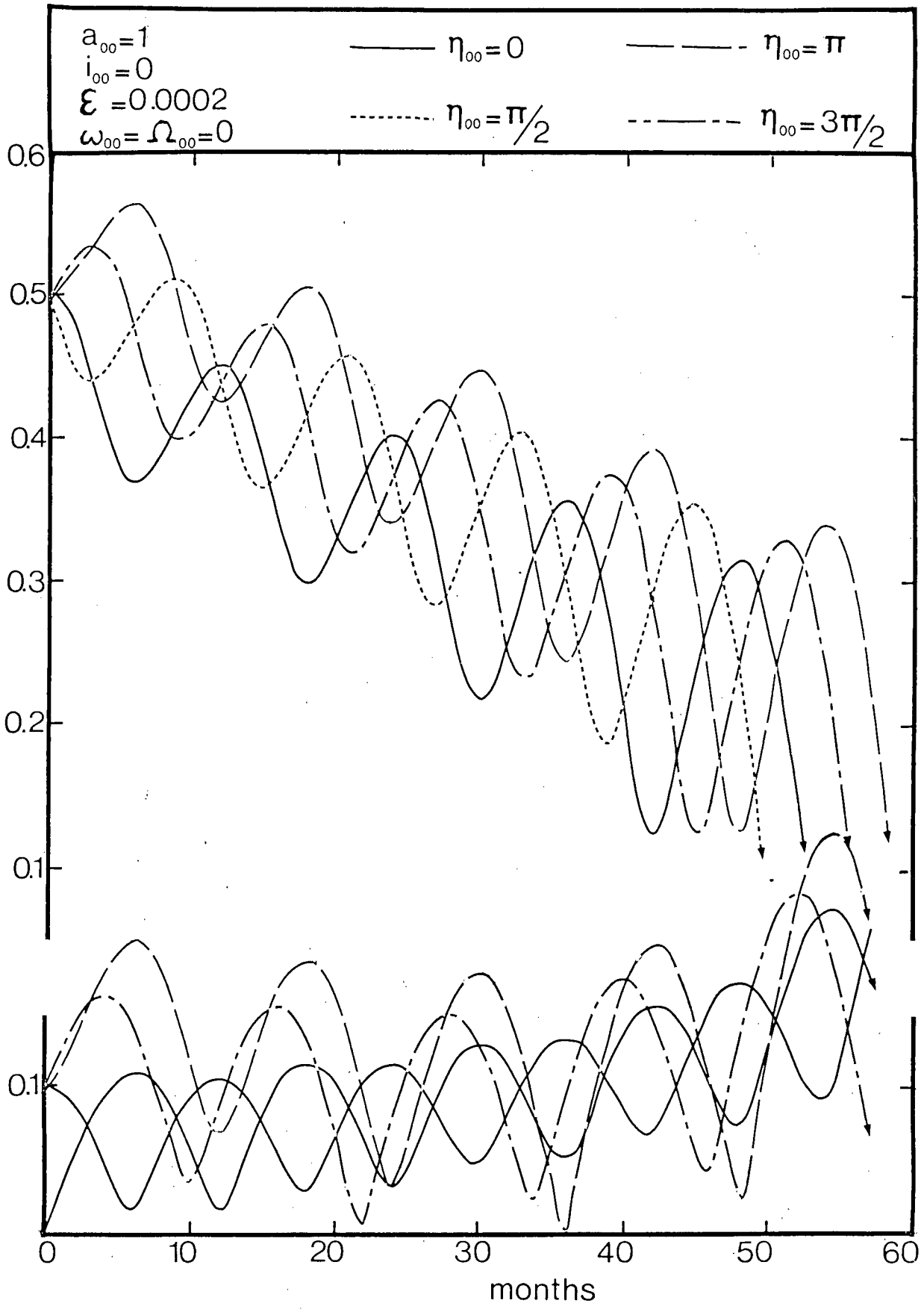

Figure 4-5 Long-term variations in eccentricity during (ν_3,ν_4) switching program

It predicts that an escape trajectory would not be reached before $\nu = \pi/(4\varepsilon\, a_{00}^2)$, i.e. about 625 revolutions or 7 years in the present example, $\varepsilon = 0.0002$, $a_{00} = 1$. This crude approximation yields remarkably good values (identical in first decimal) for the semi-major axis over the first 3 years (or 550 revolutions) for $e_{00} = 0.1$ and even over 4.5 years if $e_{00} = 0$. The same formula can also be used for predicting the major axis when the orbit is out of the ecliptic, provided that an adjustment is made for the average effective in-plane component of the force, which is accomplished by multiplying ε by the factor $1 - (\sin^2 i)/4$. For an equatorial orbit this factor amounts to about 0.96 and the approximate formula predicts the semi-major axis correctly up to the first decimal over the first 450 revolutions (about two years) for $e_{00} = 0.1$ and $\eta_{00} = \pi/2$ as compared to the results of the rectification/iteration procedure shown in Figure 4-4.

Figure 4-5 shows the behavior of the eccentricity under the influence of the present switching policy. In general, it can be concluded that for small eccentricity, the resulting orbit remains near-circular, whereas for an initially highly elliptic orbit the eccentricity decreases in the long run.

4.5 Optimal Orbit Raising

Although the on-off switching strategy of the previous section proves to be very effective for increasing the total energy of a solar sail, it is obvious that a judiciously chosen, continually varying, sail setting could be even more effective. Therefore, in the present section, the optimal control strategy yielding the maximum possible increase in total energy per revolution is determined. This is done by means of a numerical steepest-

ascent iteration procedure[118-120].

To save some computational effort, the system of equations is transformed to an autonomous form by introducing the auxiliary elements Φ, Ψ, K, L and M:

$$\begin{pmatrix} \Phi \\ \Psi \end{pmatrix} = \begin{pmatrix} \cos\nu & \sin\nu \\ \sin\nu & -\cos\nu \end{pmatrix} \begin{pmatrix} p \\ q \end{pmatrix} ;$$

$$K = \cos(i), \quad L = \sin(i)\sin(\nu - \psi), \quad M = \sin(i)\cos(\nu - \psi). \qquad .....(4.14)$$

The variations in the elements are now described by the system:

$$\begin{aligned}
a'(\nu) &= 2a^2 \ell\{F_x(\underline{\alpha})\,\Psi/(1+\Phi)^2 + F_y(\underline{\alpha})/(1+\Phi)\} ; \\
\Phi'(\nu) &= -\Psi + 2\ell^2 F_y(\underline{\alpha})/(1+\Phi)^2 ; \\
\Psi'(\nu) &= \Phi + \ell^2\{F_x(\underline{\alpha}) + F_y(\underline{\alpha})\,\Psi/(1+\Phi)\}/(1+\Phi)^2 ; \\
\ell'(\nu) &= 2\ell^3 F_y(\underline{\alpha})/(1+\Phi)^3 ; \\
t'(\nu) &= \ell^{3/2}/(1+\Phi)^2 ; \\
K'(\nu) &= -F_z(\underline{\alpha})\,\ell^2 L/(1+\Phi)^2 ; \\
L'(\nu) &= -M + F_z(\underline{\alpha})\,\ell^2 K/(1+\Phi)^3 ; \\
M'(\nu) &= L . \qquad .....(4.15)
\end{aligned}$$

The dependence of $\underline{F}$ upon the control angles $\underline{\alpha} = (\alpha,\beta)$ is due to the fact that the normal to the plate is a function of $\underline{\alpha}$: $\underline{u}^n = \underline{u}^n(\underline{\alpha})$. The system of Equations (4.15) is denoted by $\underline{a}'(\nu) = \varepsilon\, \underline{g}(\underline{a},\underline{\alpha})$ for convenience.

The various steps involved in determining the optimal control function $\underline{\alpha}^*$ yielding the maximum value for $a(2\pi)$ may be briefly described as follows. First, a reasonable starting control function $\underline{\alpha}_0(\nu)$ is chosen and the corresponding response vector $\underline{a}(\underline{\alpha}_0,\nu)$ is calculated by means of (Runge-Kutta) integration of Equations (4.15) with initial conditions $\underline{a}(0) = \underline{a}_{00}$. The results are stored in a two-dimensional array containing the elements $a_j(\underline{\alpha}_0,\nu)$, $j = 1,2,\ldots,8$ at $\nu = 2\pi\ k/n$, $k = 1,2,\ldots,n$ with n taken as 360 to start with. It may be noted that it is not necessary to take n very large or to perform a highly precise integration in this first run for $\underline{\alpha}_0(\nu)$ is usually not near the optimal control. Since the objective is to determine a more effective strategy than $\underline{\alpha}_0(\nu)$, the influence of small variations in $\underline{\alpha}_0(\nu)$ is studied. The near-by control $\underline{\alpha}(\nu) = \underline{\alpha}_0(\nu) + \delta\underline{\alpha}(\nu)$, with the norm $||\delta\underline{\alpha}||$ (defined as the integral over $(0,2\pi)$ of the dot-product of $\delta\underline{\alpha}(\nu)$ with itself) small and prescribed, is considered. An estimate for the difference in the final value of the semi-major axis for this new control function as compared to the final response for $\underline{\alpha}_0$ is found by means of a first-term Taylor expansion of Equations (4.15) around $\underline{\alpha} = \underline{\alpha}_0$, yielding:

$$\delta a(2\pi) = \int_0^{2\pi} \left[\sum_{j=1}^{2} \Lambda_j(\tau)\ \delta\alpha_j(\tau)\right] d\tau\ , \qquad \ldots\ldots(4.16)$$

where the influence functions $\Lambda_j(\nu)$ are defined by

$$\Lambda_j(\nu) = \sum_{k=1}^{8} \lambda_k(\nu) \left(\frac{\partial g_k}{\partial \alpha_j}\right)_{\underline{a}(\underline{\alpha}_0,\nu)}\ , \qquad j = 1,2, \qquad \ldots\ldots(4.17)$$

with the vector of adjoint variables $\underline{\lambda}(\nu)$ determined from the system of equations:

$$\lambda_k'(\nu) = -\sum_{i=1}^{8} \lambda_i(\nu) \left(\frac{\partial g_i}{\partial a_k} \right)_{\underline{a}(\underline{\alpha}_0,\nu)} , \quad k = 1,2,\ldots,8 , \qquad .....(4.18)$$

and final conditions $\lambda_1(2\pi) = 1$, $\lambda_j(2\pi) = 0$, $j = 2,3,\ldots,8$. One would like to know: which variation of the control, $\delta\underline{\alpha}(\nu)$, leads to the maximum possible change in response, $\delta a(2\pi)$, given in Equations (4.16), under the constraint that the stepsize $||\delta\underline{\alpha}||$ is prescribed? The answer is obtained through Lagrange multipliers, yielding the following control strategy:

$$\delta\underline{\alpha}(\nu) = \{||\delta\underline{\alpha}|| \; / \; ||\underline{\Lambda}||\}^{1/2} \; \underline{\Lambda}(\nu) . \qquad .....(4.19)$$

Upon substitution of this result into Equation (4.16), $\delta\underline{a}(2\pi)$ is written in terms of the norms $||\delta\underline{\alpha}||$ and $||\underline{\Lambda}||$. Subsequently, $||\delta\underline{\alpha}||$ can be eliminated from Equation (4.19),

$$\delta\underline{\alpha}(\nu) = \delta a(2\pi) \; \underline{\Lambda}(\nu) \; / \; ||\underline{\Lambda}|| , \qquad .....(4.20)$$

expressing the variation of the control angles explicitly in terms of the prescribed increase in the semi-major axis.

For the calculation of the influence functions, Equation (4.17), the derivatives of the right-hand-side of Equations (4.15) with respect to all state variables as well as the control angles are needed. This is a straightforward, though very tedious, process. With these results in hand, the equations for $\underline{\lambda}$ are known, Equation (4.18), and these are integrated backwards by means of the Runge-Kutta routine, using a piecewise constant approximation for the state variables stored in the array mentioned before. Now, the influence functions are also known and the new control function is determined from Equation (4.20). Subsequently, the whole procedure is repeated. While this process readily leads to a near-optimal control, con-

vergence becomes progressively slower near the optimum and special care must be taken in this region. It was found that by coupling the stepsize and the error parameter of the integration to the length of the 'gradient' $||\Lambda||$, reasonably accurate results could be obtained within about 40 iterations, which amounted to less than a minute of the computer time. Note that $||\Lambda||$ approaches zero as $\underline{\alpha} \rightarrow \underline{\alpha}^*$.

The results of the iteration program for an orbit in the ecliptic plane (β is taken zero, here) and a solar sail with perfect specular reflection are shown in Figure 4-6. Starting out with the control function indicated by N = 1, the response $a(2\pi)$ grows rapidly during the first few iterations while the control program approaches the optimal strategy. The convergence is notably faster in the highly sensitive region near $\nu = \pi/2$, even though the changes in $\underline{\alpha}$ have been subdued here (by means of a weighting function) in favor of those near $\nu = 3\pi/2$. Figure 4-6b shows the optimal orientation of the sail at a few points in the orbit. In the execution of the program, the two sides of the sail are taken to be identical. In case the properties on the two sides are different, a rotation over 180° of the sail will be required at $\nu = 3\pi/2$.

It is interesting to compare the effectiveness of the on-off switching policy, Section 4.4, and the plate having different reflectivities on either side, Section 3.5, with that of the optimal control strategy estabished here. Taking $\varepsilon = 0.0002$, the increase in semi-major axis after one revolution for the various controls is summarized in Table 4.1.

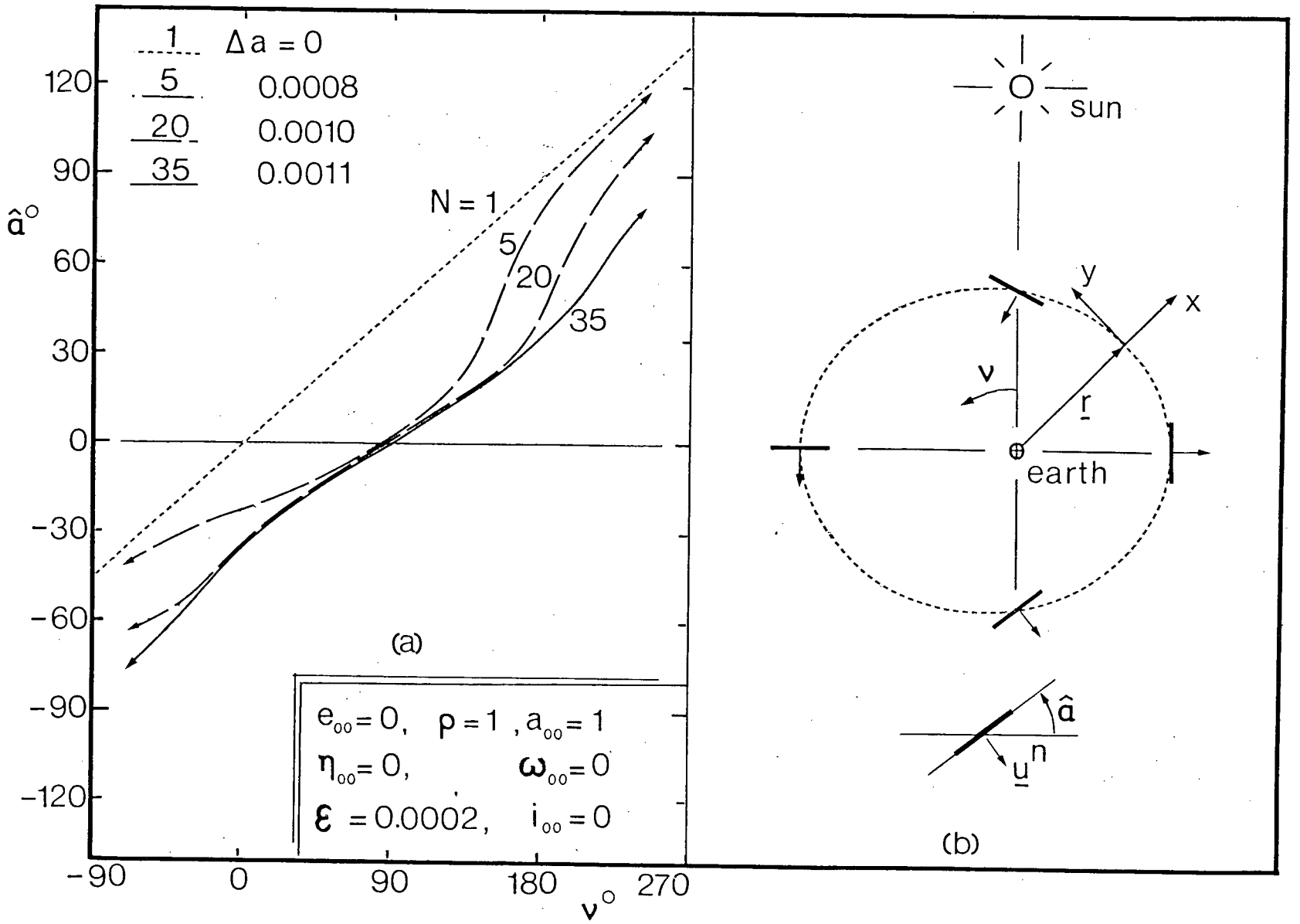

Figure 4-6 (a) Optimal control strategy for maximization of Δa;
(b) Corresponding optimal orientation of solar sail

Table 4.1 Comparison of Control Strategies ($\varepsilon = 0.0002$)

Strategy	e_{00}	ρ_f, ρ_b	$\Delta a \times 10^4$	% of optimal
Optimal Control	0	1	11.0	100
On-Off Switching (ν_3, ν_4)	0	1	8.0	73
$\alpha = 90°$ (Local Vertical), On-Off	0.1	1	6.2	56
$\alpha = 45°$, On-Off	0.1	1	4.9	45
$\alpha = 90°$, Different Reflectivity	0.1	1,0	3.1	28

Judging from Figure 4-6, a linear approximation to the optimal control would be given by $\hat{\alpha}(\nu) = (\nu - \eta - \pi/2)/2$, which remains within 10 degrees of the optimal angle at all times. The response for this steering program was calculated and an increase in the semi-major axis of 10.7×10^{-4} was obtained, amounting to about 97% of the optimal value.

Finally, it must be emphasized that the optimal control strategy determined here is valid for one revolution. For the following orbits, the best control would have to be determined using the particular initial conditions involved. Naturally, to obtain a long-term valid optimal control and corresponding response would take considerable amount of computer time. Fortunately, some idea about the long-term effectiveness of the optimal strategy may be obtained by resorting to the approximate result of Section 4.4. Presuming that the ratio of 100/73, for the increase in semi-major axis of the optimal as compared to the (ν_3, ν_4) on-off switching strategy, will be maintained throughout, Equation (4.14) with ε adjusted accordingly yields an estimate for the long-term effectiveness of the optimal control

program. The result is depicted in Figure 4-4 along with those of the on-off switching trajectories.

4.6 Orientation Control of the Orbital Plane

In this section, the feasibility of controlling orientation of the orbital plane by an on-off switching strategy is investigated. In the beginning, results for the case where the force is acting continually are interpreted so as to obtain a physical appreciation as to the nature of the solar radiation effects upon the orientation of the orbital plane. Note that perturbations of the osculating plane can be visualized by means of the rotation vector $\underline{w}^r = \varepsilon(u_z^s/\ell^{1/2})\underline{r}$, affecting the direction of $\underline{h}$ through $\dot{\underline{h}} = \underline{w}^r \times \underline{h}$, so that $\underline{h}$ rotates instantaneously in a plane normal to the radius vector. In terms of the independent variable ν, the rate of change of the vector $\underline{h}$ is written as

$$\underline{h}'(\bar{\nu}) = \dot{\underline{h}}/\dot{\nu} = \varepsilon\, r^2\, u_z^s(\underline{r} \times \underline{h})/\ell = \varepsilon\, r^3\, u_z^s(\sin\phi\ \underline{i}_n - \cos\phi\ \underline{j}_n)/\ell^{1/2}\ , \qquad .....(4.21)$$

where $\underline{i}_n$ and $\underline{j}_n$ are unit vectors along and normal to the line of nodes in the osculating plane, respectively.

While Equation (4.21) represents the instantaneous rate of change of $\underline{h}$, it is interesting to calculate the total variation in $\underline{h}$ after one full revolution of the satellite. A first-order approximation $\Delta\underline{h}$ is obtained by integrating the right-hand-side of Equation (4.21) from $\nu = 0$ to 2π keeping the slowly changing orbital elements constant. The vector $\Delta\underline{h}$ is expanded in its components along the x_n and y_n axes: $\Delta\underline{h} = \Delta h_1\ \underline{i}_n + \Delta h_2\ \underline{j}_n$, yielding:

$$\Delta h_1 = \varepsilon u_z^s \ell^2 \int_0^{2\pi} \frac{\sin(\nu - \psi)d\nu}{(1 + p\cos\nu + q\sin\nu)^3} = -3\pi \varepsilon u_z^s a^{5/2} e \sin\omega ;$$

$$\Delta h_2 = -\varepsilon u_z^s \ell^2 \int_0^{2\pi} \frac{\cos(\nu - \psi)d\nu}{(1 + p\cos\nu + q\sin\nu)^3} = 3\pi \varepsilon u_z^s a^{5/2} e \cos\omega . \quad .....(4.22)$$

The changes in orientation of the orbital plane can be visualized in terms of the vector $\Delta\underline{h}$ (Figure 3-1). Also, perturbations in the orbital elements i and Ω can be expressed in terms of $\Delta\underline{h}$: $\Delta i = -\Delta h_2/\ell^{1/2}$ and $\sin(i)\,\Delta\Omega = \Delta h_1/\ell^{1/2}$, where Δi and $\Delta\Omega$ are treated as infinitesimal angles.

It is evident that, in case of a circular orbit, the net effect of the solar radiation torque on the direction of $\underline{h}$ must vanish after one revolution, since the effective component of the torque at any position ν is equal in magnitude but opposite in sign to the one at $\nu + \pi$ (in the first-order approximation). For an elliptic orbit, variation in the orientation of the orbital plane depends upon the argument of the perigee with respect to the line of nodes: e.g. if $\omega = 0$ or π, only the inclination will be affected (provided that $\hat{\eta}$ and i are not 0 or π), whereas for $\omega = \pi/2$ $3\pi/2$, the resulting perturbation consists of a pure precession (or regression) of the line of nodes.

The changes Δi and $\Delta\Omega$ obtained by continuous exposure to sunlight pressure are small in the long run, especially for near-circular orbits (of the order ε e). In order to obtain more significant changes in i and Ω, two on-off switching strategies are proposed and their effectiveness as to the nature and magnitude of the variations in the orbital elements is assesed and interpreted.

4.6.1 Control of the inclination

Since $\Delta i = -\Delta h_2/\ell^{1/2}$, it is seen from Equations (4.22) that the inclination would increase continually if the following switching strategy is adopted:

$$\text{if } u_z^s > 0: \quad \underline{\text{on}} \text{ if } \psi - \pi/2 < \nu < \psi + \pi/2 ;$$

$$\text{if } u_z^s < 0: \quad \underline{\text{on}} \text{ if } \psi + \pi/2 < \nu < \psi + 3\pi/2 . \qquad .....(4.23)$$

The condition for the sign of u_z^s is easily translated in terms of the quadrants of the angles i and $\hat{n}$. The resulting changes in i and Ω after one on-off cycle can be determined using the integrals of Appendix I evaluated over the on-interval. In terms of $j = e\cos\omega$ and $k = e\sin\omega$, the results can be written in a compact form as follows:

$$\Delta i = \varepsilon a^2 |u_z^s| \{3 - (1 - e^2)/(1 - k^2) - 3j[\pi/2 - \arctan\{j/(1 - e^2)^{1/2}\}]/(1 - e^2)^{1/2} \};$$

$$\sin(i)\,\Delta\Omega = \varepsilon a^2 |u_z^s| k \{j[3 + 2(1 - e^2)/(1 - k^2)]/(1 - k^2) - 3[\pi/2 - \arctan\{j/(1 - e^2)^{1/2}\}]/(1 - e^2)^{1/2} \}. \qquad .....(4.24)$$

This particular control program changes the inclination appreciably, while leaving the longitude of nodes virtually untouched for near-circular orbits. Note that for near-circular orbits, the change $\Delta\Omega$ is half of that obtained for the case of continuous exposure (Equations 4.22).

It is evident that by taking the opposite strategy of Equations (4.23), i.e. replacing the on-phase by the off-interval, the results of Equations (4.24) would change sign and the inclination decreases.

Figure 4-7 illustrates the long-term effectiveness of the proposed control strategy as found by repeated rectification and iteration of the results in Equations (4.24). Starting out from the equatorial plane ($i_{00} = 23.45°$), about two degrees per year may be added to the inclination for an Echo-type satellite in an initially circular orbit. For orbits with large eccentricity, the rate of change of inclination is much higher (about 10 degrees per year for $e_{00} = 0.5$). Also, with an increase in i_{00} (up to $i_{00} = 90°$), the increase in inclination becomes larger as exemplified by the curve for $i_{00} = 68.45°$, i.e. the initial orbital plane is 45° above the equator.

It is of interest to assess the changes in the other elements under this control strategy. The resulting behavior of the eccentricity is shown in Figure 4-8. As a general rule, it may be concluded that the eccentricity increases steadily until the orbit is normal to the ecliptic plane when it starts declining. The major axis (not shown) decreases at a rate between 0.1 and 0.15 per year and the smaller the initial eccentricity, the larger the decline in the semi-major axis.

4.6.2 Control of the line of nodes

For the line of nodes to exhibit a steady precession, it is necessary that $\Delta h_1/\sin(i) > 0$ leading to the proposed switching strategy:

$$\text{if } \sin(\eta - \Omega) > 0 : \quad \underline{\text{on}} \text{ if } \psi < \nu < \psi + \pi \ ;$$
$$\text{if } \sin(\eta - \Omega) < 0 : \quad \underline{\text{on}} \text{ if } \psi + \pi < \nu < \psi + 2\pi \ . \qquad .....(4.25)$$

The changes in the elements after one revolution under this control strategy are determined using the integrals of Appendix I evaluated over the relevant interval:

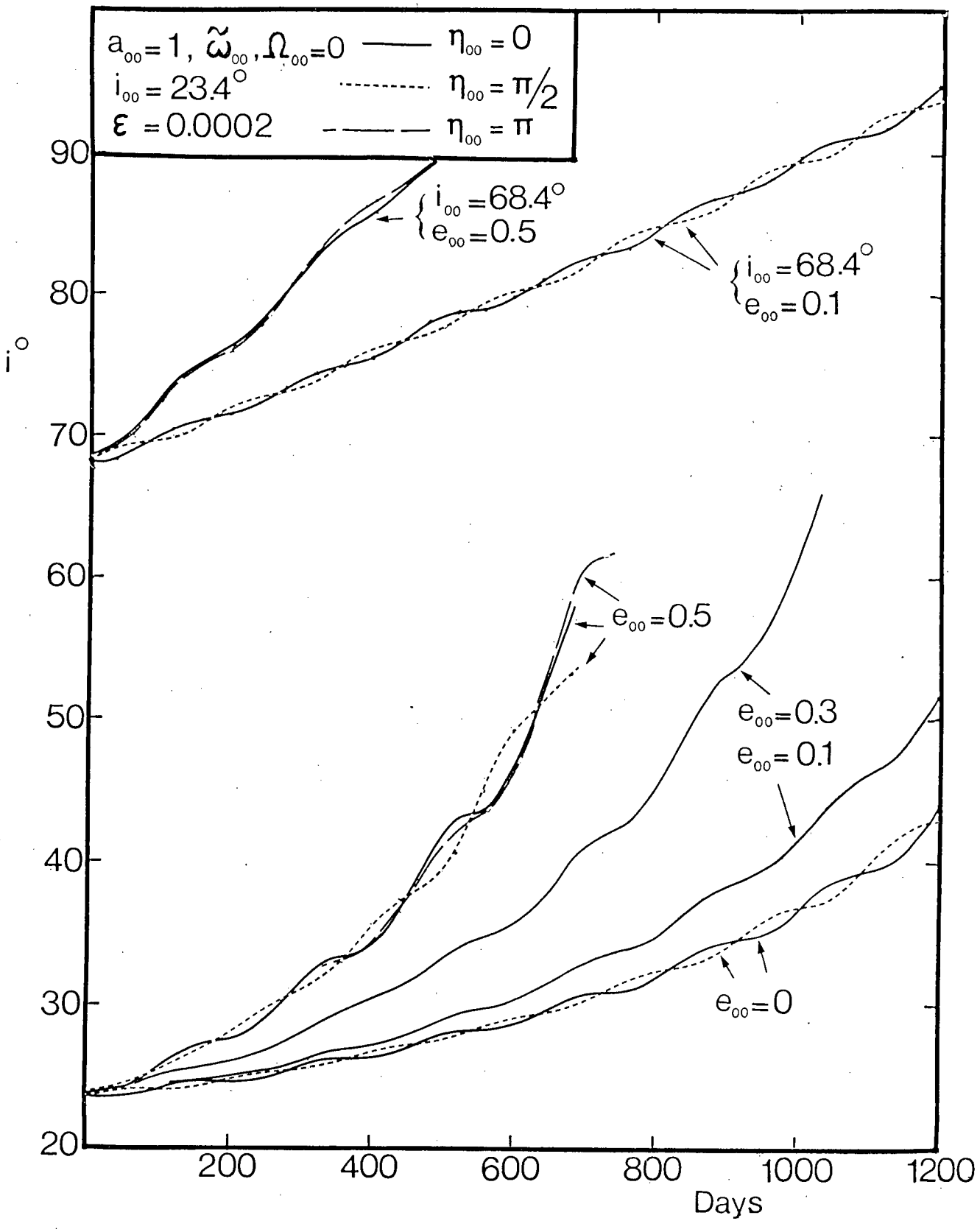

Figure 4-7 Controlled change in inclination for various initial conditions

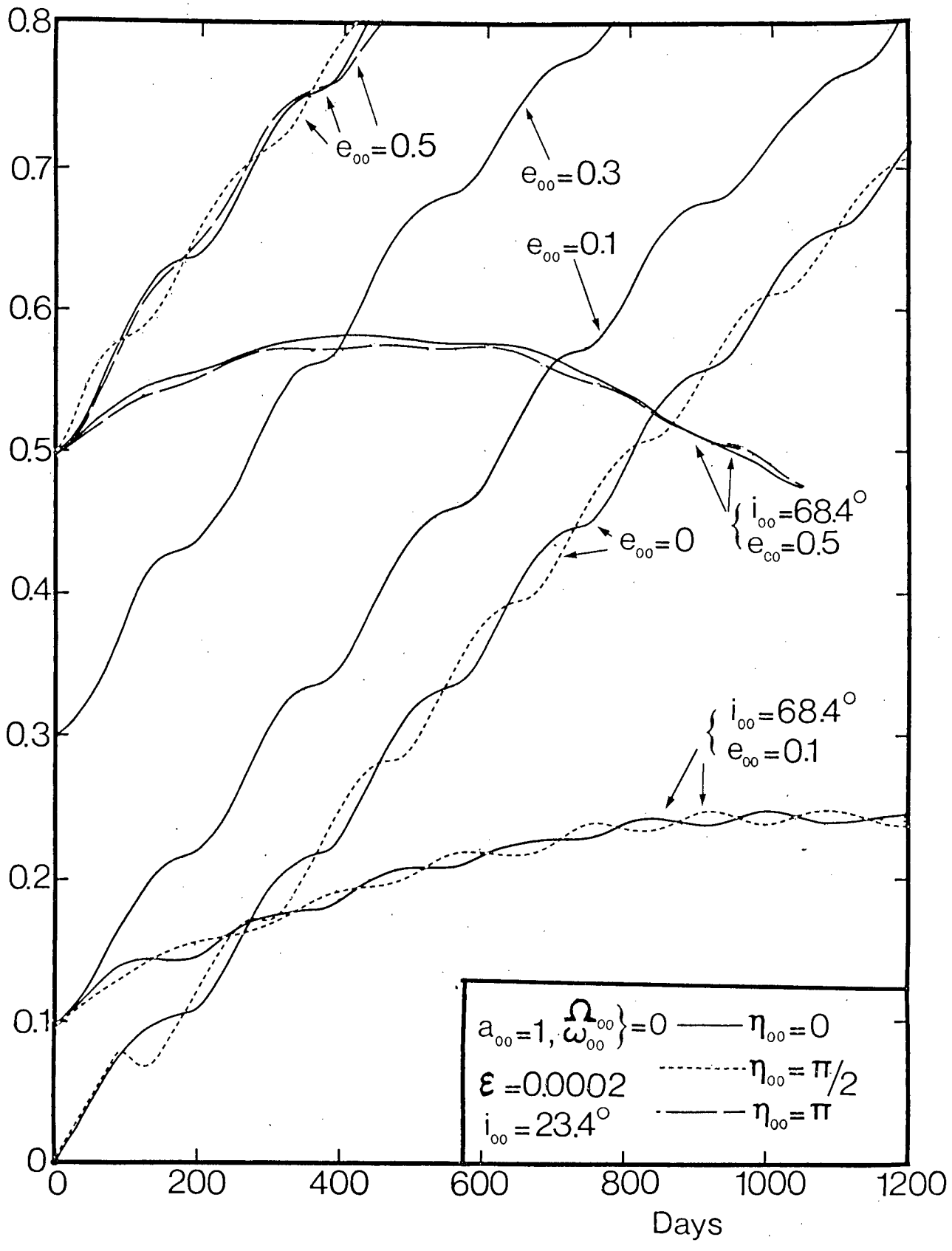

Figure 4-8 Behavior of eccentricity for switching program of Equations (4.23)

$$\Delta\Omega = \varepsilon a^2 |\sin\hat{n}| \{3 - (1 - e^2)/(1 - k^2) - 3k[\pi/2 - \arctan\{k/(1 - e^2)^{1/2}\}]/(1 - e^2)^{1/2}\} ;$$

$$\Delta i = \varepsilon a^2 \sin(i) |\sin\hat{n}| j\{k[3 + 2(1 - e^2)/(1 - k^2)]/(1 - k^2) - 3[\pi/2 - \arctan\{k/(1 - e^2)^{1/2}\}]/(1 - e^2)^{1/2}\}. \quad .....(4.26)$$

This strategy produces a substantial change in the longitude of nodes, while the changes in inclination are relatively small. Also for near-circular orbits, the change in inclination is only half that of the continuous exposure.

Figure 4-9b shows the effectiveness of the proposed switching strategy: for an Echo-type satellite, the line of nodes may precess by as much as five degrees per year, double the amount of the natural perturbations, Section 3.3.3. On the other hand, the behavior is not very sensitive to changes in the initial eccentricity or inclination. Figure 4-9a illustrates the accompanying variations in the eccentricity: in general, the eccentricity decreases for highly elliptic orbits but increases for initially near-circular trajectories. By following the opposite strategy of Equations (4.25), the line of nodes could be made to regress instead of advance.

4.7 Half-Yearly Switching

Another interesting strategy for achieving fairly large changes in the orbital elements is by switching off after a half-year instead of a half-period. The eccentricity and inclination are essentially periodic functions with a half-year period. By switching off just when an element has reached its maximum and subsequently, switching on a half-year later just when the

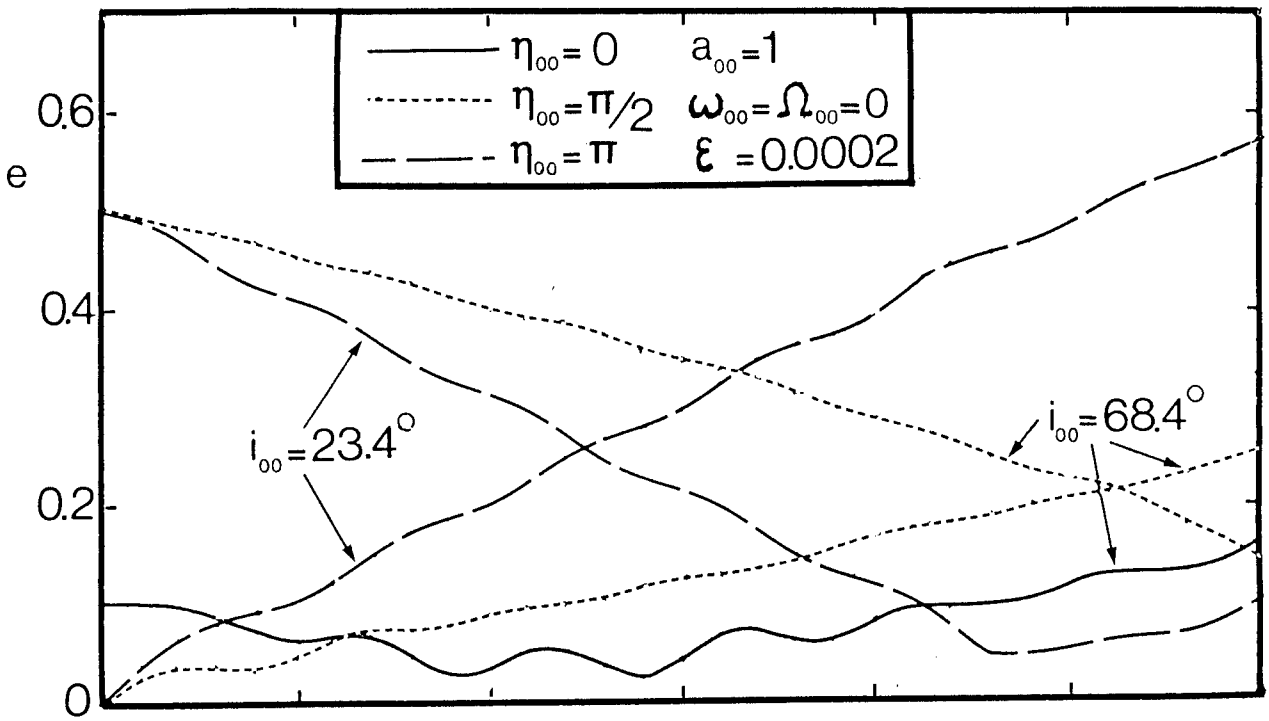

Figure 4-9 (a) Behavior of eccentricity for switching program of Equations (4.25)

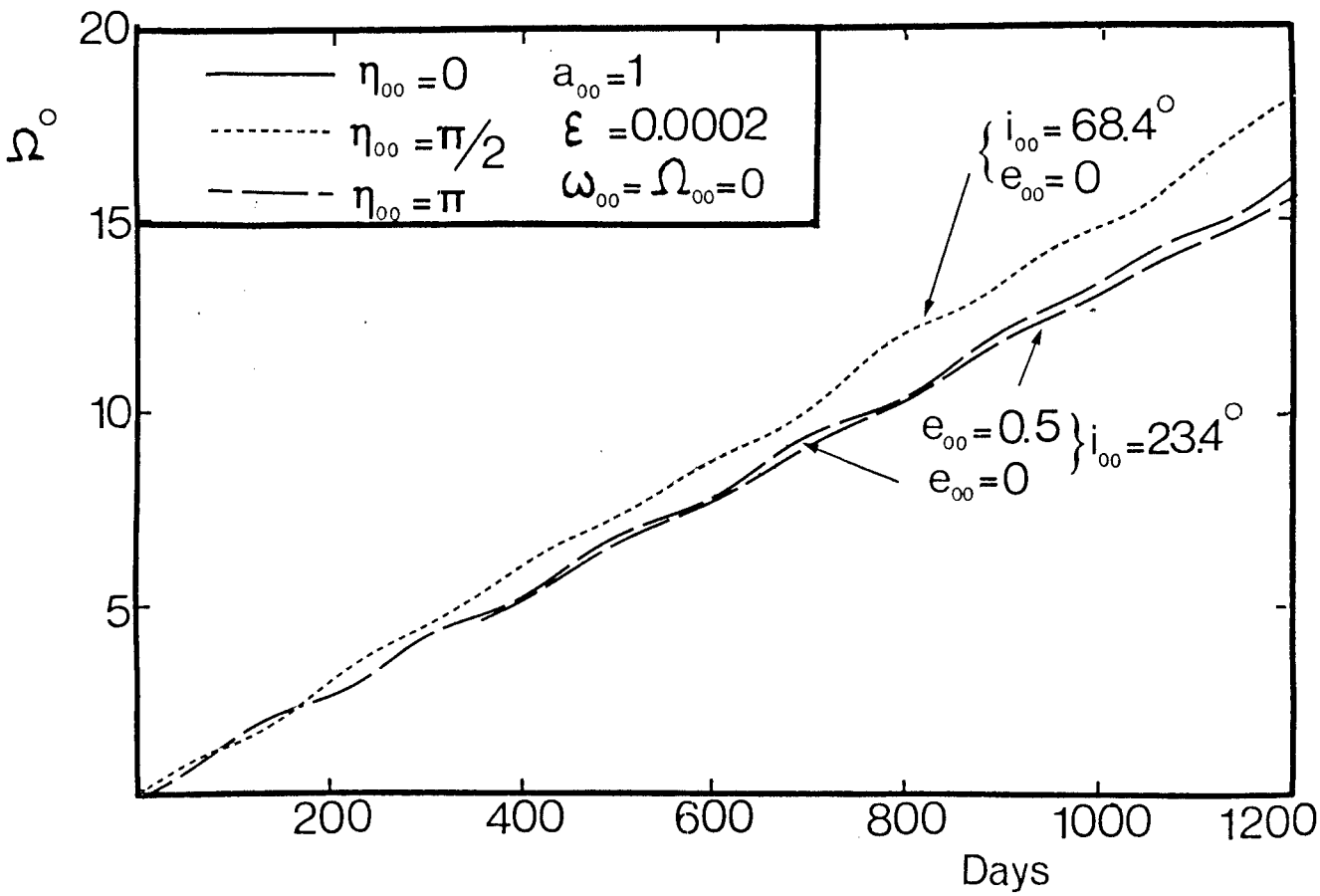

Figure 4-9 (b) Controlled change in position of line of nodes

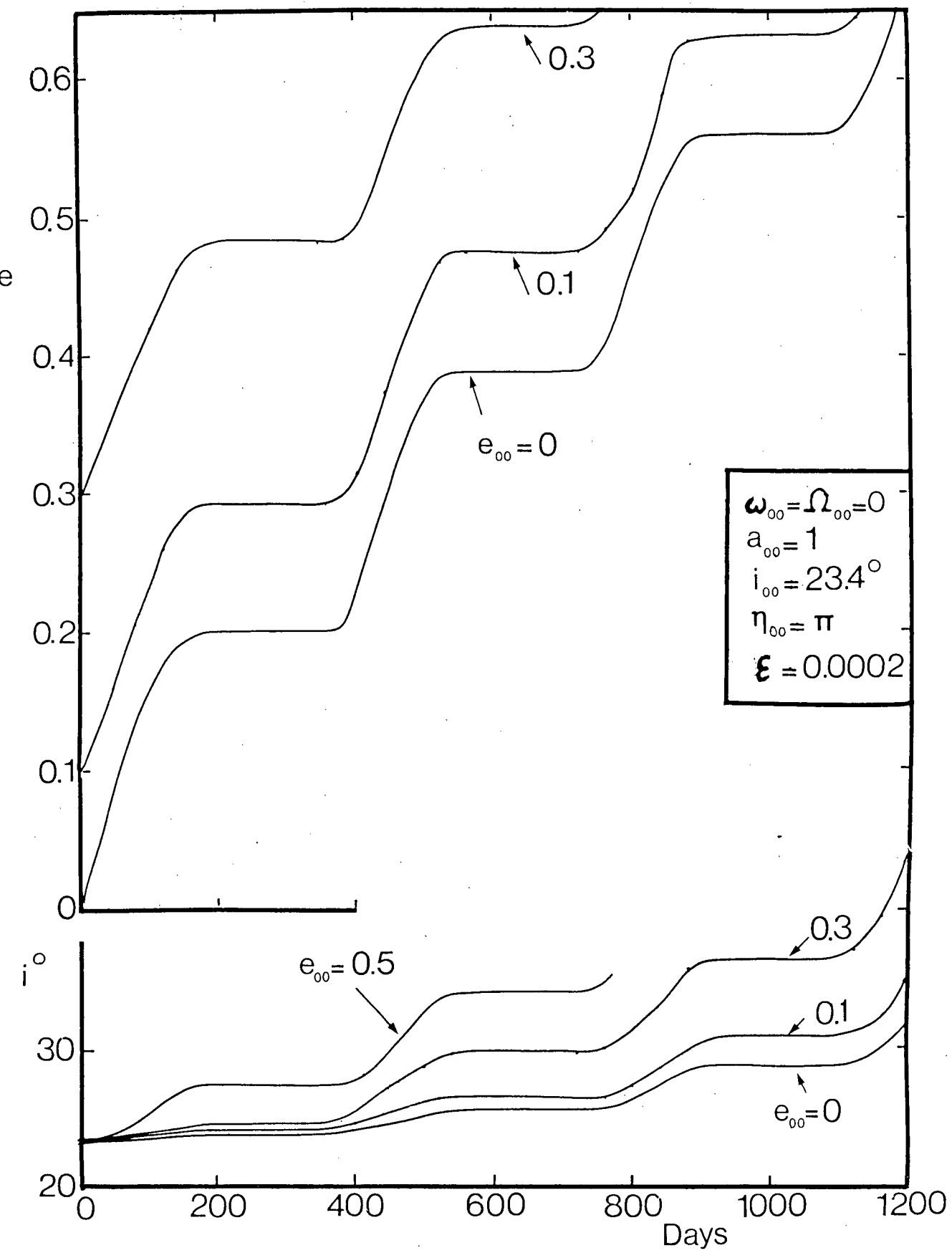

Figure 4-10 Effect of half-yearly switching upon eccentricity and inclination

up-hill phase starts again, sizable orbital changes can be achieved. Figure 4-10 illustrates this concept for an initially circular, equatorial orbit. The average rate of increase of inclination is approximately half of that attained by the switching strategy of Section 4.6.1, while the increase in eccentricity is approximately the same in the long run. As before, the changes in inclination and eccentricity increase for larger initial eccentricity.

Whereas the effectiveness of this approach upon changes in inclination is undoubtedly inferior to the strategy described in Equations (4.23), the benefit of a much lower frequency of switching (2 vs. 365 per year) could become a decisive factor in a practical situation.

4.8 Concluding Remarks

Important aspects of the analyses presented in this chapter may be summarized as follows:

(i) A few switching programs are explored and their effectiveness in achieving orbital changes established.

(ii) Whereas apogee-perigee switching does not lead to readily predictable results, the sun-earth line switching achieves a rapid increase in angular momentum and thus the semi-latus rectum.

(iii) Switching when the velocity is normal to the direction of radiation is particularly effective, since it is the best on-off switching strategy in terms of adding energy and, consequently, increasing the major axis. Under this strategy, an Echo-type satellite may increase its major axis by a factor of ten in five years, starting

from geosynchronous altitude.

(iv) The optimal time-varying orientation of a solar sail for maximum increase in semi-major axis per revolution is established. This should be of importance for raising a solar sail into a heliocentric orbit.

(v) Two switching programs for controlling orientation of the orbital plane are proposed and analysed. One strategy leads to appreciable changes in the inclination, while the other produces a precession of the line of nodes.

(vi) Changes in eccentricity and inclination in a half-yearly switching policy are relatively less pronounced, but the benefit of a much lower number of switching points could be attractive.

5. HELIOCENTRIC SOLAR SAILING WITH ARBITRARY FIXED SAIL SETTING

5.1 Preliminary Remarks

Whereas up to now the effects of solar radiation forces upon geocentric orbits were studied, in this and the following chapter, the attention is focused on heliocentric orbits. For many deep-space missions, the solar sail constitutes a viable option since it derives its motive power from an unremitting source of energy. The combination of useful payload and solar sail leads to an area over mass ratio in the range of 50 to 200 m^2/kg with characteristic accelerations between about 0.5 and 2 mm/sec^2.

This chapter studies the solar radiation effects on the orbital behavior of an arbitrarily shaped spacecraft (or a solar sail in particular) in a general fixed orientation with respect to the local coordinate frame. While a constant orientation is not necessarily the best possible setting in an actual mission, a thorough understanding of its response would facilitate the assessment of its potential as a function of area/mass ratio and initial conditions. While exact solutions in the form of logarithmic spirals have been established in the literature[51,52] for planar orbits, the analysis presented here is extended to general three-dimensional trajectories. Moreover, the parameters of the trajectories are expressed analytically by means of asymptotic series in terms of the solar parameter and a spacecraft with arbitrary material characteristics is considered. When the out-of-plane component of the thrust is kept constant, the orbital plane itself exhibits a precessional motion, returning to its original orientation after little less than one revolution. An effective out-of-plane spiral

transfer trajectory is obtained by reversing the force component normal to the orbital plane at specified positions in the orbit. By choosing the appropriate control angles for the sail orientation, any point in space can be reached eventually by this three-dimensional spiral trajectory.

Whereas a very specific initial velocity vector is required for embarking upon the spiral trajectory, other orbits emanating from different initial conditions may also be of interest. Hence, a three-dimensional short-term solution is presented for arbitrary initial conditions. Subsequently, the long-term behavior is analysed by means of the two-variable expansion procedure yielding an implicit expression for the eccentricity. By iteration, the solution can be determined up to the desired accuracy. For not too large values of the initial eccentricity, asymptotic expansions up to the order e^5 are derived. The other orbital elements are expressed in terms of the eccentricity and can be evaluated up to the desired accuracy. Higher-order terms may become important when the area/mass ratio is large. Equations for the higher-order terms can be derived. While the periodic part of the solution can be evaluated readily, secular terms can be determined analytically only for a circular initial orbit.

5.2 Formulation of the Problem

An inertial X,Y,Z reference frame with origin at the centre of the sun is introduced in Figure 5-1a where the X axis points to the initial position of the spacecraft and the X,Y plane constitutes the initial osculating plane, usually the ecliptic. The Z axis is aligned with the initial angular momentum vector. In addition, a local ξ_0,η_0,ζ_0 reference frame moving along with the spacecraft is introduced: the ξ_0, η_0 and ζ_0 axes

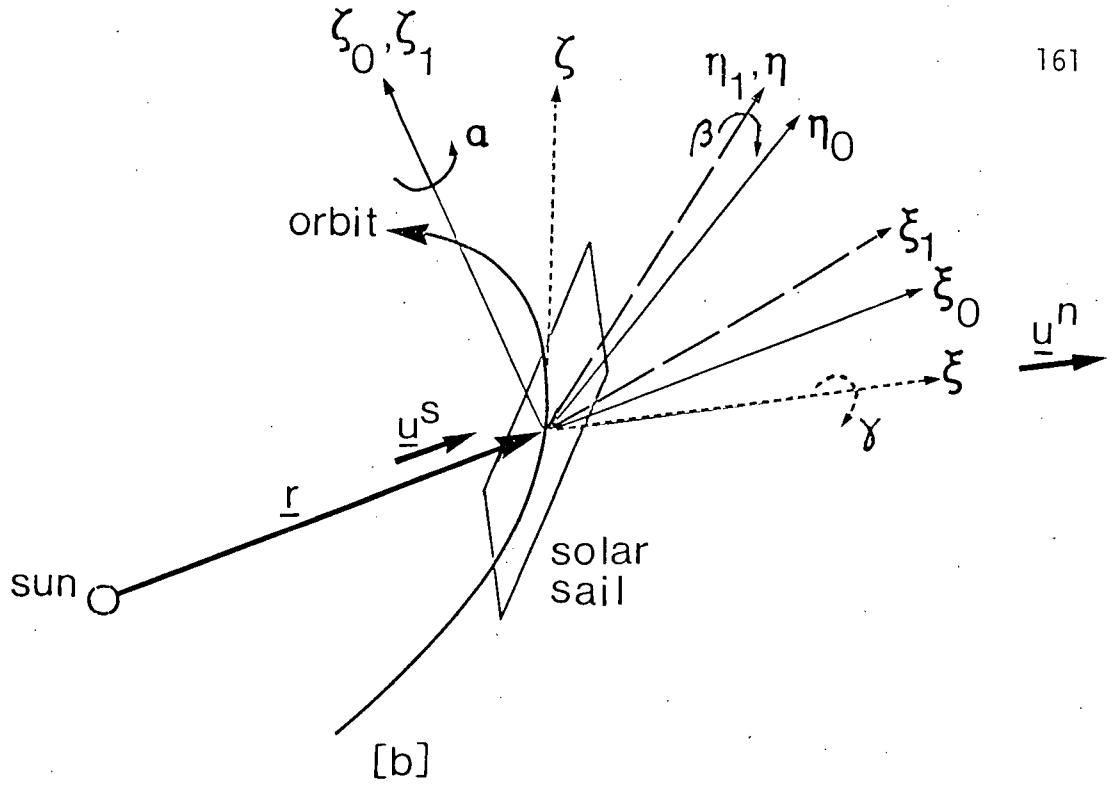

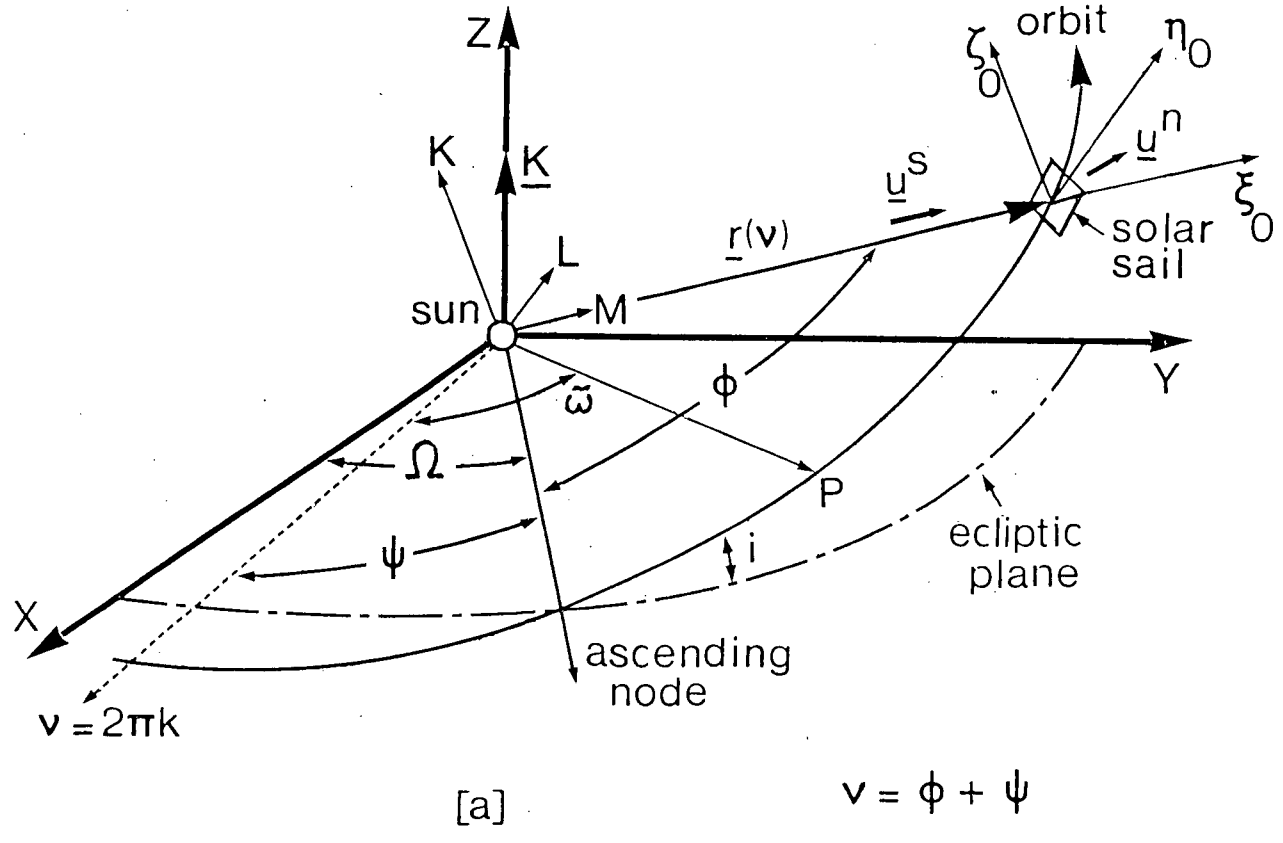

Figure 5-1 (a) Configuration of the sun and solar sail in a heliocentric trajectory;
(b) Successive rotations α, β (and γ) for defining arbitrary orientation of solar sail

point along the local vertical, local horizontal and orbit-normal directions, respectively. Any desired orientation of the solar sail in the ξ_0,η_0,ζ_0 can be described by three successive Eulerian rotations (Figure 5-1b). Taking, initially, the outward normal to the sail to be directed along the ξ_0 axis, a first rotation α about the ζ_0 axis produces the ξ_1,η_1,ζ_1 frame and brings the solar sail to the required line of intersection with the orbital plane. A subsequent rotation β about the η_1 axis yields the ξ,η,ζ frame and moves the normal to the sail out of the orbital plane to its prescribed orientation. A final rotation γ about the normal (ξ axis) could be performed for attaining the proper attitude of the sail in its η,ζ plane without affecting the resulting solar radiation force. The components of $\underline{u}^n$ taken along the local ξ_0,η_0,ζ_0 axes depend on α and β only:

$$\underline{u}^n = (\cos\alpha\cos\beta,\ \sin\alpha\cos\beta,\ -\sin\beta). \qquad .....(5.1)$$

For many satellites, solar panels form a substantial portion of the total surface area. This would particularly be so for a spacecraft designed to be propelled by solar radiation pressure. Hence, in these situations, only the area of solar panels or sails needs to be considered. In general, the spacecraft is modelled by a number of surface components, characterized by their own material parameters and orientation. In nondimensional form (unit of length equals a_e = 1 A.U. and unit of time is $1/(2\pi)$ year), the solar radiation force upon an arbitrary space structure of n homogeneous, illuminated surface components A_k in an heliocentric orbit is written as

$$\underline{F} = \varepsilon_s \sum_{k=1}^{n} |\underline{u}_k^n \cdot \underline{u}^s| \left\{\sigma_{1k}\,\underline{u}^s + [\sigma_{2k} + \rho_k(\underline{u}_k^n \cdot \underline{u}^s)]\,\underline{u}_k^n\right\} A_k/r^2, \qquad .....(5.2)$$

where the physical force is nondimensionalized through multiplication by $a_e^2/(\mu_s m)$. The small parameter ε_s denotes the ratio of solar radiation and attraction forces,

$$\varepsilon_s = 2S'(A/m)\ (a_e^2/\mu_s) = 1.57 \times 10^{-3}\ (A/m)\ . \qquad .....(5.3)$$

This illustrates that the parameter ε_s is about 200 times as large as the parameter ε in Equations (2.5) for geocentric orbits. It may be mentioned that the solar constant and hence the radiation force in Equation (5.2) varies inversely as square of the distance from the sun. This is because the total radiant energy emitted by the sun in a given time equals that passing through any concentric spherical surface around the sun in that time (taking the rate of energy output constant). Writing $\underline{F} = \varepsilon_s \underline{R}/r^2$ with auxiliary vector $\underline{R} = (R,S,T)$ the components of $\underline{R}$ can be evaluated for an arbitrarily shaped spacecraft using Equation (5.2):

$$R = \sum_{k=1}^{n} \cos\alpha_k \cos\beta_k \left\{\sigma_{1k} + [\sigma_{2k} + \rho_k \cos\alpha_k \cos\beta_k] \cos\alpha_k \cos\beta_k\right\} A_k \ ;$$

$$S = \sum_{k=1}^{n} \sin\alpha_k \cos\alpha_k \cos^2\beta_k\ [\sigma_{2k} + \rho_k \cos\alpha_k \cos\beta_k]\ A_k \ ;$$

$$T = -\sum_{k=1}^{n} \cos\alpha_k \cos\beta_k \sin\beta_k\ [\sigma_{2k} + \rho_k \cos\alpha_k \cos\beta_k]\ A_k \ . \qquad .....(5.4)$$

The normal $\underline{u}_k^n$ to a surface element A_k, $k = 1,2,\ldots,n$ is taken in such a manner that its projection along the radiation is always positive.

In general, when $T \neq 0$, the plane of the orbit will be subjected to changes in its orientation. The motion of the local ξ_0,η_0,ζ_0 frame relative to the inertial X,Y,Z frame is described in terms of the rotation vector $\underline{W} = \underline{w}^r + \dot{\underline{\nu}}$, effecting an uncoupling of the in-plane and the out-of-

plane perturbations. The equations of motion are similar to those obtained earlier (Equations 3.5) with $\underline{F}$ to be replaced by $\varepsilon_s\, u^2 \underline{R}$. Since the equation for $\Omega'(\nu)$ contains a singularity for $i = 0$, a formulation in terms of the unit vector $\underline{K}$ directed along the inertial Z axis with components $M = \sin(i)\sin(\nu - \psi)$, $L = \sin(i)\cos(\nu - \psi)$ and $K = \cos(i)$ along the local ξ_0,η_0,ζ_0 axes is favored. As the local ξ_0,η_0,ζ_0 frame moves along with the spacecraft in its orbit, the vector $\underline{K}(\nu)$ traces a path upon the sphere $(\underline{K} \cdot \underline{K}) = 1$ in the ξ_0,η_0,ζ_0 frame. The orbital elements i and ψ can be determined quite readily from the vector $\underline{K}$. The complete system of equations is written as:

$$u''(\nu) + u(\nu) = (1 - \varepsilon_s R)/\ell(\nu) - \varepsilon_s\, S\, u'(\nu)/[u(\nu)\,\ell(\nu)] ;$$

$$\ell'(\nu) = 2\varepsilon_s S/u(\nu) ;$$

$$M''(\nu) + M(\nu) = \varepsilon_s\, T\, K(\nu)/[u(\nu)\,\ell(\nu)] ;$$

$$K'(\nu) = -\varepsilon_s\, T\, M'(\nu)/[u(\nu)\,\ell(\nu)] . \qquad .....(5.5)$$

The first two equations fully describe the in-plane perturbations and the latter two equations define the orientation of the osculating plane. The component $L(\nu)$ can be shown to be equal to $M'(\nu)$. The initial conditions for the system of Equations (5.5) are written as $\ell(0) = \ell_{00}$; $u(0) = (1 + e_{00}\cos\tilde{\omega}_{00})/\ell_{00}$; $u'(0) = (e_{00}\sin\tilde{\omega}_{00})/\ell_{00}$; $K(0) = 1$ and $M(0) = M'(0) = 0$.

In a few particular situations, exact solutions for the system of Equations (5.5) can be established: in the case where the component S vanishes (e.g. when the normal to the solar sail lies in the ξ_0,ζ_0 plane

or when all of the radiation is absorbed), solutions for the orbital motion can be obtained using the classical Keplerian procedure. After modification of the sun's gravitational parameter to account for the apparent reduction in attraction because of the solar radiation force, the trajectory for the case $S = 0$ can be written as $u(\nu) = [1 + e_p \cos(\nu - \tilde{\omega}_p)]/\ell_p$ with modified orbital elements $\ell_p = \ell_{00}/(1 - \varepsilon_s R)$, $e_p = [e_{00}^2 + 2\varepsilon_s p_{00} R + \varepsilon_s^2 R^2]^{1/2}/(1 - \varepsilon_s R)$ and $\tilde{\omega}_p = \arctan[q_{00}/(p_{00} + \varepsilon_s R)]$, where all angles are measured in the osculating plane. Another, more interesting, exact solution arises when the initial velocity vector satisfies a prescribed condition leading to a trajectory in the shape of a logarithmic spiral.

5.3 Three Dimensional Spiral Trajectories

The spiral trajectory of the form $r(\nu) = r_{00} \exp(c_s \nu)$ emerges from Equations (5.5) when one looks for solutions having the properties that the product $u(\nu)\,\ell(\nu)$ remains constant, say C, and $u'(\nu) = -c_s\, u(\nu)$ at all times. The constants c_s and C can be evaluated from Equations (5.5) after substitution of these two relations:

$$c_s = \left\{(1 - \varepsilon_s R) - [(1 - \varepsilon_s R)^2 - 8\varepsilon_s^2 S^2]^{1/2}\right\} / (2\varepsilon_s S)$$

$$= 2\varepsilon_s S \left\{1 + \varepsilon_s R + \varepsilon_s^2 (R^2 + 2S^2) + \varepsilon_s^3 R(R^2 + 6S^2)\right\} + O(\varepsilon_s^5) ;$$

$$C = 2\varepsilon_s S/c_s = (1 - \varepsilon_s R)\left\{1 - 2\varepsilon_s^2 S^2 [1 + \varepsilon_s R + \varepsilon_s^2 (R^2 + 2S^2)]\right\} + O(\varepsilon_s^5) . \quad .....(5.6)$$

Taking $r(0) = r_{00}$, the complete in-plane and out-of-plane solutions of

Equations (5.5) can be expressed in terms of c_s and C:

$$r(\nu) = r_{00}\exp(c_s\nu) \ ;$$

$$\ell(\nu) = C\, r(\nu) = C\, \exp(c_s\nu)/r_{00} \ ;$$

$$M(\nu) = B\,\{1 - \cos\,(1 + B^2)^{1/2}\nu\,\}/(1 + B^2) \ ;$$

$$L(\nu) = B\,\sin[(1 + B^2)^{1/2}\nu]/(1 + B^2)^{1/2} \ ;$$

$$K(\nu) = \{1 + B^2\cos[(1 + B^2)^{1/2}\nu]\}/(1 + B^2) \ . \qquad .....(5.7)$$

Here the constant B stands for $\varepsilon_s T/C$. It is seen that the radial distance takes the form of a logarithmic spiral (outward if $S > 0$ and inward for $S < 0$), while the orbital plane exhibits a periodic wobbling motion with maximum inclination at $\nu = \pi/(1 + B^2)^{1/2}$. This is of practical interest for a solar sail since it predicts that no secular changes in the orbital orientation are induced by a constant force component normal to the plane of the orbit.

It must be emphasized that the spiral trajectory arises only when the spacecraft possesses the right velocity vector at injection. Its radial and circumferential components are given by $\dot{r} = c_s(C/r)^{1/2}$, $r\dot{\nu} = (C/r)^{1/2}$, and the spiral angle α_s equals $\arctan(c_s)$. Additional insight into the nature of the trajectory is provided by studying the osculating ellipses of the spiral. The eccentricity and perigee position at any point ν_1 are given by

$$e_1 = [c_s^2\,\exp(-2c_s\nu_1) + (1 - C)^2]^{1/2} \ ,$$

$$\tilde{\omega}_1 = \nu_1 - \pi + \arctan[c_s\exp(-c_s\nu_1)/(1 - C)] \ , \qquad .....(5.8)$$

so that the equation for the osculating ellipse at $\nu = \nu_1$ can be written as $r(\nu_1) = C \exp(c_s \nu_1)/[1 + e_1 \cos(\nu_1 - \tilde{\omega}_1)]$. It is of interest to note that the eccentricity which is of the order ε_s to start with, decreases slowly attaining the limiting value $\varepsilon_s R + O(\varepsilon_s^2)$ as $\nu_1 \to \infty$. This is of considerable importance since it predicts that a spaceprobe may be released from a spiral solar sail trajectory into a near-circular heliocentric orbit at any time. As to the position of the perigee of the osculating ellipses, it follows that $\tilde{\omega}_1$ follows ν_1 steadily, lagging behind by an angle of between $\pi/2$ and π radians in case $S > 0$ and between π and $3\pi/2$ radians if $S < 0$. As the spacecraft moves along its trajectory, the angle between the radiusvector and osculating perigee will increase (for $S > 0$) or decrease ($S < 0$) slowly until, finally, $\tilde{\omega}_1 \to \nu_1 - \pi$ for $\nu_1 \to \infty$.

An explicit expression in terms of the solar sail parameters can be obtained for the time history in the spiral trajectory,

$$t(\nu) = \int_0^{\nu} [r^2(\tau)/\ell^{1/2}(\tau)]\, d\tau = r_{00}^{3/2} [\exp(3c_s\nu/2) - 1]/c_t ,$$

with

$$c_t = 3\, \mathrm{sign}(S)/2 \{(1 - \varepsilon_s R) - [(1 - \varepsilon_s R)^2 - 8\varepsilon_s^2 S^2]^{1/2}\}^{1/2} . \qquad .....(5.9)$$

The radial distance as a function of time follows by combining Equations (5.7) and (5.9),

$$r(t) = r_{00} (1 + c_t\, t/r_{00}^{3/2})^{2/3} . \qquad .....(5.10)$$

This result is valid for both outward ($S > 0$) and inward ($S < 0$) spirals.

To obtain the most favorable sail setting for reaching the maximum radial distance at any time t, the coefficient c_t is maximized as a function of the rotation angles α and β. It follows that the maximum occurs when β

vanishes, producing a planar trajectory. The value of α is determined from

$$8\varepsilon_s S \frac{\partial S}{\partial \alpha} + \{(1 - \varepsilon_s R) - [(1 - \varepsilon_s R)^2 - 8\varepsilon_s^2 S^2]^{1/2}\} \frac{\partial R}{\partial \alpha} = 0. \qquad .....(5.11)$$

Since the exact solution of this implicit equation for α can not easily be found, it is useful to determine subsequent levels of approximation for α written as an asymptotic series in the small parameter ε_s: $\alpha = \alpha_0 + \varepsilon_s\alpha_1 + \varepsilon_s^2\alpha_2 + \ldots$. The equations for α_i, $i = 0,1,2,\ldots$, can be derived by substituting the series into Equation (5.11), developing the relation in terms of a Taylor expansion around $\alpha = \alpha_0$ and requiring that all coefficients of ε_s^n, $n = 0,1,2,\ldots$, vanish. After a considerable amount of algebra, the following asymptotic representation for α is found (taking a sail with $\sigma_2 = 0$):

$$\alpha = \arcsin(3^{-1/2}) - \varepsilon_s 3^{1/2}(\sigma_1 + 2\rho)/36 - \varepsilon_s^2 2^{1/2}(\sigma_1 + 2\rho)(5\rho + 43\sigma/6)/288$$
$$-\varepsilon_s^3 3^{1/2}(\sigma_1 + 2\rho)/2 \{1261\ \sigma_1^2 + 1252\ \rho^2 + 1588\ \rho\sigma_1 + 72\ \sigma_1 + 144\ \rho\}$$
$$/(36)^3 + 0(\varepsilon_s^4). \qquad .....(5.12)$$

Subsequently, an explicit relation for the spiral angle α_s corresponding to the optimal orientation is found by substituting the optimal angle into c_s, Equations (5.6). Expansion for small ε_s yields:

$$\alpha_s = 4\rho\varepsilon_s 3^{1/2}/9 \{1 + 6^{1/2}\ \varepsilon_s(\sigma_1 + 2\rho/3)/3$$
$$+ \varepsilon_s^2[(\sigma_1 + 2\rho)^2/48 + 2(\sigma_1 + 2\rho/3)^2/3 + 8\rho^2/81]\} + 0(\varepsilon_s^4).....(5.13)$$

In Figure 5-2a, the optimal orientation of the solar sail as well as the corresponding spiral angle have been plotted for various values of the

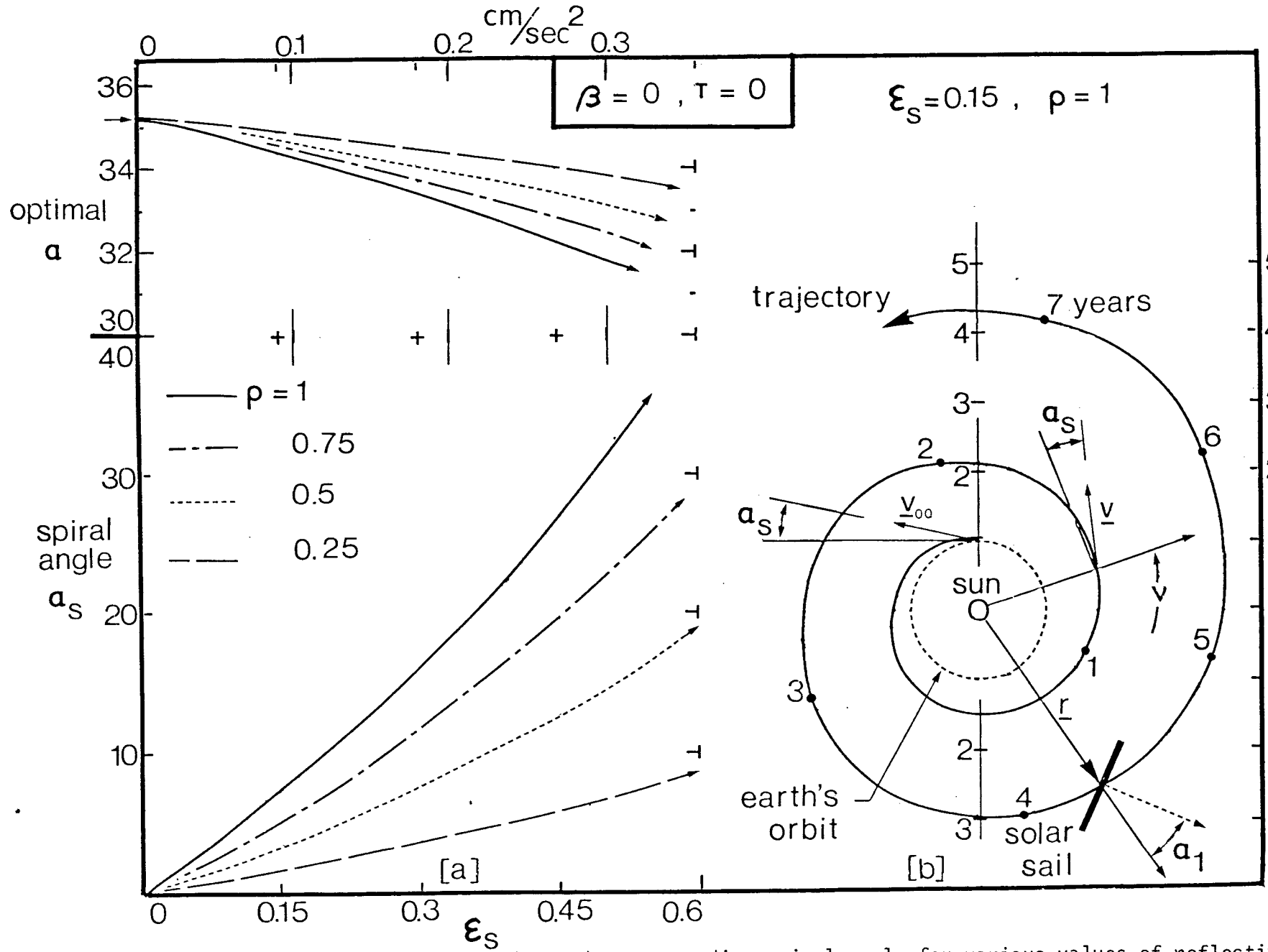

Figure 5-2 (a) Optimal sail orientation and corresponding spiral angle for various values of reflectivity; (b) Actual planar spiral trajectory for $\varepsilon_s = 0.15$ and $\rho = 1$

reflectivity ρ. For low values of ε_s, the optimal orientation can be taken as 35.26°. It is evident that the spiral angle approaches zero for $\rho \to 0$ since the case $\rho = 0$ corresponds to a closed trajectory. Figure 5-2b illustrates an example of a planar spiral trajectory, showing the spiral angle and the orientation of the sail. The value of ε_s taken here (0.15) would correspond to A/m of about 100 m^2/kg.

It is interesting to calculate the optimal radial distance over a long duration of time, showing the effectiveness of the spiral trajectory in near-circular orbital transfer, for a few values of the solar parameter ε_s. The results are summarized in Figure 5-3 for both inward and outward spirals. In case $\varepsilon_s = 0.015$, i.e. A/m = 10 m^2/kg, the orbit of Mars could be reached within 9 years and Venus in 4 years. For higher values of ε_s the opportunities increase rapidly: even a long journey to the distant planet Uranus may be feasible if a solar sail with A/m of the order of 400 m^2/kg could be constructed.

The analysis remains valid when the component T of the force is non-zero: the position and velocity vectors of the spiral trajectory lie in the osculating plane in that case. The orientation of the orbital plane described by the angles i and ψ follows from Equations (5.7):

$$i(\nu) = \arccos \{1 - 2 B^2 \sin^2[(1 + B^2)^{1/2}\nu/2]/(1 + B^2)\} ;$$

$$\psi(\nu) = \nu - \arctan \{\tan[(1 + B^2)^{1/2}\nu/2]/(1 + B^2)^{1/2}\} . \qquad .....(5.14)$$

Expansion of $\psi(\nu)$ for small ε_s leads to $\psi(\nu) = \nu/2 + 0(\varepsilon_s^2)$, $0 \leq \nu \leq 2\pi$, so that the line of nodes precesses at approximately half the orbital rate.

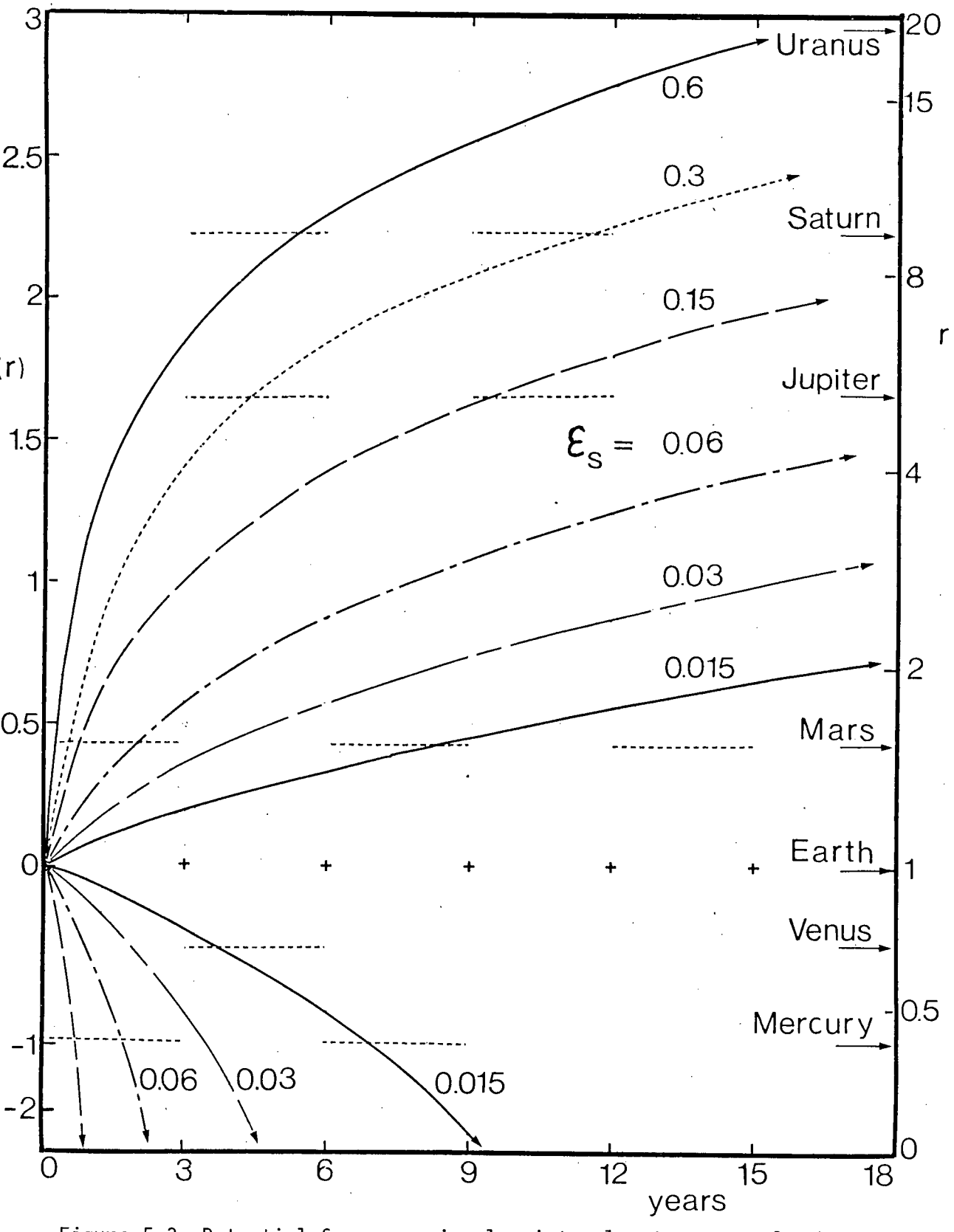

Figure 5-3 Potential for near-circular interplanetary transfer by solar sail for a few values of ε_s

The inclination reaches its maximum at $\nu = \pi/(1 + B^2)^{1/2}$ and returns to zero at $2\pi/(1 + B^2)^{1/2}$, while $\psi(\nu)$ shows a discontinuity of π radians at $\nu = 2\pi/(1 + B^2)^{1/2}$. Figure 5-4a shows the orientation of the osculating plane at a few points in the orbit.

5.4 Out-of-Plane Spiral Transfer

In order to obtain a net increase in inclination after one revolution, the orientation of the sail would have to be changed during the orbit. Obvious switching points would be the instants when $i(\nu)$ is stationary, i.e. at $\nu_1 = \pi/(1 + B^2)^{1/2}$ and $\nu_2 = 2\nu_1$. Assuming the switching to take place instantaneously from $-\beta$ to $+\beta$ (without affecting the control angle α) and repeating the procedure during each successive revolution, the out-of-plane component T becomes

$$T = \begin{cases} |T|, & \beta < 0; \quad \nu_{2j} < \nu < \nu_{2j+1} ; \\ -|T|, & \beta > 0; \quad \nu_{2j+1} < \nu < \nu_{2j+2} ; \end{cases} \qquad .....(5.15)$$

for $j = 0,1,2,...$, and the switching points $\nu_k = k\pi/(1 + B^2)^{1/2}$, $k = 0,1,2,...$. Since the operation takes place instantaneously, the force components S and R remain unchanged throughout. Writing $M_k = M(\nu_k)$ and $K_k = K(\nu_k)$, etc., $k = 0,1,2,...$, the solution $i(\nu)$ is found by repeated application of the results in Equations (5.7):

$$i(\nu) = \begin{cases} \arccos\{K_{2j} + |B|(M_{2j} - |B|K_{2j})(1 - \cos[(1 + B^2)^{1/2}\nu])/(1 + B^2)\} , \\ \arccos\{K_{2j} + 2|B|(M_{2j} - |B|K_{2j})/(1 + B^2) - |B|[(3B^2 - 1)M_{2j} \\ \qquad + |B|(3 - B^2)K_{2j}](1 + \cos[(1 + B^2)^{1/2}\nu])/(1 + B^2)^2\} , \end{cases}$$

$$.....(5.16)$$

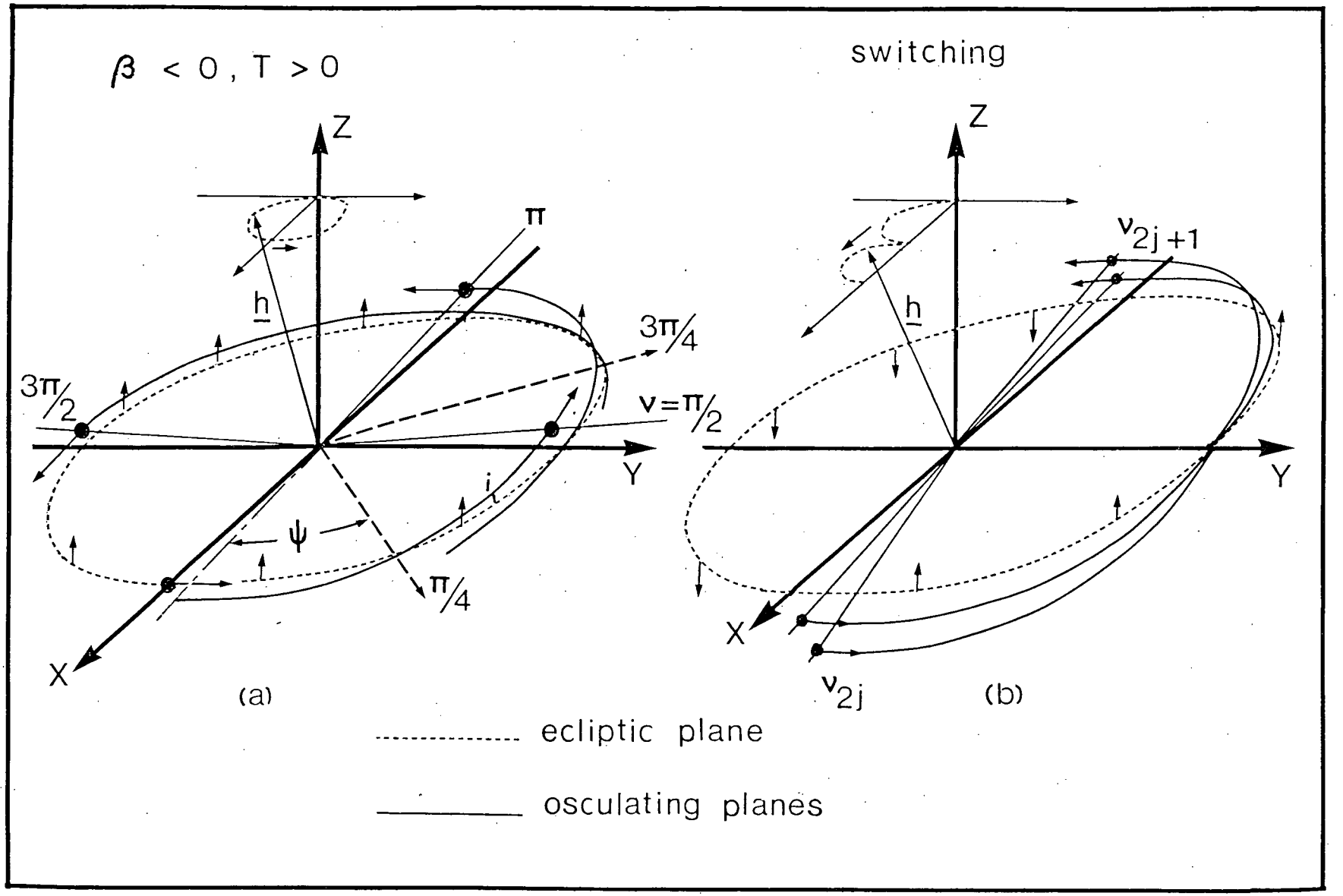

Figure 5-4 (a) Orientation of the osculating plane as affected by a constant force normal to it;
(b) Switching strategy leading to a systematic increase in orbital inclination

where the former relation holds for $\nu_{2j} < \nu < \nu_{2j+1}$ and the latter for $\nu_{2j+1} < \nu < \nu_{2j+2}$. The following recurrence relations for K_{2j} and M_{2j} can be established:

$$M_{2j} = -\{4|B|(1 - B^2)K_{2j-2} + [4B^2 - (1 - B^2)^2]M_{2j-2}\}/(1 + B^2)^2 ,$$

$$K_{2j} = -\{[4B^2 - (1 - B^2)^2]K_{2j-2} - 4|B|(1 - B^2)M_{2j-2}\}/(1 + B^2)^2 , \quad .....(5.17)$$

with $j = 1,2,3,...$ and $M_0 = 0$, $K_0 = 1$. A long-term linear approximation for $i(\nu)$, $i(\nu) = 2\varepsilon_s|T|(1 + B^2)^{1/2}\nu/\pi$, provides a good estimate as long as ε_s is sufficiently small. The line of nodes, i.e. the intersection of the instantaneous orbital plane and the X,Y plane is located at $\nu = \nu_1 - \pi/2 = \pi/2 + O(\varepsilon_s)$ when the first switching takes place. It returns to this position at all switching points while slightly deviating from this line in between. Through Equation (5.9), the switching instants are also known in terms of time.

The foregoing analysis is valid for any fixed sail orientation designated by the control angles α and β. Since the rate of increase in inclination is proportional to the magnitude of the force component $|T|$, the most effective (fixed angle) strategy is the one which maximizes $|T|$, i.e. $\alpha = 0$ and $|\beta| = \arcsin(3^{-1/2}) = 35.26°$. In this case $S = 0$ and the trajectory is a degenerate spiral maintaining a constant distance from the sun (so-called 'cranking orbit'). The behavior of the inclination for this case is illustrated in Figure 5-5c for a few values of ε_s. While it would take about 14 years to make a full 180° swing through space at 1 A.U. from the sun, the duration would be less than 5 years at 0.5 A.U. (taking $\varepsilon_s = 0.15$).

An obvious application of three-dimensional spiral trajectories in

conjunction with switching would be in a transfer mission where both inclination and radial distance are to be changed. From this consideration, it would be interesting to determine the most efficient orientation of the sail for a near-circular out-of-plane transfer with the final radial distance prescribed and the inclination to be maximized or, vice versa, the final inclination is predetermined while the distance is to be maximized (minimized). Since only constant control angles are considered, the problem may be stated mathematically as maximizing the force component $|S|$ as a function of α and β under the constraint that $|T|$ is constant and vice versa . Using Lagrange multipliers, the best control program in both cases is found to satisfy the relation $\cos^2\alpha \cos^2\beta = 2/3$. The range of inclinations and distances which can be reached within a given time by these strategies is shown in Figure 5-5a. Here the solar parameter ε_s is taken to be 0.15 ($A/m = 100\ m^2/kg$) and the results are valid for any starting radius r_{00} and for outward ($\alpha > 0$) as well as inward ($\alpha < 0$) trajectories. The plot is derived from the analytical values for $i(\nu)$, $r(\nu)$ and $t(\nu)$ involving determination of the response for various values of α and $\beta = \pm\arccos[6^{1/2}/(3\cos\alpha)]$. The arrows in Figure 5-5a indicate the direction in the r,i plane taken by a particular control strategy α,β . In the case where the radial distance is prescribed at some final time, the required ratio $|S|/|S|_{max}$ for a given value of ε_s may be established in conjunction with Figure 5-4, showing the response for the strategy with $|S| = |S|_{max}$ (i.e. $|\alpha| = 35.26°$ and $\beta = 0$). The ratio of the value for ε_s corresponding to the desired response and the actual ε_s determines the required $|S|/|S|_{max}$ with sufficient accuracy. The sail setting α,β yielding the maximum inclination is given by the point of intersection of this particular value of $|S|/|S|_{max}$ and the curve

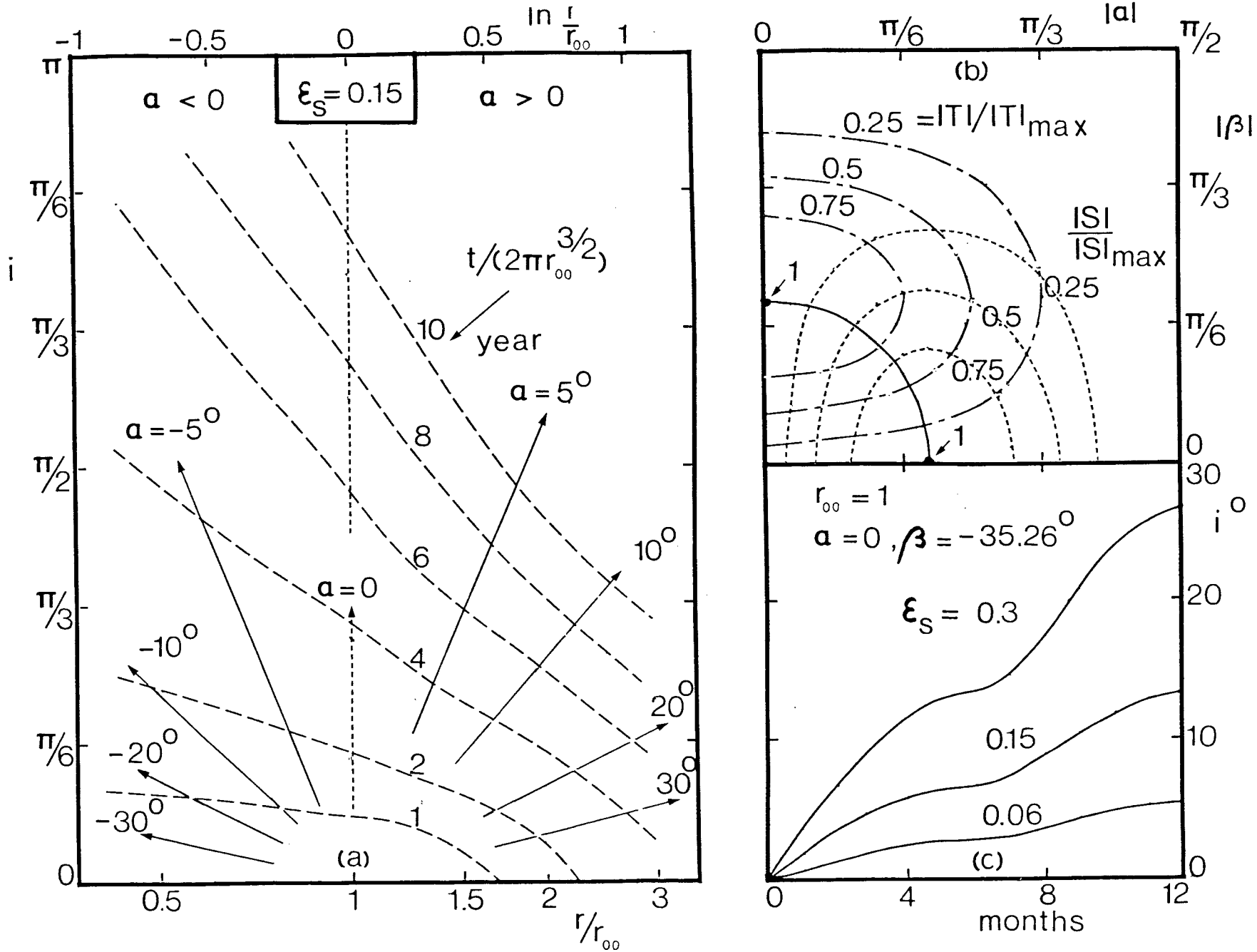

Figure 5-5 (a) Combinations of inclination and radial distance attainable after a given time;
(b) Levelcurves for constant |S| and |T|;
(c) Growth of inclination for pure out-of-plane transfer

$\cos^2\alpha \cos^2\beta = 2/3$ (i.e. the solid curve in Figure 5-5b). Conversely, if the final inclination is prescribed, the corresponding optimal control program can be determined as follows. For a given ε_s, the required value for $|T|/|T|_{max}$ may be taken equal to the ratio of the desired final inclination and the one obtained under the control program corresponding to $|T|_{max}$, i.e. $\alpha = 0$, $\beta = \pm 35.26°$. (The behavior of the inclination under the latter control strategy is shown in Figure 5-5c for a few values of ε_s). The optimal sail setting follows readily from Figure 5-5b as the intersection of this value of $|T|$ and the solid curve.

5.5 Arbitrary Initial Conditions

In this section, approximate analytical solutions for solar sail trajectories with an arbitrary but fixed sail setting and general initial conditions are developed.

5.5.1 Short-term approximate solution

By expanding the variables u, ℓ, and $\underline{K}$ in terms of a straightforward perturbation series in the small parameter ε_s, an initially valid approximate solution is obtained with the zeroth-order solution representing the unperturbed Kepler ellipse with parameters ℓ_{00}, p_{00} and q_{00}. The first-order equations are solved, yielding the expressions for in-plane perturbations as:

$$\ell_1(\nu) = 2\ell_{00} S\, A_{10}(\nu) \;;$$

$$u_1(\nu) = R(\cos\nu - 1)/\ell_{00} + S\{\cos\nu[q_{00}B_{12} + p_{00}(A_{12} - A_{10}) + 4A_{11}] + \sin\nu[p_{00}B_{12} - q_{00}(A_{12} + A_{10}) + 4B_{11}] - 4A_{10}\}/(2\ell_{00}) \quad .....(5.18)$$

It may be noted that for an initially circular orbit, the changes in a, ℓ and r after one revolution are all equal to $4\pi a_{00}S$. The short-term behavior of the orbital plane expressed in terms of i and ψ is given by

$$\psi(\nu) = \nu - \arctan\left\{\frac{T[A_{11}(\nu)\sin\nu - B_{11}(\nu)\cos\nu]}{T[A_{11}(\nu)\cos\nu + B_{11}(\nu)\sin\nu]}\right\} + O(\varepsilon_s^2) ;$$

$$i(\nu) = |T|[A_{11}^2(\nu) + B_{11}^2(\nu)]^{1/2} + O(\varepsilon_s^2). \qquad .....(5.19)$$

This result indicates that after one revolution the position of the ascending node is at $\tilde{\omega}_{00} + \pi + O(\varepsilon_s^2)$, i.e. near the aphelion, if $T > 0$ and at $\tilde{\omega}_{00} + O(\varepsilon_s^2)$ (near perihelion) for $T < 0$. This result can be understood physically: although the angular rate of the orbital plane, $W_\xi = \varepsilon_s Tu/\ell^{1/2}$, is smaller near aphelion than that near perihelion, the angular change per radian traversed by the satellite is larger near aphelion since $1/\dot{\nu}$ is proportional to r^2. Hence it is also evident that for an initially circular orbit, the orbital plane returns to its original position after one revolution (in the first-order approximation).

5.5.2 Long-term behavior of the elements

A long-term approximate solution for orbital elements of the solar sail trajectory with fixed sail setting and arbitrary initial conditions can be derived by means of the two-variable expansion procedure. Thereto, a new independent slow variable $\bar{\nu} = \varepsilon\nu$ is introduced and the variables u, ℓ and $\underline{K}$ are expanded in asymptotic series:

$$u(\nu) = \sum_{n=0}^{N-1} \varepsilon_s^n u_n(\nu,\bar{\nu}) + O(\varepsilon_s^N) ;$$

$$\ell(\nu) = \sum_{n=0}^{N-1} \varepsilon_s^n \ell_n(\nu,\bar{\nu}) + O(\varepsilon_s^N) ;$$

$$\underline{K}(\nu) = \sum_{n=0}^{N-1} \varepsilon_s^n \underline{K}_n(\nu,\bar{\nu}) + O(\varepsilon_s^N) . \qquad .....(5.20)$$

Substituting these series into Equations (5.5), using $d/d\nu = \partial/\partial\nu + \varepsilon_s \partial/\partial\bar{\nu}$ and $d^2/d\nu^2 = \partial^2/\partial\nu^2 + 2\varepsilon_s \partial^2/(\partial\nu\,\partial\bar{\nu}) + \varepsilon_s^2\, \partial^2/\partial\bar{\nu}^2$, and collecting terms of like powers in ε_s, leads to equations for the subsequent levels of approximation. The zeroth-order equations admit solutions, written as follows:

$$u_0(\nu,\bar{\nu}) = [1 + p_0(\bar{\nu})\cos\nu + q_0(\bar{\nu})\sin\nu]/\ell_0(\bar{\nu}), \quad p_0(0) = p_{00} ; \quad q_0(0) = q_{00} ;$$

$$\ell_0(\nu,\bar{\nu}) = \ell_0(\bar{\nu}) , \quad \ell_0(0) = \ell_{00} ;$$

$$M_0(\nu,\bar{\nu}) = A_0(\bar{\nu})\cos\nu + B_0(\bar{\nu})\sin\nu , \quad A_0(0) = B_0(0) = 0 ;$$

$$K_0(\nu,\bar{\nu}) = K_0(\bar{\nu}) , \quad K_0(0) = 1 . \qquad .....(5.21)$$

Physically, one can interpret the expression for u_0 as a trajectory tangent to osculating ellipses with slowly varying mean elements. These averaged orbital elements differ from the usual osculating parameters in the sense that short-term periodic variations are disregarded.

The functions p_0, q_0, ℓ_0, A_0, B_0 and K_0 of the slow variable $\bar{\nu}$ are determined from constraints imposed upon the first-order contributions. The equations for the first-order terms become:

$$\frac{\partial^2 u_1}{\partial\nu^2} + u_1 = -2\frac{\partial^2 u_0}{\partial\nu\partial\bar{\nu}} - \ell_1/\ell_0^2 - (R + S\frac{\partial u_0}{\partial\nu} / u_0)/\ell_0 ,$$

$$u_1(0) = 0; \quad \frac{\partial u_1}{\partial\nu}(0) = -\frac{\partial u_0}{\partial\bar{\nu}}(0) ;$$

$$\frac{\partial \ell_1}{\partial \nu} = -\frac{d\ell_0}{d\bar{\nu}} + 2S/u_0 \quad , \quad \ell_1(0) = 0;$$

$$\frac{\partial^2 M_1}{\partial \nu^2} + M_1 = -2\frac{\partial^2 M_0}{\partial \nu \partial \bar{\nu}} + TK_0/(u_0\ell_0), \quad M_1(0) = 0; \quad \frac{\partial M_1}{\partial \nu}(0) = -\frac{\partial M_0}{\partial \bar{\nu}}(0) \; ;$$

$$\frac{\partial K_1}{\partial \nu} = -\frac{dK_0}{d\bar{\nu}} - T\frac{\partial M_0}{\partial \nu}/(u_0\ell_0) \quad , \quad K_1(0) = 0; \qquad .....(5.22)$$

In order that the zeroth-order terms remain a valid approximation over a long duration, it is required that the first-order terms do not contain unbounded contributions (in the variable ν). Therefore, the right-hand-sides of Equations (5.22) are developed in Fourier series with slowly varying coefficients. To eliminate (mixed) secular terms in the solutions for u_1 and M_1, the coefficients of $\sin\nu$ and $\cos\nu$ need to vanish, while for suppressing unbounded contributions in ℓ_1 and K_1, the non-harmonic terms must be set equal to zero. This leads to the system of equations:

$$p_0'(\bar{\nu}) = S\, p_0[1 - (1 - e_0^2)^{1/2}]/e_0^2 \quad , \quad p_0(0) = p_{00} \; ;$$

$$q_0'(\bar{\nu}) = S\, q_0[1 - (1 - e_0^2)^{1/2}]/e_0^2 \quad , \quad q_0(0) = q_{00} \; ;$$

$$\ell_0'(\bar{\nu}) = 2S\ell_0/(1 - e_0^2)^{1/2} \quad , \quad \ell_0(0) = \ell_{00} \; ;$$

$$A_0'(\bar{\nu}) = T\, K_0\, q_0[1/(1 - e_0^2)^{1/2} - 1]/e_0^2 \quad , \quad A_0(0) = 0 \; ;$$

$$B_0'(\bar{\nu}) = -T\, K_0\, p_0[1/(1 - e_0^2)^{1/2} - 1]/e_0^2 \quad , \quad B_0(0) = 0 \; ;$$

$$K_0'(\bar{\nu}) = -T[p_0B_0 - q_0A_0][1/(1 - e_0^2)^{1/2} - 1]/\, e_0^2, \quad K_0(0) = 1 \; .$$

$$.....(5.23)$$

It follows from Equations (5.23) that $\tilde{\omega}_0(\bar{\nu}) = \tilde{\omega}_{00}$ is a constant so that the orientation of the major axis remains fixed in the long run. To analyse the

behavior of the eccentricity, the auxiliary element $w(\bar{\nu}) = 1 - [1-e^2(\bar{\nu})]^{1/2}$ is introduced and the following equation for w_0 is found from Equations (5.23),

$$w_0'(\bar{\nu}) = Sw_0/(1 - w_0), \quad w_0(0) = w_{00} . \qquad .....(5.24)$$

If $w_{00} = 0$, i.e. initial orbit is circular, it follows that the orbit will remain circular in the long run: $w_0(\bar{\nu}) = e_0(\bar{\nu}) = 0$. It may be noted that $u_0(\nu,\bar{\nu})\ell_0(\bar{\nu}) = 1$ and $\ell_0(\bar{\nu}) = \ell_{00} \exp(2\, S\bar{\nu})$ when $e_{00} = 0$ in accordance with the exact spiral solution discussed in Section 5.2.

For $w_{00} \neq 0$, integration of Equation (5.24) leads to the following implicit equation for $w_0(\bar{\nu})$,

$$w_0(\bar{\nu}) = w_{00} \exp[S\bar{\nu} + w_0(\bar{\nu}) - w_{00}] . \qquad .....(5.25)$$

Quite accurate representations for $w_0(\bar{\nu})$ can be established through a process of successive substitution. Initiating the procedure by replacing $w_0(\bar{\nu})$ with $w_0^{(0)} = w_{00}$ in the right-hand-side of Equation (5.25), subsequent more accurate approximations for $w_0(\bar{\nu})$ follow from:

$$w_0^{(n)}(\bar{\nu}) = w_{00} \exp[S\bar{\nu} + w_0^{(n-1)} - w_{00}] , \qquad .....(5.26)$$

for $n = 1,2,3,\ldots$. This iteration scheme converges very rapidly as long as e_{00} is not too close to unity. For small e_{00}, an asymptotic series in terms of powers of w_{00} can be established from the scheme in Equation (5.26). It can be shown that the errorterm in $w_0^{(n)}(\bar{\nu})$ as an approximation for $w_0(\bar{\nu})$ is of the order w_{00}^{n+1} for $w_{00} \to 0$. For most purposes, the asymptotic expansion of $w_0^{(3)}(\bar{\nu})$ for $w_{00} \to 0$ would provide sufficiently accurate results:

$$w_0^{(3)}(\bar{\nu}) = w_{00}\exp(S\bar{\nu}) + w_{00}^2[\exp(2S\bar{\nu}) - \exp(S\bar{\nu})] + w_{00}^3[3\exp(3S\bar{\nu}) - 4\exp(2S\bar{\nu}) + \exp(S\bar{\nu})]/2 + O(w_{00}^4) . \quad .....(5.27)$$

It should be emphasized that a series in terms of powers of w_{00} is more useful than the one in powers of e_{00} for small e_{00}, since $w_{00} = e_{00}^2/2 + O(e_{00}^4)$ for $e_{00} \to 0$. From the results for $w_0^{(n)}(\bar{\nu})$, Equation (5.26), the corresponding eccentricity $e_0^{(n)}(\bar{\nu})$ can readily be evaluated from the relation,

$$e_0^{(n)}(\bar{\nu}) = \{1 - [1 - w_0^{(n)}(\bar{\nu})]^2\}^{1/2} , \quad .....(5.28)$$

to any desired accuracy by taking n sufficiently large. For small e_{00}, asymptotic series in terms of powers of w_{00} can be derived. The expansion of $e_0^{(3)}(\bar{\nu})$ would serve most needs:

$$e_0^{(3)}(\bar{\nu}) = e_{00}\exp(S\bar{\nu}/2)\{1 + w_{00}[\exp(S\bar{\nu}) - 1]/4 + w_{00}^2[3 - 10\exp(S\bar{\nu}) + 7\exp(2S\bar{\nu})]/32 + O(w_{00}^3)\}. \quad .....(5.29)$$

The long-term solutions for $p_0(\bar{\nu})$ and $q_0(\bar{\nu})$ are readily expressed in terms of $e_0(\bar{\nu})$,

$$p_0^{(n)}(\bar{\nu}) = p_{00}\, e_0^{(n)}(\bar{\nu})/e_{00} , \quad q_0^{(n)}(\bar{\nu}) = q_{00}\, e_0^{(n)}(\bar{\nu})/e_{00} , \quad .....(5.30)$$

and asymptotic series are established using Equation (5.29).

The attention is focused on the behavior of the semi-latus rectum. Through Equations (5.23), $\ell_0(\bar{\nu})$ can be expressed in terms of $w_0(\bar{\nu})$:

$$\ell_0(\bar{\nu}) = \ell_{00}\exp\left\{2S\int_0^{\bar{\nu}} \frac{d\bar{\tau}}{1 - w_0(\bar{\tau})}\right\} . \quad .....(5.31)$$

For the first few approximations of $w_0(\bar{\nu})$, the integral can be evaluated explicitly:

$$\ell_0^{(1)}(\bar{\nu}) = \ell_{00}(1 - e_{00}^2)\exp(2S\bar{\nu})/[1 - w_{00}\exp(S\bar{\nu})]^2 ;$$

$$\ell_0^{(2)}(\bar{\nu}) = \ell_{00}\left\{\frac{(1 - w_{00})\exp(2S\bar{\nu})}{1 - w_{00}\exp(S\bar{\nu}) + w_{00}^2[\exp(S\bar{\nu}) - \exp(2S\bar{\nu})]}\right\} *$$

$$* \left\{\frac{2 + w_{00}[(w_{00}^2 - 2w_{00} + 5)^{1/2} + w_{00} - 1]\exp(S\bar{\nu})}{2 - w_{00}[(w_{00}^2 - 2w_{00} + 5)^{1/2} - w_{00} + 1]\exp(S\bar{\nu})}\right\}^{\frac{(1-w_{00})}{(w_{00}^2-2w_{00}+5)^{1/2}}} . \quad .....(5.32)$$

However, the following asymptotic representation is more useful for small e_{00} :

$$\ell_0^{(2)}(\bar{\nu}) = \ell_{00}\exp(2S\bar{\nu})\{1 + 2w_{00}[\exp(S\bar{\nu}) - 1]$$

$$+ w_{00}^2[4\exp(2S\bar{\nu}) - 6\exp(S\bar{\nu}) + 2] + O(w_{00}^3)\} . \quad .....(5.33)$$

A long-term approximation for the radial distance $r = 1/u$ is given by

$$r_0^{(n)}(\nu,\bar{\nu}) = \ell_0^{(n)}(\bar{\nu})/[1 + e_0^{(n)}(\bar{\nu})\cos(\nu - \tilde{\omega}_{00})] , \quad .....(5.34)$$

where the desired representations for $\ell_0^{(n)}$ and $e_0^{(n)}$ need to be substituted. Also, a long-term approximation for the semi-major axis $a_0(\bar{\nu})$ is known,

$$a_0^{(n)}(\bar{\nu}) = \ell_0^{(n)}(\bar{\nu})/[1 - w_0^{(n)}(\bar{\nu})]^2 . \quad .....(5.35)$$

Next, the time history of the satellite in its trajectory is studied. Since $t'(\nu) = r^2/\ell^{1/2}$, it is obvious that

$$t(\nu) = \int_0^{\nu} \ell^{3/2}(\bar{\tau})\, d\tau/[1 + e(\bar{\tau})\cos(\tau - \tilde{\omega}_{00})]^2 . \qquad .....(5.36)$$

Through substitution of $\ell_0^{(n)}$ and $e_0^{(n)}$ into the integrand, a long-term valid explicit approximation for $t(\nu)$ may be derived. It is more convenient, however, to determine asymptotic series for $t(\nu)$. In this regard, it must be emphasized that, due to the integration of terms depending upon $\bar{\nu}$, a consistent asymptotic series of $t(\nu)$ should be of the form:

$$t(\nu) = t_{-1}(\bar{\nu})/\varepsilon_s + t_0(\nu,\bar{\nu}) + \varepsilon_s t_1(\nu,\bar{\nu}) + O(\varepsilon_s^2). \qquad .....(5.37)$$

Substitution of $\ell_0^{(1)}$ and $e_0^{(1)}$ into Equation (5.36) and integration leads to the following approximation for $t_{-1}(\bar{\nu})$:

$$t_{-1}^{(1)}(\bar{\nu}) = a_{00}^{3/2}\{[\exp(3S\bar{\nu}) - 1]/3 + e_{00}^2[3\exp(4S\bar{\nu}) - 4\exp(3S\bar{\nu}) + 1]/4 + O(e_{00}^3)\}/S. \qquad .....(5.38)$$

It is interesting to note that this result is consistent with the exact spiral solution of Equation (5.9) when $e_{00} = 0$.

Turning to the long-term behavior of the orbital plane, it can be seen (from Equations 5.23) that the vector $K_0(\bar{\nu}) = (M_0, L_0, K_0)$ traces a path upon a spherical surface : $A_0^2 + B_0^2 + K_0^2 = 1$. Writing $A_0 = C_0 \sin\tilde{\omega}_{00}$ and $B_0 = -C_0\cos\tilde{\omega}_{00}$, an equation for C_0 can be derived and solved,

$$C_0(\bar{\nu}) = \sin\{T[\arcsin e_0(\bar{\nu}) - \arcsin e_{00}]/S\}. \qquad .....(5.39)$$

Through this expression, all of $M_0(\bar{\nu})$, $L_0(\bar{\nu})$ and $K_0(\bar{\nu})$ can now be written in terms of e_0 and are thus determined up to the required accuracy by substituting the appropriate approximation $e_0^{(n)}(\bar{\nu})$ or its expansions for small e_{00}. The orientation of the orbital plane in terms of the angles ψ_0 and i_0 is given by:

$$\psi_0(\nu) = \begin{cases} \tilde{\omega}_{00} + \pi & , \ T > 0 \ ; \\ \tilde{\omega}_{00} & , \ T < 0 \ ; \end{cases}$$

$$i_0(\bar{\nu}) = |T| \ [\arcsin e_0(\bar{\nu}) - \arcsin e_{00}] \ /S. \qquad .....(5.40)$$

5.5.3 Higher-order contributions

It may be noted that the maximum deviation of the zeroth-order solution from the actual solution is of the order ε_s only for ν up to about $1/\varepsilon_s$. Thus for large values of A/m, higher-order terms may be needed to establish sufficiently accurate long-term approximations.

After incorporating the zeroth-order solutions, the remainder of Equations (5.22) can be integrated formally, yielding the first-order results:

$$u_1(\nu,\bar{\nu}) = - [R + A_3(\bar{\nu})](1 - \cos\nu)/\ell_0(\bar{\nu}) + A_2(\bar{\nu}) \cos\nu + B_2(\bar{\nu}) \sin\nu$$
$$+ S/\ell_0(\bar{\nu}) \sum_{j=2}^{\infty} \{[2 a_{10}^j/j - p_0 d_{11}^j + q_0 c_{11}^j] \sin(j\nu)$$
$$- [2 c_{10}^j/j + p_0 b_{11}^j - q_0 a_{11}^j] \cos(j\nu)\}/(j^2 - 1) \ ;$$

$$\ell_1(\nu,\bar{\nu}) = \ell_0(\bar{\nu}) \left\{ 2S \sum_{j=1}^{\infty} \{a_{10}^j \sin(j\nu) + c_{10}^j [1 - \cos(j\nu)]\} /j + A_3(\bar{\nu}) \right\};$$

$$M_1(\nu,\bar{\nu}) = T \ K_0(\bar{\nu}) \ (1 - \cos\nu)/(1 - e_{00}^2)^{1/2} + A_4(\bar{\nu}) \cos\nu + B_4(\bar{\nu}) \sin\nu$$
$$- T \ K_0(\bar{\nu}) \sum_{j=2}^{\infty} \{a_{10}^j \cos(j\nu) + c_{10}^j \sin(j\nu)\} /(j^2 - 1) \ ;$$

$$K_1(\nu,\bar{\nu}) = T/2 \sum_{j=1}^{\infty} \{[c_{10}^{j+1} - c_{10}^{j-1}] A_0(\bar{\nu}) \sin(j\nu) - [a_{10}^{j+1} - a_{10}^{j-1}] A_0(\bar{\nu}) *$$
$$*[1 - \cos(j\nu)] - [a_{10}^{j+1} + a_{10}^{j-1}] B_0(\bar{\nu}) \sin(j\nu) - [c_{10}^{j+1} + c_{10}^{j-1}] *$$

$$*B_0(\bar{\nu})\ [1 - \cos(j\nu)]\}/j + A_5(\bar{\nu}) \quad . \qquad .....(5.41)$$

The Fourier coefficients a^j_{nk}, b^j_{nk}, etc., depend on the slow functions $p_0(\bar{\nu})$ and $q_0(\bar{\nu})$ and are evaluated in Appendix II. The functions $A_j(\bar{\nu})$, $B_j(\bar{\nu})$, $j = 2,3,4,5$, are to be determined, as usual, from constraints imposed upon the behavior of the second-order terms. Equations for these terms can readily be obtained (Appendix III), leading to lengthy equations for the functions A_j, B_j when eliminating the secular contributions to u_2, ℓ_2, etc. For instance, the least complicated one is given by,

$$\begin{aligned} A_3'(\bar{\nu}) &= - A_3\, \ell_0'/\ell_0 - S(R + A_3)\,[a^0_{20} - a^0_{21}] + S\ell_0\,[A_2\, a^0_{21} + B_2\, b^0_{21}] \\ &\quad + S^2 \sum_{j=2}^{\infty} \{c^j_{20}\,[2\, a^j_{10}/j - p_0\, d^j_{11} + q_0\, c^j_{11}] - a^j_{20} * \\ &\quad *[2\, c^j_{10}/j + p_0\, b^j_{11} - q_0\, a^j_{11}]\} \quad , \end{aligned}$$

with all Fourier coefficients depending on $\bar{\nu}$. While analytical solutions have not been found for general eccentricity, in the special case of $e_{00} = 0$ it follows that $e_0(\bar{\nu}) = 0$ and the equations for A_j and B_j can be integrated yielding the following complete first-order solutions:

$$\ell_1(\bar{\nu}) = 2\ell_{00}\, RS\bar{\nu}\, \exp(2S\bar{\nu}) \ ;$$

$$e_1(\nu,\bar{\nu}) = \{(R^2 + 4S^2)[1 + \exp(S\bar{\nu}) - 2\, \exp(S\bar{\nu}/2)\, \cos\nu]\}^{1/2} \ ;$$

$$\tilde{\omega}_1(\nu,\bar{\nu}) = \arctan\left\{ \frac{2S[\exp(S\bar{\nu}/2) - \cos\nu] - R\, \sin\nu}{R[\exp(S\bar{\nu}/2) - \cos\nu] + 2S\, \sin\nu} \right\} \ ;$$

$$\begin{aligned} r(\nu,\bar{\nu}) &= \ell_{00}\, \exp(2S\bar{\nu})\{1 + \varepsilon_s\, R[1 - \exp(S\bar{\nu}/2)\, \cos\nu] \\ &\quad -2\, \varepsilon_s\, S\, \exp(S\bar{\nu}/2)\, \sin\nu\} + O(\varepsilon_s^2) \ . \qquad .....(5.42) \end{aligned}$$

It is seen that the radial distance oscillates around the spiral solution $r = \ell_{00} \exp(2S\bar{\nu})$ with slowly increasing amplitude of oscillation.

As to the orientation of the orbital plane, it follows that

$$\psi(\nu,\bar{\nu}) = \nu - \arctan\left\{ \frac{S(1 - \cos\nu) + [2S\cos\nu - R\sin\nu][\exp(S\bar{\nu}/2) - 1]}{S\sin\nu - [2S\sin\nu + R\cos\nu][\exp(S\bar{\nu}/2) - 1]} \right\} + O(\varepsilon_s^2) ;$$

$$i(\nu,\bar{\nu}) = \varepsilon_s |T|/S\{(4S^2 + R^2)[\exp(S\bar{\nu}/2) - 1]^2 + 4S^2(\cos\nu - 1)* *[\exp(S\bar{\nu}/2) - 3/2] - 2RS\sin\nu[\exp(S\bar{\nu}/2) - 1]\} + O(\varepsilon_s^2) . \quad .....(5.43)$$

These results illustrate that the amplitude of the perturbations grows slowly.

5.5.4 Discussion of results

In order to assess the relative accuracies of the approximate results, comparisons are made with a numerical solution of the exact Equations (5.5) using a double-precision Runge-Kutta integration routine. The high value of initial eccentricity ($e_{00} = 0.6$) is chosen to illustrate a rather extreme situation, while ε_s is taken to be 0.015. Figure 5-6 shows the various approximations for the semi-latus rectum: obviously, the short-term solution has a limited range of validity, while the near-circular expansions of $\ell_0^{(1)}$ and $\ell_0^{(2)}$ may give fairly accurate long-term approximations provided a sufficient number of terms are retained for high values of e_{00} (curve a). The solution $\ell_0^{(2)}$ is more accurate, naturally, and would be the most appropriate candidate for predicting long-term, high-eccentricity trends. The effect of the first-order contributions, $\ell_1(\nu,\bar{\nu})$ from Equations (5.41) is

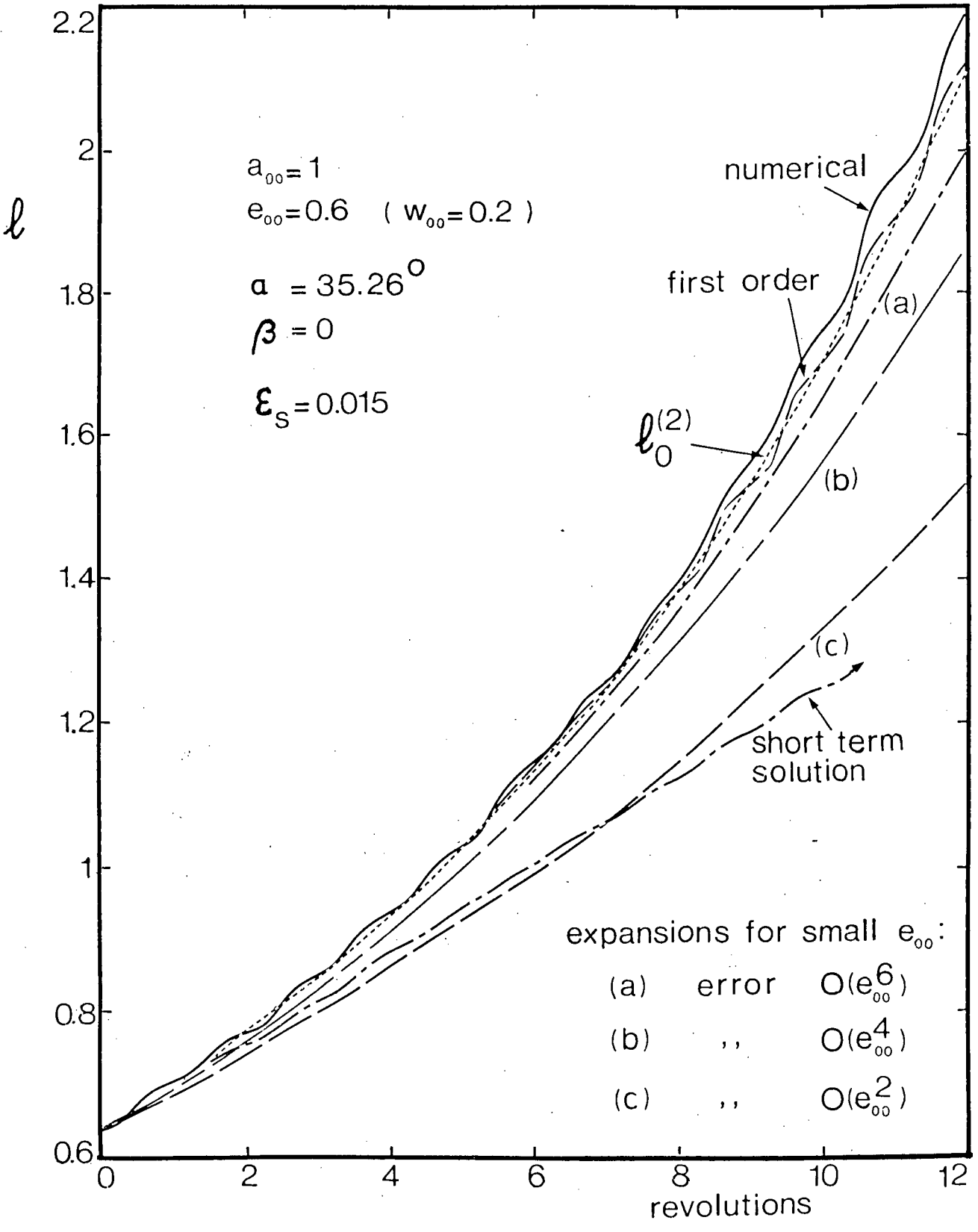

Figure 5-6 Comparison of the analytical results for the long-term behavior of the semi-latus rectum

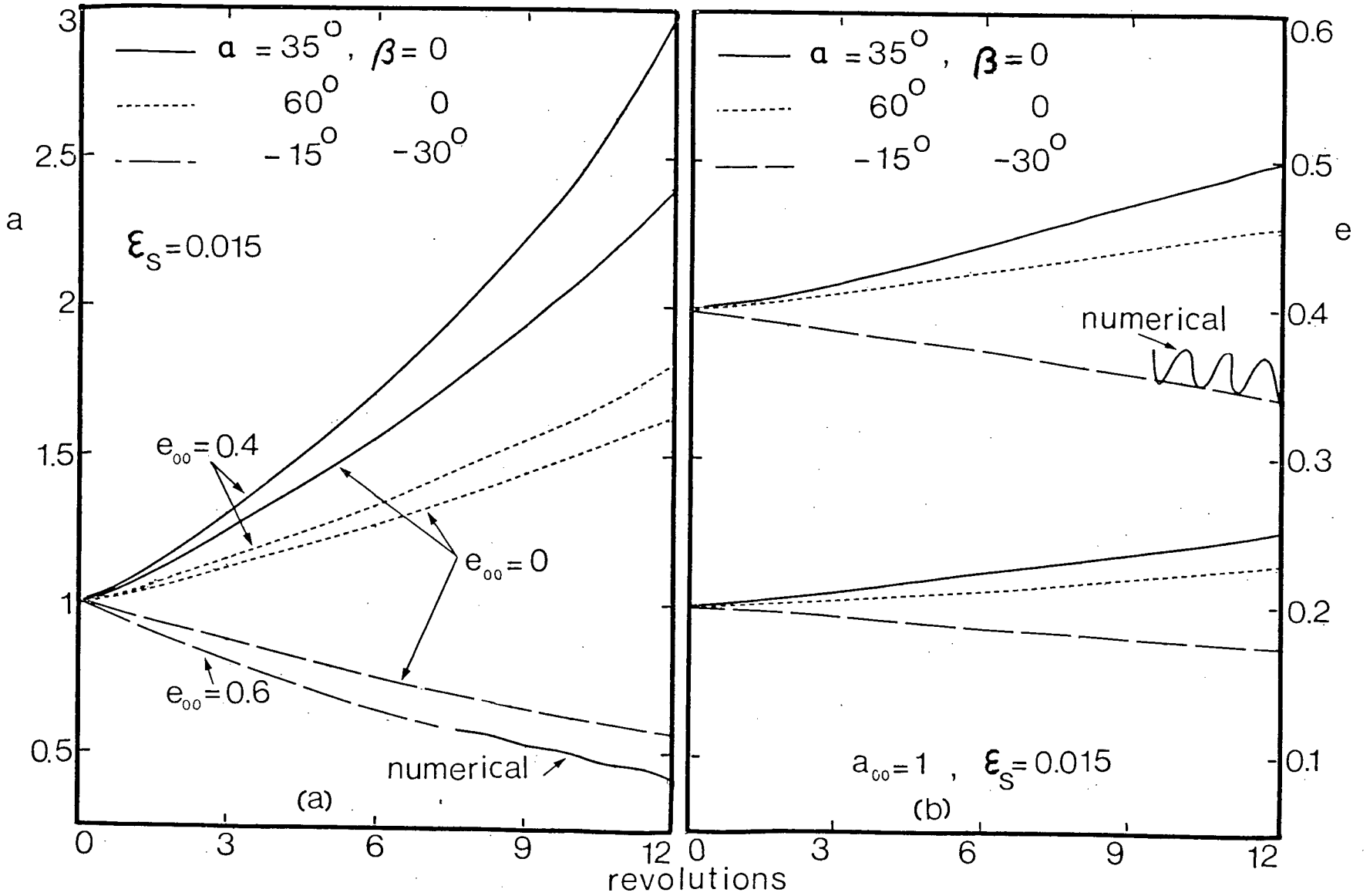

Figure 5-7 Long-term behavior of semi-major axis and eccentricity as predicted by the zeroth-order solution

added to $\ell_0^{(2)}$ illustrating the small-amplitude oscillations around the mean trend designated by $\ell_0^{(2)}$ itself. The slow function $A_3(\bar{\nu})$ was taken to be zero throughout. The discrepancy between the numerical solution and this (best) analytical approximation is largely due to the effect of $A_3(\bar{\nu})$. Other contributions to the error may be attibuted to the fact that $\ell_0^{(2)}$ represents an approximation for $\ell_0(\bar{\nu})$ and the higher-order terms are neglected.

Figure 5-7a shows the long-term trend of the semi-major axis for a few sail settings. The approximation $a_0^{(2)}(\bar{\nu})$ compares quite well with the exact numerical solution: at least to two significant digits over the first 12 revolutions. The long-term behavior of eccentricity is depicted in Figure 5-7b, where the approximation $e_0^{(2)}(\bar{\nu})$ was used. Relatively large first-order contributions separate the zeroth-order approximations from the exact solutions in this case. Nevertheless, the qualitative trend of the long-term behavior of the eccentricity is predicted correctly.

5.6 Concluding Remarks

The results of the present chapter can be summarized in the form of the following general conclusions:

(i) An exact three-dimensional solution in the form of a logarithmic spiral is presented for certain specific initial conditions by separating the out-of-plane and in-plane motions.

(ii) An effective near-circular, out-of-plane spiral transfer trajectory has been explored in detail permitting any combination of final radial distance and orbital inclination.

(iii) Short- as well as long-term approximate solutions have been established for arbitrary initial conditions. For small initial eccentricity, asymptotic series for the orbital elements should prove useful for long-term trajectory evaluation.

6. DETERMINATION OF OPTIMAL CONTROL STRATEGIES IN HELIOCENTRIC ORBITS

6.1 Preliminary Remarks

Although it is evident from the results of the previous chapter that fixed sail settings can produce effective transfer trajectories, especially if the best possible orientation of the sail is chosen, time-varying control strategies are likely to be more efficient. Therefore, the attention is focused upon the determination of optimal control strategies in this chapter. In many missions, e.g. rendezvous with a distant planet or escape from the planetary system, it is important to increase the size of the orbit in the most efficient manner. A specific optimization criterion must be formulated according to the nature and objective of the actual mission involved.

Here, two particular criteria with general applicability are selected: first, the optimal steering program of the orientation of the solar sail for maximum increase in total energy (and thus semi-major axis) after one revolution is determined. Next, the best steering program for maximum increase in angular momentum (and thus semi-latus rectum) after one revolution is derived. While the control strategy which directs the thrust along the instantaneous velocity vector at all times would likely be very effective as to the first objective, especially for near-circular orbits, a formulation in terms of optimal control theory would evaluate, for instance, the effect of steering the spacecraft relatively closer to the sun initially in order to take advantage of the larger magnitude of the force there. The solutions are found in an implicit form in terms of state and adjoint variables by means of Pontryagin's 'maximum principle'. Approximate

explicit representations can, subsequently, be determined in asymptotic series containing the small parameter ε_s denoting the ratio of solar radiation and gravity forces. In general, only the first few terms of these series can be evaluated. These approximate analytical results have been substantiated by means of a numerical iterative procedure based on the steepest-ascent method. No restrictions are placed on the position of the satellite in the initial orbit nor on the nature of the initial and ensuing osculating ellipses.

6.2 Formulation of the Problem

The governing equations of motion for the solar sail are essentially similar to Equations (5.5) except for the fact that the force components $\underline{R}$ depend on the independent variable since $\underline{R} = \underline{R}[\underline{\alpha}(\nu)]$ here.
For convenience, the solar sail is represented by a flat plate of homogeneous surface characteristics and the parameter σ_2 is neglected. Note that for a realistic solar sail surface, the magnitude of σ_2 amounts to about two percent of the reflectivity ρ, Table 2.1 . The components of $\underline{R}$ can be written as:

$$R(\underline{\alpha}) = (\sigma_1 + \rho\cos^2\alpha\,\cos^2\beta)\cos\alpha\cos\beta\ ;$$

$$S(\underline{\alpha}) = \rho\sin\alpha\,\cos^2\alpha\,\cos^3\beta\ ;$$

$$T(\underline{\alpha}) = -\rho\cos^2\alpha\,\cos^2\beta\sin\beta\ ; \qquad .....(6.1)$$

The vector $\underline{\alpha}$ stands for (α, β) and is a function of ν. For the analysis of this chapter, a more convenient alternative system of autonomous first-

order equations is derived for the in-plane orbital elements by means of Equations (5.5):

$$\Phi'(\nu) = -\Psi(\nu) + 2\varepsilon_s S(\underline{\alpha}) \; ; \qquad ; \Phi(0) = p_{00} \; ;$$

$$\Psi'(\nu) = \Phi(\nu) + \varepsilon_s \{R(\underline{\alpha}) + S(\underline{\alpha}) \Psi(\nu)/[1 + \Phi(\nu)]\}; \; \Psi(0) = -q_{00} \; ;$$

$$\ell'(\nu) = 2\varepsilon_s S(\underline{\alpha}) \ell(\nu)/[1 + \Phi(\nu)] \; . \qquad .....(6.2)$$

The variables $\Phi(\nu)$ and $\Psi(\nu)$ are defined in Equations (4.14).

The two problems to be studied here can be stated as follows:

(i) which control strategy $\underline{\alpha}(\nu)$ leads to the maximum value of the semi-major axis after one revolution ?

(ii) which control function $\underline{\alpha}(\nu)$ yields the maximum value of semi-latus rectum after one revolution ?

These problems are approached using the results of optimal control theory. To minimize algebraic complexity, new variables $\hat{a} = -1/a$ and $\hat{\ell} = \ln(\ell)$ are introduced and the complete system including the adjoint equations becomes (note that $\Phi'(\nu)$ and $\Psi'(\nu)$ are also part of this system):

$$\hat{a}'(\nu) = 2\varepsilon_s \exp(-\hat{\ell}) \{R(\underline{\alpha}) \Psi + S(\underline{\alpha}) (1 + \Phi)\} \; ; \quad \hat{a}(0) = -1/a_{00} \; ;$$

$$\hat{\ell}'(\nu) = 2\varepsilon_s S(\underline{\alpha})/(1 + \Phi) \; ; \quad \hat{\ell}(0) = \ell n(\hat{\ell}_{00}) \; ;$$

$$\lambda_0'(\nu) = 0 \; ;$$

$$\lambda_1'(\nu) = 2\varepsilon_s \lambda_0 \{R(\underline{\alpha}) \Psi + S(\underline{\alpha}) (1 + \Phi)\} \exp(-\hat{\ell}) \; ;$$

$$\lambda_2'(\nu) = -\lambda_3 - 2\varepsilon_s S(\underline{\alpha}) \exp(-\hat{\ell}) + \varepsilon_s S(\underline{\alpha}) [2\lambda_1 + \lambda_3 \Psi]/(1 + \Phi)^2 \; ;$$

$$\lambda_3'(\nu) = \lambda_2 - 2\varepsilon_s \lambda_0 R(\underline{\alpha}) \exp(-\hat{\ell}) - \varepsilon_s \lambda_3 S(\underline{\alpha})/(1 + \Phi) \; . \qquad .....(6.3)$$

The out-of-plane equations turn out to be irrelevant and are omitted here.

6.3 Maximization of Total Energy

In this section, an approximate analytical representation for the optimal control strategy $\underline{\alpha}(\nu)$ maximizing the total energy E (and thus major axis a) at $\nu = 2\pi$ is derived. The Hamiltonian for the present problem, Equations (6.3), becomes:

$$H(\underline{\alpha}) = \lambda_3\Phi - \lambda_2\Psi + \varepsilon_s R(\underline{\alpha}) \{2\lambda_0 \Psi \exp(-\hat{\ell}) + \lambda_3\}$$
$$+ \varepsilon_s S(\underline{\alpha}) \{2\lambda_0 (1 + \Phi) \exp(-\hat{\ell}) + (2\lambda_1 + \lambda_3 \Psi)/(1 + \Phi) + 2\lambda_2\} . \quad .....(6.4)$$

For $\underline{\alpha}(\nu)$ to be the optimal control vector over the fixed interval $(0, 2\pi)$, the following necessary conditions must be satisfied:

i) $\frac{\partial H}{\partial \alpha} = \frac{\partial H}{\partial \beta} = 0$;

ii) $H(\underline{\alpha})$ = constant ;

iii) $\lambda_j(2\pi) = 0$, $j = 1,2,3$; (transversality)

iv) $\lambda_0(\nu) = 1$; .....(6.5)

according to Pontryagin's Maximum Principle[107]. From the conditions ii), iii) and iv) it follows that

$$H = 2 \varepsilon_s \{[R(\underline{\alpha}) + (1 + \Phi) S(\underline{\alpha})] \exp(-\hat{\ell})\}_{\nu = 2\pi} , \quad ..... (6.6)$$

which equals $\hat{a}'(2\pi)$, Equations (6.3). The conditions in i) lead to the

following equation for α,

$$[2\,\Psi\,\exp(-\hat{\ell}) + \lambda_3]\,\frac{\partial R}{\partial \alpha} + [2(1+\Phi)\exp(-\hat{\ell}) + (2\lambda_1 + \lambda_3\Psi)/(1+\Phi) + 2\lambda_2]\,\frac{\partial S}{\partial \alpha}\,, \qquad .....(6.7)$$

and a similar one for β. It follows readily that $\beta(\nu) = 0$ is a solution for the out-of-plane rotation confirming that the optimal trajectory is a planar one since the solar radiation force remains in the plane of the orbit. The equation for the control angle $\alpha(\nu)$ is reduced to the following implicit relation:

$$\frac{\rho\cos\alpha\,(1 - 3\sin^2\alpha)}{\sin\alpha\,(\sigma_1 + 3\,\rho\,\cos^2\alpha)} = \frac{2\,\Psi + \ell\,\lambda_3}{2(1+\Phi) + (2\lambda_1 + \lambda_3\,\Phi)\,\ell/(1+\Phi) + 2\ell\,\lambda_2}\,, \qquad .....(6.8)$$

with α in the interval $(0, \pi/2)$ on physical grounds. For obtaining approximate solutions for $\alpha(\nu)$ from Equations (6.8) it is imperative to assess, carefully, the orders of magnitude of the various terms on the right-hand-side of Equation (6.8). Thereto, the orbital elements and adjoint variables are written as a system of coupled integral equations derived from Equations (6.3) by integration while taking the mixed boundary conditions into account:

$$a(\nu) = a_{00} + \varepsilon_s \int_0^{\nu} \{a^2[R\,\Psi + S(1+\Phi)]/\ell\}\,d\tau\,;$$

$$\ell(\nu) = \ell_{00} + 2\varepsilon_s \int_0^{\nu} \{\ell\,S/(1+\Phi)\}\,d\tau\,;$$

$$\Phi(\nu) = \Phi_0(\nu) + \varepsilon_s \int_0^{\nu} \{2\,S\cos(\tau - \nu) + [R + S\,\Psi/(1+\Phi)]\sin(\tau - \nu)\}\,d\tau\,;$$

$$\Psi(\nu) = \Psi_0(\nu) + \varepsilon_s \int_0^{\nu} \{[R + S\,\Psi/(1 + \Phi)] \cos(\tau - \nu) - 2S \sin(\tau - \nu)\}\, d\tau \;;$$

$$\lambda_1(\nu) = -2\varepsilon_s \int_{\nu}^{2\pi} \{[R\,\Psi + S(1 + \Phi)]/\ell\}\, d\tau \;;$$

$$\lambda_2(\nu) = \varepsilon_s \int_{\nu}^{2\pi} \{Q \sin(\tau - \nu) + P \cos(\tau - \nu)\}\, d\tau \;;$$

$$\lambda_3(\nu) = \varepsilon_s \int_{\nu}^{2\pi} \{Q \cos(\tau - \nu) - P \sin(\tau - \nu)\}\, d\tau \;. \qquad \text{.....(6.9)}$$

Here $\Phi_0(\nu) = p_{00} \cos\nu + q_{00} \sin\nu$ and $\Psi_0(\nu) = p_{00} \sin\nu - q_{00} \cos\nu$ and the auxiliary functions P and Q stand for:

$$P = 2\,S/\ell - S(2\lambda_1 + \lambda_3\,\Psi)/(1 + \Phi)^2 \;;$$

$$Q = 2\,R/\ell + \lambda_3\,S/(1 + \Phi) \;. \qquad \text{.....(6.10)}$$

An asymptotic series for $\alpha(\nu)$ in terms of the small parameter ε_s can now be constructed. By writing $\alpha(\nu) = \alpha_0(\nu) + \varepsilon_s\,\alpha_1(\nu) + O(\varepsilon_s^2)$, developing the left-hand-side of Equation (6.8) in a Taylor series around α_0 and expanding the right-hand-side using the results of Equations (6.9), successive terms in the series for $\alpha(\nu)$ can be established. The leading term satisfies the implicit relation:

$$\frac{\rho \cos\alpha_0(1 - 3\sin^2\alpha_0)}{\sin\alpha_0(\sigma_1 + 3\rho\cos^2\alpha_0)} = \frac{\Psi_0(\nu)}{1 + \Phi_0(\nu)} \;. \qquad \text{.....(6.11)}$$

A good approximation to the solution of Equation (6.11) may be obtained by

successive substitution with a starting value $\alpha_0^{(1)}(\nu) = 35.26°$, (i.e., the solution of Equation (18) for an initially circular orbit). The $(n + 1)$th approximation is obtained from $\alpha_0^{(n)}(\nu)$ as follows:

$$\alpha_0^{(n+1)}(\nu) = \arcsin\left[\{1/3 - \Psi_0 \tan\alpha_0^{(n)}\,[(\sigma_1/3\rho) + \cos^2\alpha_0^{(n)}]/(1 + \Phi_0)\}^{1/2}\right], \quad .....(6.12)$$

$n = 1,2,3,...$, which converges rapidly provided that the initial eccentricity is not too large. Geometrically, the steering angle $\alpha_0(\nu)$ in Equation (6.11) makes the resulting solar radiation force aligned with the velocity vector of the unperturbed initial osculating ellipse at each instant.

Whereas this may serve as a useful guide for very small values of ε_s, it is evident that higher-order terms relating to the slowly varying geometry of the osculating ellipse must be evaluated when practical values of ε_s are taken. For the analytical evaluation of the higher-order terms, an explicit relation for $\alpha_0(\nu)$ would be needed. In the special case when the reflection is specular ($\rho = 1$, $\sigma_1 = 0$), a closed-form result for $\alpha_0(\nu)$ can be derived from Equation (6.11),

$$\alpha_0(\nu) = \frac{1}{2}\arcsin\left[\frac{(1 + \Phi_0)\{[9\,\Psi_0^2 + 8(1 + \Phi_0)^2]^{1/2} - \Psi_0\}}{3[\Psi_0^2 + (1 + \Phi_0)^2]}\right]. \quad .....(6.13)$$

On expanding both sides of Equation (6.8) as a Taylor series in terms of the small parameter ε_s, the first-order term $\alpha_1(\nu)$ now becomes ,

$$\alpha_1(\nu) = -\frac{3}{2}\frac{\sin^2(2\alpha_0)}{[3-\cos(2\alpha_0)]}\left\{\Psi^{(1)} + \ell_{00}\,\lambda_3^{(1)}/2 - \Psi_0\,\ell_{00}[\lambda_1^{(1)} + \Psi_0\,\lambda_3^{(1)}/2]/(1+\Phi_0)^2 - \ell_{00}\,\Psi_0\,\lambda_2^{(1)}/(1+\Phi_0)\right\}, \quad \ldots\ldots(6.14)$$

where the superscript (1) denotes the coefficient of ε_s in the expressions in Equations (6.9) . The trigonometric terms in Equation (6.14) can be eliminated in favor of the orbital variables Φ_0 and Ψ_0 through Equation (6.13). Also the integrands in Equations (6.9) can be expanded for small ε_s and expressed in terms of ν. Whereas the resulting integrals are unwieldy for arbitrary eccentricity, analytical results can be obtained for near-circular orbits. Thereto, expansions of the trigonometric terms for small e_{00} are needed. These can be derived using the expansion of Equation (6.13) for small e_{00} and developing $R(\alpha)$ and $S(\alpha)$ around $\alpha = \alpha_0$. With these results, all integrands in Equations (6.9) can be evaluated and near-circular approximations for $\Psi^{(1)}$, $\lambda_3^{(1)}$, etc., in Equation (6.14) are obtained by integration. Finally, the following expression for $\alpha_1(\nu)$ with an error of the order e_{00}^3 is established:

$$\begin{aligned}\alpha_1(\nu) = {} & -3^{-3/2}\{1 - \cos\nu + 3\pi q/2 + (4\pi - 3\nu/2)\Psi_0 - (p+\Phi_0)\cos\nu \\ & + 2p - 3q/2\sin\nu - 9(2^{-3/2})\,\Psi_0\,(1-\cos\nu)\} \\ & - \nu\{7(3^{1/2})\,(p^2-q^2)\sin(2\nu) - 2(6^{1/2})\,e^2\} \\ & - \pi\{4(6^{1/2})\,e^2 + 3^{3/2}\,pq\}/18 \\ & - \sin(2\nu)\{(p^2-q^2)[6^{1/2} - 4(3^{3/2})\pi] - pq/2\}/18 \\ & - [1-\cos(2\nu)]\{(p^2-q^2)\,(3^{-1/2}+1/4) + 2(6^{1/2})pq\}/18\end{aligned}$$

$$- (1 - \cos\nu)\{(p^2 - q^2)[2(3^{-1/2} - 1/4 + 4\sin(2\nu)] - 3e^2/4$$

$$- (3^{3/2})\pi pq\}/18$$

$$- \sin\nu\{pq - 3^{3/2}(2p^2 + q^2)\pi + 3^{1/2}[4pq\cos\nu + (q^2 - 3p^2)\sin\nu]$$

$$- 4(3^{1/2})(p^2 - q^2)\sin(2\nu) + 6^{1/2}[e^2 - (p^2 - q^2)\cos(2\nu)$$

$$- 2pq\sin(2\nu)]\}/18$$

$$- 6^{1/2}\{3\pi q\Psi_0 + (8\pi - 3\nu)\Psi_0^2 - 2(p + \Phi_0)\Psi_0\cos\nu + 4p\Psi_0 - 3q\Psi_0\sin\nu$$

$$- \Psi_0[2\Phi_0 + 3(2^{-1/2})\Psi_0](1 - \cos\nu)\}/144 + O(e_{00}^3) \quad .....(6.15)$$

Here the subscripts 00 are omitted for brevity. It follows that the first-order correction $\varepsilon_s\alpha_1(\nu)$ for an initially circular orbit is at most $22\varepsilon_s$ degrees (at $\nu = \pi$) below the constant $\alpha_0 = 35.26°$ control program. It is interesting to evaluate the response of the major axis under the optimal control strategy. For a near-circular orbit, $a(\nu)$ can be written as

$$a(\nu) = a_{00}\exp\{2\varepsilon_s(1 + e_{00}^2)[2(3^{-3/2})(\nu + p_{00}\sin\nu + q_{00} - q_{00}\cos\nu)$$

$$+ 2(6^{1/2})(p_{00} - p_{00}\cos\nu - q_{00}\sin\nu)/9 + e_{00}^2\nu/2$$

$$+ (q_{00}^2 - p_{00}^2)\sin(2\nu)/4 + p_{00}q_{00}\cos(2\nu) - p_{00}q_{00}$$

$$+ O(e_{00}^3)] + O(\varepsilon_s^2)\} \quad .....(6.16)$$

If $e_{00} = 0$ this result can be reduced considerably yielding $a(2\pi) = a_{00}\exp[4.8368\ \varepsilon_s + O(\varepsilon_s^2)]$ after one revolution.

6.4 Maximization of Angular Momentum

Here, the optimal control strategy for maximum increase in angular momentum (and thus semi-latus rectum) per revolution is determined. This corresponds with maximization of $\hat{\ell}(2\pi)$. The system of Equations (6.3) remains valid provided that the equations for $\hat{a}$ and λ_0 are ignored and the equation for λ_1 is replaced by $\lambda_1'(\nu) = 0$. Now the Hamiltonian becomes

$$H_\ell(\underline{\alpha}) = \lambda_3 \Phi - \lambda_2 \Psi + \varepsilon_s \lambda_3 R(\underline{\alpha}) + \varepsilon_s S(\underline{\alpha})\{(2\lambda_1 + \lambda_3\Psi)/(1 + \Phi) + 2\lambda_2\}. \quad .....(6.17)$$

Application of Pontryagin's maximum principle leads to results as in Equations (6.5) with $\lambda_1 = 1$ now. It follows that $H_\ell = \hat{\ell}'(2\pi)$ and the out-of-plane rotation $\beta(\nu) = 0$ while the optimal control angle $\alpha(\nu)$ is given by the implicit relation,

$$\frac{\rho \cos\alpha\,(1 - 3\sin^2\alpha)}{\sin\alpha\,(\sigma_1 + 3\rho\cos^2\alpha)} = \frac{\lambda_3\,(1 + \Phi)}{2 + \lambda_3\,\Psi + 2\,\lambda_2\,(1 + \Phi)} \quad . \quad .....(6.18)$$

The orbital elements ℓ, Φ and Ψ can be written in the form of Equations (6.9) while the adjoint variables $\lambda_2(\nu)$ and $\lambda_3(\nu)$ become

$$\lambda_2(\nu) = \varepsilon_s \int_\nu^{2\pi} \{Q_\ell \sin(\tau - \nu) + P_\ell \cos(\tau - \nu)\}\, d\tau\,,$$

$$\lambda_3(\nu) = \varepsilon_s \int_\nu^{2\pi} \{Q_\ell \cos(\tau - \nu) - P_\ell \sin(\tau - \nu)\}\, d\tau\,, \quad .....(6.19)$$

with P_ℓ and Q_ℓ defined by

$$P_\ell = -S(2 + \lambda_3 \Psi)/(1 + \Phi)^2 ,$$

$$Q_\ell = \lambda_3 S/(1 + \Phi) . \qquad \text{.....(6.20)}$$

The right-hand-side of Equations (6.18) is of the order ε_s so that $\alpha(\nu)$ is written as $\alpha(\nu) = \alpha_0 + \varepsilon_s \alpha_1 + O(\varepsilon_s^2)$ with $\alpha_0 = \arcsin(3^{-1/2}) = 35.26°$. The first-order term $\alpha_1(\nu)$ is determined by expanding both sides of Equations (6.18) in Taylor series for small ε_s yielding the following explicit result,

$$\alpha_1(\nu) = -(\sigma_1 + 2\rho)\, 3^{-3/2}/2\, [1 + \Phi_0(\nu)] \left[2\, \Psi_0(\nu) * \right.$$

$$* \left\{ \pi - \arctan\left[\frac{(1 - e_{00}^2)^{1/2} \tan(\nu/2)}{1 + p_{00} + q_{00}\tan(\nu/2)} \right] \right\} /(1 - e_{00}^2)^{1/2}$$

$$\left. + 1 - [\Phi_0(\nu) + \cos\nu]/(1 + p_{00}) \right] /(1 - e_{00}^2) . \qquad \text{.....(6.21)}$$

The resulting response $\ell(\nu)$ under the optimal sail setting can be approximated by integrating $\hat{\ell}'(\nu)$ in Equations (6.3) (up to order ε_s),

$$\ell(\nu) = \ell_{00} \exp\left[8\varepsilon_s \rho\, 3^{-3/2} \arctan\left[\frac{(1 - e_{00})^{1/2} \tan(\nu/2)}{1 + p_{00} + q_{00}\tan(\nu/2)} \right] /(1 - e_{00}^2)^{1/2} \right] .$$

$$\text{.....(6.22)}$$

Considering an initially circular orbit, it follows that $\ell(2\pi) = \exp[4.8368\, \rho\varepsilon_s + O(\varepsilon_s^2)]$. This result is identical to the one found in the previous section while maximizing the semi-major axis for a near-circular starting orbit. Obviously, the control programs in Equations (6.15) and (6.21) are also identical for $e_{00} = 0$ in the present approximation.

6.5 Discussion of Results

The accuracy of the analytical solution obtained in Section 6.3 is now assessed by comparison with results from a numerical iteration procedure based upon the steepest-ascent method[119]. An arbitrary nominal control strategy is selected and the influence of a small variation in that control program upon the response is investigated. The variation leading to the maximum increase in major axis under a prescribed step-length (i.e., the integral from 0 to 2π of the square of the variation in the control function) can be determined in terms of the derivatives of the system of Equations (6.3) with respect to the control angle. Thus, a generally more effective new control strategy is obtained and the procedure is repeated. While the algorithm converges rapidly to a near-optimal control strategy, care must be taken in the neighborhood of the optimum due to the weakness of the gradient field. By making both the step-size and the error parameter in the Runge-Kutta integration routine proportional to the length of the gradient, satisfactory results are obtained. In the present case, the initial control program is taken as $\alpha(\nu) = (2\pi - \nu)/6$ and the optimal strategy is established to within, approximately, 0.1 degree in less than 30 iterations, Figure 6-1. A relatively small value of the solar parameter (based on $A/m = 10\ m^2/kg$) is taken in this example. The first-order analytical result of Equation (6.15) for a near-circular initial orbit in conjunction with the exact zeroth-order term in Equation (6.13) yields an extremely close approximation when $e_{00} = 0.2$ (Figure 6-1a): the maximum discrepancy is less than 0.1 degree. On the other hand, if $e_{00} = 0.4$ (Figure 6-1b), the near-circular analytical solution is in error by almost three degrees around $\nu = 270°$, while still providing a valid representa-

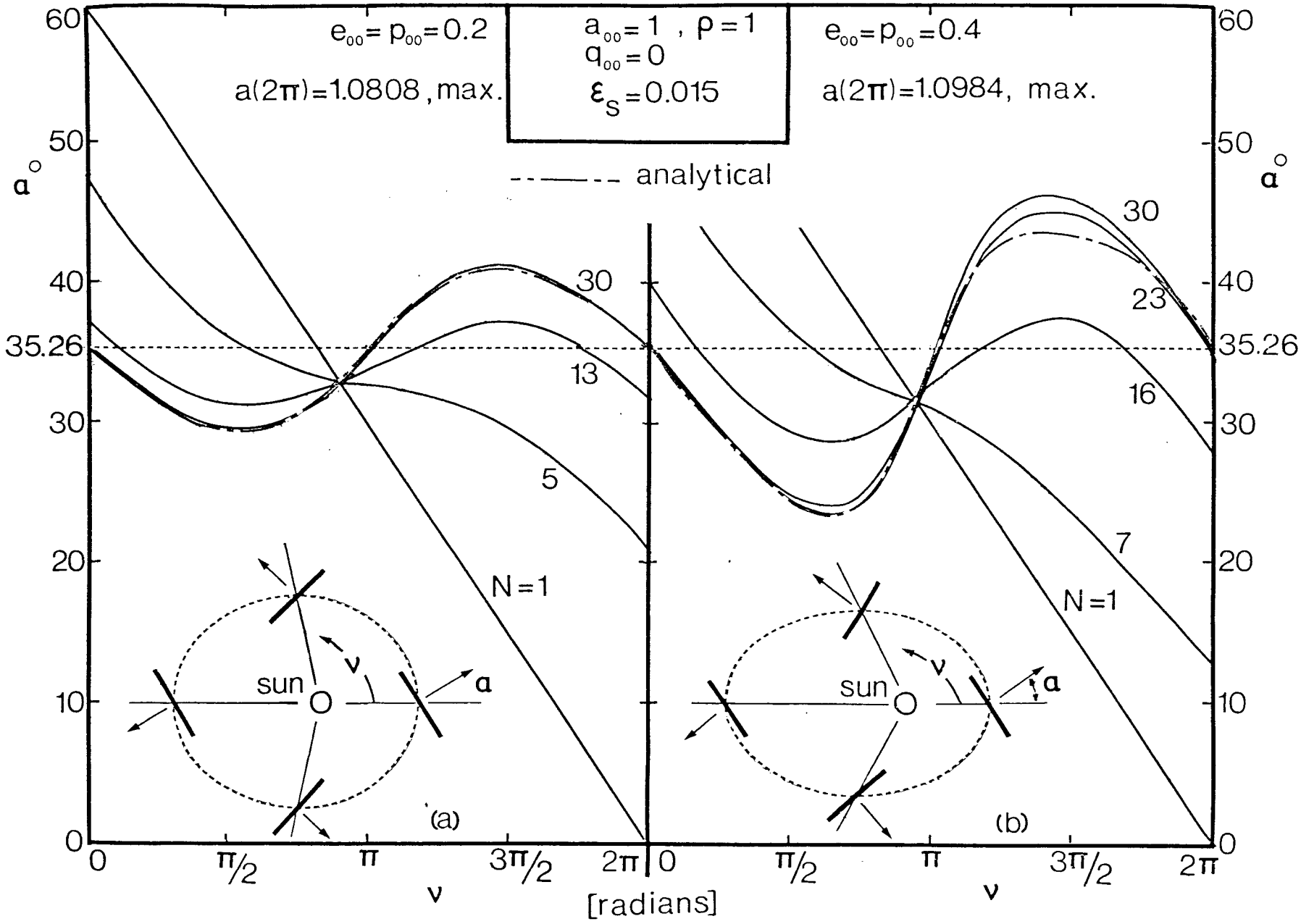

Figure 6-1 Comparison of analytical and numerical optimal controls for $\varepsilon_s = 0.015$:
(a) $e_{00} = 0.2$; (b) $e_{00} = 0.4$

tion for the optimal strategy in the remaining portion of the orbit. The breakdown in accuracy must be attributed to two reasons: first, it should be recognized that the first-order analytical result developed here does not contain terms of order e_{00}^3 and higher which are likely to be influential when the eccentricity is as high as 0.4. Secondly, the state and adjoint variables are represented as perturbation series in terms of ε_s and only the first-order solutions are taken into account leading to a rapidly growing error when away from the initial and final points.

Figure 6-2 shows the results for a higher value of ε_s, namely $\varepsilon_s = 0.09$, corresponding to $A/m = 60\ m^2/kg$. As can be expected, the analytical prediction for the optimal control is most accurate in the case $e_{00} = 0$; the maximum discrepancy of about one degree is due to higher-order (in ε_s) effects. It is interesting to note that initially the solar radiation force points slightly inwards from the velocity vector and its magnitude is smaller than that for the case where the force is aligned with the velocity. This is true for both the numerical and the first-order analytical results, although the effect is less pronounced in the latter case. This apparent waste of energy is more than recouped during the middle phase of the orbit when the spacecraft is closer to the sun and the force is larger. In this phase, the direction of the force is kept outward from the velocity vector, thus providing an additional boost to its magnitude. In the final phase the force tends to align itself with the velocity. The osculating ellipses corresponding to the resulting trajectory show that the eccentricity increases from 0 to a maximum of about 0.2 near $\nu = 190°$ and decreases to about 0.02 with the position of the perigee at about 70° in the end, $\nu = 2\pi$. The analytical result for $e_{00} = 0.2$ shows a maxi-

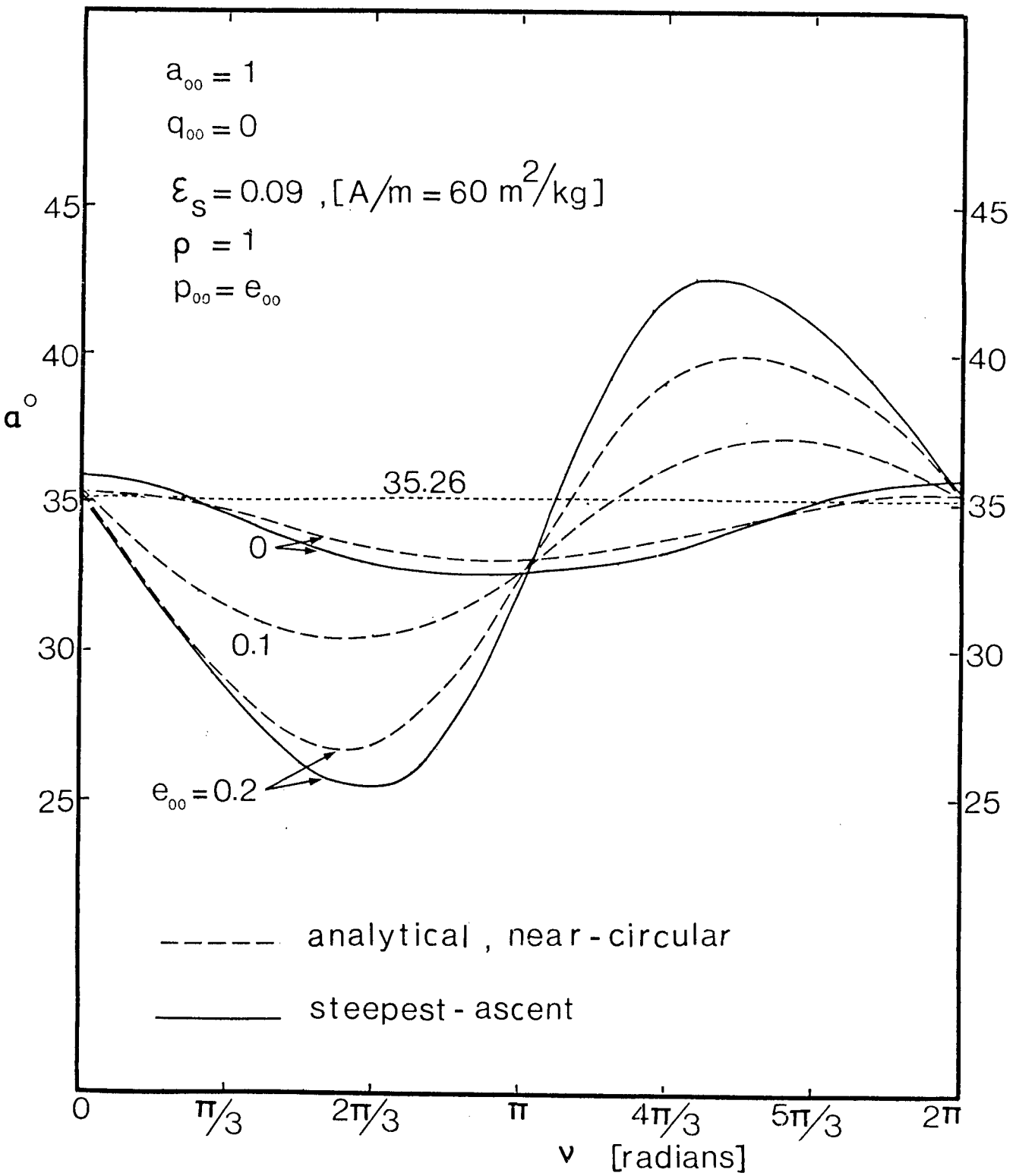

Figure 6-2 Optimal sail setting for $\varepsilon_s = 0.09$, $\omega_{00} = 0$ and a few values of e_{00}

mum error of about 2.5 degrees as compared to the steepest-ascent solution. Figure 6-3 shows the optimal steering programs for three different starting points in the same initial orbit of eccentricity $e_{00} = 0.2$ ($\varepsilon_s = 0.15$), obtained by the steepest-ascent iteration routine. It is seen that the nature of the control strategy as well as the resulting final value $a(2\pi)$ vary considerably with the position of the starting point.

It is interesting to compare the effectiveness of the optimal strategies with that of other near-optimal control programs, in particular the constant sail setting $\alpha = \arcsin(3^{-1/2}) = 35.26°$. The latter control is expected to be a very effective strategy for small ε_s and small e_{00} since it generates the maximum component of the force along the velocity for an unperturbed circular orbit. Table 6.1 gives a comparative overview of the response $a(2\pi)$ for a few values of ε_s and e_{00} (ω_{00} is taken zero).

Table 6.1 Response $a(2\pi)$ for Optimal Control Strategy and for $\alpha = \arcsin(3^{-1/2})$

e_{00} \ ε_s	0.015	0.09	0.15
0	1.0761*	1.590	2.280
	1.0760	1.587	2.258
0.2	1.0808	1.668	2.608
	1.0796	1.640	2.454
0.4	1.0984	1.962	4.314
	1.0922	1.819	3.202

*The upper values correspond to the optimal response while the lower ones represent the results for $\alpha = 35.26°$.

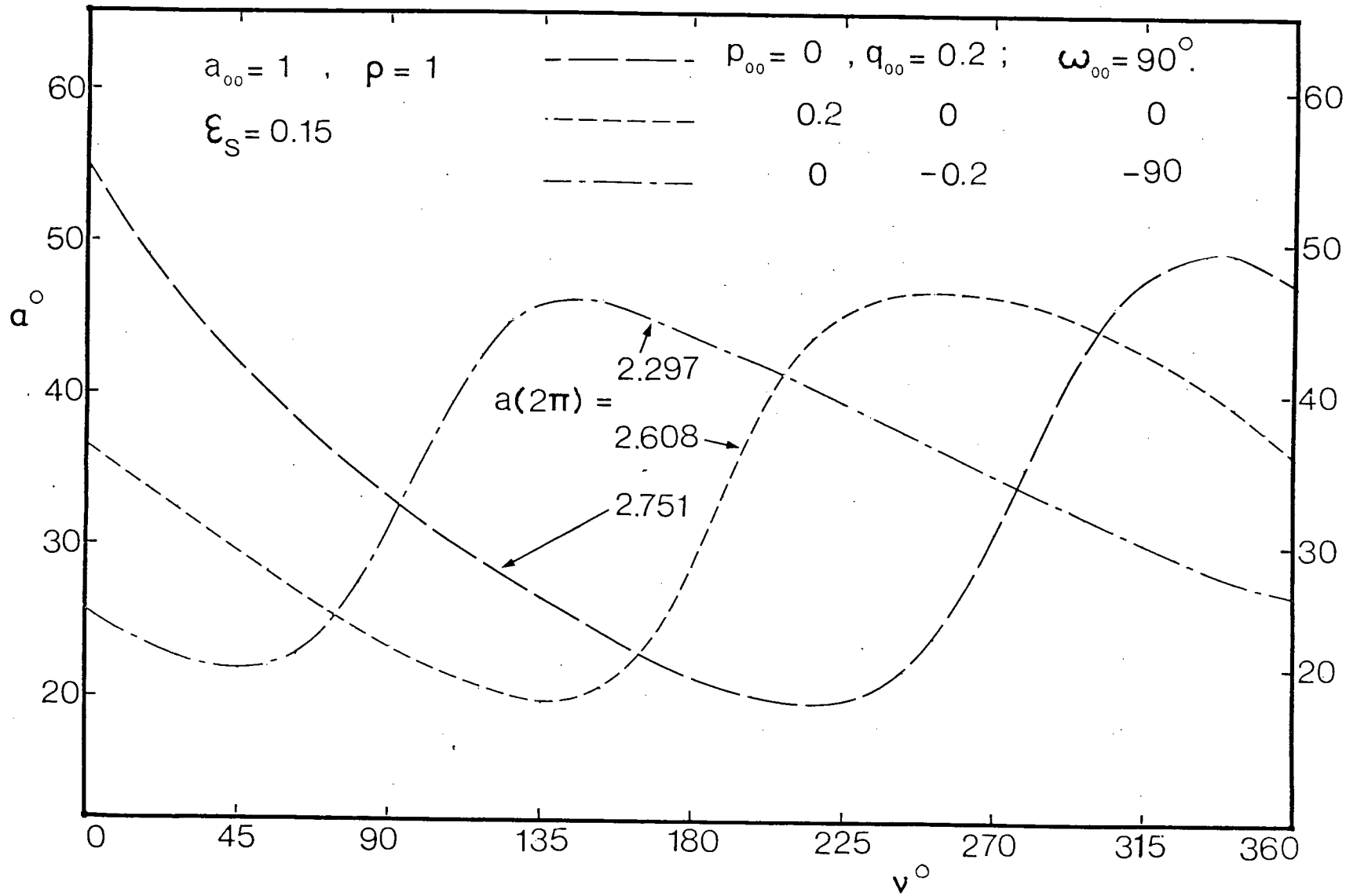

Figure 6-3 Optimal control programs for $\varepsilon_s = 0.15$, $e_{00} = 0.2$ and a few values of ω_{00}

Although the results seem to be close in most cases, it must be emphasized that a difference of one digit in the fourth decimal place represents a physical distance of about 15,000 km. On the other hand, it is evident that $\alpha(\nu) = 35.26°$ is a very effective control strategy even for eccentricities as high as 0.4. It should be mentioned that the results in Table 6.1 are derived numerically, since the analytical prediction for the response under the optimal control, Equation (6.16), yields useful values for $a(2\pi)$ only for small ε_s and e_{00} and is not capable of providing accuracy beyond three significant digits in the most favorable case, while being in error by as much as 0.3 in the most severe situation of Table 6.1.

The actual trajectory resulting from the optimal strategy for $\varepsilon_s = 0.09$ is depicted in Figure 6-4. It is seen that Mars' orbit is intercepted at about $\nu = 135°$ after approximately one year. Also the inward trajectory crossing Venus' orbit is shown. These trajectories are obtained from the steepest-ascent results. It may be mentioned that the leading term in the analytical solution of the optimal strategy for inward trajectories is equal to but opposite in sign compared to the one for the outward ones. The first-order (in ε_s) terms, however, are different and can be readily evaluated by taking $\lambda_0 = -1$ rather than $+1$. These conclusions are substantiated by the numerical results.

Finally, the optimal sail settings leading to the maximum increase in angular momentum for a few values of initial eccentricity and solar parameter are shown in Figure 6-5. The approximate analytical solution for the present case is likely to be more accurate than the ones presented before (Section 6.4) due to the fact that $\alpha_1(\nu)$ is obtained for general e_{00},

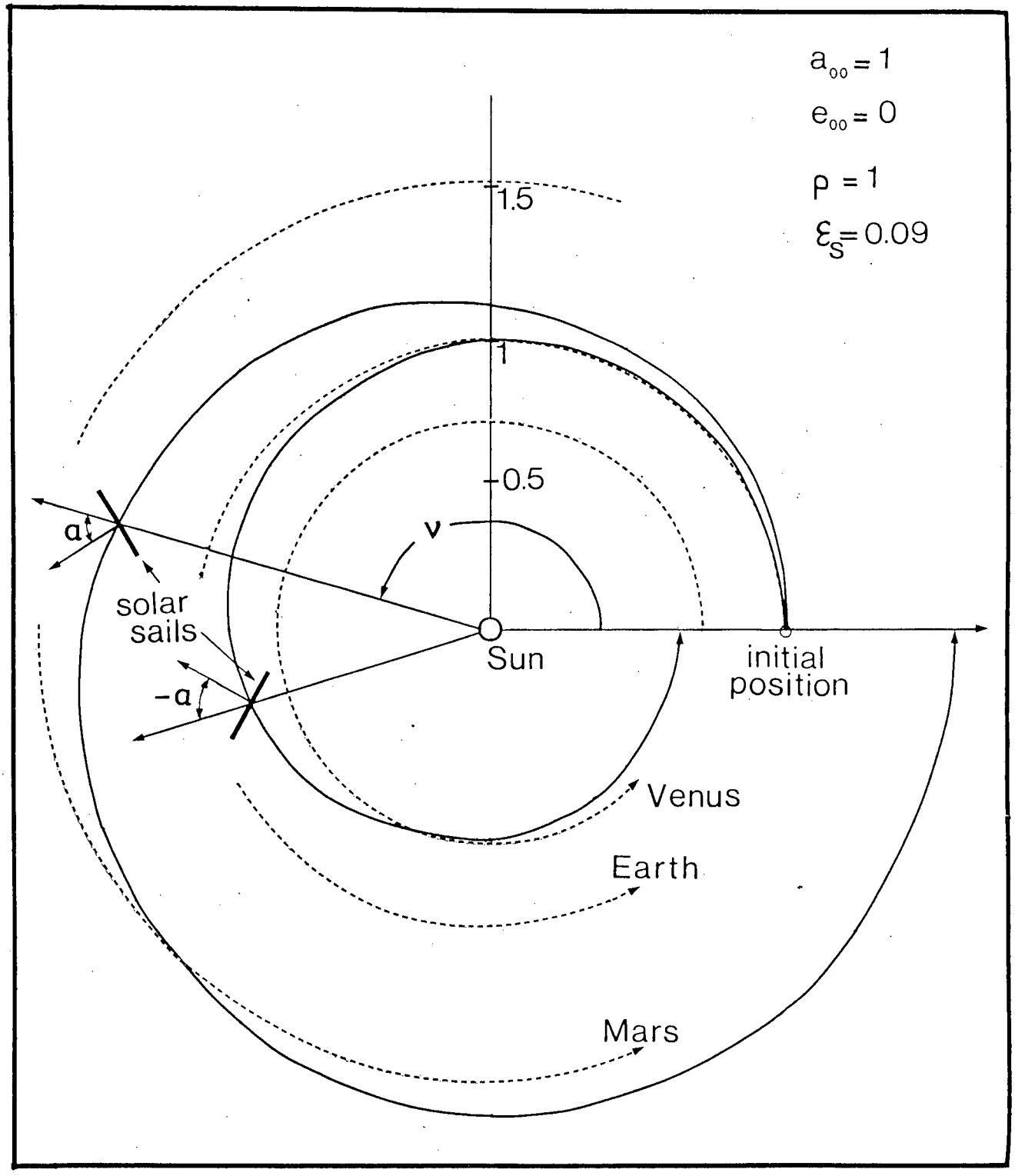

Figure 6-4 Actual trajectory under optimal sail setting showing interception with Mars' and Venus' orbits

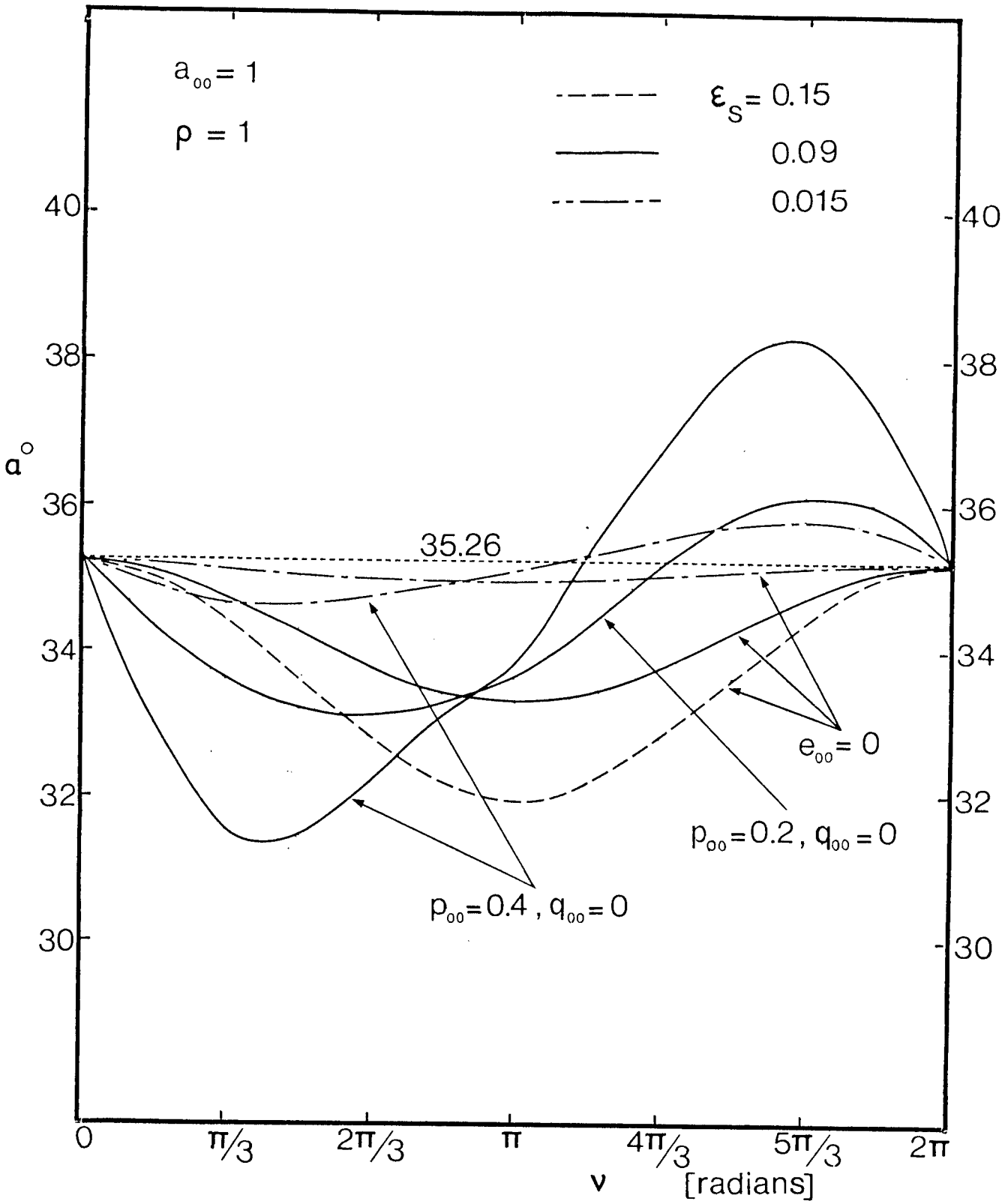

Figure 6-5 Control strategies for maximization of angular momentum

Equation (6.21), leaving only the errors caused by higher-order (in ε_s) terms. It may be noted that the resulting optimal control for $e_{00} = 0$ corresponds identically (up to first-order) to the one which maximizes $a(2\pi)$, Figure 6-2. Compared to the optimal strategy for maximization of $a(2\pi)$, the present control programs are closer to the 35.26° line, representing the zeroth-order approximation of the optimal control for circular as well as elliptic orbits.

6.6 Concluding Remarks

Important aspects of the analysis and conclusions based on them can be summarized as follows:

(i) Analytical approximate solutions for the time-dependent optimal sail setting maximizing the total energy (major axis) or the angular momentum (latus rectum) after one revolution are obtained from Pontryagin's maximum principle by means of a straightforward perturbation expansion of the state and adjoint variables.

(ii) The validity of the approximate solution is assessed by means of a numerical iteration procedure based upon the steepest-ascent method. In general, the accuracy of the analytical solution decreases with increasing ε_s and eccentricity. For values of ε_s as high as 0.1 and e up to 0.2, the maximum deviation in control angle is less than 3° (which is comparable to the expected error in manoevring the sail).

(iii) It is found that the optimal strategy as well as the response may vary considerably depending on the starting point in the orbit.

(iv) Effectiveness of the optimal sail setting is compared with that of a near-optimal constant sail orientation showing a growing divergence in responses for increasing values of ε_s and e_{00}.

(v) The optimal steering program for maximizing angular momentum stays relatively close to the 35.26° line and coincides with the optimal sail setting for maximizing $a(2\pi)$ (in first-order) when $e_{00} = 0$.

(vi) The optimal control strategies developed here should prove useful in planning missions by solar sail to the distant planets and for reaching an escape trajectory from the solar system.

7. CLOSING COMMENTS

7.1 Summary of Conclusions

The main objective of the study, to gain insight into the long-term evolution of satellite orbits under the influence of a realistically modelled solar radiation force as well as exploring possible control strategies for desired orbital change, is accomplished in some measure. The important aspects and conclusions of the thesis may be summarized as follows:

i) The long-term orbital perturbations of satellites modelled as a plate normal to the incident radiation are determined using the two-variable expansion procedure and rectification/iteration of the short-term results. The in-plane orbital changes are easily visualized through polar plots for the eccentricity vector. The long-term periodic variations in the inclination of the orbital plane are explained in terms of the in-plane perturbations, while the line of nodes regresses in a slow secular manner.

ii) Analytical representations for the short-term behavior of arbitrarily shaped space structures pointing in a fixed direction with respect to inertial space or those kept in an arbitrary fixed orientation to the solar radiation are obtained. Subsequently, long-term results are obtained by rectification and iteration. Also the perturbations of a satellite modelled as a plate in an arbitrary orientation to the local reference frame with different material properties on both sides are analysed.

iii) A few on-off switching strategies are proposed and their effectiveness in changing orbital parameters is explored. While substantial changes in the major axis can be achieved in this manner, the time-dependent optimal control strategy for maximization of total energy is derived by means of a numerical iteration scheme based on the steepest-ascent method. This result should be of interest for raising a solar sail from a geocentric into a heliocentric or escape trajectory.

iv) A detailed investigation of the long-term evolution of heliocentric trajectories for arbitrary fixed sail setting is presented which should be useful for evaluating possible solar sail missions depending on sail parameters and initial conditions. For specific initial conditions, exact three-dimensional solutions in the from of spirals and conic sections are established, while an effective near-circular out-of-plane spiral transfer trajectory is obtained by switching at appropriate locations.

v) Optimal time-dependent steering angles for maximization of total energy and angular momentum are determined both by an approximate analytical perturbation method and the numerical steepest-ascent procedure. The results are of interest for designing solar sail missions with the objective to rendezvous with a distant planet or to escape from the planetary system.

7.2 Recommendations for Future Work

While the thesis may provide an overview of the various aspects of solar radiation effects upon satellite orbits, it is by no means exhaustive and

numerous options for future work are available. An obvious extension may concern the derivation of an analytical prediction for the orbital behavior of an arbitrarily shaped space structure of general material characteristics under a suitable control strategy. An interesting manner to describe a time-dependent control would be by means of a Fourier series. The main difficulty would lie in keeping track of the continuously changing number of illuminated surface components. Conversely, after the analysis has shown its practical usefulness, it might be possible to derive conclusions as to the long-term degradation of reflecting properties of surface materials by carefully studying the orbital behavior of the spacecraft.

Various possibilities exist for extending the analysis on control strategies using solar radiation forces. For instance, the control strategy developed here for optimal orbit raising might be extended to allow for constraints on the final state and/or for a second component of the control vector. Convergence problems are expected near the optimum and a proper combination of step-size and weighting function needs to be developed for each case. Also other optimization criteria could be investigated, e.g. minimum-time transfer problems, for which a formulation in terms of radius and velocity vectors would likely be more expedient than the present one in orbital elements. As to heliocentric solar sail orbits, many topics are still open for study. Especially a generalization of the spiral out-of-plane transfer trajectory to arbitrary initial and final conditions would be of interest.

BIBLIOGRAPHY

1. Musen, P., Bryant, R., and Bailie, A., "Perturbations in Perigee Height of Vanguard I," Science, Vol. 131, No. 3404, 25 March 1960, pp. 935-936.

2. Musen, P., "The Influence of Solar Radiation Pressure on the Motion of an Artificial Satellite," Journal of Geophysical Research, Vol. 65, No. 5, May 1960, pp. 1391-1396.

3. Parkinson, R.W., Jones, H.M., and Shapiro, I.I., "Effects of Solar Radiation Pressure on Earth Satellite Orbits," Science, Vol. 131, No. 3404, 25 March 1960 pp. 920-921.

4. Shapiro, I.I., and Jones, H.M., "Perturbations of the Orbit of the Echo Balloon," Science, Vol. 132, No. 3438, 18 November 1960, pp. 1484-1486.

5. Jastrow, R., and Bryant, R., "Variations in the Orbit of the Echo Satellite," Journal of Geophysical Research, Vol. 65, No. 10, October 1960, pp. 3512-3513.

6. Shapiro,I.I., and Jones, H.M., "Loss of Mass in Echo Satellite," Science, Vol. 133, No. 3452, 24 February 1961, p. 579.

7. Jones, H.M., Shapiro, I.I., and Zadunaisky, P.E., "Solar Radiation Pressure Effects, Gas Leakage Rates, and Air Densities Inferred from the Orbit of Echo I," Space Research II, Edited by: Van de Hulst, H.C., De Jager, C., and Moore, A.F., North-Holland Publishing Company, Amsterdam, 1961, pp. 339-351.

8. Bryant, R., "A Comparison of Theory and Observation of the Echo I Satellite," Journal of Geophysical Research, Vol. 66, No. 9, September 1961, pp. 3066-3069.

9. Shapiro, I.I., and Jones, H.M., "Lifetimes of Orbiting Dipoles," Science, Vol. 134, No. 3484, 6 October 1961, pp. 973-979.

10. Allan, R.R., "Satellite Orbit Perturbations Due to Radiation Pressure and Luni-Solar Forces," Quarterly Journal of Mechanics and Applied Mathematics, Vol. 15, Pt. 3, Summer 1962, pp. 283-301.

11. Kozai, Y. "Effects of Solar-Radiation Pressure on the Motion of an Artificial Satellite," Smithsonian Contributions to Astrophysics, Vol. 6: Research in Space Science, Smithsonian Institute, Washington, D.C., 1963, pp. 109-112.

12. Bryant, R.W., "The Effect of Solar Radiation Pressure on the Motion of an Artificial Satellite," Astronomical Journal, Vol. 66, No. 8, October 1961, pp. 430-432.

13. Wyatt, S.P., "The Effect of Radiation Pressure on the Secular Acceleration of Satellites," Smithsonian Contributions to Astrophysics, Vol. 6: Research in Space Science, Smithsonian Institute, Washington, D.C., 1963, pp. 113-123.

14. Koskela, P.E., "Orbital Effects of Solar Radiation Pressure on an Earth Satellite," Journal of the Astronautical Sciences, Vol. 9, Fall 1962, pp. 71-82.

15. Cook, G.E., and Hughes, J.M., "The Orbits of Needle Satellites," Planetary and Space Sciences, Vol. 9, No. 4, April 1962, pp. 153-166.

16. Cook, G.E., "The Use of Simplified Orbital Theory for Satellites of Large Area to Mass Ratio," Planetary and Space Sciences, Vol. 11, No. 11, November 1963, pp. 1289-1295.

17. Wyatt, S.P., "The Effect of Terrestrial Radiation Pressure on Satellite Orbits," Dynamics of Satellites, Edited by: Roy, M., Springer-Verlag, Berlin, 1963, pp. 180-196.

18. Baker, Jr., R.M.L., "Radiation on a Satellite in the Presence of Partly Diffuse and Partly Specular Reflecting Body," Trajectories of Artificial Celestial Bodies, Edited by: Kovalevsky, J., Springer-Verlag, Berlin, 1970, pp. 85-150.

19. Shapiro, I.I., "The Prediction of Satellite Orbits," Dynamics of Satellites, Edited by: Roy, M., Springer-Verlag, Berlin, 1963, pp. 257-312.

20. Polyakhova, Ye.N., "Solar Radiation Pressure and the Motion of Earth Satellites," AIAA Journal, Vol. 1, No. 12, December 1963, pp. 2893-2909.

21. Brouwer, D., "Analytical Study of Resonance Caused by Solar Radiation Pressure," Dynamics of Satellites, Edited by: Roy, M., Springer-Verlag, Berlin, 1963, pp. 34-39.

22. Hori, G., "The Effect of Radiation Pressure on the Motion of an Artificial Satellite," Lectures in Applied Mathematics, Edited by: Rosser, J.B., American Mathematical Society, Providence, Vol. 7, Pt. 3, 1966, pp. 167-178.

23. Lubowe, A.G., "Orbital Behavior of Large Synchronous Satellites," Astronautica Acta, Vol. 13, No. 1, January-February 1967, pp. 49-61.

24. Levin, E., "Solar Radiation Pressure Perturbations of Earth Satellite Orbits," AIAA Journal, Vol. 6, No. 1, January 1968, pp. 120-126.

25. Zee, C.H., "Effects of the Sun and the Moon on a Near-Equatorial Synchronous Satellite," Astronautica Acta, Vol. 17, No. 6, December 1972, pp. 891-906.

26. Zee, C.H., "Effect of the Sun, the Moon and Solar Radiation Pressure on a Near-Equatorial Synchronous Satellite," Astronautica Acta, Vol. 18, No. 4, October 1973, pp. 281-287.

27. Lidov, M.L., "Secular Effects in the Evolution of Orbits under the Influence of Radiation Pressure," Cosmic Research, Vol. 7, No. 4, July-August 1969, pp. 423-438.

28. Isayev, Y.N., and Kunitsyn, A.L., "To the Problem of Satellites Perturbed Motion under the Influence of Solar Radiation Pressure," Celestial Mechanics, Vol. 6, No. 1, September 1972, pp. 44-51.

29. Isayev, Y.N., and Prokof'ev, A.I., "Secular Evolution of the Orbit of a Balloon Satellite," Cosmic Research, Vol. 13, No. 2, March-April 1975, pp. 162-166.

30. Aksnes, K. "Short-Period and Long-Period Perturbations of a Spherical Satellite Due to Direct Solar Radiation," Celestial Mechanics, Vol. 13, No. 1, February 1976, pp. 89-104.

31. Sehnal, L., "Radiation Pressure Effects in the Motion of Artificial Satellites," Dynamics of Satellites, Edited by: Morando, B., Springer-Verlag, Berlin, 1970, pp. 262-272.

32. Sehnal, L., "Non-Gravitational Forces in Satellite Dynamics," Satellite Dynamics, Edited by: Giacaglia, G.E.O., Springer-Verlag, Berlin, 1975, pp. 304-330.

33. Sehnal, L., "The Perturbations of the Orbital Elements Caused by the Pressure of the Radiation Reflected from the Earth," Dynamics of Satellites, Edited by: Morando, B., Springer-Verlag, Berlin, 1970, pp. 80-84.

34. Prior, E.J., "Earth Albedo Effects on the Orbital Variations of Echo I and Pageos I," Dynamics of Satellites, Edited by: Morando, B., Springer-Verlag, Berlin, 1970, pp. 303-312.

35. Fea, K., "The Orbital Accelerations of High Balloon Satellites," Dynamics of Satellites, Edited by: Morando, B., Springer-Verlag, Berlin, 1970, pp. 295-302.

36. Gambis, D., "On the Effect of Earth Radiation Pressure in the Motion of Pageos: Comparisons Between Different Models," Satellite Dynamics, Edited by: Giacaglia, G.E.O., Springer-Verlag, Berlin, 1975, pp. 370-375.

37. Smith, D.E., and Kissell, K.E., "Anomalous Orbital Accelerations of the Pageos Spacecraft," Space Research XII, Vol. I, Edited by: Bowhill, S.A., Jaffe, L.O., and Rycroft, M.J., Akademie-Verlag, Berlin, 1972, pp. 1523-1527.

38. Patterson, W.B., and Kissell, K.E., "Comparison of the Theoretical Solar Radiation Effects and the Observed Accelerations of the Pageos Satellite," Journal of Spacecraft and Rockets, Vol. 12, No. 9, September 1975, pp. 539-543.

39. Georgevic, R.M., "The Solar Radiation Pressure on the Mariner 9 Mars Orbiter," Astronautica Acta, Vol. 18, No. 2, April 1973, pp. 109-115.

40. Escobal, P.R., "Orbital Entrance and Exit from the Shadow of the Earth," ARS Journal, Vol. 32, No. 12, December 1962, pp. 1939-1941.

41. Karymov, A.A., "Determination of the Period of Solar Illumination of an Artificial Earth Satellite," Cosmic Research, Vol. 5, No. 2, May-June 1967, pp. 257-260.

42. Zhurin, B.L., "The Longest Eclipse Time of Earth Satellites," Cosmic Research, Vol. 5, No. 2, May-June 1967, pp. 261-264.

43. Ferraz Mello, S., "Action de la Pression de Radiation sur le Mouvement d'un Satellite Artificiel de la Terre," Proceedings of the 14th International Astronautical Congress of the I.A.F., Paris, 1963, Vol. 4, Edited by: Brun, E., and Hersey, I., Gauthier-Villars, Paris,1965, pp. 41-50.

44. Ferraz Mello, S., "Analytical Study of the Earth's Shadowing Effects on Satellite Orbits," Celestial Mechanics, Vol. 5, No. 1, January 1972, pp. 80-101.

45. Vilhena de Moraes, R., "Solar Radiation Pressure and Balloon Type Artificial Satellites," Satellite Dynamics, Edited by: Giacaglia, G.E.O., Springer-Verlag, Berlin, 1975, pp. 331-341.

46. Lála, P., "Short-Periodic Perturbations of the Satellite Orbits Caused by Solar Radiation Pressure," Bulletin of the Astronomical Institutes of Czechoslovakia, Vol. 19, No. 4, July-August 1968, pp. 233-239.

47. Lála, P., and Sehnal, L., "The Earth's Shadowing Effects in the Short-Periodic Perturbations of Satellite Orbits," Bulletin of the Astronomical Institutes of Czechoslovakia, Vol. 20, No. 6, November-December 1969, pp. 327-330.

48. Lála, P., "Semi-Analytical Theory of Solar Pressure Perturbations of Satellite Orbits During Short Time Intervals," Bulletin of the Astronomical Institutes of Czechoslovakia, Vol. 22, No. 2, March-April 1971, pp. 63-72.

49 Meeus, J., "Note on the Period of the Balloon Satellites," Journal of the British Astronomical Association, Vol. 78, No. 2, February 1968, pp. 108-109.

50. Garwin, R.L., "Solar Sailing - A Practical Method of Propulsion Within the Solar System," Jet Propulsion, Vol. 28, No. 3, March 1958, pp.188-190.

51. Tsu, T.C., "Interplanetary Travel by Solar Sail," ARS Journal, Vol. 29, No. 6, June 1959, pp. 422-427.

52. London, H.S., "Some Exact Solutions of the Equations of Motion of a Solar Sail with Constant Sail Setting," ARS Journal, Vol. 30, No. 2, February 1960, pp. 198-200.

53. Pozzi, A., and De Socio, L., "Some Remarks on Solar Sail," ARS Journal, Vol. 31, No. 8, August 1961, pp. 1164-1165.

54. Kiefer, J.W., "Feasibility Considerations for a Sail-Powered Multi-Mission Solar Probe," Proceedings of the 15th International Astronautical Congress of the I.A.F., Warszawa, 1964, Vol. 1, Editor-in-chief: Lunc, M., Gauthier-Villars, Paris, 1965, pp. 383-416.

55. Modi, V.J., Pande, K.C., and Nicks, G.W., "On the Semi-Passive Propulsion of Space Vehicles Using Solar Radiation Pressure," Proceedings of the 10th International Symposium on Space Technology and Science, Editor-in-chief: Kobayashi, S., AGNE Publishing Company, Tokyo, 1973, pp.375-382.

56. Sands, N., "Escape from Planetary Gravitational Fields by Use of Solar Sails," ARS Journal, Vol. 31, No. 4, April 1961, pp. 527-531.

57. Fimple, W.R., "Generalized Three-Dimensional Trajectory Analysis of Planetary Escape by Solar Sail," ARS Journal, Vol. 32, No. 6, June 1962, pp. 883-887.

58. Cohen, M.J. and Freestone, M.M., "Spiral Trajectories in the Plane of the Ecliptic Using Solar Sails," Proceedings of the 15th International Astronautical Congress of the I.A.F., Warszawa, 1964, Vol. 1, Editor-in-chief: Lunc, M., Gauthier-Villars, Paris, 1965, pp. 363-382.

59. Bosch, H.B., "Effects of Sunlight Pressure on the Motion of an Earth-Orbiting Mirror," Astronautica Acta, Vol. 16, No. 1, January 1971, pp. 37-43.

60. Ahmad, S., and Stuiver, W., "Effects of Solar Radiation on the Orbits of Flat Plates," Astronautica Acta, Vol. 18, Supplement, 1974, pp. 163-170.

61. Shrivastava, S.K., and Rajasingh, C.K., "Optimum Orbital Control Using Solar Radiation Pressure," Journal of Spacecraft and Rockets, Vol. 12, No. 8, August 1975, pp. 502-504.

62. Shrivastava, S.K., Hablani, H.B. and Gopinath, N.S., "SPACTS: Semi-Passive Attitude Control and Trajectory Stabilization System for a Geostationary Satellite," Presented at the 26th International Astronautical Congress of the I.A.F., Lisbon, 21-27 September 1975, Paper No. 75-105.

63. Modi, V.J., Pande, K.C., and Misra, A.K., "Solar Pressure Induced Perturbations of Orbital Elements for the Communications Technology Satellite," Advances in the Astronautical Sciences, Vol. 33, 1976, pp. 3-25.

64. Buckingham, A.G., Lim, Y.C., and Miller, J.A., "Orbit Position Control Using Solar Pressure," Journal of Spacecraft and Rockets, Vol. 2, No. 6, November-December 1965, pp. 863-867.

65. Black, W.L., Crocker, M.C., and Swenson, E.H., "Stationkeeping a 24-Hr Satellite Using Solar Radiation Pressure," Journal of Spacecraft and Rockets, Vol. 5, No. 3, March 1968, pp. 335-337.

66. Perkins, F.M., "Flight Mechanics of Low-Thrust Spacecraft," Journal of the Aero/Space Sciences, Vol. 26, No. 5, May 1959, pp. 291-297.

67. Copeland, J., "Interplanetary Trajectories Under Low Thrust Radial Acceleration," ARS Journal, Vol. 29, No. 4, April 1959, pp. 267-271.

68. Arthur, P.D., Karrenberg, H.K., and Stark, H.M., "Simple Method for Approximating the Characteristics of Low Thrust Trajectories," ARS Journal, Vol. 30, No. 7, July 1960, pp. 649-652.

69. Lass, H. and Lorell, J., "Low Acceleration Take-Off From a Satellite Orbit," ARS Journal, Vol. 31, No. 1, January 1961, pp. 24-28.

70. Rider, L., "Low Thrust Correction of Orbital Orientation," ARS Journal, Vol. 30, No. 7, July 1960, pp. 647-648.

71. Lass, H., and Solloway, C.B., "Motion of a Satellite Under the Influence of a Constant Normal Thrust," ARS Journal, Vol. 32, No. 1, January 1962, pp. 97-100.

72. Zee, C.H., "Low Constant Tangential Thrust Spiral Trajectories," AIAA Journal, Vol. 1, No. 7, July 1963, pp. 1581-1583.

73. Zee, C.H., "Low-Thrust Oscillatory Spiral Trajectory," Astronautica Acta, Vol. 9, Fasc. 3, May-June 1963, pp. 201-207.

74. Bogoliubov, N.N., and Mitropolskii, Y.A., Asymptotic Methods in the Theory of Nonlinear Oscillations, Hindustan Publishing Corporation, Delhi, 1961.

75. Laricheva, V.V., and Rein, M.V., "The Asymptotic Behavior of the Celestial-Mechanics Equations Applicable to Broad-Range Variation in Eccentricity," Cosmic Research, Vol. 3, No. 1, January-February 1965, pp. 21-33.

76. Laricheva, V.V., and Rein, M.V., "A Method for Formulating Solutions to the Celestial-Mechanics Equations of Plane Perturbed Motion," Cosmic Research, Vol. 3, No. 3, May-June 1965, pp. 359-367.

77. Okhotsimskii, D.E., "Investigation of Motion in a Central Field Under the Influence of a Constant Tangential Acceleration," Cosmic Research, Vol. 2, No. 6, November-December 1964, pp. 715-736.

78. Cohen, M.J., "Low-Thrust Spiral Trajectory of a Satellite of Variable Mass," AIAA Journal, Vol. 3, No. 10, October 1965, pp. 1946-1949.

79. Johnson, D.P., and Stumpf, L.W., "Perturbation Solutions for Low-Thrust Rocket Trajectories," AIAA Journal, Vol. 3, No. 10, October 1965, pp. 1934-1936.

80. Ting, L., and Brofman, S., "On Take-Off from Circular Orbit by Small Thrust," Zeitschrift für Angewandte Mathematik und Mechanik, Vol. 44, Heft 10/11, October-November 1964, pp. 417-428.

81. Brofman, W., "Approximate Analytical Solution for Satellite Orbits Subjected to Small Thrust or Drag," AIAA Journal, Vol. 5, No. 6, June 1967, pp. 1121-1128.

82. Nayfeh, A.H., "Take-off From a Circular Orbit by a Small Thrust," Progress in Astronautics and Aeronautics: Methods in Astrodynamics and Celestial Mechanics, Edited by: Duncombe, R.L. and Szebehely, V.G., Academic Press, New York, Vol. 17, 1966, pp. 139-157.

83. Shi, Y.Y., and Eckstein, M.C., "Ascent or Descent from Satellite Orbit by Low Thrust," AIAA Journal, Vol. 4, No. 12, December 1966, pp. 2203-2208.

84. Shi, Y.Y., and Eckstein, M.C., "An Approximate Solution for Ascending Low-Thrust Trajectories without Singularity," AIAA Journal, Vol. 5, No. 1, January 1967, pp. 170-172.

85. Moss, J.B., "Perturbation Techniques and Orbit Expansion by Continuous Low Thrust," Journal of the British Interplanetary Society, Vol. 27, No. 3, March 1974, pp. 213-225.

86. Flandro, G.A., "Analytic Solution for Low Thrust Out of Ecliptic Mission Design," AIAA Journal, Vol. 14, No. 1, January 1976, pp. 33-38.

87. Cole, J.D., and Kevorkian, J., "Uniformly Valid Asymptotic Approximations for Certain Nonlinear Differential Equations," Proceedings of the International Symposium on Non-Linear Differential Equations and Non-Linear Mechanics, Edited by: LaSalle, J.P., and Lefschetz, S., Academic Press, New York, 1963, pp. 113-120.

88. Kevorkian, J., "The Two Variable Expansion Procedure for the Approximate Solution of Certain Nonlinear Differential Equations," Lectures in Applied Mathematics, Edited by: Rosser, J.B., American Mathematical Society, Providence, Vol. 7, Part 3, 1966, pp. 206-275.

89. Morrison, J.A., "Comparison of the Modified Method of Averaging and the Two-Variable Expansion Procedure," SIAM Review, Vol. 8, No. 1, January 1966, pp. 66-85.

90. Perko, L.M., Higher Order Averaging and Related Methods for Perturbed Periodic and Quasi-Periodic Systems," SIAM Journal of Applied Mathematics, Vol. 17, No. 4, July 1968, pp. 698-724.

91. Klimas, A., "On the Compatibility Problem for the Uniformization of Asymptotic Expansions," Journal of Mathematical Analysis and Applications, Vol. 32, No. 3, December 1970, pp. 482-504.

92. Kevorkian, J., "Von Zeipel Method and the Two-Variable Expansion Procedure," The Astronomical Journal, Vol. 74, No. 9, November 1966, pp. 878-885.

93. Nayfeh, A.H., Perturbation Methods, John Wiley and Sons, New York, 1973.

94. Lee, E.B., and Markus, L., Foundations of Optimal Control Theory, John Wiley and Sons, New York, 1967.

95. Bryson, A.E., Jr., and Ho, Y.C., Applied Optimal Control, John Wiley and Sons, New York, 1971.

96. Lawden, D.F., "Optimal Escape from a Circular Orbit," Astronautica Acta, Vol. 4, Fasc. 3, May-June 1958, pp. 218-233.

97. Lawden, D.F., "Optimal Intermediate-Thrust Arcs in a Gravitational Field," Astronautica Acta, Vol. 8, Fasc. 2-3, March-June 1962, pp. 106-123.

98. Faulders, C.R., "Optimum Thrust Programming of Electrically Powered Rocket Vehicles in a Gravitational Field," ARS Journal, Vol. 30, No. 10, October 1960, pp. 954-960.

99. Faulders, C.R., "Minimum-Time Steering Programs for Orbital Transfer with Low-Thrust Rockets," Astronautical Acta, Vol. 7, Fasc. 1, January-February, 1961, pp. 35-49.

100. Melbourne, W.G., "Three-Dimensional Optimum Thrust Trajectories for Power Limited Propulsion Systems," ARS Journal, Vol. 31, No. 12, December 1961, pp. 1723-1728.

101. Melbourne, W.G., and Sauer, Jr., G.G., "Optimum Thrust Programs for Power-Limited Propulsion Systems," Astronautica Acta, Vol. 8, Fasc. 4, July-August 1962, pp. 205-227.

102. Hinz, H.K., "Optimal Low-Thrust Near-Circular Orbital Transfer," AIAA Journal, Vol. 1, No. 6, June 1963, pp. 1367-1371.

103. Edelbaum, T.N., "Propulsion Requirements for Controllable Satellites," ARS Journal, Vol. 31, No. 8, August 1961, pp. 1079-1089.

104. Breakwell, J.V., and Rauch, H.E., "Optimum Guidance for a Low Thrust Interplanetary Vehicle," AIAA Journal, Vol. 4, No. 4, April 1966, pp. 693-704.

105. McIntyre, J.E., and Crocco, L., "Higher Order Treatment of the Optimal Transfer of a Thrust-Limited Vehicle Between Coplanar Circular Orbits," Astronautica Acta, Vol. 13, No. 1, January-February 1967, pp. 3-21.

106. Bell, D.J., "Optimal Space Trajectories - A Review of Published Work," The Aeronautical Journal of the Royal Aeronautical Society, Vol. 72, No. 686, February 1968. pp. 141-146.

107. Pontryagin, L.S., Boltyanskii, V.G., Gamkrelidze, R.V., and Mishchenko, E.F., The Mathematical Theory of Optimal Processes, Interscience, New York, 1962.

108. Lebedev, V.N., "Some Problems of the Optimal Transfer Theory," Proceedings of the 14th International Astronautical Congress of the I.A.F., Paris, 1963, Vol. 4, Edited by: Brun, E. and Hersey, I., Gauthier-Villars, Paris, 1965, pp. 389-408.

109. Zhukov, A.N., and Lebedev, V.N., "Variational Problem of Transfer Between Heliocentric Circular Orbits by Means of a Solar Sail," Cosmic Research, Vol. 2, No. 1, January-February 1964, pp. 41-44.

110. Moiseyev, N.N., and Lebedev, V.N., "Problems of Theory of Vehicles Optimal Controls," Proceedings of the 16th International Astronautical Congress of the I.A.F., Athens, 1965, Guidance and Control, Editor-in-chief: Lunc, M., Gauthier-Villars-Dunod, Paris, 1966, pp. 301-320.

111. Avramchuk, N.A., and Klikh, Yu. A., "Solution of an Optimal Control Problem by the Averaging Method," Cosmic Research, Vol. 9, No. 2, March-April 1971, pp. 196-202.

112. Grodzovskii, G.L., Ivanov, Yu.N., and Tokarev, V.V., Mechanics of Low-Thrust Spaceflight, Israel Program for Scientific Translations, Jerusalem, 1969.

113. Brusch, R.G., and Vincint, T.L., "Low-Thrust, Minimum-Fuel, Orbital Transfer," Astronautica Acta, Vol. 16, No. 2, February 1971, pp. 65-74.

114. Anthony, M.L., and Sasaki, F.T., "Analytical Determination of Optimal Escape with Constant Thrust," Astronautica Acta, Vol. 16, No. 3, May-June 1971, pp. 173-179.

115. Jacobson, R.A., and Powers, W.F., "Asymptotic Solution to the Problem of Optimal Low-Thrust Energy Increase," AIAA Journal, Vol. 10, No. 12, December 1972, pp. 1679-1680.

116. Reidelhuber, O.J., and Schwenzfeger, K.J., "Analytical Approximate Calculation of Optimal Low-Thrust Energy Increase Trajectories," AIAA Journal, Vol. 13, No. 3, March 1975, pp. 395-397.

117. Paiewonsky, B., "Optimal Control: A Review of Theory and Practice," AIAA Journal, Vol. 3, No. 11, November 1965, pp. 1985-2006.

118. Kelley, H.J., "Gradient Theory of Optimal Flight Paths," ARS Journal, Vol. 30, No. 10, October 1960, pp. 947-954.

119. Bryson, A.E., and Denham, W.F., "A Steepest-Ascent Method for Solving Optimum Programming Problems," Transactions of the ASME, Series E, Journal of Applied Mechanics, Vol. 29, No. 2, June 1962, pp. 247-257.

120. Campbell, T.K., and Gold, T.T., "Three Dimensional Trajectory Optimization Program for Ascending and Descending Vehicles," Proceedings of the 16th International Astronautical Congress of the I.A.F., Athens, 1965, Astrodynamics, Editor-in-chief: Lunc, M., Gauthier-Villars-Dunod, Paris, 1966, pp. 161-177.

121. Glaser, P.E., "Power from the Sun," Mechanical Engineering, Vol. 91, No. 3, March 1969, pp. 20-24.

122. Glaser, P.E., "Solar Power Via Satellite," Astronautics and Aeronautics, Vol. 11, No. 8, August 1973, pp. 60-68.

123. Williams, J.R., "Geosynchronous Satellite Solar Power," Astronautics and Aeronautics, Vol. 13, No. 11, November 1975, pp. 46-52.

124. Raine, H.R., "CTS Flight Performance," Presented at the 27th International Astronautical Congress of the I.A.F., Anaheim, California, October 10-16, 1976, Paper 76-223.

125. Wright, J.L., "Physical Principles of Solar Sailing," Presented at the Solar Sail Small Symposium, American Astronautical Society, Jet Propulsion Laboratory, Pasadena, California, April 20-21, 1977.

126. Lubowe, A.G., "Order of a Perturbation Method," AIAA Journal, Vol. 3, No. 3, March 1965, pp. 568-570.

127. Geyling, F.T., and Westerman, H.R., Introduction to Orbital Mechanics, Addison-Wesley, Reading, Massachusetts, 1971, Chapter 9.

APPENDIX I

EVALUATION OF THE INTEGRALS A_{nk} AND B_{nk}

The integrals A_{nk} and B_{nk} are defined as

$$A_{nk}(\nu) = \int_0^{\nu} \cos(k\tau)\, d\tau/(1 + p\cos\tau + q\sin\tau)^n \quad ,$$

$$B_{nk}(\nu) = \int_0^{\nu} \sin(k\tau)\, d\tau/(1 + p\cos\tau + q\sin\tau)^n \quad , \qquad .....(I.1)$$

for k = (0),1,2,...; n = 1,2,3.... The parameters p and q represent the initial conditions p_{00} and q_{00} or the slow functions $p_0(\bar{\nu})$ and $q_0(\bar{\nu})$. While the integral A_{10} can be evaluated by elementary means, the integrals A_{n0} for higher values of n can be obtained from A_{10} by repeated differentiation within the integrand ,

$$A_{10}(\nu) = 2\arctan\left\{\frac{(1-e^2)^{1/2}\tan(\nu/2)}{1+p+q\tan(\nu/2)}\right\}/(1-e^2)^{1/2} \quad ,$$

$$A_{20}(\nu) = \left\{A_{10}(\nu) - \Psi(\nu)/[1+\Phi(\nu)] - q/(1+p)\right\}/(1-e^2) \quad ,$$

$$A_{30}(\nu) = \frac{1}{2}\left\{(2+e^2)A_{10}(\nu) - 3\Psi(\nu)/[1+\Phi(\nu)] - 3q/(1+p)\right.$$

$$\left. - (1-e^2)\Psi(\nu)/[1+\Phi(\nu)]^2 - q(1-e^2)/(1+p)^2\right\}/(1-e^2)^2 .$$

$$.....(I.2)$$

The integrals $A_{nk}(\nu)$ and $B_{nk}(\nu)$ for $k \geq 1$ may be expressed in terms of $A_{n-1,k-1}$, $B_{n-1,k-1}$, $A_{n,k-1}$, and $B_{n,k-1}$ according to the following recurrence formulae

$$e^2 A_{n+1,k+1} = p\left\{\frac{(n+k)}{n} A_{nk} - A_{n+1,k}\right\} - q\left\{\frac{(n+k)}{n} B_{nk} - B_{n+1,k}\right\} - \frac{[p \sin(k\nu) + q\cos(k\nu)]}{n[1+\Phi(\nu)]^n} + \frac{q}{n(1+p)^n},$$

$$e^2 B_{n+1,k+1} = q\left\{\frac{(n+k)}{n} A_{nk} - A_{n+1,k}\right\} + p\left\{\frac{(n+k)}{n} B_{nk} - B_{n+1,k}\right\} + \frac{[p\cos(k\nu) - q\sin(k\nu)]}{n[1+\Phi(\nu)]^n} - \frac{p}{n(1+p)^n}, \quad \ldots\ldots(I.3)$$

for $k = 0,1,2,\cdots$ and $n = 1,2,3,\cdots$. The following results can be obtained from Equations (I.3):

$$A_{21}(\nu) = \left\{-p A_{10}(\nu) + (q + \sin\nu)/[1+\Phi(\nu)] - q/(1+p)\right\}/(1-e^2);$$

$$B_{21}(\nu) = \left\{-q A_{10}(\nu) - (p + \cos\nu)/[1+\Phi(\nu)] + 1\right\}/(1-e^2);$$

$$A_{31}(\nu) = \frac{1}{2}\left\{-3p A_{10}(\nu) + [3q + (1+2e^2)\sin\nu]/[1+\Phi(\nu)] - 3q/(1+p) + (1-e^2)(q+\sin\nu)/[1+\Phi(\nu)]^2 - q(1-e^2)/(1+p)^2\right\}/(1-e^2)^2;$$

$$B_{31}(\nu) = \frac{1}{2}\Big\{ -3q\,A_{10}(\nu) - [3p + (1+2e^2)\cos\nu]/[1+\Phi(\nu)]$$
$$+(1+3p+2e^2)/(1+p) - (1-e^2)(p+\cos\nu)/[1+\Phi(\nu)]^2$$
$$+(1-e^2)/(1+p)\Big\}/(1-e^2)^2 \quad . \qquad \ldots\ldots(I.4)$$

The integrals with $n \leq k$ can usually be determined quite readily:

$$A_{11}(\nu) = \left\{ p[\nu - A_{10}(\nu)] + q\ \ell n \left| \frac{1+\Phi(\nu)}{1+p} \right| \right\} / e^2 \quad ;$$

$$B_{11}(\nu) = \left\{ q[\nu - A_{10}(\nu)] - p\ \ell n \left| \frac{1+\Phi(\nu)}{1+p} \right| \right\} / e^2 \quad ;$$

$$A_{12}(\nu) = -2[q+\Psi(\nu)]/e^2 - (p^2-q^2)[(2-e^2)A_{10}(\nu)$$
$$-2\nu]/e^4 - 4pq\ \ell n \left| \frac{1+\Phi(\nu)}{1+p} \right| / e^4 \quad ;$$

$$B_{12}(\nu) = 2[p-\Phi(\nu)]/e^2 + 2pq[(2-e^2)A_{10}(\nu) - 2\nu]/e^4$$
$$- 2(p^2-q^2)\ell n \left| \frac{1+\Phi(\nu)}{1+p} \right| / e^4 \quad . \qquad \ldots\ldots(I.5)$$

These results are not suited for $e \to 0$, and are to be replaced by:

$$A_{11}(\nu) = -p\nu/2 + [1 + 3p^2/4 + q^2/4]\sin\nu - p\sin(2\nu)/4$$
$$+ pq(1-\cos\nu)/2 - q[1-\cos(2\nu)]/4 + (p^2-q^2)\sin(3\nu)/12$$
$$+ pq[1-\cos(3\nu)]/6 + O(e^3) \quad ;$$

$$B_{11}(\nu) = -q\nu/2 + pq \sin\nu/2 + [1 + p^2/4 + 3q^2/4](1 - \cos\nu)$$
$$+ q \sin(2\nu)/4 - p[1 - \cos(2\nu)]/4 - pq \sin(3\nu)/6$$
$$+ (p^2 - q^2)[1 - \cos(3\nu)]/12 + O(e^3) \quad ;$$

$$A_{12}(\nu) = \sin(2\nu)/2 - p/2 \sin\nu + q(1 - \cos\nu)/2 - p \sin(3\nu)/6$$
$$- q[1 - \cos(3\nu)]/6 + O(e^2) \quad ;$$

$$B_{12}(\nu) = [1 - \cos(2\nu)]/2 - q/2 \sin\nu + p(1 - \cos\nu)/2 + q \sin(3\nu)/6$$
$$- p[1 - \cos(3\nu)]/6 + O(e^2) \quad . \qquad .....(I.6)$$

In many applications, the values of $A_{nk}(\nu)$ and $B_{nk}(\nu)$ for $\nu = 2\pi$ are required. These can be determined from the integral

$$I_{nk}(p,q) = \int_0^{2\pi} \frac{\exp(ik\tau)\ d\tau}{[1 + p\cos\tau + q\sin\tau]^n} \quad ,$$

$$n = 1,2,3,\cdots \ ; \qquad k = 0,1,2,\cdots \ ; \qquad .....(I.7)$$

with $i = (-1)^{1/2}$ and $(p^2 + q^2)^{1/2} = e < 1$. The integral I_{nk} can be evaluated by means of residues:

$$I_{nk}(p,q) = 2\pi \exp(ik\omega)\ e^{-k}(1 - e^2)^{-(n-k)/2} \sum_{j=0}^{n-1} 2^{j-n+1} *$$
$$* \binom{n+k-1}{j} \binom{-n}{n-j-1} [1 - (1 - e^2)^{-1/2}]^{n+k-j-1} \quad , \quad .....(I.8)$$

where $\omega = \arctan(q/p)$. The binomial coefficients are defined by

$$\binom{-n}{j} = (-n)(-n-1)\cdots\cdots[-n-(j-1)]/j! \quad , \quad j = 1,2,\cdots, \quad .....(I.9)$$

and $\binom{-n}{0} = 1$. The values $A_{nk}(2\pi)$ and $B_{nk}(2\pi)$ are simply:

$$A_{nk}(2\pi) = \mathrm{Re}\left\{ I_{nk}(p,q) \right\} = 2\pi \cos(k\omega)[\cdots\cdot] \quad ,$$

$$B_{nk}(2\pi) = \mathrm{Im}\left\{ I_{nk}(p,q) \right\} = 2\pi \sin(k\omega)[\cdots\cdot] \quad . \qquad .....(I.10)$$

The following explicit results are obtained:

$$A_{10}(2\pi) = 2\pi/(1-e^2)^{1/2} \; ; \quad A_{20}(2\pi) = 2\pi/(1-e^2)^{3/2} \; ;$$

$$A_{30} = \pi(2+e^2)/(1-e^2)^{5/2} \; ;$$

$$A_{11}(2\pi) = 2\pi p[1-(1-e^2)^{-1/2}]/e^2 \; ;$$

$$B_{11}(2\pi) = 2\pi q[1-(1-e^2)^{-1/2}]/e^2 \; ;$$

$$A_{12}(2\pi) = -2\pi(p^2-q^2)\left\{2-(2-e^2)/(1-e^2)^{1/2}\right\}/e^4 \; ;$$

$$B_{12}(2\pi) = -4\pi pq\left\{2-(2-e^2)/(1-e^2)^{1/2}\right\}/e^4 \; ;$$

$$A_{21}(2\pi) = -2\pi p/(1-e^2)^{3/2} \; ; \quad B_{21}(2\pi) = -2\pi q/(1-e^2)^{3/2} \; ;$$

$$A_{22}(2\pi) = 2\pi(p^2-q^2)\left\{2+(3e^2-2)/(1-e^2)^{3/2}\right\}/e^4 \; ;$$

$$B_{22}(2\pi) = 4\pi pq \left\{ 2 + (3e^2 - 2)/(1 - e^2)^{3/2} \right\} / e^4 \quad ;$$

$$A_{23}(2\pi) = -2\pi p(p^2 - 3q^2)\left\{ 8 - 3(2 - e^2)/(1 - e^2)^{1/2} + (3e^2 - 2)/(1 - e^2)^{3/2} \right\} / e^4 \quad ;$$

$$B_{23}(2\pi) = -2\pi q(3p^2 - q^2)\left\{ 8 - 3(2 - e^2)/(1 - e^2)^{1/2} + (3e^2 - 2)/(1 - e^2)^{3/2} \right\} / e^4 \quad ;$$

$$A_{31}(2\pi) = -3\pi p/(1 - e^2)^{5/2} \quad ; \quad B_{31}(2\pi) = -3\pi q/(1 - e^2)^{5/2} \quad ;$$

$$A_{32}(2\pi) = 3\pi(p^2 - q^2)/(1 - e^2)^{5/2} \quad ; \quad B_{32}(2\pi) = 6\pi pq/(1 - e^2)^{5/2} \quad ;$$

$$A_{33}(2\pi) = \pi p(p^2 - 3q^2) \left\{ 8 + (12e^2 - 8)/(1 - e^2)^{3/2} - 3e^4/(1 - e^2)^{5/2} \right\} / e^4 \quad ;$$

$$B_{33}(2\pi) = \pi q(3p^2 - q^2) \left\{ 8 + (12e^2 - 8)/(1 - e^2)^{3/2} - 3e^4/(1 - e^2)^{5/2} \right\} / e^4 \quad . \qquad \ldots\ldots(I.11)$$

APPENDIX II

EVALUATION OF THE FOURIER COEFFICIENTS a^j_{nk}, ..., d^j_{nk}

The Fourier coefficients of the functions

$$\cos(k\nu)/[1 + p\cos\nu + q\sin\nu]^n = a^0_{nk}/2 + \sum_{j=1}^{\infty} \left\{a^j_{nk}\cos j\nu + c^j_{nk}\sin j\nu\right\} ,$$

$$\sin(k\nu)/[1 + p\cos\nu + q\sin\nu]^n = b^0_{nk}/2 + \sum_{j=1}^{\infty} \left\{b^j_{nk}\cos j\nu + d^j_{nk}\sin j\nu\right\} ,$$

.....(II.1)

for k = (0),1,2,... and n = 1,2,3,... can be expressed in terms of the integrals $A_{nk}(2\pi)$ and $B_{nk}(2\pi)$ as follows:

$$a^j_{nk} = \frac{1}{\pi}\int_0^{2\pi} \frac{\cos(k\tau)\cos(j\tau)\,d\tau}{(1 + p\cos\tau + q\sin\tau)^n} = [A_{n,j+k}(2\pi) + A_{n,j-k}(2\pi)]/(2\pi) ;$$

$$b^j_{nk} = \frac{1}{\pi}\int_0^{2\pi} \frac{\sin(k\tau)\cos(j\tau)\,d\tau}{(1 + p\cos\tau + q\sin\tau)^n} = [B_{n,j+k}(2\pi) - B_{n,j-k}(2\pi)]/(2\pi) ;$$

$$c^j_{nk} = \frac{1}{\pi}\int_0^{2\pi} \frac{\cos(k\tau)\sin(j\tau)\,d\tau}{(1 + p\cos\tau + q\sin\tau)^n} = [B_{n,j-k}(2\pi) + B_{n,j+k}(2\pi)]/(2\pi) ;$$

$$d^j_{nk} = \frac{1}{\pi}\int_0^{2\pi} \frac{\sin(k\tau)\sin(j\tau)\,d\tau}{(1 + p\cos\tau + q\sin\tau)^n} = [A_{n,j-k}(2\pi) - A_{n,j+k}(2\pi)]/(2\pi) ;$$

.....(II.2)

It may be noted that $A_{n,j-k} = A_{n,k-j}$ and $B_{n,j-k} = -B_{n,k-j}$.

By means of the results of Equations(I.10), the following explicit expressions for the Fourier coefficients can be derived:

$$\begin{Bmatrix} a_{10}^{j} \\ c_{10}^{j} \end{Bmatrix} = 2 \begin{Bmatrix} \cos(j\omega) \\ \sin(j\omega) \end{Bmatrix} [(1 - e^2)^{1/2} - 1]^j \, e^{-j}/(1 - e^2)^{1/2} \quad ;$$

$$\begin{Bmatrix} a_{20}^{j} \\ c_{20}^{j} \end{Bmatrix} = 2 \begin{Bmatrix} \cos(j\omega) \\ \sin(j\omega) \end{Bmatrix} [(1 - e^2)^{1/2} - 1]^j [1 + j(1 - e^2)^{1/2}] e^{-j}/(1 - e^2)^{3/2}$$

$$\begin{Bmatrix} a_{30}^{j} \\ c_{30}^{j} \end{Bmatrix} = \frac{[(1 - e^2)^{1/2} - 1]^j}{e^j \, (1 - e^2)^{5/2}} \begin{Bmatrix} \cos(j\omega) \\ \sin(j\omega) \end{Bmatrix} [2 + e^2 + 3j(1-e^2)^{1/2} + j^2(1-e^2)]$$

$$\begin{Bmatrix} a_{11}^{j} \\ c_{11}^{j} \end{Bmatrix} = - \frac{2[(1 - e^2)^{1/2} - 1]^j}{e^{j+1}} \left\{ \frac{\cos \omega}{(1 - e^2)^{1/2}} \begin{Bmatrix} \cos(j\omega) \\ \sin(j\omega) \end{Bmatrix} + \sin\omega \begin{Bmatrix} \sin(j\omega) \\ -\cos(j\omega) \end{Bmatrix} \right\}$$

$$\begin{Bmatrix} b_{11}^{j} \\ d_{11}^{j} \end{Bmatrix} = - \frac{2[(1 - e^2)^{1/2} - 1]^j}{e^{j+1}} \left\{ \frac{\sin \omega}{(1 - e^2)^{1/2}} \begin{Bmatrix} \cos(j\omega) \\ \sin(j\omega) \end{Bmatrix} + \cos\omega \begin{Bmatrix} -\sin(j\omega) \\ \cos(j\omega) \end{Bmatrix} \right\}$$

$$\begin{Bmatrix} a_{21}^{j} \\ c_{21}^{j} \end{Bmatrix} = - \frac{2[(1 - e^2)^{1/2} - 1]^j}{e^{j+1}(1 - e^2)^{3/2}} \left\{ [e^2 + j(1 - e^2)^{1/2}]\cos\omega \begin{Bmatrix} \cos(j\omega) \\ \sin(j\omega) \end{Bmatrix} \right.$$

$$\left. + j(1 - e^2)\sin\omega \begin{Bmatrix} \sin(j\omega) \\ -\cos(j\omega) \end{Bmatrix} \right\} \quad ;$$

$$\begin{Bmatrix} b_{21}^{j} \\ d_{21}^{j} \end{Bmatrix} = - \frac{2[(1 - e^2)^{1/2} - 1]^j}{e^{j+1}(1 - e^2)^{3/2}} \left\{ [e^2 + j(1 - e^2)^{1/2}]\sin\omega \begin{Bmatrix} \cos(j\omega) \\ \sin(j\omega) \end{Bmatrix} \right.$$

$$+ j(1 - e^2)\cos\omega \begin{Bmatrix} -\sin(j\omega) \\ \cos(j\omega) \end{Bmatrix} \Big\} \quad ;$$

$$\begin{Bmatrix} a_{31}^{j} \\ c_{31}^{j} \end{Bmatrix} = -\frac{[(1 - e^2)^{1/2} - 1]^{j}}{e^{j+1}(1 - e^2)^{5/2}} \Big\{ [3e^2 + j(1 + 2e^2)(1 - e^2)^{1/2} + j^2(1 - e^2)]*$$

$$*\cos\omega \begin{Bmatrix} \cos(j\omega) \\ \sin(j\omega) \end{Bmatrix} + j(1 - e^2)[1 + j(1 - e^2)^{1/2}]\sin\omega \begin{Bmatrix} \sin(j\omega) \\ -\cos(j\omega) \end{Bmatrix} \Big\};$$

$$\begin{Bmatrix} b_{31}^{j} \\ d_{31}^{j} \end{Bmatrix} = -\frac{[(1 - e^2)^{1/2} - 1]^{j}}{e^{j+1}(1 - e^2)^{5/2}} \Big\{ [3e^2 + j(1 + 2e^2)(1 - e^2)^{1/2} + j^2(1 - e^2)]*$$

$$*\sin\omega \begin{Bmatrix} \cos(j\omega) \\ \sin(j\omega) \end{Bmatrix} + j(1 - e^2)[1 + j(1 - e^2)^{1/2}]\cos\omega \begin{Bmatrix} -\sin(j\omega) \\ \cos(j\omega) \end{Bmatrix} \Big\};$$

.....(II.3)

The coefficients a_{n1}^{0} , b_{n1}^{0} are equal to a_{n0}^{1} , b_{n0}^{1} respectively. For values of k larger than 1, the dominant coefficients can be expressed in terms of the results of Equations (II.3):

$$a_{nk}^{j} = a_{nj}^{k} \; ; \; \ldots\ldots \; ; \; d_{nk}^{j} = d_{nj}^{k} \; ; \qquad j = 0, 1, 2, \ldots \qquad \ldots\ldots(II.4)$$

APPENDIX III

DERIVATION OF HIGHER-ORDER EQUATIONS

The unknown secular terms in the first-order solutions obtained by the two-variable expansion method may become of importance eventually, especially in the heliocentric case and when the A/m ratio is large. These terms are to be determined from the boundedness constraint imposed upon the second-order solutions. In assessing the nature of the various contributions, products of (sometimes incomplete) Fourier expansions need to be analysed. Thereto, the following formal result is employed:

$$\left\{ \sum_{j=1}^{\infty} [\{\alpha\}^j \cos(j\nu) + \{\beta\}^j \sin(j\nu)] \right\} \left\{ \sum_{j=1}^{\infty} [\{\gamma\}^j \cos(j\nu) + \{\delta\}^j \sin(j\nu)] \right\}$$

$$= \{a\}^0 + \sum_{k=1}^{\infty} [\{a\}^k \cos(k\nu) + \{b\}^k \sin(k\nu)] ,$$

with:

$$\{a\}^0 = \sum_{n=1}^{\infty} [\{\alpha\}^n \{\gamma\}^n + \{\beta\}^n \{\delta\}^n]/2 ;$$

$$\{a\}^1 = [\{\alpha\}^1 \{\gamma\}^2 + \{\beta\}^1 \{\delta\}^2]/2 + \sum_{n=2}^{\infty} [\{\alpha\}^n (\{\gamma\}^{n+1} + \{\gamma\}^{n-1}) + \{\beta\}^n (\{\delta\}^{n+1} + \{\delta\}^{n-1})]/2 ;$$

$$\{b\}^1 = [\{\alpha\}^1 \{\delta\}^2 - \{\beta\}^1 \{\gamma\}^2]/2 + \sum_{n=2}^{\infty} [\{\alpha\}^n (\{\delta\}^{n+1} - \{\delta\}^{n-1}) - \{\beta\}^n (\{\gamma\}^{n+1} - \{\gamma\}^{n-1})]/2 ;$$

etc. .....(III.1)

Depending upon the nature of the left-hand-side of the differential equations, either the non-harmonic or the first-harmonic terms are required to vanish. The equations for the secular first-order as well as for the second-order periodic terms can now be derived readily; these equations are untractable in general. Solutions have been obtained only for circular starting orbits. It may be mentioned that numerical integration of the original equations is preferable in the general case.